UNIVERSITAT DE BARCELONA

Exploiting hPSCs-derived kidney organoids to study the mechanobiology of nephrogenesis

Zarina Nauryzgaliyeva

PhD program in Biomedicine

Exploiting hPSCs-derived kidney organoids to study the mechanobiology of nephrogenesis

Dissertation submitted by Zarina Nauryzgaliyeva for the degree of Doctor of Philosophy

Barcelona, 2024

Supervisors:

Dr. Nuria Montserrat Pulido

Dr. Xavier Trepat Guixer

IBEC
Institute for Bioengineering of Catalonia

UNIVERSITAT DE BARCELONA

¨ Рукописи не горят ¨

- Мастер и Маргарита,

Булгаков

Acknowledgments

First and foremost, I would like to thank my supervisors Nuria Montserrat and Xavier Trepat, for allowing me to be a part of this exiting project and the members of my PhD jury – Jordi Alcaraz, Berta Alsina, Vikas Trivedi, Raymon Sunyer, and Esteban Hoijman, for offering their time to read and evaluate my PhD thesis.

The time I´ve spent at IBEC in the labs of Nuria Montserrat and Xavier Trepat have been exceptionally educational and enriching to say the least. I've been given the opportunity to learn so much about kidney development and mechanobiology, fields that were very new to me at the beginning of the thesis, as well as gain valuable research experience. I've gotten the chance to experience science in a high-quality research environment, where hard work, communication, and mutual support between the members of the research groups are present all around.

Nuria and Xavi, thank you both for allowing me to join a truly stimulating research environment and for showing me the beauty of collaboration. Thank you for all the support and guidance throughout these years. It has been a privilege working under your supervision and getting to experience research with both of you.

I would also like to extend my acknowledgments to Pere Roca-Cusachs and Florencio Serras, for serving as my follow-up committee during the PhD and for all their insightful comments.

I have been very lucky to experience two distinct yet stimulating environments and have had the pleasure of working with some of the smartest and kindest people throughout the PhD.

To all the past and present members of the NM laboratory, thank you for the truly enriching experience. Elena, thank you for your guidance and support in all scientific matters, discussing experiments with you has always given me very valuable insights. Thank you for sharing your knowledge and experience with me. Carolina and Daniel, thank you for all your support for the laboratory, for the hard work that you do in the many projects of the lab, you are truly invaluable members, and I am grateful to have had the chance to work by your side.

Gaia, Anisha, Andres, Miriana, Lucia, Patricia, - it has been so much fun sharing this PhD journey with you and becoming more than just lab-mates. Thank you for all the support, the encouragements and all the laughs we´ve shared together. I´ve learned so much from each one of you. A special thank you to Andres for all the encouragements

and the help during the past years. I´m excited for all your journeys and can´t wait to keep celebrating your accomplishments.

To the newer members, Iphigenie, Agnes, Andrea, Beatrice and Aina, - thank you for your positivity and for the laughter you bring into the office, it´s a pleasure to share the spaces with you. Good luck with all your future endeavours. Maria, while you spent a short time in the lab, I associate your time with only positive memories, so for that, thank you and good luck with your PhD.

To all the past and present members of the XT-PRC labs, thank you for welcoming me into this large community, I´m truly grateful to have become a part of it. I´ve learned so much about different research fields, countries, cultures and more with each one of you.

I´m eternally grateful to Miquel, from whom I´ve learnt so much in this PhD. You have saved me from drowning in my own data, and have always been available to discuss ideas, TFM analysis and MATLAB troubleshooting whenever I got stuck. Thank you for your kindness and enthusiasm in science and outside of the lab, whether it was breakfast in Montferry or hiking in Montserrat.

To Miguel, Ignasi, Marc, Gerardo, Sefora, Isabela, Clement, Ona, Thomas, Aina, Irina, Nimesh and Sri, sharing the PhD with you has been so much fun. Thank you for all the deep conversations, the laughs, the climbing, the theatre, the cinema and more. I´ve loved learning something new from each one of you, be it about Galicia and cinema, or basket weaving, you´ve become more than lab-mates and I´m very grateful for that. A special thank you to Alice, for the instantaneous friendship and for your unconditional support, throughout the good and the bad, in this entire journey. I´m grateful to have found a friend like you.

Marija, JuanFra and Leone, thank you for all your support regarding science and life, somehow talking with you has always given me peace of mind and I´m very grateful for that. Thank you for sharing life outside of the lab, through concerts, cinema and art, life in Barcelona has been a lot more fun with you.

There are still so many wonderful people that I haven´t mentioned that are a part of this lab, who made the past few years so enjoyable. Laura, Amy, Ozge, Steffen, Tom, Elena, Guillermo, Anabel-lise, Margherita, Janet, Elia, Rohit, Pau, Emmanuel, Pau, Ibrahim, Jorge, Mamatha, Manu, Valeria, Evelyn, Meng, Yudish, thank you all for the conversations, for sharing your culture with me and for making the environment so welcoming.

And of course, I would like to thank Anghara, Susana, Monica, Evelyn and the members of the different teams: microscopy, cell culture, stocks, etc. The lab functions thanks to your commitment and hard work, and for that I am very grateful.

The helix building has also brought me closer to other wonderful humans, such as Annie, Chris, Pilar, Juan, Aina and Sujey. Thank you for all the conversations and the support, you make the helix building a more enjoyable place.

To my dear friends outside of the lab, thank you for your unconditional support and love. Celine, Morgane, Chrysanthi, Tere, Kunya, Sam, Aizat, and Aliya you are always there for me, and I appreciate that a lot. To the ones in Barcelona, Ivan, Jacob, Maria, and Luis, thank you for making it feel like home. Thank you for all the support in the PhD and in life, these years have been filled with fun thanks to all of you.

And of course, I can´t miss the little community of climbers that have become like family. Marcos, Clara, Maria, and Oliver, thank you for the past year of adventures, for the immense support in climbing, in the PhD and in life in general.

I would not be writing these words here if it wasn´t for the unconditional support from my family. Мама, Папа, сіздерге оқу жолымда көрсеткен мейіріміңіз бен көмектеріңізге мен ризамын. Бұл жетістікке жетуым сіздердің арқаларыныз. Сіздің махаббатыңыз бен қолдауыңыз болмаса, мен бұл жұмысты жасай алмас едім. Сіздерді жақсы көремін. Дана, Дариа спасибо и вам за бесконечную веру в меня, за очень нужные слова поддержки по телефону и за то что вы просто есть. You are my strength, and I am very lucky to have you both.

Last, but definitely not the least, Joel. Thank you for your contagious optimism on days full of failure. For your never-ending energy, that fuels the both of us, when I´m feeling low. For your undying hope in a dry crag after 3 days of rain. And for your unconditional and unbeatable belief in me. You´ve been my biggest pillar of support these years, and I am truly grateful that you came into my life.

And lastly, thank you to the reader, for enduring these long pages of acknowledgements and for taking the time to read this thesis.

Abstract

The isolation and generation of human pluripotent stem cells (hPSCs) has allowed research in human organogenesis to excel, by allowing the reproduction of the fundamental principles of tissue morphogenesis *in vitro*. Particularly in the field of kidney development, cutting edge research has led to the successful generation of kidney organoids from hPSCs by mimicking *in vitro* biochemical renal inductive signals that occur during organogenesis. However, tissue formation and morphogenesis don't solely rely on biochemical and genetic instructions they are also influenced by mechanical signals that drive migration, differentiation, and growth within the forming organ, regulated through local internal forces and dynamics of ECM stiffness and viscosity. While the key morphogens and signalling pathways involved in kidney morphogenesis have been identified, the role of mechanical cues during kidney development and formation of congenital anomalies of the kidneys and urinary tract (CAKUT) has remained elusive.

This thesis describes the development of a high throughput system for 2D kidney differentiation (namely RV emergence and nephron-like formation) on soft PDMS substrates which allows the exposure of hPSCs-derived kidney progenitor cells to physical constraints in the form of substrate rigidity and geometry, compatible with traction force measurements. We have validated the system for supporting RV emergence and nephron-like formation in 2D in the background of male ES[4] and female CB40 kidney progenitor cells, as well as measured traction forces exerted by kidney progenitors in wildtype and CAKUT-related phenotypes. We found that wildtype kidney progenitors exert increasing traction forces as differentiation progresses, while in the CAKUT-related backgrounds these forces are diminished. We identified a correlation between extent of kidney differentiation and exposure to increasing curvature of micropattern geometry. In this regard, wildtype progenitors seeded on triangular geometries displayed lower extent of differentiation (as described by immunofluorescence expression) and higher traction forces compared to circle and square counterparts. As such, our experimental pipeline and quantitative analysis have set the bases for further experiments to mechanistically couple how RV emergence and nephron differentiation is driven by changes in the expression of specific renal markers and cell force generation.

Funding

The project that gave rise to these results received the support of a fellowship from La Caixa Foundation (ID 100010434). The fellowship code is LCF/BQ/DI20/11780019.

Table of Contents

Introduction

The kidneys: anatomy and function

The kidney

The kidneys are vital excretory organs responsible for maintaining blood volume and electrolyte composition, thus ensuring overall organism homeostasis (Bertram et al., 2011). They achieve this through a highly vascularized architecture facilitating efficient glomerular filtration of blood plasma. Selective reabsorption of essential solutes and water occurs within the nephron tubules, with waste products and excess water ultimately excreted as urine via the ureter. This intricate process is tightly regulated by the renin-angiotensin-aldosterone system (RAAS), ensuring precise control of blood pressure, electrolyte balance, and acid-base equilibrium. Here, the kidneys also contribute to the production of some of the hormones in RAAS, erythropoietin and vitamin D3 (Davis et al., 1961; Sahay et al., 2012). Less known is the fact that the kidneys are also the second organ after the heart in total number of mitochondria and oxygen consumption (Pagliarini et al., 2008). This is specifically important to produce ATP to fuel active transport of glucose and ions from the bloodstream, further highlighting the irreplaceable importance of the kidneys as an organ (Forbes, 2016).

Each human kidney (depending on ethnicity) harbours between one and one point five million nephrons, the microscopic workhorses responsible for blood filtration (Bertram et al., 2011). These intricate structures comprise two key components: the renal corpuscle, where blood plasma undergoes ultrafiltration at the glomerular filtration barrier, and the tubular epithelium, responsible for selective reabsorption and secretion of solutes. Waste products and excess water are then directed into a collecting duct network, ultimately eliminated via the ureters.

Embryonic kidney development

Prior knowledge from kidney development in model organisms

The morphogenetic events leading to proper embryonic kidney development in vertebrates have been widely studied with the use of mouse, *xenopus*, and avian model organisms.

During mammalian embryonic kidney development, three precursor kidney structures form. The first two, the pronephros and mesonephros, are temporary but essential for early development. The pronephros is rudimentary, while the mesonephros contains primitive nephrons that eventually degenerate and contribute to the developing reproductive system. In humans, in the absence of these structures, a condition called renal agenesis occurs, where kidneys fail to develop altogether. In contrast, the third structure, the metanephros, persists and differentiates into the permanent, functional adult kidney. It begins development around five weeks of gestation and becomes functional by the end of the first trimester (Reidy & Rosenblum, 2009; Romagnani et al., 2013).

Early commitment of the urinary system starts at the blastula stage of embryonic development, from a primitive tissue termed the primitive streak (PS) (Figure 1). Embryonic mouse experiments [reviewed in (Dressler, 2009; Halt & Vainio, 2014)] have demonstrated that the posterior end of the PS further evolves into the Intermediate Mesoderm (IM), that gives rise to all specialized cells of the mature kidneys. It arises at embryonic day 8 in mice (E8) and is termed "intermediate" due to its localization between axial and lateral plate mesoderm's of the developing embryo (Little & McMahon, 2012). Upon polarization, the IM is segmented into the anterior IM (AIM) and posterior IM (PIM). This event is crucial and sets the basis for the development of the two main components of the developing kidney: the ureteric bud (UB), formed from the Wolffian duct (epithelialized AIM) and the metanephric mesenchyme (MM), formed from the PIM, around the UB as a cap-like structure. Pioneering dissociation and reaggregation experiments in chick embryonic kidneys have demonstrated the fundamental reciprocal inductive signalling events necessary for proper kidney morphogenesis (Grobstein, 1956; Moscona & Moscona, 1952; Saxen & Sariola, 1987). At embryonic day 12.5 (in the mouse), reciprocal

interactions between the UB and MM promote their co-development: the UB, under the influence of GDNF produced by the MM, undergoes branching morphogenesis, while the MM, influenced by canonical Wnt signalling from the UB, undergoes mesenchymal-to-epithelial transition (MET). Isolated MM has been shown to be responsive to inductive signals from several embryonic tissues, such as the spinal cord, and ultimately contributing to the proper formation of the renal epithelial tubules (Saxen & Sariola, 1987).

Upon activation of the Wnt pathway, nephron progenitor cells (NPCs) arising from the MM undergo a series of structural changes. They first cluster together to form pre-tubular aggregates (PTAs), which over time form a lumen and become renal vesicles (RVs). These in turn polarize, elongate, and eventually segment into different sections of the mature nephron (proximal, medial, and distal segments) a process termed nephron patterning and segmentation (Dressler, 2006; Khoshdel Rad et al., 2020; Lindström, Tran, et al., 2018).

Following birth, the mammalian kidney exhibits remarkable cellular diversity, encompassing over 30 distinct cell types. These cell types can be broadly categorized into epithelial cells, endothelial cells, and stromal cells, each playing a specific role in kidney function, filtration, and hormone production.

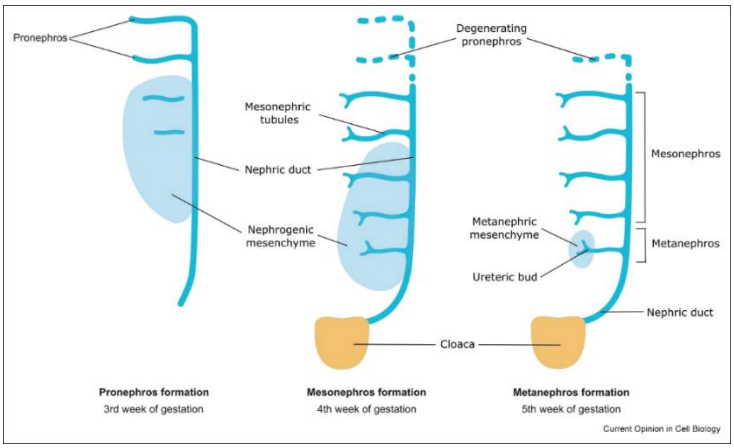

Figure 1. Urogenital system development in humans, resulting in the formation of the metanephric mesenchyme and ureteric bud. Following the development and subsequent regression of the pronephros, the mesonephros emerges caudally, giving rise to mesonephric tubules. These tubules, readily irrigated with blood flow, temporally contribute to urine production and drainage into the nephric duct, ultimately reaching the cloaca. The mesonephric structures eventually degenerate upon the formation of the metanephros, which comprises the metanephric mesenchyme and ureteric bud. Taken with permission from: (Pahuja et al., 2024)

Methods for ex vivo organ culture in kidney research

As research into kidney development progressed, the need for improved culture methods for isolated organs (*ex vivo* organ culture) grew in parallel. It started from Trowell in 1954, who introduced a novel method for *ex vivo* organ culture using a metal grid and a cotton sheet to support the embryonic kidney at an air-liquid interface (Trowell, 1954). Later, with the aims of studying the induction of the metanephric mesenchyme, Grobstein slightly modified the methodology of Trowell. He created a ¨sandwich type culture¨ which included sandwiching an inducer tissue, such as the spinal cord, in between two filters, on top of which the uninduced mesenchyme would be placed (Grobstein, 1956). All of this was then held on top of either a glass cloth or plexiglass ring, to create the same air-liquid interface. Later, Saxen created a combined and simplified version of the previous two, by culturing the uninduced mesenchyme and the spinal cord separated by a filter, which laid directly on top of a metal grid in a culture dish (Saxen, 1987). These methodologies opened doors to the possibilities of organ culture by fine-tuning their environment and the cues received, which significantly accelerated the field of kidney development (Rak-Raszewska et al., 2015).

Genes identified to be important players during kidney development

The advancement in *ex vivo* organ culture coincided with the development of genetically modified mice and other model organisms, which played a critical role in identifying genes and signalling pathways essential for triggering nephrogenesis (kidney formation) in mammals.

Studies comparing embryonic kidney development across various mammals revealed a remarkable degree of similarity. Research by Lindström et al. documented shared morphological features between mouse and human embryonic and adult kidney tissues (Lindström, Tran, et al., 2018). This suggests a strong conservation of tissue architecture across species at corresponding gestational stages. This conservation extends to the basic layout of the nephron: both mouse and human nephrons share a similar blueprint in terms of their morphology and relative positioning within the kidney (Lindström, Tran, et al.,

2018). Additionally, immunocytochemistry studies have shown a high degree of conservation in nephron patterning events across mammals including the polarization of renal vesicles (early nephron structures), their segmentation into proximal and distal parts, and their overall orientation within the developing kidney.

The remarkable conservation of embryonic development across mammals has allowed insights gained from animal models to be translated to human kidney development (L. Cullen-McEwen et al., 2015). These studies have been instrumental in elucidating the various stages of kidney morphogenesis and identifying key signalling pathways and genes governing this process. Notably, the canonical Wnt pathway has been established as a crucial player in nephrogenesis, as evidenced by research in various models (Carroll et al., 2005; Lindström, Tran, et al., 2018).

Studies using targeted mutagenesis in mice have revealed a vast number of genes critical for normal kidney development [reviewed in (Kuure et al., 2000)]. Most of these genes are indispensable for proper morphogenesis of the metanephros. Notably, mutations that inactivate specific transcription factor genes, such as *Lim1* (Shawlot & Behringer, 1995), *Pax2* (Favor et al., 1996; Torres et al., 1995), *WT1* (Kreidberg et al., 1993), *Hnf1a/b* (Naylor et al., 2013) and *Ret* (S. Jain, 2009), among others, result in the most severe kidney and urogenital malformations, or cancer (*WT1*).

LHX1

LIM homeobox 1 (LHX1) is a transcription factor first identified in Xenopus *Xlim-1* to be important, during gastrulation, for establishing body patterning of the developing embryo (Taira et al., 1992). Later on, expression of *Xlim-1* has been identified to be concentrated in the neural plate, the precursor of the central nervous system, and the lateral plate mesoderm that develop into the pro- and mesonephros (Taira et al., 1994). Interestingly, functional genetic studies have demonstrated a critical role of *Xlim-1* in kidney development: the expression of a dominant negative form of this gene resulted in the lack of proximal tubules (Chan et al., 2000), while the co-overexpression (with *Pax8*) resulted in kidney

enlargement and ectopic pronephric tubules (Carroll & Vize, 1999). Murine *Lim-1* depletion has been demonstrated to be lethal, however in some cases pups developed lacking the head, kidneys and gonads (Shawlot & Behringer, 1995). MM-specific ablation of *Lim-1* in mice has resulted in a complete abolishment of nephrogenesis, with mutant pups developing kidneys empty of nephrons (Kobayashi et al., 2005). In humans, mutations in *LHX1* have been registered in women suffering from Mayer-Rokitansky-Kuster-Hauser syndrome (MRKH), a disorder presenting uterus and vaginal aplasia (Cheroki et al., 2008). While these cases validate that *LHX1* plays a similar role in the development of the female reproductive system across species, further investigation into its other potential functions during human embryonic development is challenging. This difficulty likely stems from the lethality associated with the loss of *LHX1*.

PAX2

Paired box gene 2 (*PAX2*) is a critical player in kidney development, expressed throughout nephron differentiation (Torres et al., 1995). It has been identified to be expressed starting from the development of the three precursor kidney structures (pro-, meso- and metanephros) (Dressler et al., 1990). In mice, *Pax2* is essential for the MM to transition into NPCs and for UB positioning and outgrowth (Brophy et al., 2001). In the absence of *Pax2*, nephric ducts in mouse embryonic kidneys are still able to form, however quickly degenerate resulting in a renal agenesis, as observed in *Pax2*-deficient mice (Torres et al., 1995). In humans, *PAX2* frameshift mutations are associated with renal coloboma, a less severe defect (Bower et al., 2012; Chang et al., 2022; Sanyanusin et al., 1995). Mice models carrying identical *Pax2* mutations (*1Neu)* to human patients with renal coloboma, have demonstrated an increased apoptosis in the UB, resulting in a reduction in UB branching and consequently lower total nephron numbers in the developing kidneys (Favor et al., 1996). Such murine studies have pointed to the functional role of *Pax2* in both UB branching morphogenesis and nephron patterning, validating its role as a key molecular regulator at different steps of kidney development.

WT1

Wilm´s Tumour 1 (*WT1),* first characterized in a case of nephroblastoma, a childhood kidney cancer (Call et al., 1990), has been shown to play an important role in embryonic kidney development (J. F. Armstrong et al., 1993). Early *Wt1* murine models developed in the 90s demonstrated the important role of this gene in different stages of kidney morphogenesis. *Wt1* null mice developed complete kidney and gonad agenesis and resulted in lethality of the pups at E13.5 (Kreidberg et al., 1993). Later studies using silencing (siRNA) in E11.5 mice kidney cultures have validated the role of *Wt1* in MET and the formation of the cap mesenchyme (Davies et al., 2004). Studies using conditional knockout of *Wt1* only in the renal condensing mesenchyme in mice have further validated the importance of *Wt1* for MET, since the resulting pups developed kidneys with poor nephron formation, with an overall abundance of mesenchyme over epithelial structures (Essafi et al., 2011). In humans, mutations in *WT1* have been associated with tumours in the kidney (Wilms Tumour) and renal developmental abnormalities like Denys-Drash and Frasier syndromes. The later syndromes typically present as glomerulosclerosis with predisposition for Wilms Tumour (Drash et al., 1970; Frasier et al., 1964; Pelletier et al., 1991).

HNF1B

Hepatocyte nuclear factor 1-β (*HNF1B*) plays a vital role in nephrogenesis. Studies in zebrafish lacking *hnf1ba/b* revealed its role in nephron patterning and segmentation, as these embryos formed epithelial tubules but lacked markers for distal and proximal segments (Naylor et al., 2013). Similar findings were observed in mice and Xenopus, where disruption or overexpression of this gene disrupted SSB patterning and segmentation (Naylor et al., 2013). Mutations in *HNF1B*, along with *PAX2* mutations, contribute to roughly 15% of human congenital anomalies of the kidneys and urinary tract (CAKUT) (Nicolaou et al., 2015).

RET

Mutations in the receptor tyrosine kinase *RET* gene are frequently associated with congenital urinary anomalies like renal agenesis and aplasia (Chatterjee et al., 2012). Studies using mutant mice with alterations along the *GDNF-Gfra1-Ret* axis have shed light on *Ret* expression patterns throughout the kidney and lower urinary tract (S. Jain, 2009). *Ret* plays a crucial role in early UB induction and branching, and its absence leads to severe phenotypes like renal agenesis or prenatal death. A study by Chatterjee et al. (2012) found that mutations in the GDNF-RET signalling pathway occur in about 5% of CAKUT patients, and the mutation type influences the severity of clinical presentation.

Disruption of kidney development can lead to CAKUT

Considering the established roles of the above-described genes in embryonic kidney development, dysregulation of their expression or dosage is likely to contribute to the pathogenesis of congenital kidney anomalies.

CAKUT – congenital anomalies of the kidneys and urinary tract

Congenital anomalies of the kidneys and urinary tract (CAKUT) is a broad term encompassing a diverse range of congenital malformations of the kidney and urinary system, with an estimated prevalence of 1 in 100 to 500 newborns (Westland et al., 2021). The phenotypic spectrum of CAKUT anomalies is highly heterogeneous, with aplasia, hypoplasia, dysplasia, agenesis, and ureteral abnormalities being among the most observed presentations [reviewed in (Schedl, 2007)]. Mutations in over twenty genes have been implicated in the pathogenesis of both syndromic and non-syndromic CAKUT, potentially explaining the varied clinical presentations of these congenital anomalies (Nicolaou et al., 2015). Examples include key regulatory genes such as *PAX2, HNF1B, BMP7, RET, GATA3, SALL1, SIX5*, and *EYA1*, all of which play crucial roles in kidney development.

The development of mouse models harbouring genetic mutations that disrupt kidney development, leading to phenotypes like renal aplasia, agenesis, horseshoe kidneys, ureteral duplication, polycystic kidney disease, interstitial fibrosis (scarring), hypertension, and diabetic nephropathy, has significantly advanced our comprehension of the pathogenesis and underlying mechanisms of congenital kidney anomalies [reviewed in detail in (Kuure & Sariola, 2018)].

While mouse models have been extremely useful in gaining an understanding of embryonic kidney morphogenesis, it is important to note that models of CAKUT in mice have so far been developed by a complete inactivation of genes, rather than mimicking patient specific mutations.

In human patients, mutations associated with CAKUT are typically heterozygous. Homozygous mutations in critical regulatory genes likely result in severe developmental consequences, leading to early pregnancy loss (miscarriage or abortion) rather than manifesting as a specific disease syndrome or isolated organ defect. Similarly in mice, certain homozygous or heterozygous mutations have caused either embryonic or postnatal lethality, making it difficult to study the underlying pathophysiology (Stone et al., 2016). Additionally, the presence of gene families in humans introduces the concept of redundancy. Genes within a family might share similar functions, potentially

allowing remaining members to compensate for the loss of a single mutated gene, for example members of the *PAX* gene family (Bouchard et al., 2002). Furthermore, the possibility exists that additional genetic modifiers, involving alterations in other genes, might be necessary for CAKUT to manifest.

Unfortunately, most CAKUT cases in patients are idiopathic, with the genetic alteration sometimes causing different presentations (or non-symptomatic) in members of the same family (Murugapoopathy & Gupta, 2020).

These limitations call for a better approach to phenocopy CAKUT anomalies in humans by taking advantage of techniques, such as CRISPR/Cas9 gene editing technology, to generate patient specific mutations.

Animal models in kidney research: advances and challenges

Unveiling the intricate mechanisms of organ development requires a multi-faceted approach. A combination of genetic techniques, like forward and reverse genetics, to pinpoint the genes that orchestrate this process, together with techniques like *in situ* hybridization and immunohistochemistry can help understand gene expression and protein localization within developing embryos.

All these techniques take advantage of model organisms, from zebrafish to mice, that, due to their rapid development and genetic similarities to humans' ability to have enhanced our understanding of embryonic organ development.

The following section will give an overview of different model organisms historically utilized for studying embryonic kidney development and novel techniques for studying the role of CAKUT associated genes.

Zebrafish (Danio Rerio)

The zebrafish (*Danio rerio*) has become a crucial vertebrate model organism for investigating human biological processes. Several key features contribute to its exceptional utility. First, zebrafish exhibit prolific breeding, generating offspring ranging between 50 to 200 embryos that develop rapidly, reaching adulthood within just 3 months. Additionally, zebrafish share a high degree of genetic similarity with humans, possessing roughly 70% of all human genes and a remarkable 82% of human disease-associated genes (Howe et al., 2013). This genetic conservation extends to the presence of nearly all organ systems found in humans. Furthermore, the transparent nature of zebrafish embryos during their larval stage allows the direct visualization of biological processes within the intact organism, using techniques like live cell imaging with fluorescent reporters. This approach enables the study of these processes at high resolution, encompassing cellular and even subcellular levels.

While adult zebrafish possess a mesonephric kidney, a more primitive structure compared to the mammalian metanephric kidney, their larval stage offers a valuable model for studying basic kidney function. During this period, the zebrafish kidney exists in the form of a pronephros, an even simpler structure.

This pronephros consists of two bilateral glomeruli connected to two pronephric ducts. Remarkably, these ducts share a high degree of genetic and functional similarity with their counterparts in the mammalian nephron (Wingert & Davidson, 2008). For instance, the proximal segments of both the zebrafish pronephric duct and the mammalian nephron express proteins like *megalin* and *slc4a4*, pointing towards the tubule like nature of specific regions of the zebrafish pronephros, once considered as the duct (Wingert & Davidson, 2008). The remarkable conservation of proximodistal specialization across vertebrate species in the pronephros challenges the traditional view of these structures as "simple" nephrons in the zebrafish. This observation suggests a deeper level of complexity within the pronephros, with evidence indicating that these early excretory organs share many segmental characteristics with their more advanced counterparts, the metanephric nephrons found in mammals.

The zebrafish pronephros has emerged as a popular model for investigating genes and processes associated with various diseases. Notably, the field of ciliopathies has particularly benefitted from utilizing the pronephros in zebrafish larvae for gene validation (Ross et al., 2005). All cells lining the pronephric duct possess motile cilia on their apical surfaces. The transparent nature of the zebrafish allows researchers to readily observe cilia-related abnormalities, such as renal cyst formation. However, a crucial distinction exists between zebrafish and mammalian nephrons: all cilia in the zebrafish pronephros are motile 9+2 cilia, sometimes arranged in bundles, unlike the differentiated cilia found in mammals (Zhu et al., 2021). This dissimilarity suggests that cyst formation in zebrafish might primarily stem from impaired fluid movement rather than disruptions in fluid flow sensing and signalling pathways, which are implicated in human diseases like polycystic kidney disease (PKD) and nephronophthisis (NPH) (Kramer-Zucker et al., 2005).

Frog (Xenopus Laevis)

The African clawed frog (*Xenopus laevis*) emerged as a prominent embryological model organism in the early 20th century. This rise to prominence stemmed from the pioneering work of UK zoologists who successfully established breeding

protocols for xenopus in laboratory aquaria. A key advantage of the xenopus model lies in the remarkable accessibility of its eggs and embryos. Females lay large clutches containing thousands of eggs, each with a substantial diameter of roughly 1 mm, facilitating microinjection directly into targeted cells within the early embryo, even after several rounds of cell division. This capability is particularly valuable for generating mosaic tissues, where different cell populations within an organism possess distinct genetic compositions (Blum & Ott, 2019).

Perhaps the most celebrated contribution of the xenopus model is the groundbreaking nuclear transfer experiments of John Gurdon. This pioneering research culminated in the cloning of the first-ever vertebrate organism – a frog – achieved by transferring a nucleus from a differentiated somatic cell into a denucleated fertilized egg (Gurdon et al., 1958). Since then, the xenopus has proved itself as a versatile and valuable model organism for developmental mechanisms including cell cycle regulation, expression of key developmental genes and morphogen pathways (such as Wnt and BMP signalling) [reviewed in detail in (Bier & De Robertis, 2015; Cruciat & Niehrs, 2013; De Robertis et al., 2000; Philpott & Yew, 2008; Sha et al., 2003)].

A remarkable degree of gene collinearity exists between the xenopus and human genomes, signifying that long stretches of genes reside in the same relative chromosomal order. This conservation extends to the identification of orthologs – genes in different species that share a common evolutionary origin and similar function. Significantly, a high percentage (79%) of human disease genes have a verified ortholog in xenopus. This substantial overlap offers a powerful bridge between human disease and developmental biology research (Hellsten et al., 2010).

In regards to kidney diseases, the xenopus has been extensively used to model and understand CAKUT-related gene mutations [reviewed in (Blackburn & Miller, 2019)]. For example, *xenopus laevis* have been used to generate loss-of function mutations in *pax* family genes to study the specific role of *pax2* and *pax8* on xenopus pronephros development(Buisson et al., 2015). As discussed earlier in this thesis, *Pax2* null mice have previously been shown to result in complete

kidney agenesis (or renal hypoplasia in humans with heterozygous mutations) (Torres et al., 1995).

While *Pax2* and *Pax8* have been shown to have redundant functions in mice (Bouchard et al., 2002), in xenopus they are required at specific steps of pronephros development (Buisson et al., 2015). In xenopus, the absence of *pax8* leads to a complete lack of the pronephric tubule, while *pax2* plays a more important role towards the end of pronephric development, after the establishment of the pronephric tubule anlage. Interestingly, the same study found that *pax8* is crucial for the expression of *hnf1b* and cell proliferation of pronephric precursors via *wnt/b-catenin* signalling in the developing kidney field of the *xenopus* (Buisson et al., 2015).

Xenopus has also emerged as a valuable model organism for investigating genotype-phenotype relationships of mutations in the *HNF1B* gene, which has been shown to exhibit a spectrum of CAKUT phenotypic presentations (Bohn et al., 2003).

Two independent studies successfully employed different approaches in Xenopus to model the phenotypic diversity associated with *HNF1B* mutations. The first study utilized a heat-shock inducible Cre-loxP system to generate transgenic xenopus lines expressing two distinct human *HNF1B* mutations – an insertion and a deletion. The deletion mutation resulted in impaired pronephric development, while the insertion mutation led to an enlarged pronephros. Notably, both phenotypes primarily affected the proximal tubules (Sauert et al., 2012).

The second study compared the effects of nine different human *HNF1B* mutations, encompassing insertions/deletions (indels), missense mutations, and nonsense mutations, by injecting mutant mRNA into xenopus embryos. Like the observed variations in humans, these mutations induced distinct renal disease phenotypes in Xenopus. Six of the mutations caused an enlargement of the pronephric structures, while the remaining three resulted in reduced or absent tubules and an anterior duct defect (Bohn et al., 2003).

The remarkable recapitulation of human kidney phenotypes in Xenopus offers a powerful platform for establishing correlations between specific *HNF1B*

mutations and patient phenotypes. This approach has the potential to streamline the identification of pathogenic genetic variants and elucidate the underlying mechanisms responsible for the variable expressivity observed in patients with *HNF1B* mutations.

In humans, deletions within the chromosomal region 17q12, a region spanning two genes – *HNF1B* and *LHX1* - have been associated CAKUT (Nagamani et al., 2010). Given that *LHX1* is an important gene for many developmental processes, mice embryos carrying KO mutations for this gene often result in prenatal lethality. Interestingly, xenopus carrying homologous KO mutations in *lhx1* do not result in embryonic lethality, rather only in kidney developmental disruptions (DeLay et al., 2018).

Mouse (Mus Musculus)

The laboratory mouse (*Mus musculus*) serves as a remarkably powerful model organism for biomedical research. Its short gestation period of approximately three weeks, followed by a litter size of three to ten pups, facilitates rapid generation of experimental cohorts. Additionally, the mouse boasts a lifespan of roughly two to three years, allowing for longitudinal studies. A significant advantage lies in the high degree of genetic conservation between humans and mice, with a vast majority of human disease genes having functional counterparts in the mouse genome. Furthermore, most established research tools are accommodated for mouse studies. The availability of numerous antibodies specific to mice, as well as the well-annotated mouse genome enable comprehensive transcriptomic and proteomic investigations. Perhaps the most compelling strength of the mouse model lies in the development of a diverse array of innovative genetic technologies that enable the creation of genetically modified mice, allowing researchers to dissect the function of specific genes and their contribution to various disease processes.

In kidney development, the mouse has become an indispensable tool, contributing to a vast body of publications and groundbreaking discoveries. This stems primarily from the inherent complexity of the human kidney, which is sufficiently replicated within a mammalian model system, such as the mouse.

Consequently, the mouse allows researchers to investigate a broad spectrum of genetic kidney diseases, encompassing developmental defects, glomerular dysfunction, and tubular disorders.

In the context of CAKUT modelling, spatial and temporal expression patterns of candidate genes during mouse kidney development can be effectively studied using techniques like *in situ* hybridization, immunohistochemistry, and transcriptomic analysis.

Furthermore, the availability of diverse *Cre* recombinase lines allows the generation of conditional gene knockouts. This approach allows for the targeted deletion of genes within specific renal cell types, not only during development but also in adulthood. This capability provides unparalleled flexibility for investigating gene function across different stages of life.

Despite a high degree of evolutionary conservation in the fundamental processes of embryonic kidney development across mammals, subtle variations exist at the molecular and anatomical levels between different species (Lindström, Tran, et al., 2018; O'Brien et al., 2016). Indeed, comparative studies between mouse and human nephrogenesis have some revealed divergent features (O'Brien et al., 2016). For instance, only a small subset of previously identified mouse "anchor genes" exhibit a conserved pattern of expression in the developing human kidney (Lindström, Guo, et al., 2018). Variations in nephron number are observed between mammalian species. While measuring the absolute number of nephrons in any species remains technically difficult, an estimate in mouse kidneys is around 12,000 nephrons, whereas human kidneys, depending on the race, have an average of 1 million (Bertram et al., 2011; L. A. Cullen-McEwen et al., 2003). This significant difference can be attributed to two key factors: gestational length and the overall rate of nephrogenesis. Compared to the extended gestation period of approximately 9 months in humans, mice undergo nephrogenesis within a considerably shorter timeframe of 20 days. This disparity in gestational timing translates to a prolonged window for nephron generation in humans, ultimately resulting in a far greater number of nephrons (O'Brien & McMahon, 2014).

Ethical concerns and limitations of human studies

While genetic studies in the zebrafish, frog and mouse have provided us with the current fundamental knowledge on embryonic kidney development, studying the mechanisms of human specific congenital anomalies has been proven more difficult. While kidney development is a process remarkably conserved among vertebrates (and even more so among mammals), species specific differences still exist (specifically regarding disease onset), where in mice, for example, heterozygous or homozygous CAKUT related mutations often lead to embryonic or postnatal lethality. Moreover, the phenotypical manifestations in knock-out animals for CAKUT related genes often result in interspecies differences, making the translation of patient specific mutations more difficult (Khan et al., 2022).

On the other hand, investigating the intricacies of human kidney development throughout gestation with human specific samples presents significant challenges. These challenges stem from two primary factors: the limited availability of human embryonic kidney samples and the complex ethical considerations surrounding their origin.

In this regard, the advancements of human pluripotent stem cell (hPSCs) based technologies are pushing the boundaries of our understanding of organogenesis and disease progression in complex human organs, such as the kidneys.

Pluripotent stem cells (PSCs)

Recent studies have described the isolation and culture conditions of nephron progenitor cells (NPCs) from the mouse embryonic kidney as a source of studying nephrogenesis *in vitro* (A. C. Brown et al., 2015). The isolation of similar NPCs of human origin, on the other hand, is not affordable and raises important ethical concerns. In this regard, there is a need for alternative human cell sources with renal differentiation potential.

The development of human embryonic stem cells (hESCs) and induced pluripotent stem cells (hiPSCs), collectively termed hPSCs (Takahashi et al., 2007; Takahashi & Yamanaka, 2006; Thomson et al., 1998), has revolutionized how scientists' study human development and disease outside the human body. Their ability to self-renew indefinitely while retaining pluripotency (the potential to differentiate into all three embryonic germ layers) allows researchers to probe the early stages of cell lineage specification and differentiation (Thomson et al., 1998). This has led to the identification of specific cell culture conditions that promote differentiation, now routinely used for developmental research (P. B. Armstrong, 1989).

Initial hPSC differentiation studies focused on early lineage specification and commitment in two-dimensional cultures (Laflamme et al., 2007). However, groundbreaking work by (L. Yang et al., 2008) and (Chambers et al., 2009) utilized embryoid bodies (EBs) as surrogates for studying differentiation and cell specification along all three germ layers in the human embryo. This approach paved the way for the explosion of the organoid field. The seminal work of (Eiraku et al., 2008) established the first self-patterned stratified cortical tissues by plating EBs on coated surfaces in serum-free medium, marking the birth of the modern organoid concept.

Organoids: mimicking organs in vitro

Organoids are three-dimensional (3D) cell cultures that resemble specific organs (Lancaster & Knoblich, 2014). They comprise multiple cell types - characteristic of the native organ, - recapitulating, to some extent, specific

organ functions. *In vivo*, different cell types arise from stem cells through lineage commitment and cell sorting, leading to the spatial organization observed in organs during development. *In vitro*, hPSC-derived cell types can self-organize into organoids that partially mimic that organization and organ function.

State of the art in kidney organoids

Cutting-edge research in the field has pushed the generation of kidney organoids from hPSCs by mimicking the *in vitro* renal inductive signals that occur during kidney organogenesis (Freedman et al., 2015; Garreta et al., 2019; Garreta, Moya-Rull, et al., 2022; Garreta, Prado, et al., 2022; Taguchi & Nishinakamura, 2017; Xia et al., 2014). These studies have identified specific morphogens and cytokines that drive hPSC differentiation towards a renal lineage *ex vivo* (Morizane et al., 2015; Taguchi & Nishinakamura, 2017; Takasato et al., 2014, 2015, 2016; Uchimura et al., 2020; Xia et al., 2014). Procedures have been established to generate organoids resembling separate components of the mammalian kidney (Figure 2), including nephron progenitor (NP), ureteric bud (UB), and even stromal progenitor (SP) organoids (Palakkan et al., 2022; Tanigawa et al., 2022; Vanslambrouck et al., 2022; Zeng et al., 2021).

While current state-of-the-art kidney organoids show remarkable resemblance to first/second trimester human embryonic kidneys (Garreta et al., 2019), they lack the higher order of anatomical organization needed for functional filtration and reabsorption. Researchers are exploring specialized tissue culture techniques, such as bioreactors for nephron development, patterned substrates for collective duct development, and microfluidics for vascularization, to drive organoid maturation and better mimic physiologically relevant cues (Czerniecki et al., 2018; Homan et al., 2019; Przepiorski et al., 2018a; Shi et al., 2023).

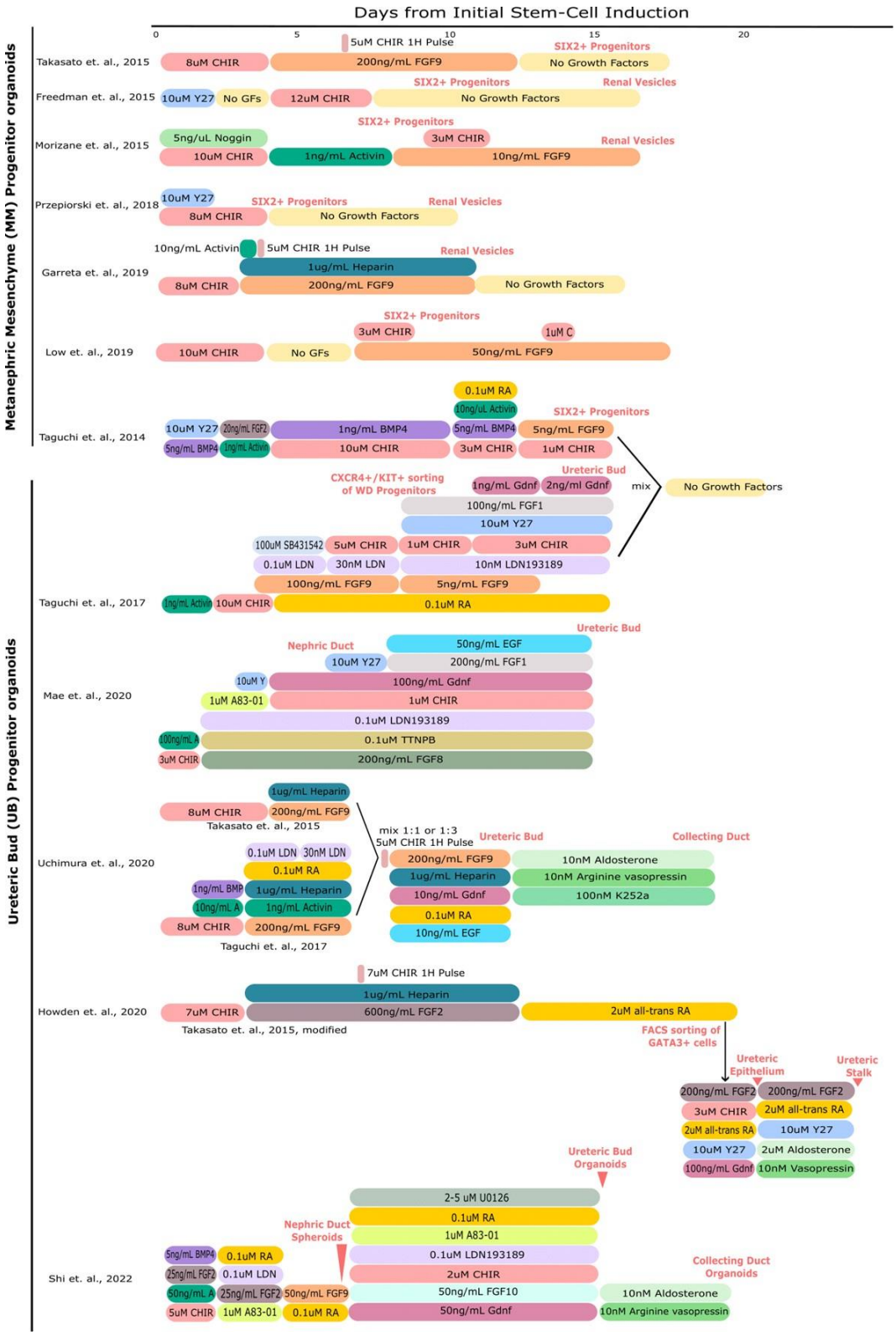
Days from Initial Stem-Cell Induction
0
5
10
15
20
Metanephric Mesenchyme (MM) Progenitor organoids
Takasato et. al., 2015
5uM CHIR 1H Pulse
8uM CHIR
200ng/mL FGF9
SIX2+ Progenitors
No Growth Factors
Freedman et. al., 2015
10uM Y27
No GFs
12uM CHIR
SIX2+ Progenitors
No Growth Factors
Renal Vesicles
Morizane et. al., 2015
5ng/uL Noggin
3uM CHIR
SIX2+ Progenitors
10uM CHIR
1ng/mL Activin
10ng/mL FGF9
Renal Vesicles
Przepiorski et. al., 2018
10uM Y27
8uM CHIR
SIX2+ Progenitors
No Growth Factors
Renal Vesicles
Garreta et. al., 2019
10ng/mL Activin
5uM CHIR 1H Pulse
1ug/mL Heparin
8uM CHIR
200ng/mL FGF9
Renal Vesicles
No Growth Factors
Low et. al., 2019
SIX2+ Progenitors
3uM CHIR
1uM C
10uM CHIR
No GFs
50ng/mL FGF9
Taguchi et. al., 2014
0.1uM RA
10ng/uL Activin
SIX2+ Progenitors
10uM Y27
20ng/mL FGF2
1ng/mL BMP4
5ng/mL BMP4
5ng/mL FGF9
5ng/mL BMP4
1ng/mL Activin
10uM CHIR
3uM CHIR
1uM CHIR
Ureteric Bud
CXCR4+/KIT+ sorting of WD Progenitors
1ng/mL Gdnf
2ng/ml Gdnf
mix
No Growth Factors
100ng/mL FGF1
10uM Y27
100uM SB431542
5uM CHIR
1uM CHIR
3uM CHIR
0.1uM LDN
30nM LDN
10nM LDN193189
100ng/mL FGF9
5ng/mL FGF9
Taguchi et. al., 2017
1ng/mL Activin
10uM CHIR
0.1uM RA
Ureteric Bud (UB) Progenitor organoids
Ureteric Bud
Nephric Duct
50ng/mL EGF
10uM Y27
200ng/mL FGF1
Mae et. al., 2020
10uM Y
100ng/mL Gdnf
1uM A83-01
1uM CHIR
0.1uM LDN193189
100ng/mL A
0.1uM TTNPB
3uM CHIR
200ng/mL FGF8
1ug/mL Heparin
8uM CHIR
200ng/mL FGF9
Takasato et. al., 2015
mix 1:1 or 1:3
5uM CHIR 1H Pulse
Ureteric Bud
Collecting Duct
Uchimura et. al., 2020
0.1uM LDN
30nM LDN
0.1uM RA
1ng/mL BMP
1ug/mL Heparin
10ng/mL A
1ng/mL Activin
8uM CHIR
200ng/mL FGF9
200ng/mL FGF9
10nM Aldosterone
1ug/mL Heparin
10nM Arginine vasopressin
10ng/mL Gdnf
100nM K252a
0.1uM RA
10ng/mL EGF
Taguchi et. al., 2017
7uM CHIR 1H Pulse
1ug/mL Heparin
Howden et. al., 2020
7uM CHIR
600ng/mL FGF2
2uM all-trans RA
Takasato et. al., 2015, modified
FACS sorting of GATA3+ cells
Ureteric Epithelium
Ureteric Stalk
200ng/mL FGF2
200ng/mL FGF2
3uM CHIR
2uM all-trans RA
2uM all-trans RA
10uM Y27
10uM Y27
2uM Aldosterone
100ng/mL Gdnf
10nM Vasopressin
Ureteric Bud Organoids
2-5 uM U0126
Nephric Duct Spheroids
0.1uM RA
1uM A83-01
5ng/mL BMP4
0.1uM RA
0.1uM LDN193189
25ng/mL FGF2
0.1uM LDN
2uM CHIR
Collecting Duct Organoids
50ng/mL A
25ng/mL FGF2
50ng/mL FGF9
50ng/mL FGF10
10nM Aldosterone
Shi et. al., 2022
5uM CHIR
1uM A83-01
0.1uM RA
50ng/mL Gdnf
10nM Arginine vasopressin

Figure 2. Comparison of protocols for hPSC-derived kidney organoid differentiation. A schematic detailing the compounds used for driving PSCs towards Metanephric Mesenchyme (MM) or Ureteric Bud (UB) progenitor states. The cell types induced by each step of differentiation are denoted above in pink. More specific details regarding the protocols can be found in the corresponding publications. Taken with permission from: (Nauryzgaliyeva et al., 2023)

hPSC-derived organoids for modelling CAKUT

A significant strength of hPSC-based organoid systems lies in their amenability to genetic manipulation. This enables researchers to create *in vitro* models of genetic kidney diseases by introducing targeted alterations in the corresponding genes. Patient-derived or gene-edited hPSCs have become valuable tools for investigating adult kidney disorders such as chronic kidney disease (CKD) and polycystic kidney diseases (PKD) (Karp et al., 2022; M. Liu et al., 2022). While studies employing hPSC-derived organoids recapitulating the PKD genetic background have proven instrumental in modelling cyst formation (Freedman et al., 2015) and drug response (Cruz et al., 2017; Tran et al., 2022), the relative immaturity of these *in vitro* models hinders their application to diseases manifesting adult-onset anomalies. In contrast, CAKUT, encompassing a spectrum of congenital anomalies affecting the embryonic kidney and urinary tract, presents itself as a highly suitable target for investigation using hPSC-derived kidney organoids.

Kaku et al., have successfully generated *PAX2* null kidney organoids from hPSCs and demonstrated that *PAX2* may not be necessary for human NP formation *in vitro*. Their hPSC-derived *PAX2*-null cells could still become NPs and even form epithelial structures resembling tubules and glomeruli. However, *PAX2* appears to be crucial for proper differentiation of parietal epithelial cells within the glomeruli (Kaku et al., 2017).

Przepiorski et al., utilized human induced pluripotent stem cell (iPSC)-derived kidney organoids to model *HNF1B*-related CAKUT. By generating biallelic deletions in the *HNF1B* gene, they observed organoids lacking regions positive for proximal and distal tubule markers, mirroring phenotypes seen in *Hnf1b*-deficient mice (Przepiorski et al., 2018b).

Zeng et al., successfully employed human PSC-derived UB organoids to model congenital anomalies arising from *RET* mutations. Their *RET*-null organoids failed to undergo branching and exhibited a phenotype resembling renal agenesis, demonstrating the feasibility of modelling such diseases using *in vitro* genetic editing and 3D culture (Zeng et al., 2021).

These studies highlight the potential of hPSC-derived kidney organoids for investigating CAKUT pathogenesis. Further research focusing on other CAKUT-associated genes and utilizing advanced techniques like single-cell RNA sequencing will provide a deeper understanding of the complex interplay between genetic factors and early kidney development. Although it should be noted that given the architectural and structural complexity of any organ, re-associating single-cell RNA-seq data back to its functional anatomy is not a straightforward task. In this regard, recent studies employing microdissection and cell dissociation strategies for scRNA-seq analysis have managed to conserve certain structural features of the organization of the kidney, by combining anatomy guided RNA sequencing, cell lineage tracing and *in situ* expression (Ransick et al., 2019). Such studies allow an in-depth view into cell diversity in the developing kidney, along with differences in sex and between species, all in relation to the location and function within the organ.

The role of mechanobiology in embryonic development

The field of developmental biology has traditionally focused on elucidating the roles of morphogens and the intricate molecular pathways governing embryogenesis and tissue formation. However, a growing body of evidence suggests that these processes are not solely driven by biochemical and genetic cues. Mechanical forces, both intrinsic and extrinsic, also play a significant role in morphogenesis [reviewed in detail in (Goodwin & Nelson, 2021; Heisenberg & Bellaïche, 2013)].

At the subcellular level, cells experience various biomechanical forces such as actomyosin contractility, membrane tension during cell division or upon exposure to stiff microenvironments (Colombo et al., 2003; Daley et al., 2011; Krieg et al., 2008). Extracellularly, cells encounter forces such as compression and extrusion during apoptosis and tissue remodelling (Eisenhoffer et al., 2012; Y. Yang et al., 2000). These forces can also manifest at the tissue level, exemplified by muscle fibre contractions (Harrington, 1979), and even at the organismal level, as evident from the influence of gravity.

This recognition has led to a paradigm shift in developmental biology, with a growing focus on how mechanical forces impact tissue development and morphogenesis. Pioneering work in the 1980s and 1990s laid the groundwork for this shift, proposing that tissue morphogenesis is a fundamentally biomechanical process (Beloussov et al., 1994; Wolpert, 1981). These early studies highlighted the interplay between biochemical and mechanical cues. The physical properties of a local region can influence the distribution of morphogen gradients, and conversely, cell movements can alter how tissues respond to these molecular gradients.

In essence, the field is moving towards a more comprehensive understanding of how both biochemical and biomechanical forces orchestrate the complex processes of development.

Analogous to how biochemical signalling molecules initiate intracellular cascades leading to gene expression changes, mechanical stimuli can trigger similar signalling pathways within cells. This process is divided into two fundamental steps – mechanosensing and mechanotransduction. Cells

possess specialized membrane structures called cell adhesion complexes, which bind to components of the surrounding extracellular matrix (ECM), forming connections like cell-to-ECM and cell-to-cell junctions. These junctions function as mechanosensors, transmitting forces exerted by the microenvironment towards the nucleus (Elosegui-Artola et al., 2016, 2017b). The received mechanical signals initiate a signalling cascade known as mechanotransduction. This cascade translates the physical cues into biochemical responses that influence various cellular processes, including migration, differentiation, proliferation, and cell death [reviewed in detail in (Kechagia et al., 2019)].

The ECM, a complex network of proteins and polysaccharides surrounding cells, plays a critical role in mechanotransduction during embryo development and organogenesis. Its composition, stiffness, and viscoelasticity (combining elastic and viscous properties) all significantly influence stem cell fate and differentiation [reviewed in detail in (Elosegui-Artola, 2021; Guilak et al., 2009)]. Indeed, the *in utero* embryonic microenvironment is rich in ECM proteins like fibronectin, collagen, and laminin, and exhibits a highly viscoelastic nature (stiffness ranging from 0.1 to 100 kPa) (Chaudhuri et al., 2020; Guilak et al., 2009; Rozario & DeSimone, 2010). Studies have demonstrated that these specific properties significantly impact the differentiation pathways of stem cells within developing tissues.

The impact of the ECM on cell behaviour extends far beyond just providing structural support. A prime example is the influence of ECM elasticity on lineage specification of mesenchymal stem cells (MSCs). Studies have demonstrated that soft matrices favour differentiation of these multipotent cells into adipocytes (fat cells) while stiffer environments promote osteogenesis (bone formation) from the same initial population (Engler et al., 2006; Guilak et al., 2009; Huebsch et al., 2010). Similarly, vascular progenitors cultured on soft matrices differentiate into endothelial cells, while stiffer environments guide them towards a smooth muscle cell fate (Wong et al., 2019).

The composition and physical properties of the ECM are also crucial for tissue homeostasis. For instance, mammary gland tissue requires a soft, laminin-rich microenvironment to maintain its normal function (Alcaraz et al., 2008).

Conversely, alterations in ECM stiffness and composition, often associated with increased stiffness and changes in protein density, are linked to tumour growth and metastasis (Bauer et al., 2020; Wullkopf et al., 2018). A compelling study linked the stiffened adipose tissue microenvironment in obese mice, characterized by an enrichment of myofibroblasts, to an increased malignant potential of breast cancer cells, highlighting the role of ECM mechanics in tumorigenesis (Ling et al., 2020; Seo et al., 2015). Recent research suggests that beyond just stiffness, the viscoelasticity (combining elastic and viscous properties) of the ECM plays a significant role in regulating cell fate decisions (Chaudhuri et al., 2020; Elosegui-Artola et al., 2022). This property influences not only individual cell behaviour but also collective behaviours like spheroid/organoid growth and differentiation (Elosegui-Artola et al., 2022).

Fluid flow within the embryonic environment has also been shown to impact cell behaviour [reviewed in (Freund et al., 2012)]. Studies have demonstrated its role in establishing left-right asymmetry during organ development, regulating vascularization, and sprouting, and maintaining normal kidney function (Nauli et al., 2003; Song & Munn, 2011; Tanaka et al., 2005).

Exploring the role of mechanical cues in kidney development

As discussed above, microenvironmental cues from the surrounding microenvironment encompassing both biophysical (ECM stiffness, fluid flow) and biochemical factors ultimately influencing stem cell behaviour and organization (Vining & Mooney, 2017). As in any other organ, the intricate architecture of the kidney is built upon a complex network of extracellular matrix (ECM) components, that are not simply passive scaffolding, but rather actively contribute to kidney development and function, through mechanical support and mediating signalling (Bülow & Boor, 2019). During kidney development, the cell arrangement plays a crucial role in tubule formation and overall organ function. This organization is initiated by cells attaching to their surrounds through adhesion proteins. Some recent studies have demonstrated the effect of matrix stiffness on tubule formation, giving rise to the possibility of using material stiffness for guiding cell organization (Hamon et al., 2023).

Homan et al. demonstrated that applying fluid flow to kidney organoids enhanced vascularization and promoted the maturation of podocytes, specialized kidney cells (Homan et al., 2019). Additionally, studies by Garreta et al. and Ruiter et al. employed soft synthetic hydrogels to mimic the *in-utero* environment. These soft matrices facilitated the maturation of kidney organoids *in vitro,* highlighting the importance of mechanical stiffness in kidney development (Garreta et al., 2019; Ruiter et al., 2022).

The mechanisms governing the intricate branching of the ureteric bud and the subsequent organization of collecting tubules within the developing kidney have emerged as a topic of intense research interest. While compelling evidence demonstrates that morphogenetic signalling pathways play a key role in driving UB branching into the metanephric mesenchyme, the precise mechanisms by which biomechanical defects translate into CAKUT phenotypes remain elusive. To address this knowledge gap, recent studies have begun to investigate the role of tissue forces and the dynamic processes involved in tubule organization within the geometrically constrained environment of the developing kidney bud tips (Prahl, Viola, et al., 2023; Viola et al., 2022). Indeed, these studies offer a compelling model that elucidates the packing of collecting duct tubules during murine kidney development, encompassing both healthy scenarios and those involving UB defects. While the critical influence of morphogenetic signalling pathways on healthy kidney development is well-established, this work sheds new light on the crucial role of tissue forces and their dynamic interplay in the proper organization of these complex organs(Prahl, Viola, et al., 2023).

Recent work from Mederacke *et. al.*, have demonstrated the effect of geometrical confinement on morphogen up-concentration, necessary for the development of renal vesicles from the MM (Mederacke et al., 2023). Through computational modelling and mouse embryonic kidney explant experiments, they address the question of precise RV positionality under the branching UB and how certain geometrical confinements and angles contribute to an increase in morphogen gradients promoting regional differentiation.

Mechanical forces also play a crucial role in adult kidney function. Choudhury et al. explored the role of these forces in fluid transport across kidney tubule cells. Their findings revealed differences in fluid movement and pressure

gradients between healthy and diseased (autosomal dominant polycystic kidney disease, ADPKD) cells, suggesting the importance of mechanical cues in both normal kidney function and disease states (Choudhury et al., 2022). Cruz et al. investigated the microenvironment's influence on cyst formation in ADPKD, a condition characterized by fluid-filled cysts in kidney tubules. Their study revealed that the microenvironment within tubule organoids can significantly influence cyst formation, suggesting a potential role for mechanical factors in ADPKD progression (Cruz et al., 2017).

All these recent findings highlight the need for a more comprehensive research model that integrates both signalling pathways and biomechanical forces for a complete picture of kidney development and potential CAKUT pathogenesis. They emphasize the crucial role of mechanical input from the environment and the cell's ability to mechano-sense and translate these signals into cellular responses, ultimately influencing healthy tissue development and disease progression. Nowadays, current research continues to unravel the mechanisms by which cells perceive and interpret mechanical cues to trigger genetic responses (De Belly et al., 2022; Discher et al., 2005; Heisenberg & Bellaïche, 2013).

Approaches to studying the mechanobiology of kidney morphogenesis

While the influence of mechanical stimuli on cell fate decisions within simplified 2D *in vitro* environments is well-documented [see reviewed in (Mammoto et al., 2012; Wagh et al., 2021)] (substrate stiffness, physical confinement, and fluid flow), these findings may not directly translate to the complexities of living tissues. *In vivo*, tissues are subjected to viscoelasticity, fluid flow, stresses and pressures, properties that can significantly influence cellular behaviour (Cheng et al., 2008; Geerligs et al., 2008; Safshekan et al., 2017). This intricate environment comprises a multitude of cellular and extracellular components, including the cytoskeleton, ECM proteins, membrane adhesion complexes, and the cellular cortex. These elements collectively orchestrate a biomechanical signalling pathway that dictates variable cellular responses across space and time. Furthermore, the practical challenges of accessing and manipulating developing organs and tissues *in vivo* significantly complicate the study of their mechanical properties. While some studies utilize embryonic kidney explants, the samples are almost always of mouse origin and span a limited developmental timeframe. Consequently, measuring and probing the mechanical environment of living human tissues remains a complex endeavour.

However, the emergence of organoid technologies offers a promising solution. These 3D self-organizing structures can more closely mimic the complexities of human embryonic organ development in a culture dish. This advancement allows the investigation of the dynamic mechanical changes occurring during early stages of organogenesis. By strategically combining organoid technology with cutting-edge mechanobiology techniques, it becomes possible to explore the mechanical properties of cells and tissues within a more controlled and physiologically relevant environment. This powerful approach holds immense potential to elucidate the critical role of mechanical forces in human organ development and disease pathogenesis. The knowledge gained from such studies can pave the way for the development of novel therapeutic strategies for a wide range of diseases.

The following section will discuss in more detail several research methodologies instrumental to studying the mechanobiology of human organoid development:

1) bioengineering the microenvironment (exposure to synthetic and natural hydrogels, micropatterning, microfluidics etc.), 2) application and measurement of physical forces (micro-rheology, traction measurements, optical tweezers, laser ablation etc.), and 3) genetic manipulation of key genes in mechanosensing and mechanotransduction pathways (*YAP/TAZ – HIPPO* pathway, *WNT* signalling pathway, *SRF* pathway).

Bioengineering the microenvironment

Mimicking the complex extraembryonic environment that surrounds and influences developing organs is crucial for studying organogenesis *in vitro*. Hydrogels, with their tuneable properties, offer a powerful tool for bioengineering this niche. By encapsulating organoids within hydrogels with varying stiffness, composition, and viscoelasticity, it is possible to re-create environments that closely resemble the native tissues.

The discovery of Matrigel, a natural basement membrane extract derived from mouse tumours (Orkin et al., 1977), revolutionized *in vitro* research, leading to a surge in studies (Kibbey et al., 1992; Kubota et al., 1988). This ubiquitous ECM surrogate has proven highly valuable in assays examining cell invasion, angiogenesis, spheroid formation, and organoid growth (Barker et al., 2010; Huch et al., 2013; Stange et al., 2013; W. Wang et al., 2017). However, the limitations of Matrigel in translational research, particularly for organ disease modelling and drug screening, are becoming increasingly apparent. Firstly, the poorly defined composition and inherent cancerous origin of Matrigel raise concerns about its suitability for these applications. Secondly, significant batch-to-batch variability in Matrigel production can dramatically impact the degree of organoid differentiation, hindering the reproducibility and comparability of studies.

To address these limitations, the organoid research field has begun exploring the development of well-defined, synthetic materials for generating organoid models suitable for disease modelling and interrogation. This advancement has led to the creation of substrates with tuneable properties, including stiffness, elasticity, and protein composition.

The next mini section will delve deeper into the use of both natural and synthetic substrates for organoid generation and disease modelling applications, exploring options such as decellularized ECM, natural ECM proteins, and various synthetic hydrogels.

Natural hydrogels

Decellularized Extracellular Matrix (dECM) retains the intricate architectural composition of native tissues, making it ideal for promoting the long-term maturation of human pluripotent stem cell (hPSC)-derived organoids *in vitro* [reviewed in (Garreta et al., 2017)]. Depending on the de-cellularization method used, dECM-derived scaffolds can preserve both the mechanical and biological properties of the original tissue. This allows for cell attachment, migration, and differentiation of newly introduced cells within the empty scaffold. This approach has been successfully applied to various cell types derived from liver, intestine, pancreas, and kidney (Batchelder et al., 2015; Guyette et al., 2014; Hong et al., 2018; Orlando et al., 2013). However, utilizing dECM scaffolds presents several challenges. These include variations in decellularization protocols depending on the tissue source; difficulty in precisely repopulating the dECM with the diverse cell types present in the native tissue; the need for oxygen perfusion in thicker tissue formations; and limited availability of human material, often relying on organ donation.

Naturally occurring ECM proteins like collagen and laminin can also be used to generate scaffolds for tissue engineering [reviewed in (Glowacki & Mizuno, 2008)]. Collagen scaffolds, typically composed of types I, II, and III collagen, offer a specific biomechanical architecture that can support cancer cell migration, metastasis, and the maintenance of certain organoids (Dong & Lv, 2016; W. Han et al., 2016; Jee et al., 2019; Kopanska et al., 2016; P. C. Wang, 2005). However, collagen-based matrices often require additional support from co-cultured cells and other ECM proteins for full tissue development (Y. Wang et al., 2016).

Another option is using natural polysaccharides like alginate, a cost-effective, biocompatible, and tuneable substrate well-suited for

biological applications [reviewed in (Cattelan et al., 2020; Chen et al., 2020)]. Studies have demonstrated the use of various alginate modifications to study the growth and development of brain, kidney, lung, intestine, and pancreas organoids (Capeling et al., 2019; Cassel De Camps et al., 2022; Geuens et al., 2021; H. Liu et al., 2020; Wilkinson et al., 2018). However, like Matrigel, alginate is a biologically derived material, leading to potential batch-to-batch variability (Fu et al., 2010).

Synthetic hydrogels

Synthetic polymers offer a compelling alternative to natural substrates, enabling precise control over the mechanical, chemical, and structural properties of the culture environment. By meticulously manipulating the composition of these synthetic substrates, it is possible to effectively mimic the viscoelasticity, porosity, and density of specific tissues. This allows for the investigation of how mechanical and chemical cues influence cell fate decisions.

One such material is polyethylene glycol (PEG), a non-toxic and biocompatible polymer increasingly used in cell culture and for the controlled release of biomolecules within *in vitro* tissues (Drury & Mooney, 2003; Mellott et al., 2001) [see detailed review in (C. C. Lin & Anseth, 2009)]. PEG's unique advantage lies in its high tunability. A variety of cross-linkers and functional groups can be incorporated, essentially creating a customizable "blank slate" for bioengineering purposes. PEG hydrogels can encapsulate entire cell clusters or organoids and have been shown to support a diverse range of cell types in culture (Chaudhuri et al., 2016; Gjorevski et al., 2016; Lutolf et al., 2003; Moon et al., 2010; Ng et al., 2017; Phelps et al., 2012).

Polyacrylamide (PAA) hydrogels offer another powerful tool. Their stiffness can be precisely controlled across a wide range (0.2 kPa to 200 kPa) by adjusting the ratio of acrylamide to bis-acrylamide within the formulation. In a landmark study (Pelham & Wang, 1997), PAA hydrogels were used to demonstrate for the first time that substrate stiffness can significantly impact cell adhesion, spreading, and migration. This finding

paved the way for the widespread adoption of PAA and other synthetic materials to investigate the role of stiffness as a mechanical cue in directing cell fate decisions (Engler et al., 2006; Wen et al., 2014).

Polydimethylsiloxane (PDMS), initially developed for microfluidic applications (Duffy et al., 1998), has emerged as a promising material for cell culture in mechanobiology and bioengineering research (X. Q. Brown et al., 2005; Chuah et al., 2015). Its tuneable stiffness, transparency, minimal autofluorescence, and ease of use make it well-suited for studying cell-biomaterial interactions and the effects of substrate stiffness on cell fate (Mata et al., 2005). Notably, advancements in surface chemistry activation techniques have enabled cell attachment to the originally hydrophobic PDMS surface.

The utilization of these versatile biocompatible materials, both natural and synthetic, allows for a far more accurate representation of the *in vivo* tissue microenvironment within *in vitro* culture conditions.

The impact of these engineered microenvironments on organoid development can be assessed through a combination of qualitative and functional assays. Qualitative evaluation focuses on the rate of organoid maturation, as evidenced by the expression of specific markers using techniques like immunofluorescence microscopy, histology, and gene expression analysis. Additionally, the attainment of organ-specific functionalities can be assessed, providing a more comprehensive understanding of how the engineered niche influences organoid development and function.

Emerging evidence suggests that organoids exhibit a dynamic mechanical response throughout their development, requiring distinct mechanical cues from the surrounding extracellular matrix (ECM) at different stages. For instance, studies have shown that intestinal stem cell expansion thrives in a stiff, fibronectin-rich ECM, while their differentiation and subsequent formation of intestinal organoids necessitate a softer laminin-decorated matrix (Broguiere et al., 2018; Gjorevski et al., 2016). This highlights the stage-specific influence of ECM stiffness and composition.

Similarly, recent research demonstrates the benefits of encapsulating kidney organoids derived from hPSCs within synthetic PEG-based hydrogels during later differentiation stages. This approach has been shown to reduce unwanted fibrosis and promote a further degree of maturation in these organoids (Geuens et al., 2021; Ruiter et al., 2022). This dynamic mechano-responsiveness extends beyond the kidney, with similar observations reported in brain organoids (Cassel De Camps et al., 2022).

While encapsulating organoids within elastic hydrogels offers a strategy to provide mechanically stimulating environments that mimic native tissues, a significant drawback is their potential to restrict the physical expansion and morphogenesis of the developing organoid (Ranga et al., 2016; H. Wang & Heilshorn, 2015). To circumvent this limitation, researchers have explored engineered PEG-based hydrogels with dynamic bond properties. These hydrogels can rearrange their constituent bonds, allowing the surrounding synthetic extracellular matrix (ECM) to adapt to the expanding organoid and accommodate its morphogenesis (Chrisnandy et al., 2022). This dynamic characteristic presents a significant advantage, enabling the engineered matrix to more closely resemble the evolving mechanical environment experienced by a developing organoid over time. Consequently, these PEG-based hydrogels provide a more reliable culture system for studying the interplay between mechanics and organ formation.

Using geometry and microfluidics to guide organoid morphogenesis

While substrate stiffness is a well-established factor influencing *in vitro* tissue morphogenesis, recent studies highlight the additional influence of geometric cues on tissue organization and differentiation. Pioneering work by Warmflash et al. demonstrated that simple geometric confinement can induce self-organization in hPSCs (Warmflash et al., 2014). Further research has explored how these geometries establish focal points of cell adhesion tension, known to guide mesoderm specification in hESCs (Muncie et al., 2020).

The impact of geometry extends beyond early developmental stages, influencing morphogenesis past gastrulation in *in vitro* organoids. Curved geometries have

been shown to enhance brain region specification in human cerebral organoids, while controlled circular patterns promote cardiac beating in human cardiac organoids (Ma et al., 2015; Sen et al., 2021).

Micropatterning techniques in 2D offer even greater control over tissue morphogenesis. Karzbrun et al. elegantly demonstrated how precise control over pattern size, shape, and 2D hPSC monolayer density can guide the process of neural tube folding and lumenogenesis (Karzbrun et al., 2021). Similarly, Gjorevski et al. engineered geometrically defined microwells to enable controlled generation of intestinal crypts and villi from stem cells (Gjorevski et al., 2022). These innovative approaches pave the way for a deeper understanding of human synthetic morphogenesis *in vitro*.

Certain organs, like the brain and gut, undergo extensive tissue folding during organogenesis. These processes are particularly captivating: epithelial monolayers transform over time through buckling and folding, giving rise to complex structures like the brain's gyri and the villi of the intestine [reviewed in (Nelson, 2016)]. With the advent of organoid technology, researchers are now effectively exploring the mechanical and physical stimuli guiding these events, such as brain folding (Karzbrun et al., 2018). Similarly, microfluidic organ-on-a-chip models offer a powerful approach to study the physical forces associated with morphogenesis. By engineering microfluidic models that mimic specific organs, it is possible to measure bending angles, bulging, deformations, and flow rates during development [reviewed in (Polacheck et al., 2013)].

Measurement and application of mechanical forces

The influence of mechanical stimuli like stiffness, viscoelasticity, and fluid flow on cell fate decisions has been extensively documented (Vining & Mooney, 2017). This understanding has fuelled the development of mechanobiology techniques to investigate the forces experienced and exerted by cells. Currently, a diverse toolbox exists for these measurements, described in detail below and in Table 1 [reviewed in (Campàs, 2016; Polacheck & Chen, 2016; Roca-Cusachs et al., 2017)].

Many techniques in mechanobiology are based on direct measurements of degrees of deformation of a elastic material of know mechanical properties. Examples include traction force microscopy (TFM), micropillars, microdroplets/micro-inserts, and cantilevers/atomic force microscopy (AFM) (Dembo & Wang, 1999; Harris et al., 2012; Rajagopalan & Saif, 2011; Tan et al., 2002; Zimmermann et al., 2000). These methods are applicable *in vitro* (most commonly), *ex vivo* (AFM), and even *in vivo* (AFM, microdroplets) (Feroze et al., 2015; Mongera et al., 2023; Moore et al., 1995).

Technique	Principle of Action	Citations
Traction Force Microscopy (2D & 3D TFM) 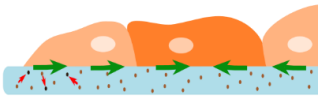	• Uses compliant elastic substrate and fluorescent microbeads. • Cells seeded on top (2D) or embedded within (3D) a hydrogel. • Cells exert forces that generate a deformation in the hydrogel. Gel deformation allows the generation of a displacement map. • Computational methods can be used to obtain traction forces exerted by the cells.	(Bergert et al., 2016; Butler et al., 2002; Dembo & Wang, 1999; S. J. Han et al., 2015; Trepat et al., 2009)
Cantilevers (AFM) 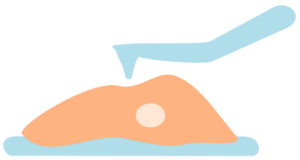	• Allows the application and quantitative measurement of mechanical force on a cell/tissue. • Based on the use of a calibrated cantilever with known mechanical properties that can deflect when in contact with a surface (for example cells). • The displacement/bending of the cantilever can be used to calculate the forces exerted by the cell as well as determine the stiffness/rheology of the tissue.	(Badique et al., 2013; Krieg et al., 2008; Schillers et al., 2017; Taubenberger et al., 2014)
Micropillars 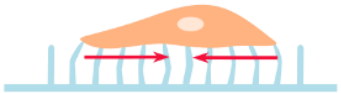	• An array of cylindrical columns made of a deformable elastic substrate with cells on top. • Depending on the stiffness of the pillars, cells can exert forces that are able to deform these pillars. • Mapping the deformations of the pillars and comparing to their undeformed state, allows to calculate the forces exerted by the cells.	(Rajagopalan & Saif, 2011; Tan et al., 2002)
Droplets & Inserts 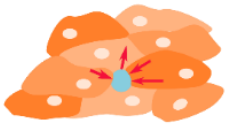	• Microdroplets of deformable compliant elastic materials. • Can be used to evaluate the mechanical properties of a tissue *in vivo*.	(Mongera et al., 2023; Träber et al., 2019)

	• Can be injected into a tissue of interest, imaged, and compared to their undeformed state, to gain a map of local tissue stresses.	
Fluorescence Resonance Energy Transfer (FRET) 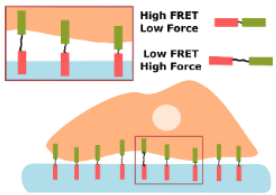 sensors	• Used to study cellular forces like tension between cell, and their surround ECM. • Contain two fluorescent proteins (energy acceptor and donor), linked by a tension sensitive linker (spring). • When a force is applied to the linker, the distance between the fluorophores changes, resulting in a change in energy transfer. This change can be recorded by fluorescence lifetime imaging microscopy (FLIM) and translated to tension measurements.	(Grashoff et al., 2010)
Micropipette aspiration 	• Involves a glass micropipette of 0.5-10um diameter to apply a controlled suction force to a single cell. • The suction force generates an indentation in the cellular membrane. • The deformation of the membrane can be measured through microscopy and can help determine other mechanical properties of the cell: elasticity, viscosity, and tension along the membrane.	(Irianto et al., 2016; Maître et al., 2015; von Dassow et al., 2010)
Laser ablation (LA) 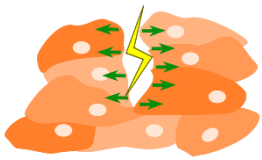	• Uses a focused laser beam to dissect/disrupt a local tissue or cellular structures. • Can be specifically targeted at mechanical components of the cell: focal adhesions, cytoskeletal components, intercellular junctions etc. • The movement /deformation of tissues can be used to infer whether the tissue before was in a tense or compressed state, and to further calculate the extent of these forces.	(Kiehart et al., 2000; Samarage et al., 2015)
Optical Tweezers (OT) 	• Uses focused laser beam to trap a microbead that can be used to apply force to another subject, such as a cell. • Position of the laser beam can be manipulated to control the forces being exerted by the trapped object. • Resulting deformations on the cell membrane can be measured: cell indentation, cell stretching, and active rheology.	(Zhang & Liu, 2008)

Table 1. Techniques to measure cellular and tissue level forces. Taken with permission from:(Nauryzgaliyeva et al., 2023)

Another approach uses techniques such as FRET tension-based sensors to measure the tensile forces between cells and their surrounding environment (Grashoff et al., 2010). These sensors can even detect forces at the nuclear level (Andreu et al., 2022).

Techniques like micropipette aspiration and laser ablation have been used to assess the mechanical properties of whole embryos (xenopus, zebrafish) during early development (Chaigne et al., 2013; Maître et al., 2015; von Dassow et al., 2010). These methods have allowed the investigation of tissue viscoelasticity, tension, and contractile forces maintaining the embryonic structure (Rauzi et al., 2008; Samarage et al., 2015). While the mechanical properties of early embryos have been extensively studied in animals, ethical considerations and limited availability of human embryonic material make it challenging to investigate these properties in humans. Culturing human embryos beyond day 14 of development is prohibited, hindering *in vivo* studies of mechanical forces within developing human organs.

Traction force microscopy (TFM)

Traction force microscopy (TFM) using fluorescent microbeads embedded within a hydrogel with defined elastic properties offers a powerful approach to quantitatively assess the mechanical forces exerted by developing organoids (Bergert et al., 2016). This 3D TFM technique, when applied to encapsulated organoids, provides valuable insights into the directionality of tissue growth, the stress and tension required to maintain their morphology, and the internal pressures guiding their growth patterns (Ban et al., 2018; Broguiere et al., 2018; Mulligan et al., 2019; Steinwachs et al., 2016). Interestingly, studies on epithelial tissue morphogenesis suggest that 3D dimensionality may not always be essential for guiding tissue growth and differentiation (Pérez-González et al., 2021). In 2D organoid systems, a simpler environment facilitates more reliable cellular force measurements using 2.5D TFM, without compromising the morphogenetic process [reviewed in (Matejčić & Trepat, 2023)].

Alternatively, deformations on hydrogel-based microdroplets implanted within organoids can be used to investigate the internal forces exerted by developing cells. By analysing these deformations, it becomes possible to identify the local forces generated by specific cell structures (Girardo et al., 2018). While primarily employed for studying forces within developing embryos (Mongera et al., 2023; Träber et al., 2019), this technique can be readily adapted to investigate local forces within organoids during organogenesis. Furthermore, functionalization of microbeads with cell-specific antibodies could enable targeted placement within organoids, facilitating force measurements at specific structures.

It is important to acknowledge the limitations of these methods despite their ability to provide a general overview of the forces acting on and within tissues. Both 2D and 3D TFM often assume a linear elastic model for the surrounding matrix, neglecting inelastic effects. This assumption can lead to inaccuracies, particularly when calculating forces within large 3D tissue structures like organoids, especially over extended timeframes involving significant ECM remodelling by surrounding cells.

While the development of more precise force measurement techniques remains a priority, current methods based on displacement measurements can still offer valuable insights into the mechanics of tissue systems (Clark et al., 2022). In the case of inelastic materials, where relaxation/trypsinization-based force calculations are impractical, alternative approaches like monitoring tissue and cell dynamics can still provide reliable data (Godeau et al., 2022; Yamaguchi et al., 2022). The field of organoid mechanobiology remains young, with many unexplored avenues for research. One promising area could involve the quantification of load history, offering a deeper understanding of how mechanical cues influence organoid development.

Bottom-up approach to investigate organoid morphogenesis and mechanics

While the introduction so far has focused on a top-down approach to studying organoid mechanics (manipulating the environment to elicit cellular responses), a complementary approach, the bottom-up approach, offers valuable insights as well. This method involves modulating key players within the

mechanotransduction signalling pathway to understand how the activation of mechanosensitive proteins and gene transcription influences tissue morphogenesis (Mammoto et al., 2012).

The first responders to external mechanical stimuli are mechanosensitive membrane proteins, such as the Piezo family of ion channels [reviewed in (Ranade et al., 2015)]. Piezo1, a well-studied example, functions as a mechanotransducer and has been implicated in vascular, neural, and bone development (Li et al., 2019; Pathak et al., 2014; Ranade et al., 2014). In the urinary system, Piezo proteins play a crucial role in sensing shear stress and wall tension for proper filtration (Li et al., 2022). While the exact role of these proteins in kidney development and disease remains to be explored (Dalghi et al., 2019), their importance in the urinary tract is undeniable. The high sensitivity of these membrane proteins makes them attractive candidates for tissue engineering. By regulating them (e.g., through light-activated genetic manipulation), it might be possible to control cellular responses even in the absence of mechanical stimuli.

Further downstream in the mechanotransduction pathway lie mechanosensitive transcription factors like *YAP/TAZ*, which initiate gene activation in the nucleus to orchestrate the cellular response to mechanical cues (Mosqueira et al., 2014; Piccolo et al., 2014). These factors are modulated by both biochemical (Hippo signalling) and mechanical (ECM stiffness, shear stress, stretching) signals, which determine their subcellular localization (cytoplasm or nucleus) and subsequent activity (Aragona et al., 2013; Elosegui-Artola et al., 2016).

In the context of the kidney, *TAZ* activity has been linked to cystogenesis in polycystic kidney disease (PKD), highlighting the potential impact of mechanotransduction during disease progression (Lee et al., 2020). Interestingly, depletion of YAP in stem cells leads to a loss of pluripotency, while its expression promotes stemness (Lian et al., 2010). Studies have demonstrated that mechanical stimuli, such as substrate stiffness, can control stem cell fate by regulating *YAP* localization through the stretching of nucleopores (Andreu et al., 2021, 2022; Elosegui-Artola et al., 2017a; Mosqueira et al., 2014; Musah et al., 2014; Totaro et al., 2017). These findings suggest that

directly regulating *YAP/TAZ* localization could effectively direct mechanotransduction and ultimately cell fate, even without external mechanical forces.

Understanding the mechanotransduction machinery offers a powerful bottom-up approach to controlling morphogenetic events during development. Human PSCs-derived organoids provide a valuable framework to investigate the mechanical aspects of organ development where bioengineering advancements can further facilitate these studies in a controlled and reproducible manner.

Objectives

The general aim:

This thesis aimed to map RV emergence and nephron differentiation in human kidney development. Towards this goal, we first developed a series of differentiation procedures (kidney organoids in 3D and 2D) based on the use genetically engineered hPSCs in combination with micropatterning techniques, confocal and traction force microscopy analysis. This multifaceted approach allowed us to start mechanistically coupling how RV emergence and nephron differentiation is driven by changes in the expression of specific renal markers and cell force generation.

The specific objectives of the thesis were:

1. To characterize RV emergence and nephron differentiation in hPSCs through the development of different cell culture set ups (including 3D and 2D) and the definition of several quantitative read outs, including:
    a. The characterization of RV emergence and nephron like structure differentiation in 3D hPSC-derived kidney organoids.
    b. The definition of cell culture conditions sustaining for the emergence of RV and the differentiation of nephron-like structures on compliant substrates in 2D.
    c. The definition of experimental conditions to externally control RV emergence and nephron differentiation through the definition of geometrical and mechanical constraints.
    d. The measurement of traction forces during RV emergence and nephron differentiation under the experimental set up achieved in b-c.

2. To mechanistically couple how changes in renal markers expression results in disturbances on RV emergence and nephron differentiation through the development of different cell culture set ups (including 3D and 2D) and the definition of several quantitative read outs, including:

a. The application of cell culture conditions developed in Objective 1 for the differentiation of PAX2 KO and LHX1 KO hPSCs into RV and nephron-like structures.
b. To quantitatively assess how geometrical constraints and rigidity impact on RV emergence and differentiation into nephron-like structures in PAX2 and LHX1 KO hPSCs through the determination of changes in renal markers expression by confocal microscopy analysis and mapping cell force generation.

Materials and Methods

Culture and maintenance of hPSCs

Origin of hPSC lines

The work in this thesis was performed using the ES[4] human embryonic stem cell line (hESC) and the human induced pluripotent stem cell line CBiPS1sv-4F-40 (CBiPSC) (Arellano-Viera et al., 2019). Both hESCs and hiPSCs were obtained from the National Bank of Stem Cell Lines-BNLC (ISCIII, Madrid). This work also includes genome edited lines for PAX2 and LHX1 genes (knock out lines) which are currently under characterization of ulterior registry at the BNLC.

Maintenance of hPSC lines

Both hESCs and CBiPSCs (human pluripotent stem cells, hPSCs) were maintained in Essential 8 (E8) medium (Thermo Fisher Scientific, #A1517001) supplemented with 1% Penicillin/Streptomycin (Pen/Strep) (10.000 U/ml, Thermo Fisher Scientific, #15140122). hPSCs were grown in cell culture plates previously coated with 5 µg/ml vitronectin (VTN) (Thermo Fisher Scientific, #A14700) and kept at 37 °C and 5% CO_2. Cell passages was performed every 4-6 days, at a confluency of 80%, with 0.5 mM EDTA (Thermo Fisher Scientific, #15575-038) to avoid single-cell disaggregation. Briefly, cells were rinsed once with 1X PBS (Thermo Fisher Scientific, #10010056) and further incubated with 0.5 mM EDTA solution for 3-5 min at 37°C. Afterwards, EDTA was aspirated, and cells were recovered with a gentle flush of E8 media to detach the hPSCs into small clusters. Cell clusters were then collected and diluted for passaging (at ratios of 1:12 to 1:20, depending on the cell line). Finally, cells were seeded onto a VTN-coated 6-well plate (Thermo Fisher Scientific, #140675), and maintained until the next passage. When necessary, hPSCs were cryopreserved with 10% DMSO (Sigma, D2650) in E8 media.

Genetically altered hPSC lines

A large proportion of the work in this thesis was performed using knockout (KO) ES[4] hPSC lines previously generated in the Montserrat laboratory (Aspiroz,

2021; Gimenez, 2021). Briefly, KO ES[4] hPSC lines were generated by making use of an iC2 platform (Gimenez, 2021), which essentially consists of the ES[4] F51 hPSC line integrated with a doxycycline inducible Cas9 expression cassette into one AAVS1 allele through homologous recombination. PAX2 KO and LHX1 KO ES[4] F51 iC2 hPSC lines were generated by transfecting the ES[4] iC2 F51 hPSC lines with sgRNAs targeting relevant coding sequences of PAX2 and LHX1 genes, respectively. As such, Cas9 was induced in these cell lines by doxycycline treatment. After recovery cells were replated at single cell to establish clonal cell lines. These lines were then screened for biallelic KO mutations at the target genes of interest by target amplicon sequencing (miseq and CRISPResso analysis) (https://doi.org/10.5281/zenodo.6457752). The resulting successful KO lines were then validated and characterized (Aspiroz, 2021; Gimenez, 2021).

Generation of kidney progenitors from hPSCs

Seeding hPSCs for differentiation

The differentiation of hPSCs towards kidney organoids in 3D was performed following a previously published step-wise methodology (Garreta et al., 2019; Garreta, Moya-Rull, et al., 2022; Garreta, Prado, et al., 2022; Monteil et al., 2020; Selfa et al., 2021). Briefly, hPSC colonies at 80% confluency grown on VTN/E8 media were washed once with 1X PBS and incubated with 0.5mM EDTA for 3-5 mins, to allow dissociation of hPSCs colonies into cell clusters. After removal of EDTA, cell clusters were resuspended in fresh E8 medium. Further, 100 µl of the cell suspension was mixed with Accumax™ (Stem Cell Technologies, #07921) in a 1:4 ratio and allowed to incubate at 37°C for dissociation into single cells. The single cell suspension was then used to calculate an accurate cell concentration, which was ultimately used to seed the cell clusters at a cell density of 1 x 10^5 cells per well of a VTN coated 24-well plate. To allow an even distribution of the cell clusters inside the wells, the 24-well plate was vigorously shaken 2-3 times every 5 minutes after placing into the incubator. For the following 1-3 days the cells are maintained in E8 media, which is refreshed daily, until the cell clusters reach about 80% of confluency. From this moment on,

hPSCs are considered ready to initiate differentiation towards the posterior primitive streak (PPS) and intermediate mesoderm (IM).

Guiding hPSCs towards PPM and IM fate: D0 of Differentiation

At D0 of differentiation, the E8 medium in the 24 well plate was replaced by 500 µl/well of basal differentiation media (Advanced RPMI 1640 (Thermo Fisher Scientific, #12633-012) supplemented with 1% GlutaMAX (200 mM, Thermo Fisher Scientific, #35050–038) and 1% Pen/Strep). For the duration of 3 days from day (D) D0 until D2, the basal differentiation media is supplemented with 8 µM CHIR99021 (CHIR) (Sigma-Aldrich, #SML1046-5MG), to allow the hPSCs to differentiate towards the PPS-related fate. At D3, the cells are driven towards the IM-fate with the supplementation of 200 ng/ml FGF9 (Peprotech, #100–23B), 1 µg/ml heparin (Sigma-Aldrich, # H3149-10KU) and 10 ng/ml activin A (Sigma-Aldrich, #338-AC-050) into the basal differentiation media.

Generation of 3D kidney organoids

At D4, 24 hours after the addition of 200 ng/ml FGF9, 1 µg/ml heparin and 10 ng/ml activin A into the basal differentiation media, the cells obtained a tight monolayer morphology. As previously described in (Garreta et al., 2019; Garreta, Moya-Rull, et al., 2022; Garreta, Prado, et al., 2022; Monteil et al., 2020; Selfa et al., 2021), the cells at this stage are in a nephron progenitor cell (NPC) state. From this point on, the basal differentiation media was refreshed, and the monolayer was subjected to a CHIR pulse: 5 µM CHIR, 200 ng/ml FGF9 and 1 µg/ml heparin in basal differentiation medium for 1H at 37°C. Following this, the monolayer was carefully rinsed with 1X PBS and incubated for 1 minute with TrypLE Express Enzyme (Thermo Fisher Scientific, #12604021) to detach the monolayer. The dissociated NPCs from each well of the 24 well plate were then collected, counted, and resuspended in basal differentiation medium supplemented with 200 ng/ml FGF9 and 1 µg/ml heparin to generate 3D organoids. Here, the size of the organoid was determined based on the number of cells (8×10^3 or 100×10^3 cells) resuspended in 100 µl of each well of a conical-

bottom 96-well plate (Thermo Fisher Scientific, #249935), which was then centrifuged at 300g for 3 min. From D6 onwards, the basal differentiation media of the organoids was refreshed every 2 days and supplemented with growth factors (200 ng/ml FGF9 and 1 µg/ml heparin). From D11 onwards until D20 of differentiation, the media was refreshed without the addition of growth factors.

Note: At D4 of differentiation, after the 1H CHIR pulse treatment, some of the NPCs were frozen in basal differentiation medium supplemented with 10% DMSO (Sigma, #D8418) and maintained in liquid nitrogen for long term storage.

Generation of PAA hydrogels

Glass bottom 35mm dishes (Mat-Tek, #P35G-0-20-C) were incubated with a 1:12:1 volume ratio mixture of Bind-silane (Sigma, #M6514), absolute ethanol (PanReac, #131086.1214) and acetic acid (Sigma, #27225) for 10 min at room temperature. Following incubation, the dishes were washed 2x with absolute ethanol, after which 22.5 µl of PAA mixture (see table 1) was added on top of the glass, and covered with a 18mm coverslip (Paul Marienfield, #0111580). Following 1H of polymerization at room temperature, PBS was added, and the coverslips were detached using a scalpel. For traction measurements 0.2 µm far-red fluorescent carboxylate-modified microbeads were used (Invitrogen, #C37480). The surface of the PAA gels was activated using Arylic Acid NHS chemistry and incubated further with 100 µg/ml Fibronectin (Merck, #440159) overnight.

Acrylamide %	Bis-acrylamide %	Beads % solid	APS %	TEMED %	Stiffness (kPa)
5	0.04	0.04	0.05	0.2	1
7.46	0.044	0.04	0.05	0.05	5

Table 1. PAA gel composition. Acrylamide (BioRad, #1610140), Bis-Acrylamide (BioRad, #1610142), beads, Ammonium persulfate (APS, Sigma, #A3678), Tetramethylethylenediamine (TEMED, Sigma, #T9281) were mixed in the specified proportions and diluted in PBS.

Differentiation of kidney progenitors in 2.5D on PAA substrates

Either fresh or frozen NPCs were resuspended in fresh basal differentiation media with differentiation factors (200 ng/ml FGF9, 1 µg/ml heparin) at a concentration of 4 x 10^6 cells / ml) and seeded as a drop of 200 µl onto the PAA gels. The gels were then carefully placed into the incubator for 1-2H, to allow the attachment of the cells. After the indicated time, each individual MatTek dish was filled with 2 ml of media with factors and maintained untouched in the incubator until day 6 of differentiation. Media was refreshed every two days and supplemented with factors until day 11, after which no additional factors were added.

Generation of PDMS gels

Soft PDMS preparation

Soft polydimethylsiloxane (PDMS) substrates of 3 and 18kPa were prepared by mixing the two components of the DOWSIL™ CY 52-276 A&B Kit (Dow, #2624028 and #2624052). The ratio of components A to B would determine the bulk elastic modulus of the PDMS substrate (see Table 2).

PDMS A/B mixing ratio (w/w)	Bulk elastic modulus (kPa)
1:1	3
5:6	18.6

Table 2. PDMS substrate composition.

Briefly, the PDMS mixture of desired stiffness was vigorously mixed on ice and further degassed under vacuum for 30 mins. Once the mixture was free of bubbles, it was spin-coated at a volume of 100 µl onto clean pre-heated (at 65°C) glass bottom dishes (MatTek, #P35G-0-20-C) for 90 seconds at 400 r.p.m. The samples were further cured in an oven at 65°C overnight.

Regular (Stiff) PDMS substrates preparation

Stiff PDMS substrates were used to create large circular confinements (6 mm diameter) for optimizing reagent usage during functionalization of the soft PDMS substrates. First, a mixture of stiff PDMS was created by mixing two components

of Sylgard™ - 184 Silicone Elastomer KIT (Dow Corning, #2401673921) at a ratio of 10:1, degassing for 60 minutes and allowing polymerization on a flat 150mm cell culture petri dish (TPP, #07177926 (93150)) in an oven at 65°C overnight. Once cured, the PDMS was cut into ¨donut¨ shapes with an inner ring diameter of 6 mm and outer ring diameter of 12.5 mm using two punchers. The resulting donut stencils were carefully placed on top of soft PDMS coated MatTek dishes, ready for functionalization.

Functionalization of PDMS substrates

The soft PDMS coated MatTek dishes were passivated with a 5% (3-aminopropil) trietoxisilano (APTES) (Sigma Aldrich, #175560) in absolute ethanol (EtOH) (Merck, #1009831011) for 3 mins and further washed 3x with absolute EtOH. The samples were then washed once with Boric Buffer [5 mg/ml Boric acid (Merck, #B1934), 3.8 mg/ml Sodium tetraborate (Merck, #221732)). For traction force measurements, FluoSpheres with a diameter of 0.2 µm (Invitrogen, #F8807) were diluted in Boric Buffer at a ratio of 1:40 and allowed to settle on top of the passivated soft PDMS-coated MatTek dishes for 1H at room temperature (RT). The PDMS substrates were then washed 3x with Boric Buffer and further incubated with a 1% solution of Poly-L-Lysine (PLL) (Merck, #P2636) in Boric Buffer for 1H at RT. Further, the PDMS substrates were washed 3x with 10mM HEPES buffer at pH 8.24 (Merck, #H3375-25G) and incubated with 50 mg/ml mPEG-SVA (Laysan Bio, #MPEG-SVA-5000) diluted in the same buffer, for 1H at RT. Finally, the samples were washed with 1xPBS and stored at 4°C until the generation of micropatterns.

Generation of micropatterns with PRIMO

Micropatterns were created with the help of the PRIMO system (Alvéole) (Strale et al., 2016a) mounted on an inverted microscope Nikon Eclipse Ti-2. Briefly, this system relies on contactless and maskless photopatterning on substrates via UV-mediated mPEG scission. The mPEG-SVA coated on top of the PDMS substrate acts as an antifouling layer. Upon exposure to UV light, and in the

presence of a photo initiator agent (PLPP) (Alvéole), the passivating properties of the mPEG become weakened, hence exposing the PLL to the surface, which can be further decorated with adhesion proteins to bind cells onto PEG-free motifs.

In the context of this work, 5x5 circular (300 µm in diameter), square (488 µm x 488 µm) and triangular (297 µm height x 475 µm base) micropatterns, as well as annotations were designed in Inkscape 1.2 (inkscape.org) and photopatterned onto PLPP coated soft PDMS substrates using the Leonardo Software (Alvéole) (Strale et al., 2016a). Once the UV exposure was finished, the gels were washed 1x with 1X PBS, and incubated with 100 µg/ml Fibronectin (Merck, #440159) for 5 minutes. The samples were then washed 3x with 1X PBS and kept at 4°C until NPC seeding.

Note: In the case of traction force microscopy experiments, a mix of 100 µg/ml unlabelled fibronectin and 100 µg/ml fluorescent Fibronectin HiLyte488™ (Tebubio, #FNR02-A) in a ratio of 1:3, was used for pattern annotation purposes.

Differentiation of kidney progenitors in 2.5D on PDMS substrates

Either fresh or frozen NPCs were resuspended in fresh basal differentiation media with differentiation factors (200 ng/ml FGF9, 1 µg/ml heparin) at a concentration of 4 x 10^6 cells / ml) and seeded as a drop of 50 µl onto the micropatterned PDMS substrates. The gels were then carefully placed into the incubator for 15-30 minutes, to allow the attachment of the cells. After the indicated time, the PDMS substrates were gently washed with fresh media with a 1000 µl pipette, to reveal the attached cells on the surface of the micropatterned substrates. Finally, each individual MatTek dish was filled with 2 ml of media with factors and maintained untouched in the incubator until day 6 of differentiation. Media was refreshed every two days and supplemented with factors until day 11, after which no additional factors were added.

TFM pipeline for kidney progenitors on PDMS substrates

In this thesis, traction force measurements were taken in a non-traditional (reverse) method. Here, images of the relaxed state of fluorescent beads were performed prior to cell seeding, allowing post TFM fixation of samples and their further immunofluorescence staining for markers of interest (see below more detailed information regarding TFM data analysis). Briefly, micropatterned soft PDMS substrates decorated with fibronectin were incubated with cell culture media for at least 1H before imaging (to ensure the same osmolarity conditions of the PDMS substrates during TFM measurements). Confocal Z-stack images of fluorescent fibronectin annotations were taken together with z-stack images of the fluorescent microbeads, to ensure accurate pre-TFM and TFM image correlation. Following this, the PDMS substrates were maintained in cell culture media and kept in the incubator until NPC seeding. On the differentiation day of interest, TFM images were obtained in the exact same manner as the pre-TFM images: fluorescent fibronectin annotations + fluorescent microbeads channels (see below for details regarding microscopy set-up + imaging conditions). Following the TFM image acquisition, samples were fixed and kept until further immunofluorescence staining (details follow below).

Immunofluorescence staining

In 3D kidney differentiation experiments, immunofluorescence (IF) staining was performed on either whole (in toto) organoids, or in 5 to 10 µm sections. IF staining on 2D kidney differentiation experiments were performed either in combination with TFM measurement or as separate (IF) experiments.

3D kidney differentiation – Immunofluorescence staining in toto

In the 3D kidney differentiation experiments, IF staining was performed to study and characterize the extent of kidney organoid differentiation by taking advantage of protein expression at different stages of nephron development.

Briefly, organoids were collected at different stages of differentiation (D9-D20) and fixed overnight at 4°C with a 4% solution of paraformaldehyde (PFA) (1:4 dilution of 16% PFA, ANAME, #15710-S). the following day, the organoids were washed thrice with 1X PBS and permeabilized with a blocking buffer (#1): 1X Tris Buffer Saline (TBS) [10x TBS: 24 gr TRIZMA base (Sigma, #T6791) and 88 gr NaCl (Sigma, # S7653) in 800 mL MiliQ H_2O], 1% Triton X-100 (Sigma-Aldrich, #T8787) and 6% donkey serum (Sigma-Aldrich, #S30-KC) for 24H at 4°C, under agitation. The next day, organoids were incubated with the primary antibodies (see table 2) of interest (diluted in blocking buffer #1) and incubated at room temperature for 2H followed by 72H incubation at 4°C. The organoids were then washed thrice with blocking buffer #1 for periods of 1H each and incubated with secondary antiobodies (see table 2) of interest (diluted in blocking buffer #1) for an additional 2H at room temperature and 72H at 4°C. Finally, the organoids were then washed 2x with blocking buffer #1 and 1x with 1X TBS and incubated with 4',6-Diamidino-2-Phenylindole, Dihydrochloride (DAPI) (Invitrogen, #D1306) at a 1:2500 dilution in 1X TBS for 60 minutes. The organoids were then placed on top of a glass microscopy slide (Thermo Fisher Scientific, #J1800AMNZ), mounted with 50 - 100 µl Fluoromount-G (Southern Biotech, #0100-01), sealed with a round coverslip (Thermo Fisher Scientific, #CBAD00120RAC20MNZ#0) and kept at 4°C until imaging.

3D kidney differentiation – Immunofluorescence staining in sections

For a more detailed IF analysis, 100K and 8K 3D organoids were embedded in paraffin and sectioned on a vibrotome to obtain slices ranging between 5 and 10 µm. These slices were further subjected to antigen retrieval in citrate buffer pH 6 and stained for Hematoxylin and Eosin (H&E). Images were captured using the AF7000 Leica microscope. Sections of interest were further permeabilized with a blocking buffer (#2): 1X TBS, 1% Triton X-100 and 3% donkey serum for 1H at room temperature. For nephron structure analysis, lectins (see table 2) were used to stain tubule-like structures. Here, an additional blocking step with Streptavidin/Biotin blocking kit (SP-2002, Vector Labs) was used for 1H each at room temperature, consecutively (with 1X TBS washes in between). Further, primary antibodies of interest were diluted in a blocking buffer (#3) consisting of

1X TBS, 1% Triton X-100, 1% Bovine Serum Albumin (BSA) (Sigma-Aldrich, #A4503) and incubated for 2H at room temperature and overnight at 4°C. The following day, the samples were washed with blocking buffer #3 thrice for periods of 1H at room temperature, after which the secondary antibodies (diluted in blocking buffer #3) were incubated for 2H at room temperature and overnight at 4°C. Finally, the samples were washed thrice with 1X TBS for periods of 1H each at room temperature and incubated with DAPI at a 1:2500 dilution in 1X TBS for 30 minutes. The samples were further mounted with 50 µl Fluoromount-G, sealed with a rectangular glass coverslip (VWR, #631-1335) and kept at 4°C until imaging.

2.5D kidney differentiation – Immunofluorescence staining

For each timepoint (day 8-16), individual MatTek dishes with the 2.5D kidney organoids were washed with sterile 1X PBS and fixed overnight at 4°C with 4% PFA. The next day, the solution was rinsed away 3 times for 15 minutes each with 1X PBS.

The samples were further subjected to blocking and permeabilization overnight at 4°C with blocking buffer (#1) consisting of 1X TBS, 1% Triton X-100 and 6% donkey serum (further always used in 2D samples). The following day, samples were incubated for an initial 2H at room temperature and further 72H at 4°C with primary antibodies diluted in blocking buffer #1 (see Table 3 for antibodies used in this work). Samples were further washed 3x with blocking buffer #1 for 1H periods at room temperature, before adding secondary antibody solutions (diluted in blocking buffer #1) for an additional initial 2H at room temperature and further 72H at 4°C. Finally, the samples were washed 2x with blocking buffer #3 for 1H periods, followed by a final 1H wash with 1X TBS. The stained samples were then mounted with 50 µl Fluoromount-G and kept at 4°C until imaging.

Primary and Secondary Antibodies			
Primary Antibodies	Host	Dilution	Cat #
PAX2	Goat	1:20	AF3364
WT1	Rabbit	1:100	MA5-32215
LHX1	Mouse	1:100	MAB2725
JAG1	Goat	1:200	AF599
E-CADHERIN	Mouse	1:50	610181
β-CATENIN	Mouse	1:50	610153
WGA	-	1:100	b-1025
LTL	-	1:200	B-1325
LAMININ	Rabbit	1:50	L9393
CASPASE – 3	Rabbit	1:100	9661S
Anti-GFP	Chicken	1:250	GFP-1020
Secondary Antibodies	Host	Dilution	Cat #
Anti-Goat IgG (H+L) Alexa Fluor Plus 405	Donkey	1:250	A48259
Anti-rabbit IgG Alexa fluor 488-conjugated	Donkey	1:200	A21206
Anti Mouse Alexa Fluor 488-conjugated	Donkey	1:200	A28175
Anti Goat Alexa Fluor 488-conjugated	Donkey	1:200	705-545-147
Anti Chicken IgY CyTM2-conjugated	Donkey	1:200	703-225-155
Anti-rabbit IgG Alexa fluor 555-conjugated	Donkey	1:200	A11015
Anti Mouse Alexa Fluor 555-conjugated	Donkey	1:200	A31570
Anti-Goat IgG Alexa Fluor 555-conjugated	Donkey	1:200	A-21432
Anti Rabbit Alexa Fluor 647-conjugated	Donkey	1:200	711-605-152
Anti-Mouse IgG Alexa Fluor 647-conjugated	Donkey	1:200	715-605-151
Dylight 649 Streptavidin	-	1:200	SA-5649

Table 3. Primary and Secondary Antibodies for Immunofluorescence staining.

Microscopy set-up and image acquisition

3D organoid (both in toto and sections) experiments were acquired using a laser-scanning confocal microscope (LSM880. Carl Zeiss) at a resolution of 1024 x 1024 (pixel size = 0.2076 μm) with bidirectional scanning. A Plan-Apo x10 (NA=0.45, dry, Ph1), x20 (NA=0.8, dry) and x40 (NA=1.2, Glycerol, DIC) objectives were used. The Zeiss ZEN software was used to carry out acquisitions.

2D organoid experiments were imaged using a Nikon TiE inverted microscope with a spinning disk confocal unit (CSU-WD, Yokogawa) and a Zyla-4.2-CL10 sCMOS camera (Andor). A built-in temperature and CO_2 box (Life Imaging Services), maintaining 37°C and 5% CO_2, was used for live TFM experiments. All images were acquired using a x20 objective (Nikon, Plan Apo, NA=0.75, Ph2, DM WD1, Dry). The multidimensional image acquisition was operated by the open-source software Micromanager ((Edelstein, Arthur et al., 2015), with custom made scripts.

TFM analysis

In the context of this thesis, tractions forces exerted by NPCs during their transition towards the nephron-like fate were measured by relying on the displacement of fluorescent microbeads on the surface of an elastic substrate (soft PDMS). Three-dimensional tractions were calculated as described previously (Latorre et al., 2018). Confocal z-stack images of fluorescent microbeads coated on the surface of soft PDMS substrates were taken in a relaxed (before cell seeding) and deformed (during cell attachment) states with a z-step of 0.2 µm. From these two states, the displacement of the fluorescent microbeads and the deformation of the gels were calculated by using a homemade iterative 3D PIV software, with a square interrogation window size of 32 pixels and an overlap of 0.5. A Finite Element Method (FEM) solution was implemented to compute 3D tractions from the 3D deformations of the soft PDMS. Calculation of displacements and traction forces were carried out using custom MATLAB scripts (Trepat et al., 2009).

Image analysis

Average IF intensity quantifications

Raw images were processed with Image J. Quantifications of average fluorescence intensities were performed with custom made Image J macros. Briefly, Z-stacks of individual images were projected as a sum of all pixel grey values per each channel. These sum projection images were then added using

the ImageCalculator tool (to ensure that the entire organoid is being taken), after which the Autothresholding tool was used to generate binary masks of the 2D organoid. This mask was then used as a guideline to calculate the average fluorescence intensity of the organoid per channel (marker). In a similar manner, a rectangle outside of the organoid mask was selected to calculate the average fluorescence intensity of the background, making it possible to subtract the background signal. Finally, all values were normalized to the number of slices per Z-stack.

Inner vs Outer IF quantifications

Z-stack images of the first 100 µm of cells (in contact with the surface of the gel) were projected as a sum of all pixel grey values per each channel. These sum projection images were then added using the ImageCalculator tool (to ensure that the entire organoid is being taken), after which the Autothresholding tool was used to generate binary masks of the 2D organoid. This mask was then used together with the Geometry to Distance function of Image J, to create a distance map of IF expression in relation to the center of the pattern. As such, a distance threshold of 20-30% was defined from the edge of the pattern – to define the inner and outer regions. Following this, the average fluorescence intensities were measured per channel, per region. All values were then normalized to number of slices per z-stack and to the background.

Statistical analysis

Traction maps and kymographs were generated in MATLAB. The remaining plots were created in GraphPad Prism 10.1.0. All immunostaining images were processed in Image J. All data are represented as the mean ± s.d. Sample size (n) and the number of independent repetitions is indicated in the figure captions. All statistical analyses are indicated in the figure captions.

Results

Chapter 1.

Generation of hPSC-derived kidney organoids

In the context of this chapter, three pluripotent stem cell lines were used to generate kidney organoids: ES[4] (male hESCs), CB40 (female hiPSCs) and ES[4]-WT1-GFP (male hESCs).

The generation of kidney organoids was performed using a previously established methodology (Figure 1A) (Garreta, Moya-Rull, et al., 2022; Garreta, Prado, et al., 2022). Briefly, ES[4], CB40 and ES[4] – WT1 – GFP background hPSCs (Figure 1B) were cultured in a monolayer until confluency and were guided towards PPS induction by making use of an agonist of Wnt signalling – CHIR for a duration of 3 days. The monolayers were then driven towards the IM fate by exposing them to FGF9, Activin A and Heparin for 24 hours. At this stage of differentiation Activin A (analogue of Retinoic Acid, RA) was used as a potent inducer of the PIM, phenocopying earlier stages of embryogenesis when the neural tube secrets RA (Tanigawa et al., 2019; Wilson et al., 2003). Following this, at day 4 (Days = D) of the differentiation protocol, the monolayers were disintegrated into single cells, which were then subjected to either aggregation in 3D or seeding on 2D surfaces (discussed in detail in the next section). From this point onwards, the cultures (both 3D and 2D) were supplemented with FGF9 and Heparin (FGF9 to maintain the progenitor niche, and Heparin for aiding Wnt signalling) until the appearance of renal vesicles (D11) (Barak et al., 2012; Binari et al., 1997). Importantly, after the induction of RVs, the cultures were maintained growth factor free, where in a cell autonomous process, the RV driven cell populations further develop into multiple nephron-like structures that were segmented into typical nephron components, including proximal tubules, loop of Henle, distal tubules and glomeruli, as described previously (Garreta et al., 2019; Garreta, Moya-Rull, et al., 2022; Garreta, Prado, et al., 2022).

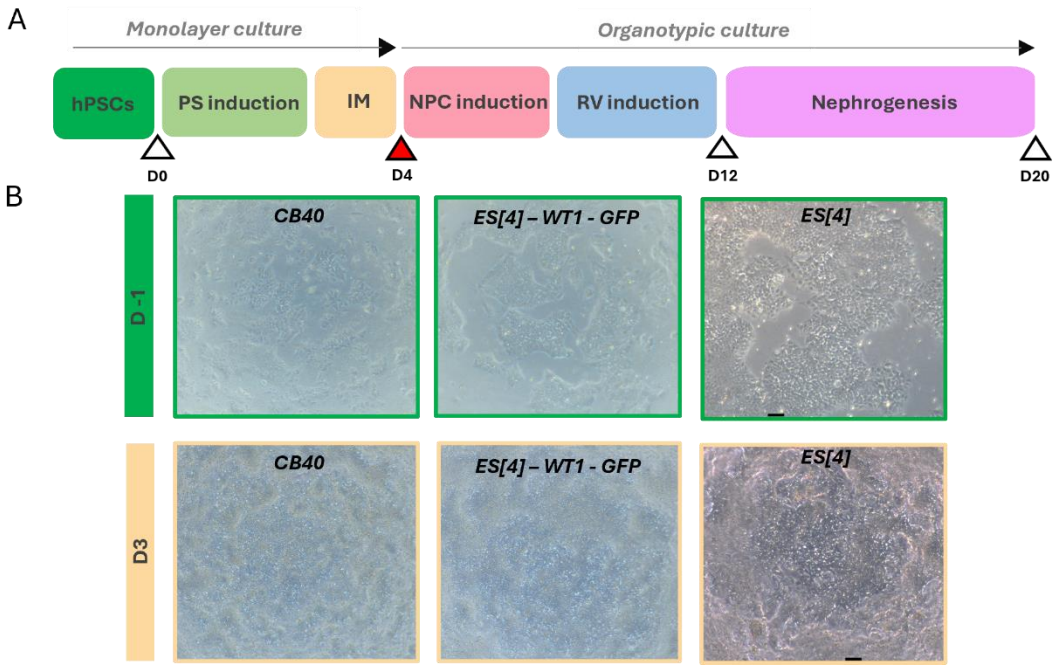

Figure 1. Generation of hPSC derived kidney organoids. A) Stepwise methodology starting from a monolayer culture of hPSCs, at D0 induction of primitive streak (PS), at D3 induction of intermediate mesoderm (IM). From D4 the culture is organotypic, induction of Nephron Progenitor Cells (NPCs), induction of renal vesicles (RV) and nephrogenesis. B) Representative brightfield images of CB40, ES[4] and ES[4]-WT1-GFP hPSCs at D-1 and D3 of culture.

In the interest of studying Nephron Progenitor Cells (NPC) differentiation into nephron like structures in hPSC-derived kidney organoids, and to further dissect early steps of patterning and segmentation (by assessing specific time frame where this occurs *in vitro*), this chapter describes three distinct methodologies used throughout the thesis (Figure 2). In the 3D free-floating kidney organoid culture methodology, IM-driven cultures at D4 of differentiation (Figure 2A) are dissociated into single cells and aggregated into 3D spheroids by centrifugation in a non-adherent v-bottom 96 well plate (Figure 2B top schematic). This methodology allows for the robust and high-throughput generation of organoids of varying sizes [cell aggregation number, 8K ($8x10^3$) – 100K ($100x10^3$) (Dhillon et al., 2021; Garreta et al., 2019; Garreta, Prado, et al., 2022; Monteil et al., 2020)] and is convenient for performing many types of characterization analyses, such

as immunofluorescence (IF) staining, protein extraction, and RNA analysis, due to the easy availability of large numbers of samples (Figure 2C top panel).

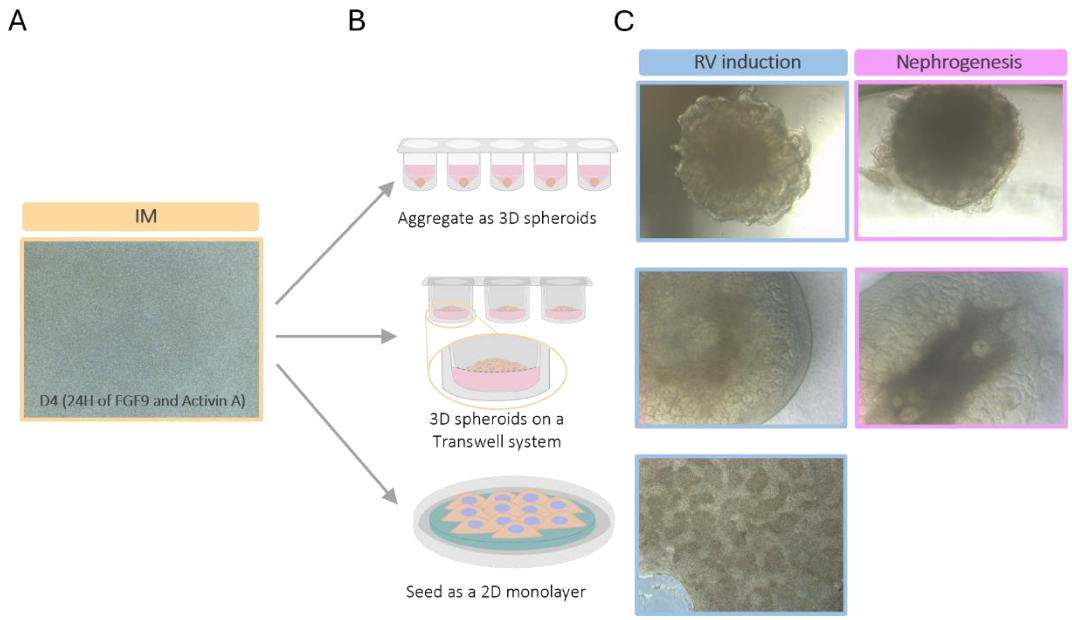

Figure 2. Different methodologies used to culture hPSC-derived kidney organoids. A) Representative brightfield image of hPSC-derived IM cells at D4 of differentiation. B) Schematic representations of three methodologies used for kidney differentiation: aggregated 3D spheroids cultured in a v-bottom 96 well plate (top), 3D spheroids cultured on a trans-well insert in a 6 well plate (middle), 2D monolayer on a substrate in a Mat-tek dish (bottom). C) Representative brightfield images of 3D kidney organoids (top), Trans-well organoids (middle) and 2D differentiation (bottom).

Several studies have demonstrated improved extent of kidney organoid differentiation (comprising segmented nephrons with endothelial and stromal cells, transcriptionally similar to a human fatal kidney) upon culture on an air-liquid interface, such as an insert trans-well system (Figure 2B middle schematic) (Gupta et al., 2021; Taguchi et al., 2014; Takasato et al., 2015). To utilize this system, at D4 of differentiation IM-derived cells were aggregated into 3D spheroids, similarly, to the 3D free-floating organoid methodology. Further, at D6 of differentiation, individual organoids were carefully picked one by one and placed onto the membrane of an insert trans-well, where it can be in contact with both the cell culture media and air. In the insert trans-well system, the 3D organoids were flatter, making it easier to visualize RVs and more complex structures by brightfield microscopy (Figure 2C middle panel). While the use of

an insert trans-well system is relatively low throughput (compared to the 3D free-floating methodology), the resulting organoids can be easily characterized by IF, protein, and RNA analysis.

While many studies have demonstrated the amenability of hPSCs to generating 3D kidney organoids (either free-floating or on insert trans-wells), not much has been described regarding the 2D kidney differentiation potential of hPSCs (Garreta et al., 2019; Morizane et al., 2015; Taguchi & Nishinakamura, 2017; Takasato et al., 2016). Others have utilized non-3D approaches, such as ¨sandwiching¨ hPSCs between two layers of Matrigel, to generate either lumenized spheroids (in 3D) or monolayer colonies (in 2D) (Freedman et al., 2015). However, the study of NPC transition onto RVs and subsequent nephron-like structures has not yet been explored. In this regard, work in the Montserrat laboratory has initiated the study of 2D kidney differentiation on tissue culture plastic and compliant substrates (from NPC derivation to RV induction to nephron like structures).

In 2D, hPSCs can differentiate into the kidney lineage as effectively as in the 3D methodology (Garreta et al., unpublished). Similar to the previous two hPSC -derived kidney culture approaches described above, the 2D methodology relies on increased cell-cell contact at D4 of differentiation, therefore the dissociated single IM-induced cells were seeded on to a 2D surface as a tight monolayer (for example 800K on a single Mat-Tek dish) (Figure 2B and C middle panel). One advantage of using a 2D methodology is the potential for mimicking the mechanical properties of the extraembryonic environment by taking advantage of compliant substrates. The substrates used in this thesis include polyacrylamide (PAA) and polydimethylsiloxane (PDMS), both of which were generated at stiffness values of 1-5kPa (similar to that of the embryo). Furthermore, both these substrates allow the incorporation of fluorescent microbeads on their surface, making it possible to obtain direct measurements of traction forces exerted by cells/tissues onto the substrate (discussed in detail further in the thesis).

The next sections of this chapter will describe characterization experiments performed in these three distinct systems, each providing unique insights into the process of NPC formation and differentiation into nephron-like structures in

hPSC-derived kidney differentiation. From now onwards the cell cultures resulting from the three systems will be referred to as: 3D organoids, trans-well organoids and 2D differentiation, respectively.

Characterization of nephrogenesis in 3D kidney organoids

Mouse embryonic kidney samples have been a valuable tool for identifying the key genes involved in the different steps of nephrogenesis, prior and after RV emergence to nephron patterning and segmentation (schematic representation in Figure 3).

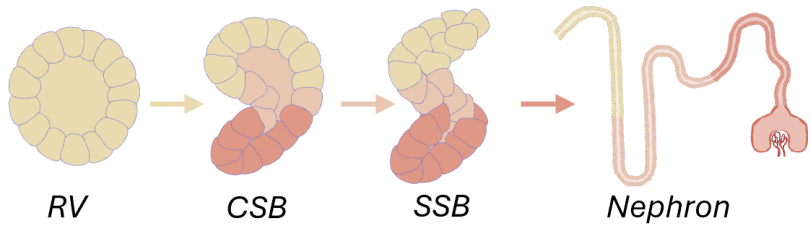

Figure 3. Schematic representation of nephrogenesis: renal vesicle (RV), comma shaped body (CSB), S-shaped body (SSB) and nephron consisting of distal, medial, and proximal segments.

Previous studies have demonstrated the capacity of NPCs to self-organize *in vitro* and form RV-like structures in 3D kidney organoids. These observations have been extensively replicated among different laboratories, overall providing a useful toolkit to monitor RV emergence. Initially in mouse embryonic tissue samples, RVs have been characterized for the expression of markers such as *Wnt4, Fgf8, Pax8, Lhx1*, *Brn1* (Kobayashi et al., 2005; Park et al., 2007). Further proximal-distal specification and segmentation of the developing nephron has been extensively studied and characterized by the Wnt/β-catenin and Notch signalling pathways (Deacon et al., 2019; Heliot et al., 2013; Lindstrom et al., 2013; Lindström et al., 2015; Park et al., 2007). Notch ligands such as *Dll1, Jag1,* members of the *Pax* family – *Pax2 and Pax8, Wt1, Hnf1b, Cdh1, Cdh6* among others, have all been previously described in the context of mouse nephron patterning and segmentation. In the human kidney organoid context, these studies have been extremely useful in validating the extent of kidney differentiation by the use of markers *WT1, PAX2, LHX1, E-CADHERIN, HNF1B* – at the renal vesicle stage; *JAG1* – for medial segments / late RVs; *SLC3A1*, *LTL* -

for proximal tubules; E-*CADHERIN, UMOD* – for loop of Henle; *E-CADHERIN* – for distal tubules and *PODXL, PODOCIN, NEPHRIN, NEPH1, WT1* – for glomeruli (Garreta et al., 2019; Morizane et al., 2015; Taguchi & Nishinakamura, 2017; Takasato et al., 2015, 2016).

3D kidney organoids derived from the ES[4] hPSC background express keys markers such as *PAX2, WT1* and *E-CADHERIN* from D12 (RV emergence) to D20 of differentiation in different structures over time (Figure 4A and B). At D12 of differentiation, epithelialized lumen containing vesicles can be observed (in both 100K and 8K organoids) by expression of *PAX2* and *WT1*. At D14, *WT1* expressing cells are observed in clusters resembling intermediate elongated structures such as comma-shaped (CSB) and s-shaped bodies (SSB) (Figure 4B, D14). At this time point, *E-CADHERIN* can be observed in emerging tubular like structures (Figure 4A, D14). By D20, distal tubular structures demarked by *E-CADHERIN* and *PAX2* appear more elongated and bent. *WT1* can be observed on the outer edges of 100K organoids, demarking the emerging podocyte – like cells (Figure 4A, D20). In 8K organoids *WT1* can be observed in proximal tubule-like structures (Figure 4B, D20).

Other markers such as *JAG1* start their expression at the distal domain in pre-tubular aggregates, where proximal recruitment of mesenchymal cell types is still taking place over an extended period relative to the mouse kidney (Figure 5A, D12 and D14). *LAMININ* in 3D kidney organoids highlights the basal membrane, where at D12 of differentiation it surrounds individual RVs, and as differentiation progresses, its expression becomes concentrated around larger, more elongated structures (Figure 5B).

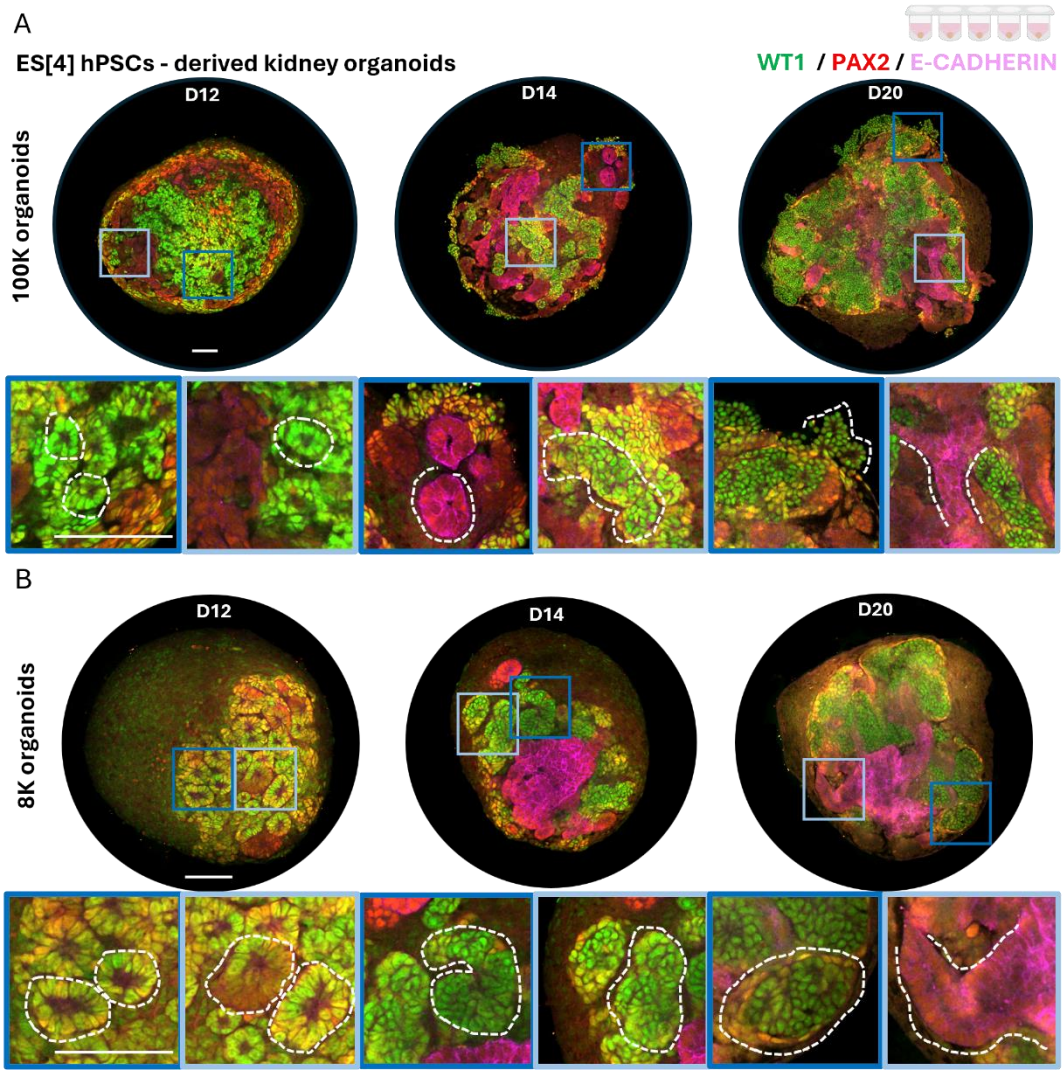

Figure 4.3D Kidney organoids derived from ES[4] hPSCs. Immunofluorescence images of A) 100K organoids and B) 8K organoids at D12, 14 and 20 of differentiation. Organoids stained for *WT1* in green, *PAX2* in red and *E-CADHERIN* in magenta. Dark blue and light blue boxes contain magnification images. White dashed lines indicate RVs (at D12), CSBs/SSBs (at D14) and nephron like tubular structures (at D20). Scale bar 100µm.

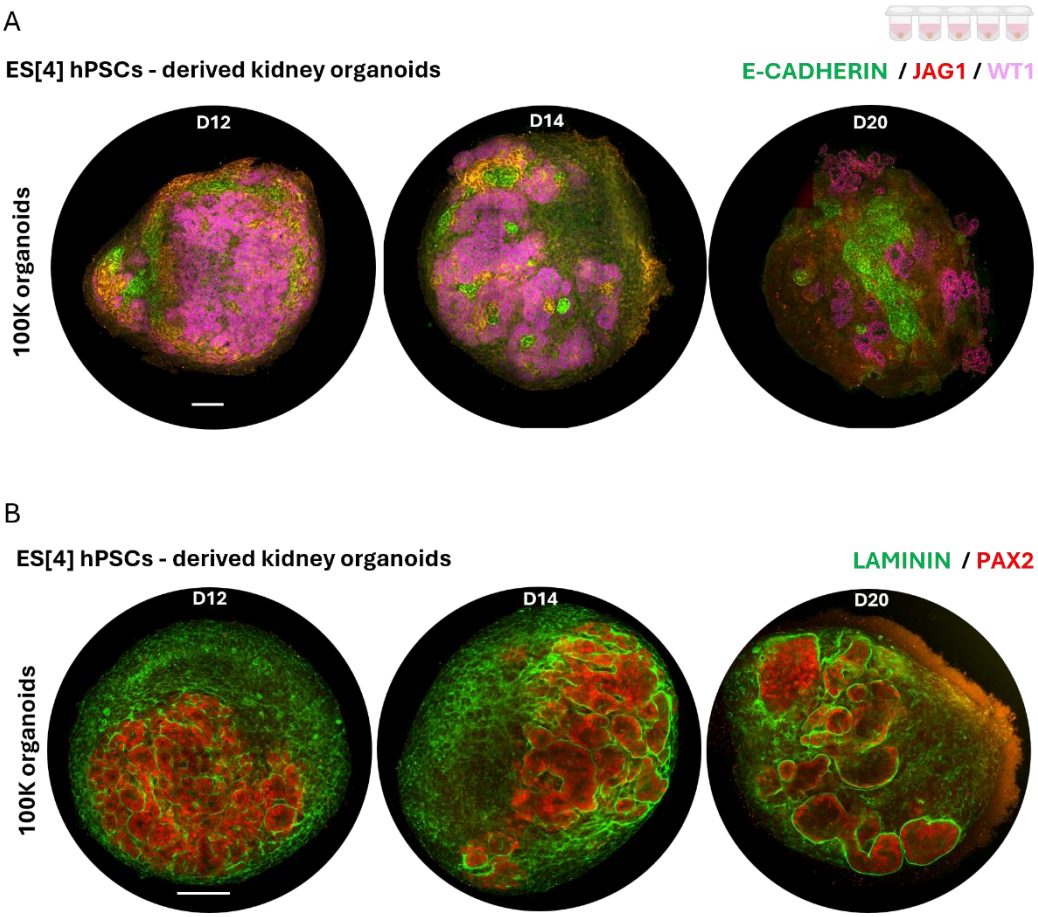

Figure 5. 3D Kidney organoids derived from ES[4] hPSCs. Immunofluorescence images of A) 100K organoids and B) 8K organoids at D12, 14 and 20 of differentiation. Organoids stained for A*) E-CADHERIN* in green, *JAG1* in red, *WT1* in magenta; B) *LAMININ* in green, *PAX2* in red. Scale bar 100µm.

Like most 3D spheroid systems, 3D kidney organoids, although containing CD31+ cells, lack proper vascularization. In long term culture and, as a consequence of cell number aggregation, they can in some instances develop a necrotic core due to the lack of nutrient supply to the centre. In CB40 3D kidney organoids this phenomenon was observed by immunofluorescence staining for *CASPASE-3* (Figure 6A). Upon closer examination, *CASPASE-3* expression was observed within *PAX2* positive RVs at D15 of differentiation (Figure 6B), hinting at a potential way by which RVs develop/increase their lumen. At D20, we see the expression of *CASPASE-3* lining the inner wall of *PAX2* positive structures (Figure 6C). To further correlate the extent of differentiation and cell death in the system, specific markers to distinguish the different cell types in the system such as *WT1* for the podocyte-like cells, *MEIS1* to demark the stromal cells, could provide a better overview.

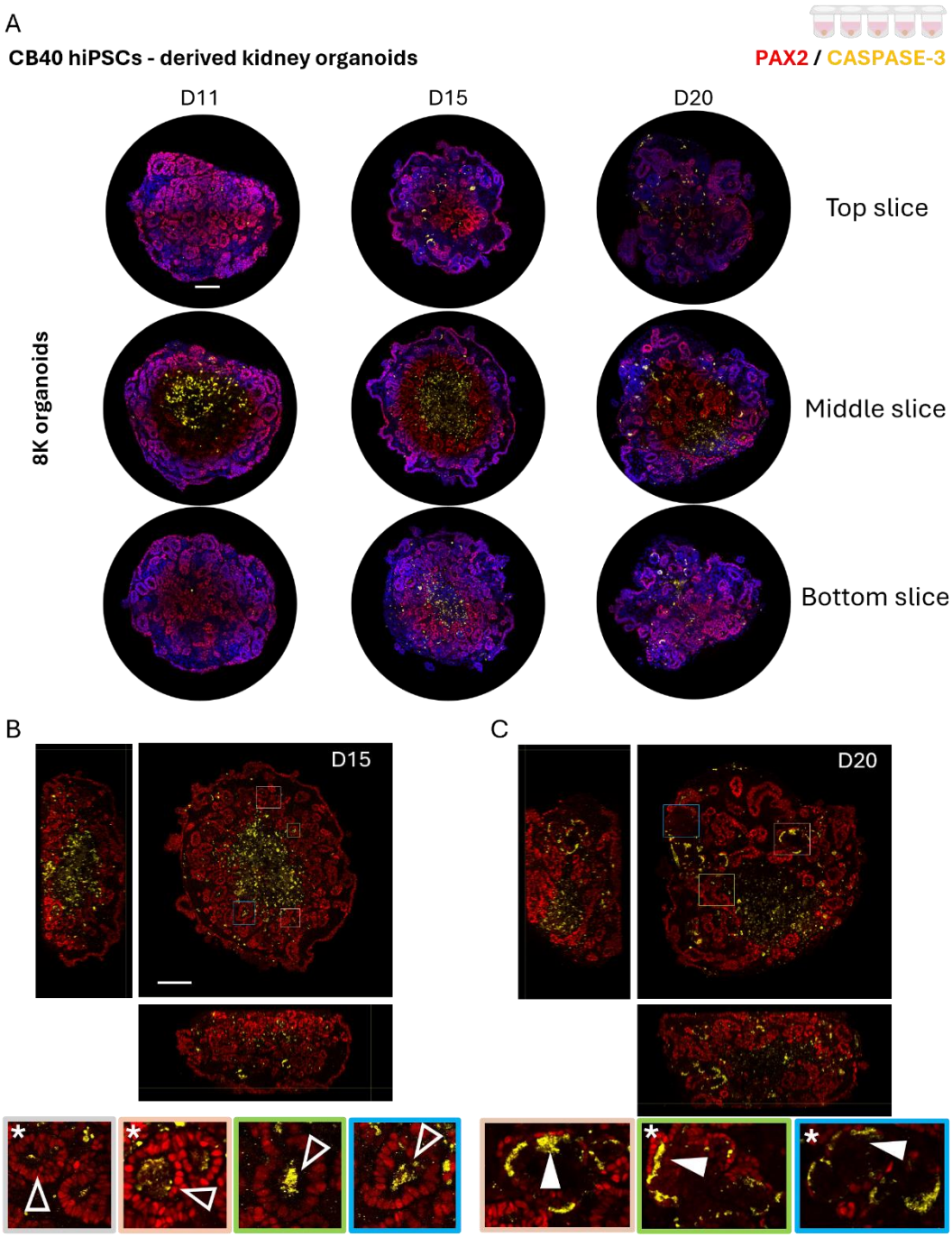
A
CB40 hiPSCs - derived kidney organoids
PAX2 / CASPASE-3
D11
D15
D20
Top slice
Middle slice
Bottom slice
8K organoids
B
D15
C
D20

Figure 6. 3D Kidney organoids derived from CB40 hiPSCs. Immunofluorescence images of 8K organoids at A) D11, 15 and 20 of differentiation. Organoids stained for *PAX2* in red and *CASPASE-3* in yellow. Single z slice representative image of B) D15 and C) D20 organoids, with orthogonal views (on the left and bottom). Coloured boxes represent magnified images, white arrow heads pointing towards *CASPASE-3* expression. Asterix represent close up images taken from other Z-slices of the same organoid. Scale bar 100µm.

In the trans-well system organoids present a flatter morphology, allowing better visualization of RV emergence by brightfield microscopy (Figure 7A). Embedding organoids in agarose and subjecting them to sectioning allows for a more in-depth histological and immunofluorescence analysis of nephron patterning across closely related sections of the same organoid (Figure 7B). By taking advantage of these techniques, it was possible to visualize key time points in nephron patterning in trans-well organoids in the ES[4] – WT1 – GFP background (Figure 7C). The ES[4] – WT1 – GFP hPSCs were previously generated in the Montserrat laboratory and presented as a useful approach for monitoring first, RV emergence (as demarked by *WT1*), and then the progression throughout differentiation until obtaining a *WT1* positive podocyte like cells fate. A variety of other reporter hPSC lines have been previously described for *CITED1, SIX2, GATA3, MAFB, LRP2, HNF4A* and have been useful in fate tracing and understanding the role of different genes throughout development (Howden et al., 2019; Vanslambrouck et al., 2019).

Haematoxylin and Eosin (H&E) stainings of trans-well kidney organoids between D10 and D20 of differentiation carry notable similarities to human embryonic kidney sections at 11 weeks of gestation (Figure 7C middle panel) (Faa et al., 2012). Immunofluorescence expression of *E-CADHERIN* at D12 of differentiation indicates the mesenchymal to epithelial transition ongoing in the developing organoid, and from D14 to D20, *E-CADHERIN* (distal) and *LTL* (proximal) expression can be observed in different segments of nephron like structures (Figure 7C, bottom panel).

WT1 and *PAX2* demark distinct populations as NPCs progress to RVs and resulting nephron-like structures (Figure 8A). At D12 they are both expressed in the RVs, at D14 polarization of expression can be observed in intermediate structures and by D20 *WT1* gets localized towards glomerular and proximal tubule like structures (Figure 7C bottom panel, Figure 8B), while *PAX2* localizes in distal tubular structures (Figure 8B).

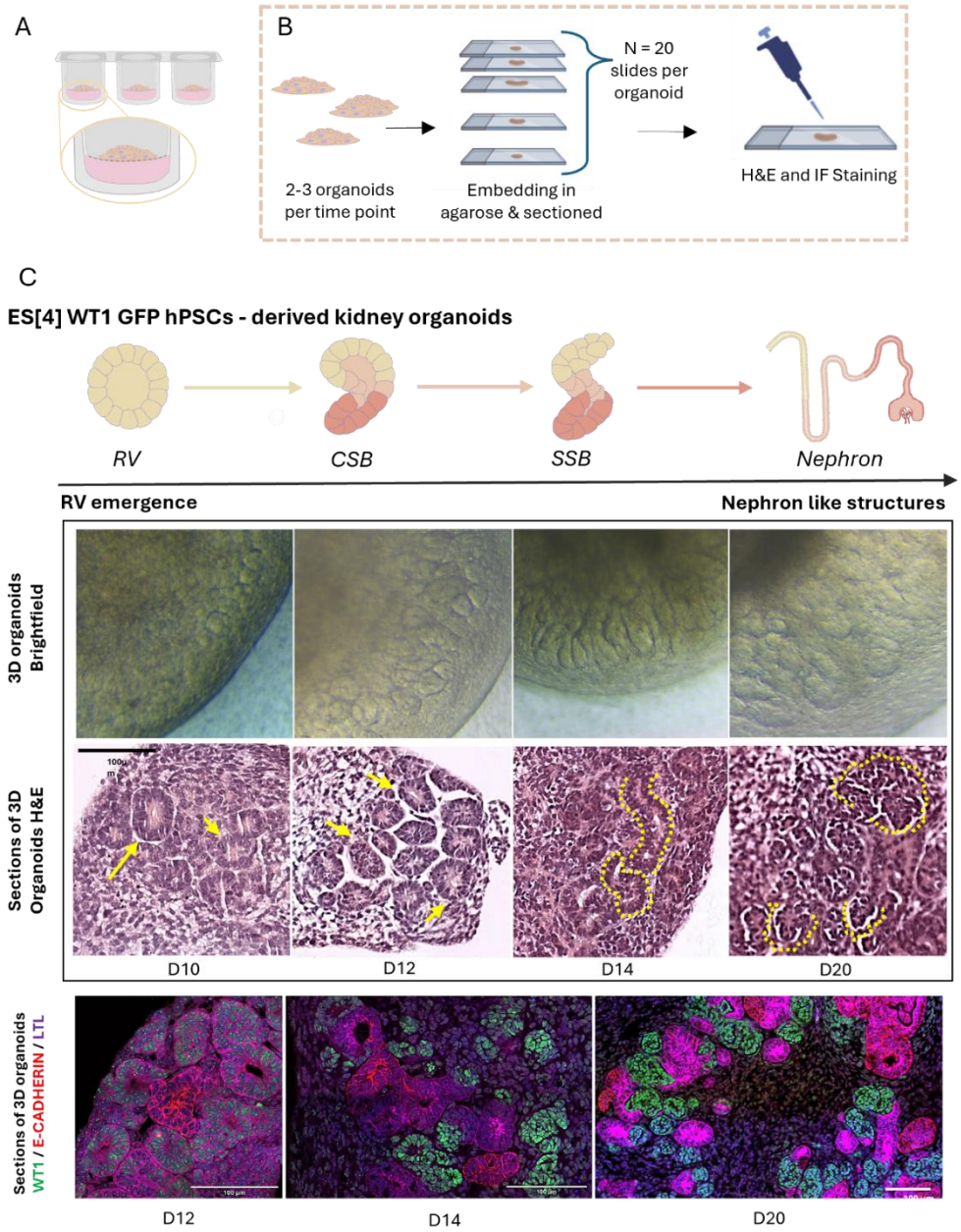

Figure 7. 3D kidney organoids cultured in a trans-well system. A) Schematic representation of the trans-well insert. B) Schematic representation of methodology for embedding organoids in agarose, sectioning, and staining. C) 3D kidney organoids derived from ES[4]-WT1-GFP hPSCs cultured in a trans-well insert. Brightfield images (top panel) and Haematoxylin and Eosin (H&E) staining images of sectioned organoids (middle panel). Yellow arrows indicate RVs at D10 and D12. Yellow dashed lines indicate SSB and tubular like structures at D14 and glomeruli at D20.Immunofluorescence staining of sectioned organoids for *WT1* in green, *E-CADHERIN* in red and *LTL* in magenta (bottom panel). Scale bar 100µm.

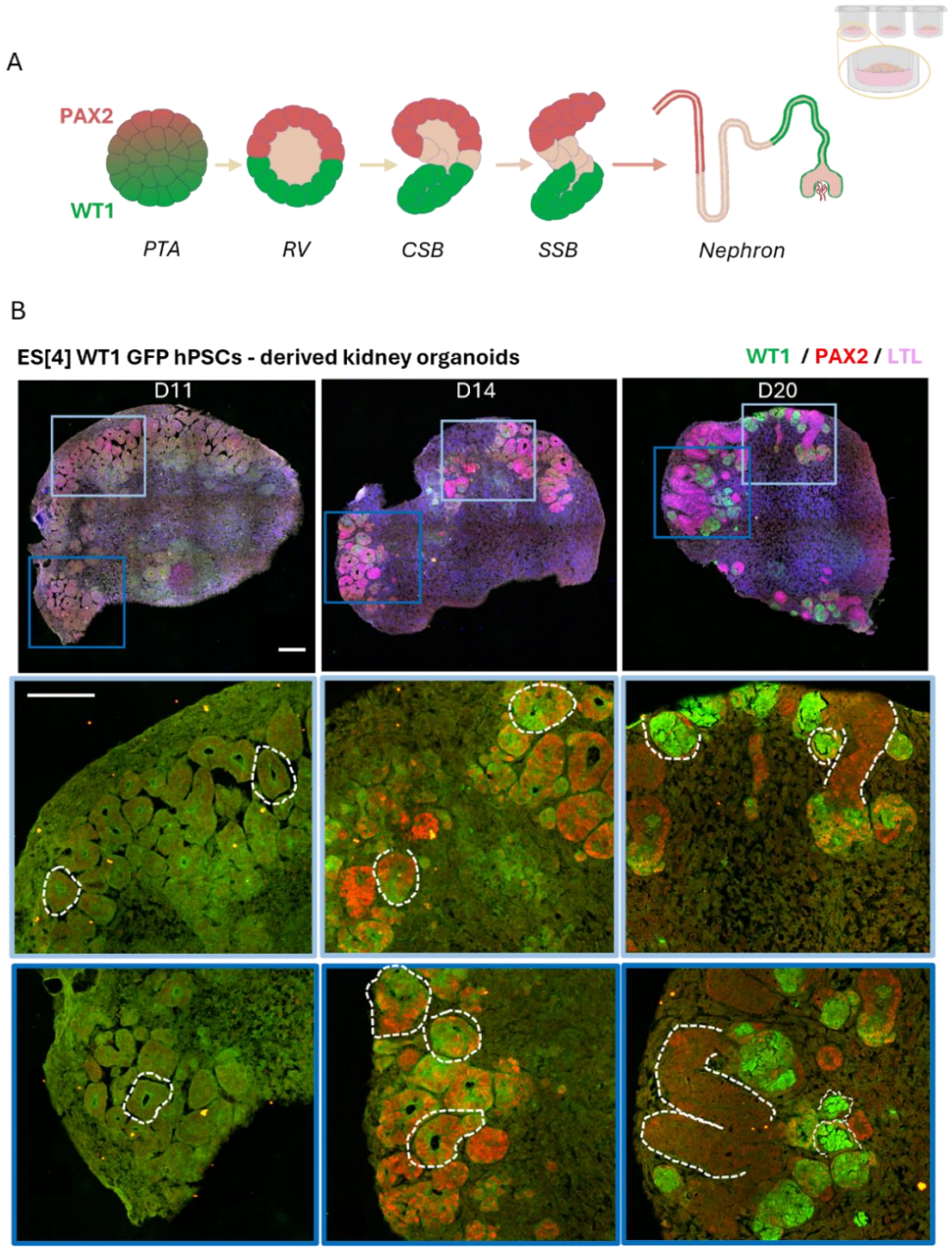

Figure 8. Sections of 3D kidney organoids cultured in a trans-well system. A) Schematic representation of *PAX2* in red and *WT1* in green expression during nephron patterning. B) Sections of 3D kidney organoids derived from ES[4]-WT1-GFP hPSCs cultured in a trans-well insert at D11,D14 and D20. Dark blue and light blue boxes contain magnification images. White dashed lines indicate RVs (at D11), CSBs/SSBs (at D14) and nephron like tubular structures and glomeruli (at D20). Scale bar 100µm.

Differentiation of NPCs on 2D compliant substrates

Previous findings have demonstrated how exposure of hPSCs to soft substrates can guide mesodermal commitment, while stiff matrices resulted in Wnt-dependent inhibition of differentiation(Przybyla et al., 2016).

In terms of kidney differentiation, preliminary findings by Garreta et al (2019) have demonstrated that short term exposure of hPSCs to a soft PAA hydrogel (1kPa) prior to cell aggregation for 3D spheroids, resulted in accelerated kidney organoid maturation, higher number of RVs, increased expression of late stage nephron markers, in comparison to exposure to stiff PAA gel (60kPa) (Garreta et al., 2019) . Indeed, conventional 2D substrates such as tissue culture plastic or glass have a stiffness value of around 1GPa, which is far greater in magnitude than the embryonic microenvironment (1kPa) (Kolahi et al., 2012).In the context of this thesis, 2D differentiation of kidney organoids was explored on soft PAA and PDMS substrates ranging between 1 and 5kPa of rigidity.

2D differentiation on Polyacrylamide (PAA) hydrogels

PAA hydrogels were polymerized on single Mat-Tek glass bottom dishes and coated with fibronectin prior to NPC seeding at D4 of differentiation (Figure 9A). The cell cultures were further guided through differentiation by the addition of FGF9 and Heparin until D11 of differentiation, similar to the 3D culture system, after which they were maintained growth factor free (Figure 9B).

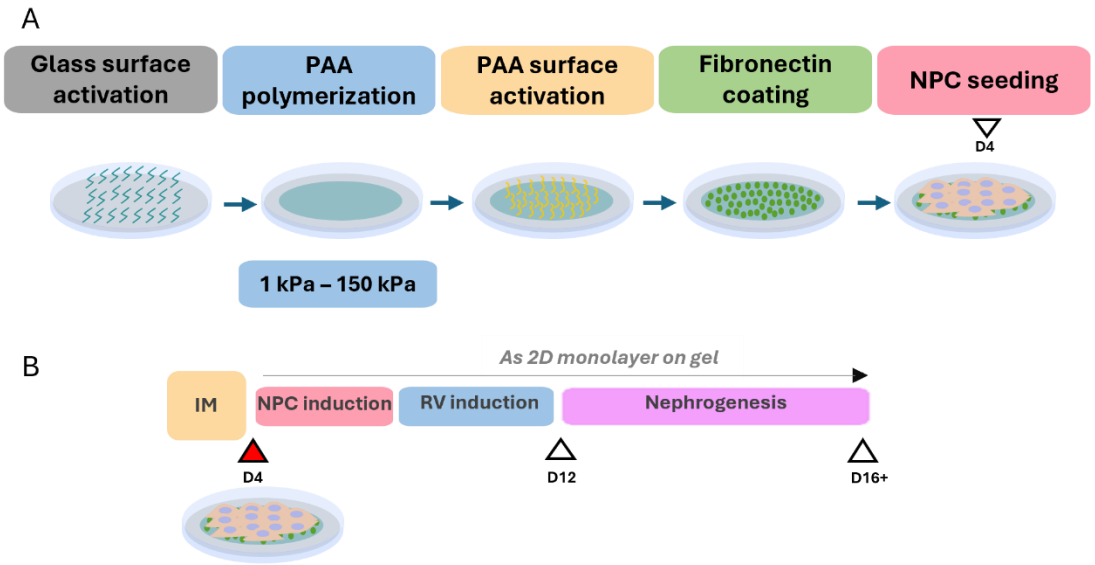

Figure 9. 2D differentiation on Polyacrylamide (PAA) gels. A) Schematic representation of steps for glass surface activation, PAA polymerization, PAA surface activation, fibronectin coating and NPC seeding. B) Schematic representation of 2D kidney differentiation on PAA gels.

NPCs of the ES[4]-WT1-GFP and CB40 backgrounds were differentiated on 1kPa PAA and glass substrates (Figure 10A). At D7 of differentiation, monolayers cultured on both types of substrates did not show obvious differences at morphological level (i.e., overgrow, cell death, among others) as determined by brightfield microscopy (Figure 10A). As expected morphological changes started to be visible by brightfield microscopy at the time point of expected RV emergence (D11/12) in the monolayers generated on 1kPa PAA compared to glass substrates, especially in the ES[4]-WT1-GFP background (Figure 10B).

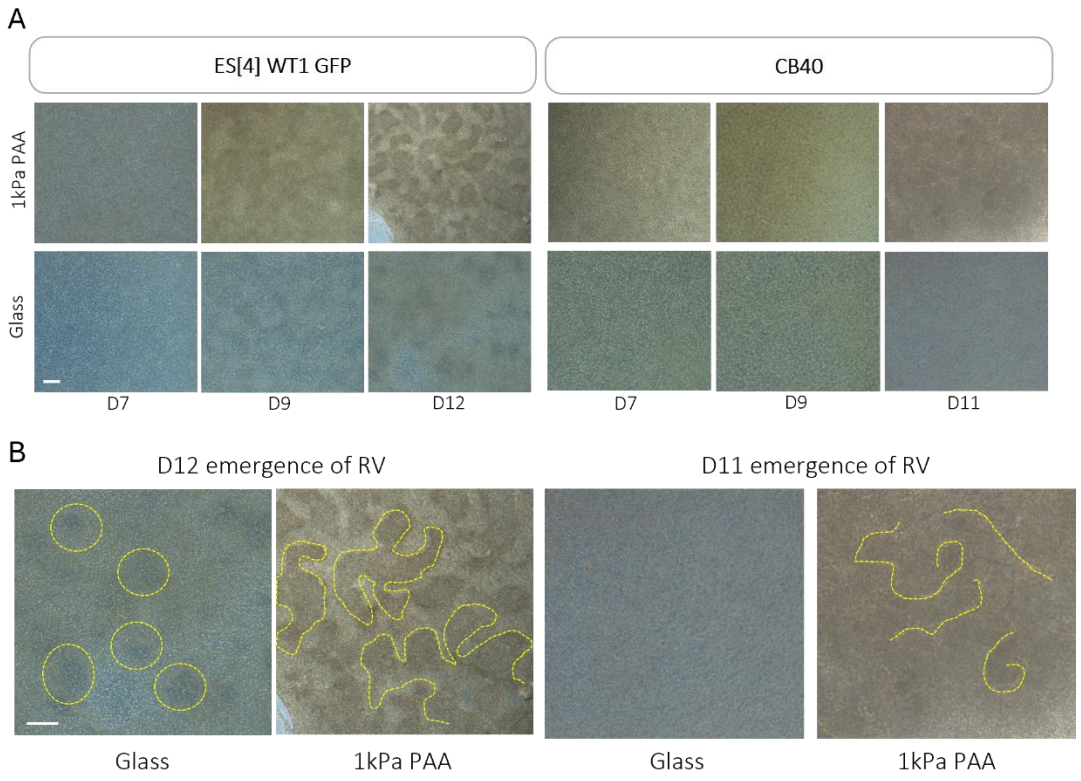

Figure 10. 2D differentiation of kidney progenitors on PAA gels. A) Brightfield images of ES[4]-WT1-GFP and CB40 hPSC-derived kidney differentiation on 1kPa PAA and glass substrates over D7, D9 and D12/11 of differentiation. B) Close-up magnification brightfield images of RV emergence in the corresponding cell lines. Yellow dashed lines indicate morphological changes observed in the monolayers.

Upon IF staining of ES[4]-WT1-GFP and CB40 2D differentiation cultures on soft PAA (1kPa and 5kPa respectively) at timepoints of RV emergence (D11/12), differences in RV structures and abundance could be observed, compared to glass substrates (Figure 11). RV clusters expressing PAX2 and surrounded by an outer layer of *LAMININ* could be observed in ES[4]-WT1-GFP 2D differentiation on 1kPa PAA, which appeared larger than RV structures seen on glass (Figure 11A). A similar phenomenon was observed in the CB40 background (Figure 11B). Total RV number in 3D kidney organoids, derived from hPSCs cultured on either 1kPa or 60kPa PAA gels revealed a higher value in the softer condition, compared to the stiff PAA, further supporting our findings (Garreta et al., 2019).

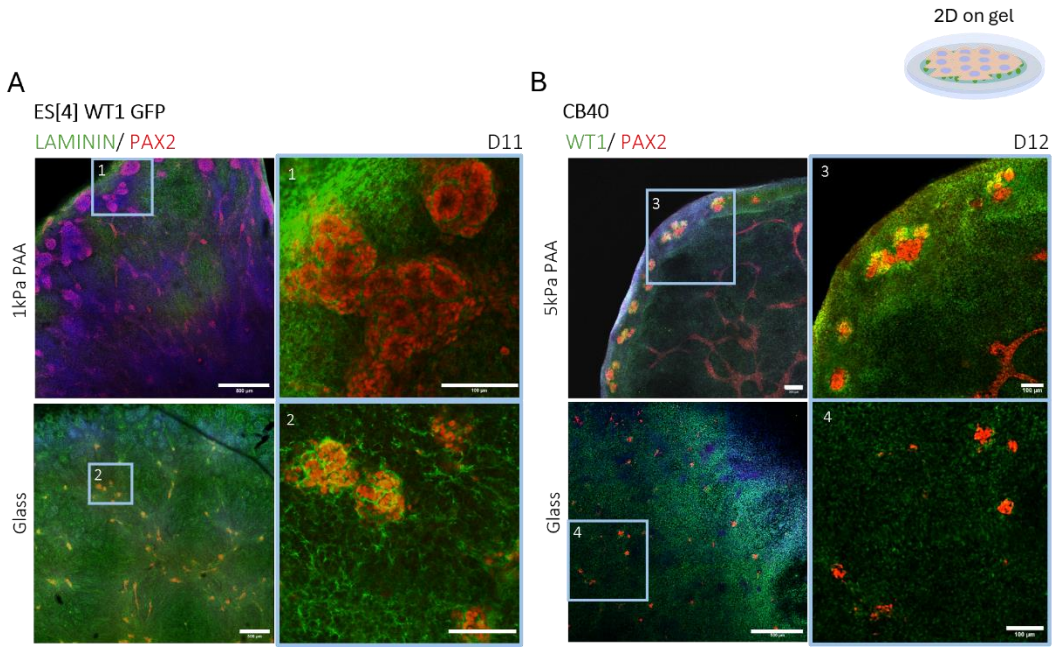

Figure 11. Immunofluorescence staining of 2D differentiation of kidney progenitors on PAA gels. A) ES[4]-WT1-GFP derived 2D kidney differentiation at D11 on 1kPa PAA (top) and glass (bottom). Staining for *LAMININ* in green and *PAX2* in red, scale bar 500µm (left images). Light blue boxes indicate magnified images, scale bar 100µm (right images). B) CB40 derived 2D kidney differentiation at D12 on 5kPa PAA (top) and glass (bottom). Staining for *WT1* in green and *PAX2* in red, scale bar 200µm (top) and 500µm (bottom). Light blue boxes indicate magnified images, scale bar 100µm (right images).

At later stages, more complex nephron-like structures, such as proximal tubule segments (as demarked by *WT1*), medial tubule segments (as demarked by *JAG1*) and distal tubule segments (as demarked by *E-CADHERIN*) could be observed in CB40 background cells on 1kPa PAA at D15 of differentiation (Figure 12A). Unfortunately, we observed that 2D kidney differentiation monolayers tended to detach from the PAA substrates when maintained over long periods of time. Unlike on PAA however, ES[4]-WT1-GFP 2D kidney differentiation could be maintained on glass for up to 21 days (Figure 12B).

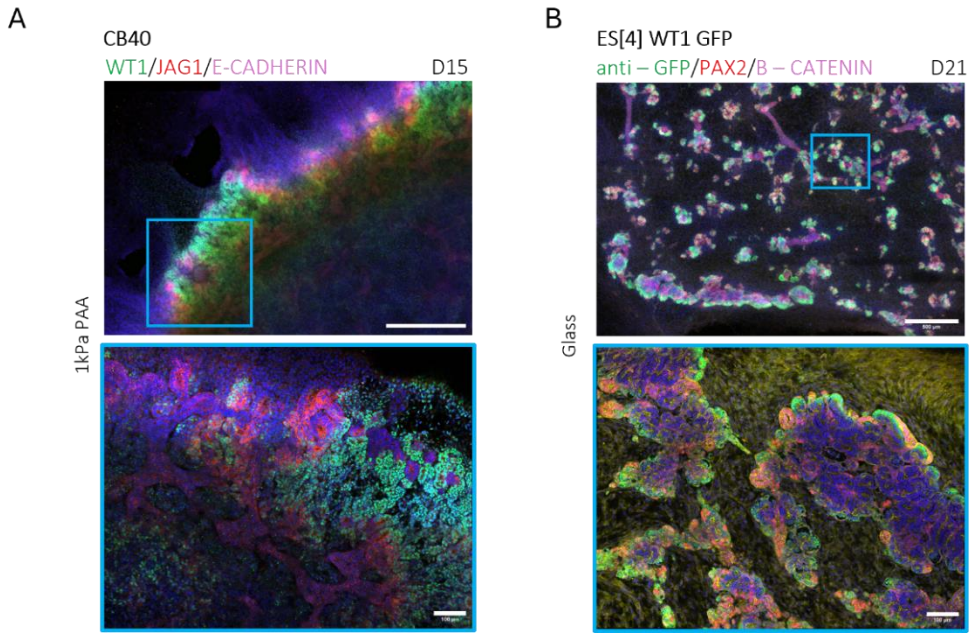

Figure 12. Immunofluorescence staining of 2D differentiation of kidney progenitors on PAA gels and glass at later stages. A) CB40 derived 2D kidney differentiation at D15 on 1kPa PAA gel. Staining for *WT1* in green, *JAG1* in red and *E-CADHERIN* in magenta scale bar 500µm. Light blue box indicates magnified image, scale bar 100µm. B) ES[4]-WT1-GFP derived 2D kidney differentiation at D21 on glass. Staining for *anti-GFP* in green, *PAX2* in red and *B-CATENIN* in magenta, scale bar 500µm. Light blue boxes indicate magnified images, scale bar 100µm.

A diverse array of *in vivo* processes, encompassing cell differentiation, morphogenesis, and migration, are orchestrated by forces generated by the cells themselves. Traction force microscopy (TFM) has emerged as a prominent technique within the spectrum of methods used to assess cellular mechanics. Standard TFM protocols rely on fiducial markers embedded within the extracellular environment to quantify the deformations induced by cellular forces. Traditionally, fluorescent microbeads served as these fiducial markers. However, recent advancements highlight the advantages of employing fluorescently labelled DNA structures. These DNA markers offer a diminished size compared to beads and the potential for customization, enabling the extraction of orthogonal information and the realization of switchable surface functionalization for further analysis. (Juskowiak, 2011; Prahl, Porter, et al., 2023). Here, we made use of the amenability of PAA hydrogels and incorporated fluorescent microbeads for measuring displacements and inferring traction

forces exerted by cells upon the gel (Figure 13A). Brightfield microscopy allowed the visualization of emerging RVs and CSBs in ES[4]-WT1-GFP and CB40 background 2D kidney differentiation (Figure 13B), while confocal imaging of the fluorescent enabled the measurement of traction forces surrounding such structures on 1kPa PAA (Figure 13C). Briefly, to be able to infer traction forces from the displacement field of fluorescent microbeads, we compare confocal z-stack images of the beads in the presence of cells and the same regions after trypsinization. This allows the comparison of bead displacement and by using particle image velocimetry (PIV), the substrate deformations can be calculated. Here, a finite element method is used to calculate traction fields (Figure 13C). As such, it was possible to observe the displacements of beads in z (Figure 13C middle panel) and the corresponding tractions indicating a pushing down force on the substrate (Figure 13C right panel), in the region which correlated with a vesicle like structure by brightfield microscopy (Figure 13C left panel). While such preliminary force measurements could hint at some mechanical activity around RV emergence, the technical difficulties of maintaining long term 2D kidney differentiation on PAA gels and imaging multi-cell-layer structures by brightfield microscopy resulted in a low throughput and reproducibility of such experiments.

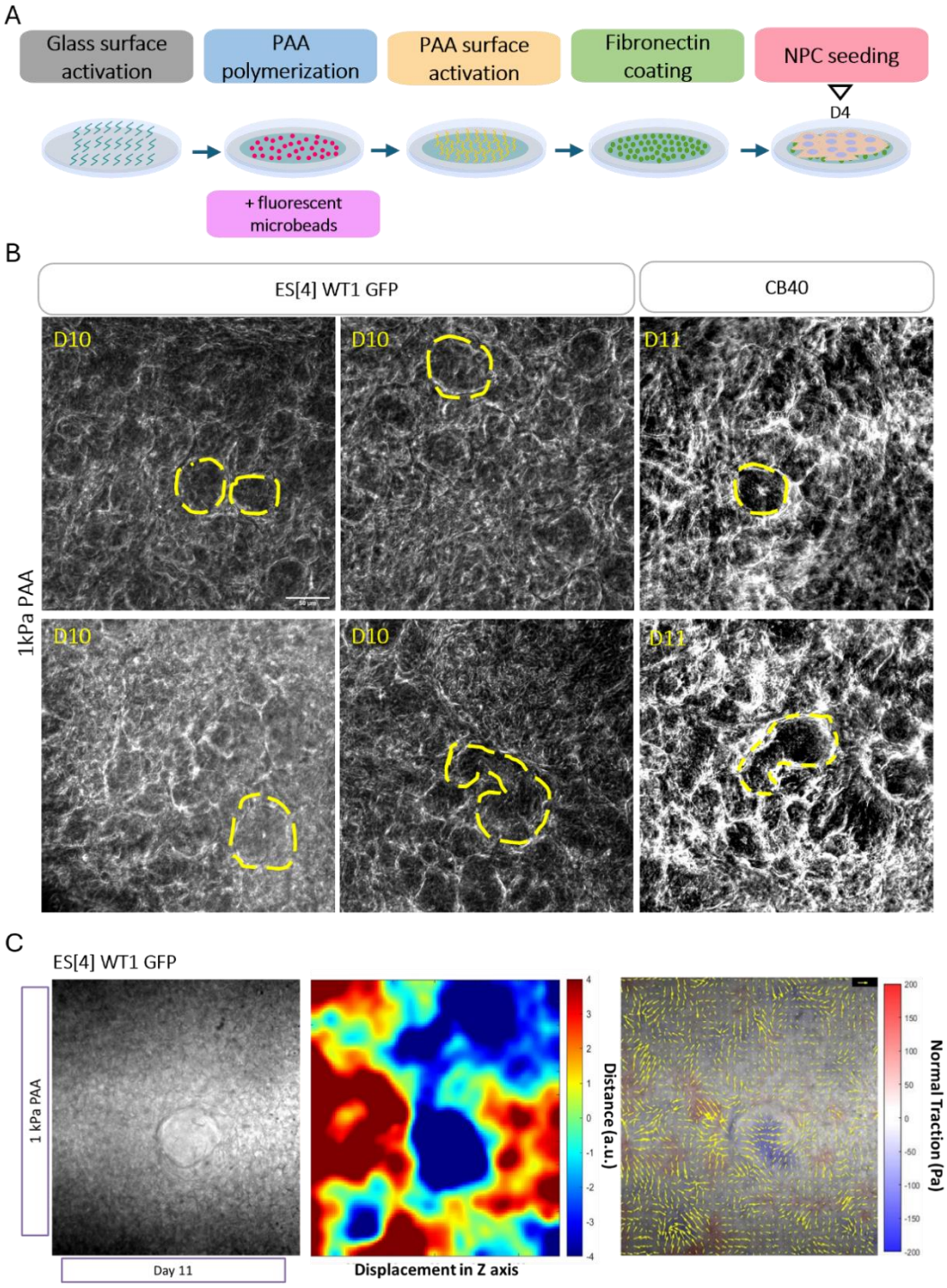
A
Glass surface activation
PAA polymerization
PAA surface activation
Fibronectin coating
NPC seeding
D4
+ fluorescent microbeads
B
ES[4] WT1 GFP
CB40
D10
D10
D11
1kPa PAA
D10
D10
D11
C
ES[4] WT1 GFP
1 kPa PAA
Day 11
Displacement in Z axis
Distance (a.u.)
Normal Traction (Pa)

Figure 13. Measuring traction forces in 2D kidney differentiation on Polyacrylamide (PAA) gels. A) Schematic representation of steps for glass surface activation, PAA polymerization with fluorescent microbeads, PAA surface activation, fibronectin coating and NPC seeding. B) Brightfield images of ES[4]-WT1-GFP and CB40 derived 2D kidney differentiation at D10 and 11 on 1kPa PAA gels. Yellow dashed lines indicate RVs and CSBs observable by brightfield microscopy, scale bar 50µm. C) Preliminary traction measurements of a RV identified by brightfield imaging (left panel), displacements in Z-axis (middle panel) and normal tractions (right panel).

2D differentiation on Polydimethylsiloxane (PDMS) substrates

Like PAA, soft PDMS can also be fabricated to a stiffness value of 3kPa, while maintaining its elasticity, making it a suitable candidate for 2D differentiation and traction force measurements (Figure 14A) (Bergert et al., 2016). RV clusters (demarked by *PAX2* and *WT1* expression) could be observed in CB40 2D kidney differentiation cultures on 3kPa PDMS at D12 of differentiation (Figure 14B). Higher levels of mRNA expression of *LHX1, WT1, PAX2* and *E-CADHERIN* (markers of early RVs and MET) were observed in CB40 kidney differentiation on 3kPa PDMS compared to conventional tissue culture plastic as detected by the RT-qPCR (Figure 14C). This hints at the capability of soft substrates, such as 3kPa PDMS at promoting NPC differentiation towards RV fate.

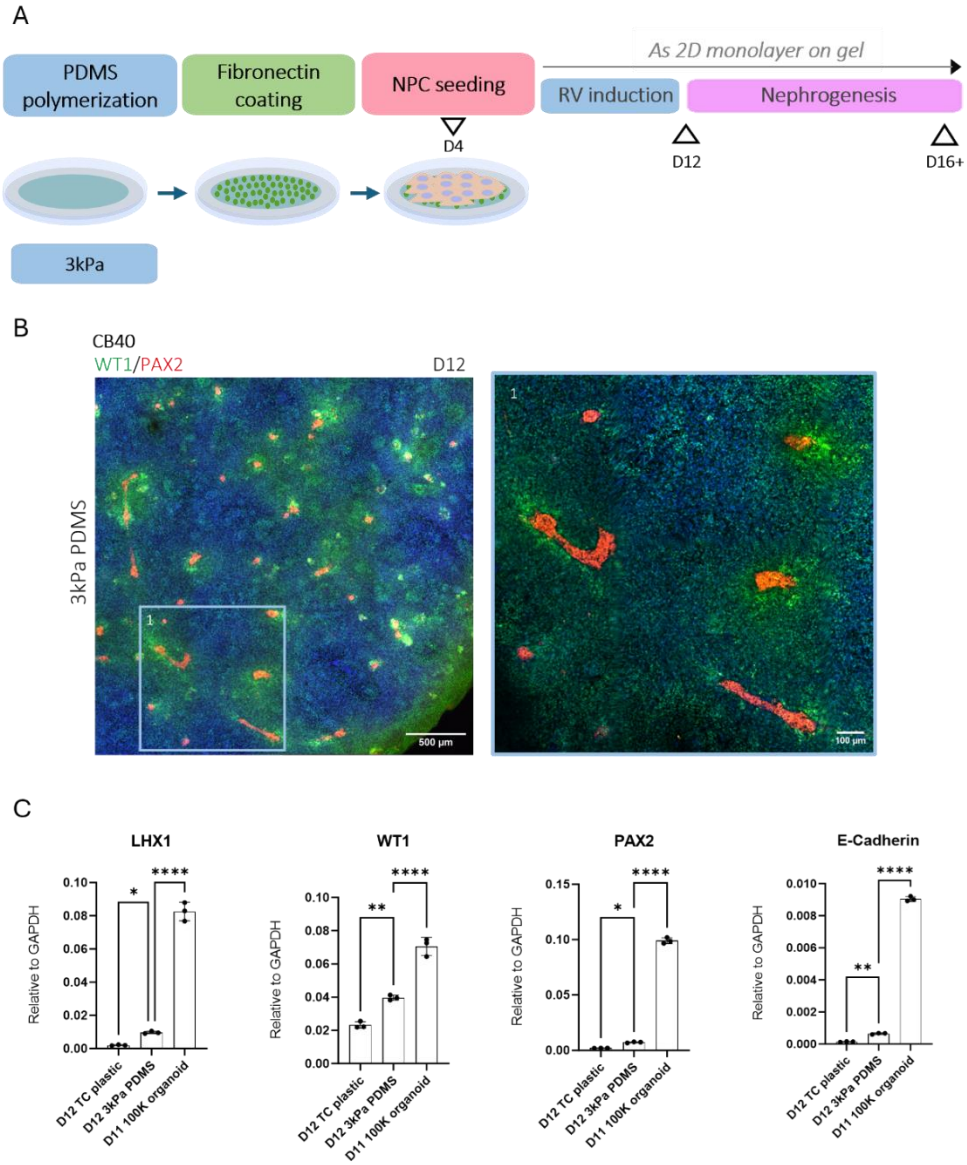

Figure 14. 2D differentiation on Polydimethylsiloxane (PDMS) substrates. A) Schematic representation of steps for PDMS polymerization, fibronectin coating and NPC seeding, followed by 2D kidney differentiation on PDMS substrates. B) CB40 derived 2D kidney differentiation at D12 on 3kPa PDMS, staining for *WT1* in green and *PAX2* in red, scale bar 500µm. Light blue box indicates magnified image, scale bar 100µm. C) qPCR results of CB40 derived kidney differentiation in three conditions: cultured on tissue culture plastic, cultured on 3kPa PDMS and cultured as 100K 3D spheroids. Expression of *LHX1*, *WT1*, *PAX2* and *E-CADHERIN* at D12/11 of differentiation, n=3 technical replicates from 1 biological experiment.

Presenting physical constraints onto 2D NPC differentiation

Unlike PAA gels, soft PDMS is compatible with photopatterning through the technology from Alveole Lab (PRIMO) (Strale et al., 2016b). By taking advantage of a passivating compound, photo-initiator agent, and UV illumination, 3kPa PDMS substrates could be photopatterned into circles (300µm diameter), squares and triangles of equal area coated with fibronectin (Figure 15A). NPC at D4 of differentiation could then be seeded onto the photopatterned PDMS substrates (Figure 15B and C).

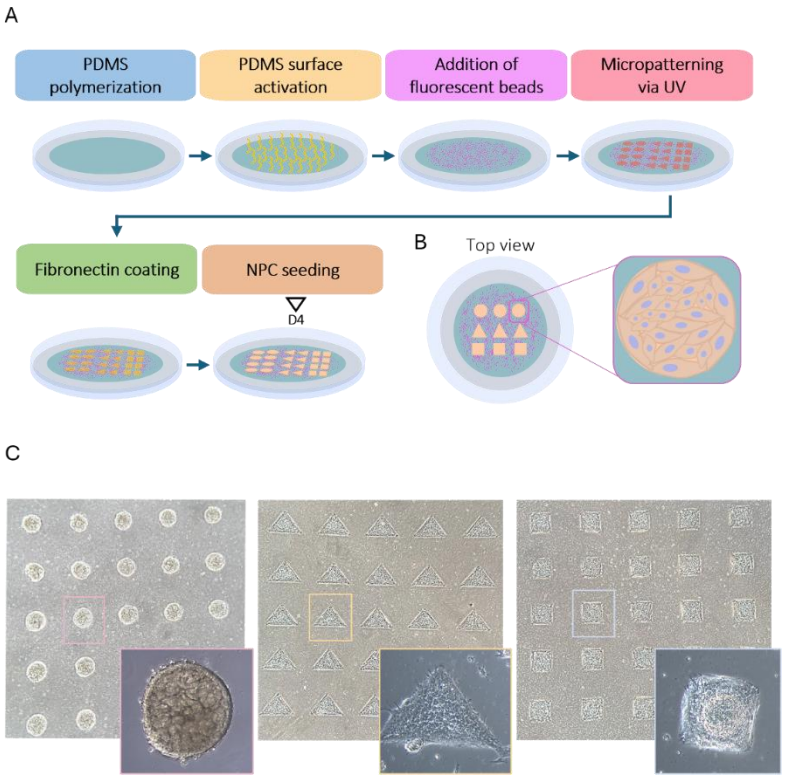

Figure 15. Micropatterning on PDMS substrates. A) Schematic representation of steps PRIMO photopatterning: PDMS polymerization, PDMS surface activation, addition of fluorescent microbeads, micropatterning via UV illumination, fibronectin coating and NPC seeding. B) Schematic representation of top view of 2D kidney differentiation on micropatterned PDMS substrates. C) Brightfield microscopy images at 4x magnification of 2D kidney differentiation micropatterned onto circles, squares, and triangles. Pink, yellow, and blue squares represent magnified images.

To further investigate the effect of physical constraints on 2D NPC differentiation towards RVs and further nephron like structures, CB40 – derived NPCs were seeded onto 3kPa PDMS substrates micropatterned with 300µm diameter circular geometries and observed by brightfield microscopy until D11 of differentiation. RV emergence could be observed as early as D8 of differentiation, and by D11 larger, elongated structures could be observed (Figure 16). Immunofluorescence staining confirmed the presence of *WT1* and *PAX2* expressing clusters at D8 of differentiation, and their evolution to elongated tubular structures by D11 (Figure 17). Distal tubular-like structures (demarked by *E-CADHERIN)* could be observed at D11 of differentiation on micropatterned 3kPa PDMS substrates (Figure 17). Interestingly, relative consistencies in the appearance and expression of *WT1, PAX2* and *E-CADHERIN* could be observed between the individual patterns of each time point. This points to the self-organization capacity of NPCs and their amenability to be guided to differentiation by geometry.

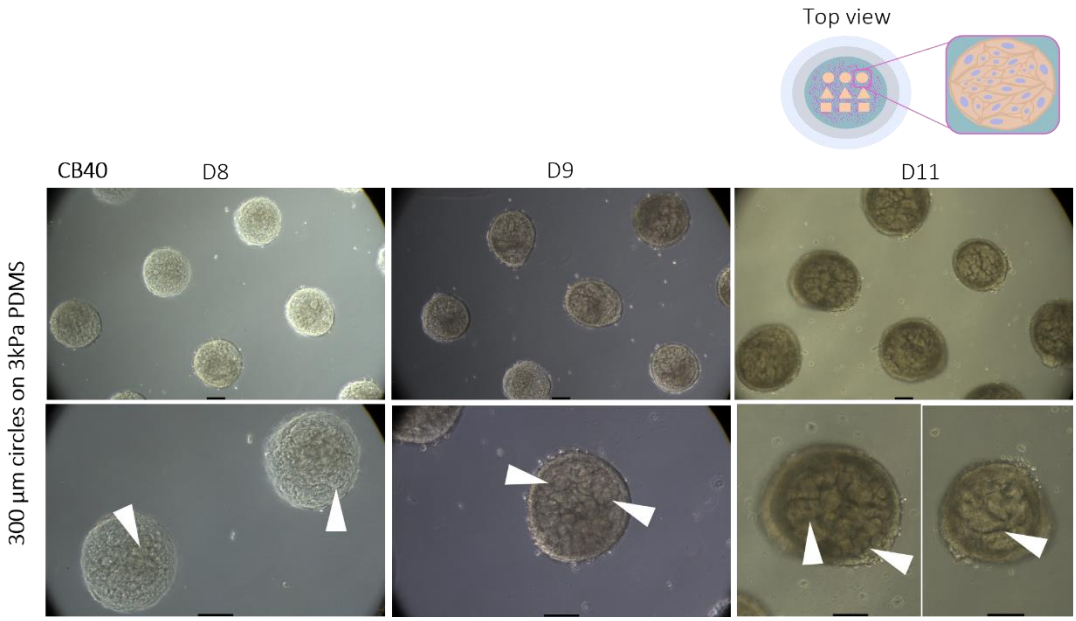

Figure 16. 2D kidney differentiation on micropatterned 3kPa PDMS substrates. CB40-derived kidney differentiation over D8, D9 and D11 of culture on 300µm diameter circles. White arrowheads point towards emerging RVs at D8 and 9, and towards more complex structures at D11. Scale bar 100µm.

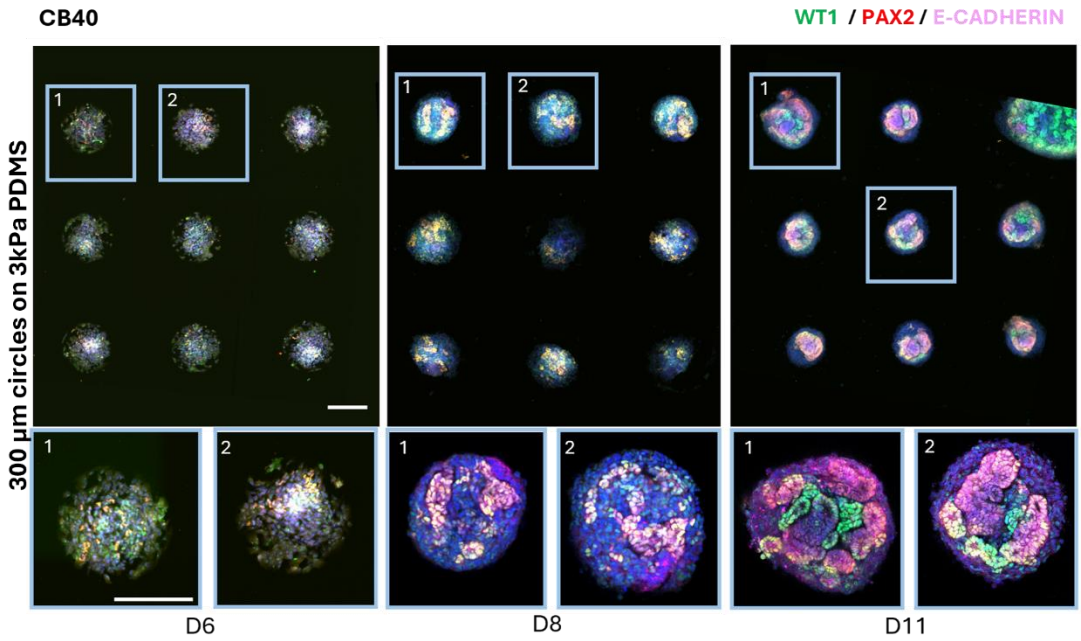

Figure 17. Immunofluorescence images of 2D kidney differentiation on micropatterned 3kPa PDMS substrates. CB40-derived kidney differentiation over D6, D8 and D11 of culture on 300µm diameter circles. Staining for *WT1* in green, *PAX2* in red and *E-CADHERIN* in magenta. Light blue boxes indicate magnified images. Scale bar 100µm.

The elastic nature of soft 3kPa PDMS and the presence of fluorescent microbeads on the surface of the substrate allowed for traction measurements to be performed in the micropattern confinement setting (Figure 18). To gain a better resolution and visualization of the structures during 2D differentiation, cells were labelled with Flipper TR – a membrane tension marker used here simply for the purpose of fluorescence imaging (as demonstrated by the Morizane lab for live imaging of kidney tubule like structures). The marker was useful in visualizing the 2D micropatterned organoid as a whole and sometimes in identifying rosette like structures within RVs (Figure 18A), while measuring tractions in three dimensions (Figure 18B and C). However, the Flipper TR membrane marker was non-specific, therefore could not provide accurate information on cell identity during differentiation, nor could it allow for the resolution of forces of specific structures / cell clusters.

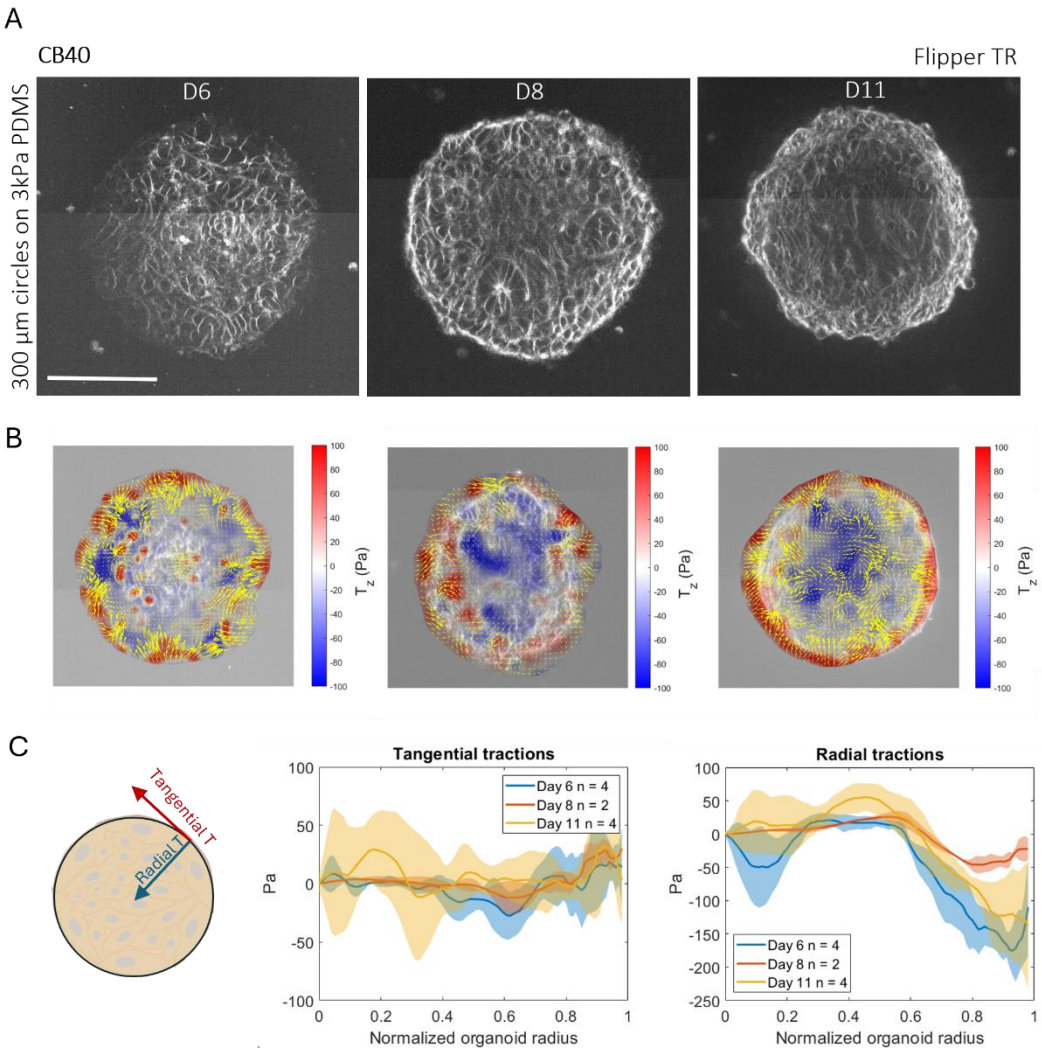

Figure 18. Traction force measurements on micropatterned 3kPa PDMS substrates. A) CB40 derived 2D kidney differentiation stained with Flipper TR membrane tension marker at D6, D8 and D11. B) Traction maps of Z tractions at D6, D8 and D11 of differentiation, blue and red indicate inward and outward forces, yellow vectors represent tractions. C) schematic representation (left) of tangential (middle) and radial (right) tractions in micropatterned circles on 3kPa PDMS substrates over D6, D8 and D11 of differentiation. Scale bar 100µm.

The traditional traction force microscopy approach (shown in Figure 18 and as described earlier) relies on the calculation of displacements of fluorescent microbeads between confocal images of a ¨stressed state¨ (when cells are exerting forcing onto the gel) and a ¨relaxed state¨ (when cells are then trypsinized and the gel is released to its original elastic state). This method, therefore, relies on a live imaging marker or reporter that could demark the cells of interest, to be able to correlate force measurements with cell identity.

In this thesis, a different approach to traction force microscopy was undertaken. By taking advantage of the high-resolution micropatterning capabilities of PRIMO, it was possible to create annotations for each micropatterned circle and to label them with fluorescent fibronectin (Figure 19A and B). This quickly made each 2D micropatterned kidney differentiation traceable and allowed the imaging of the ¨relaxed state¨ of the gel prior to the seeding of the NPCs (Figure 19C, D and E). This adaptation no longer required the trypsinization of cells, allowing us to fix them and perform immunofluorescence staining (see example in Figure 19F). This approach has opened the possibility of directly correlating traction measurements and cell cluster identity without requiring live fate reporters (see representative example in Figure 19G).

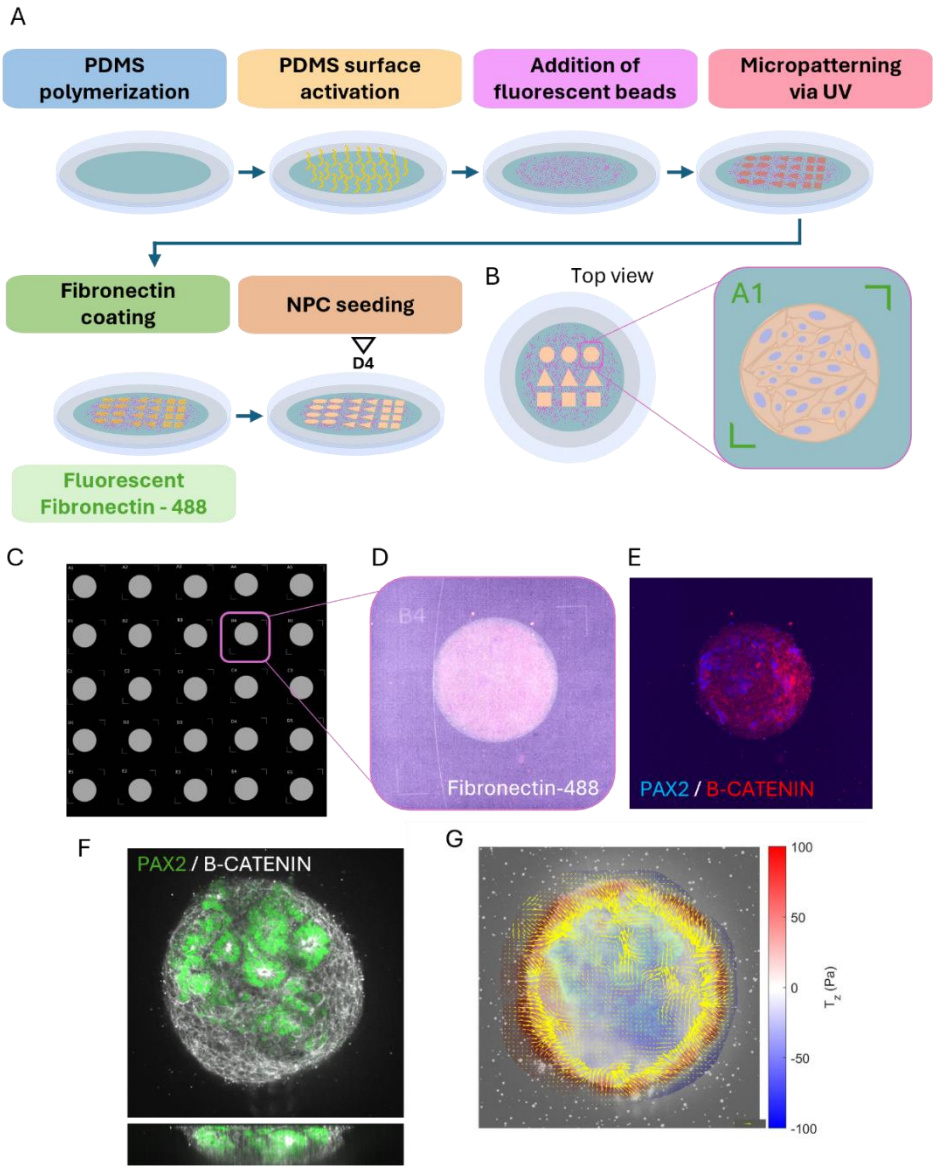

Figure 19. Annotated micropatterning on PDMS substrates. A) Schematic representation of steps of PRIMO photopatterning: PDMS polymerization, PDMS surface activation, addition of fluorescent microbeads, micropatterning via UV illumination, fluorescent fibronectin coating and NPC seeding. B) Schematic representation of top view of 2D kidney differentiation on annotated micropatterned PDMS substrates. C) Overview of annotations on 5x5 circular micropatterns. D) Example of fibronectin labelled annotations, overlayed on top of IF image of 2D kidney differentiation (see E) labelled with *PAX2* in blue and *B-CATENIN* in RED. F) Immunofluorescence representation of stained micropatterned 2D kidney differentiation, *PAX2* in green and *B-CATENIN* in white. G) Example of traction map of traction in Z overlayed on top of IF image of 2D kidney differentiation (see F).

Chapter 2.

2D micropatterned differentiation of wild type and CAKUT knockout NPCs

The 2D micropatterning set-up described in *Chapter 1* allowed us to start monitoring the emergence and differentiation of RVs towards nephron like structures and observing their response to the mechanical microenvironment through different quantitative and qualitative approaches. To further assess the potential role of mechanobiology in RV emergence and differentiation, we exploited the true potential of hPSCs, which are their inherent differentiation capacity and amenability towards genome editing. To this aim, hPSC lines carrying knock-out mutations for genes important in kidney development (such as *PAX2* and *LHX1*) were investigated [lines previously developed and characterized in (Aspiroz, 2021; Gimenez, 2021)]. The Monserrat laboratory has previously established and characterized the phenotypes of hPSC-derived kidney organoids carrying mutations in *PAX2* or *LHX1* via CRISPR/Cas9 technology. The use of non-inducible Cas9 in hPSCs has given the possibility to elucidate the role of a particular gene in both pluripotency and differentiation(Aspiroz, 2021; Gimenez, 2021).

In both backgrounds, the hPSCs were able to correctly establish posterior intermediate mesoderm (PIM) commitment. At the renal vesicle emergence stage, NPCs of the PAX2 KO background were able to self-organize into renal vesicles, which resulted in the correct formation of several glomerular like structures. However, in the PAX2 KO background, a complete disruption of distal tubulogenesis was observed (Aspiroz, 2021). In the background of LHX1 KO NPCs, there was a complete disruption of RV formation at the RV stage, followed by an abolition of nephrogenesis all together (Gimenez, 2021).

The data presented in this chapter come from 2D kidney differentiation experiments in the 4 following cell lines: ES[4] (from now on termed ES[4] CTRL), ES[4] F51 iC2 LHX1 KO clone E4 (from now on termed LHX1 KO), ES[4] F51 iC2 PAX2 CTRL clone C5 (from now on termed PAX2 CTRL) and ES[4] F51 iC2 PAX2 KO clone B5 (from now on termed PAX2 KO).

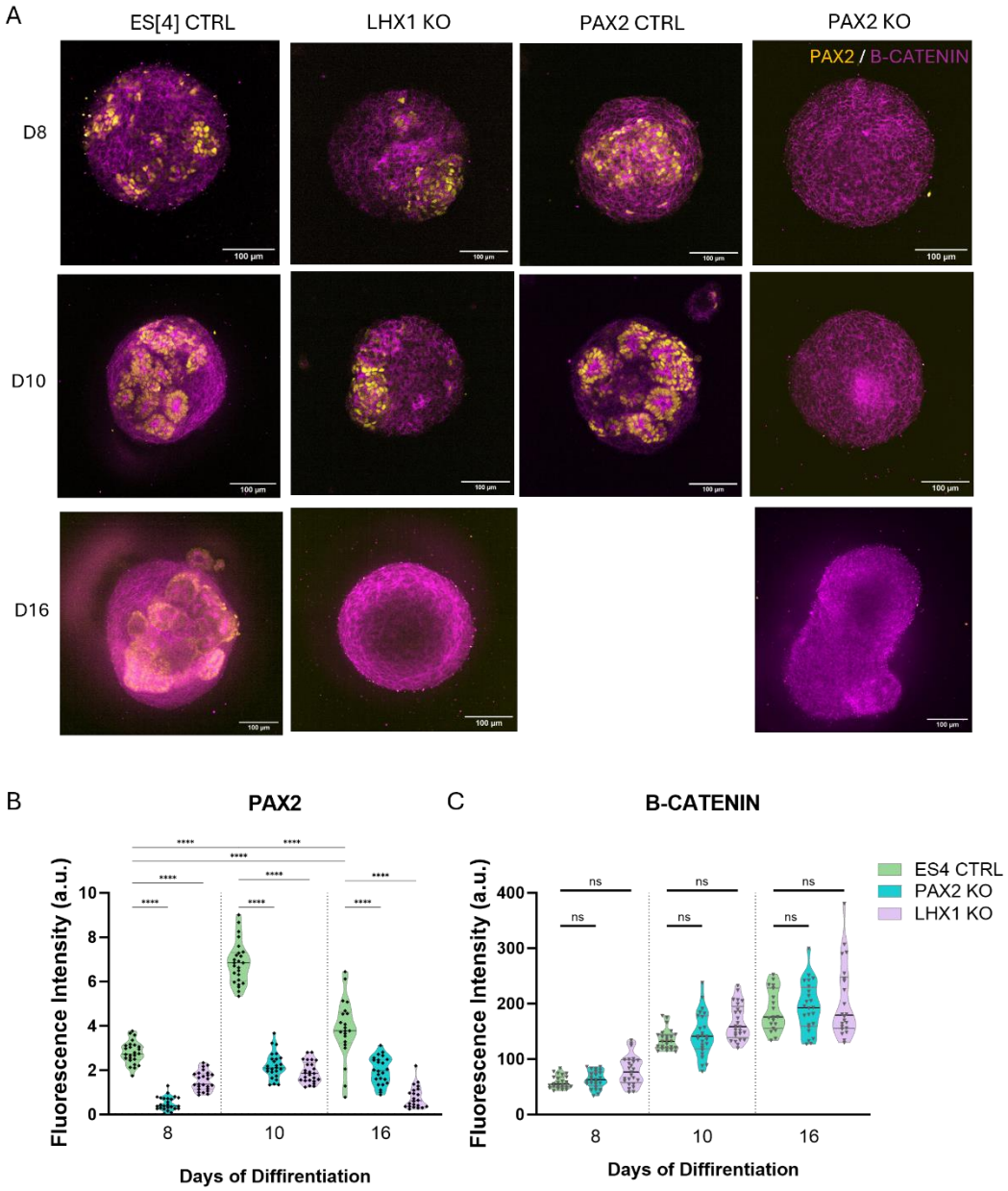

Figure 20. 2D differentiation of ES[4] CTRL, LHX1 KO, PAX2 CTRL and PAX2 KO lines on 300 µm circle micropatterned 3kPa PDMS. A) Representative immunofluorescence staining images of D8, D10 and D16 samples. *PAX2* in yellow, *B-CATENIN* in magenta. Scale bar 100 µm. Average fluorescence intensity measurements of B) *PAX2* and C) *B-CATENIN*, normalized by z slice and background intensity values. Images and data represent N=3 biological experiments with 20-25 micropatterns per experiment, across all cell lines, except PAX2 CTRL (D8 and D10 data only from N=1 biological experiment). Statistical significance was determined by a two-way ANOVA test: **** P < 0.0001, *** P < 0.001, ** P < 0.01, * P < 0.05, ns > 0.05.

ES[4] CTRL, LHX1 KO, PAX2 CTRL and PAX2 KO hPSCs were subjected to 2D kidney differentiation following the different procedures established and described in *Chapter 1,* with a particular focus on the use of soft (3kPa) PDMS substrates micropatterned with 300 µm diameter circles (Figure 20). To assess mechanical properties of mesenchymal renal progenitor cells in the establishment of RV (D8-D10) and the subsequent generation of nephron-like structures (D14-D16), traction forces were measured on D8, 10 and 16 of differentiation. Immunofluorescence microscopy was further used to correlate potential changes in traction force generation with the expression and localization of *PAX2* and B-*CATENIN* at the indicated time points.

As described in the introduction, *PAX2* is a key kidney developmental gene, expressed throughout differentiation, playing a critical role in mesenchymal to epithelial transition of NPCs, their further evolution into nephron like structures, and the outgrowth of the ureteric bud (Brophy et al., 2001; Dressler et al., 1990; Torres et al., 1995). Early kidney development involves the formation and caudal extension of the nephric duct (Wolffian duct), followed by the subsequent branching of the ureteric bud. Studies in Pax2 null mice reveal a disruption in the epithelial integrity of the nephric duct, potentially hindering the proper formation of the ureteric bud. This compromised ureteric budding is hypothesized to be a contributing factor to the kidneys agenesis observed in Pax2 null mice (Brophy et al., 2001).

Interestingly, in the context of hPSC-derived kidney organoids, *PAX2* has been shown to be dispensable during nephron differentiation (Kaku et al., 2017). Given these interesting previous *in vivo* and *in vitro* findings regarding *PAX2* deficiencies, and the incidences of *PAX2* associated CAKUT cases in humans, we made use of *PAX2* as a readout marker for our study.

At the same time, studies have demonstrated that MET of NPCs and induction of renal vesicles is dependent on Wnt/β-catenin signalling. Genetic removal of β-catenin activity from the mesenchymal progenitors in mice resulted in a blockade of RV emergence, while a genetic stabilization in the same progenitors resulted in an ectopic expression of *Fgf8, Pax8, Wnt4* (early inductive markers), functionally replacing the need for *Wnt9b* and *Wnt4* signalling form the ureteric bud *in vivo* (Lindström et al., 2015; Park et al., 2007; Schmidt-Ott & Barasch,

2008). At the same time, stabilization of β-catenin has been associated with an expanded NPC population and arrested MET, resulting in the formation of Wilms Tumour (WT) (Drake et al., 2020). Overall, canonical Wnt signalling (mediated by β-catenin) is both necessary and sufficient for initiating and maintaining inductive pathways during nephron differentiation. For these reasons, we also made use of *B-CATENIN* as a readout marker for our study.

In wildtype hPSC-derived 2D kidney differentiation on micropatterned PDMS, *PAX2* is present throughout the entire nephrogenesis process, and *B-CATENIN* is highly expressed in the apical sides of RVs and forming nephron like structures (Figure 20A). In the two control cell lines *PAX2* expression could be observed starting from D8 of differentiation and at D10 lumen containing RVs were seen, as demarked by *PAX2* and rosette-like structures demarked by *B-CATENIN* (Figure 20A). By D16, elongated tubular-like structures could be observed. In LHX1 KO circles at D8 and 10 of differentiation, clusters of *PAX2* positive cells were observed along the edges of the patterns and reduced their expression by D16 (Figure 20A). In PAX2 KO patterns, *PAX2* expression was not observed, with the exception of 1 experiment (data not shown), where it was observed at low levels. In this regard, *in vivo* studies in mice and frog have demonstrated the redundancy of proteins in the Pax *(*pax*)* family during kidney development (Bouchard et al., 2002; Buisson et al., 2015). Indeed, in hPSC-derived kidney organoids, *PAX8* expression was identified in a subset of *PAX2* positive cells during the renal vesicle stage of differentiation (Kaku et al., 2017). Immunofluorescence staining demonstrated the presence of *PAX8* positive cells within RVs in *PAX2* mutant kidney organoids and supported speculations of the compensatory mechanisms by which MET transition could still occur in the KO conditions. Although not stained for in these experiments (Figure 20A), we speculate that in our system *PAX8* protein cross reactivity with the antibody used for *PAX2* could explain the expressions observed in *PAX2* KO hPSC-derived differentiation (Figure 20B). *B-CATENIN* expression remained unchanged in all cell lines and grew equally over time (Figure 20B).

Traction measurements were taken at D8, D10 and D16 in the four cell lines (except for PAX2 CTRL D16). From traction maps, average strain energies were calculated and compared among samples, indicating the total energy

transferred by the cells on their underlying substrate (Figure 21). For comparative analysis, a total of N=3 biological experiments (with n=15-25 technical replicates per experiment) were used. At D8 strain energies were similar among all samples, and the differences between control and KO cell lines were non-significant (Figure 21A (top panel) and B). In the ES[4] CTRL background strain energies were significantly increasing over time (by D10 and D16). Interestingly, at D10 of differentiation, strain energies measured in the LHX1 KO background were significantly lower compared to ES[4] CTRL D10, seemingly maintaining the same levels as D8 samples (Figure 21B), overall highlighting that LHX1 expressing cells do have a role in RV emergence. Samples of the PAX2 KO background, on the other hand, at D10 of differentiation demonstrated similar levels of strain energy, being non-significantly different from PAX2 CTRL, overall highlighting that indeed, *PAX2* seems to be dispensable during RV formation (Kaku et al., 2017). At D16 however, both LHX1 KO and PAX2 KO background samples displayed equal levels of strain energies, significantly lower than in ES[4] CTRL samples, overall suggesting that RV emergence and subsequent differentiation into nephron like structures is indeed a mechanically active process, in which *LHX1* and *PAX2* play a vital role.

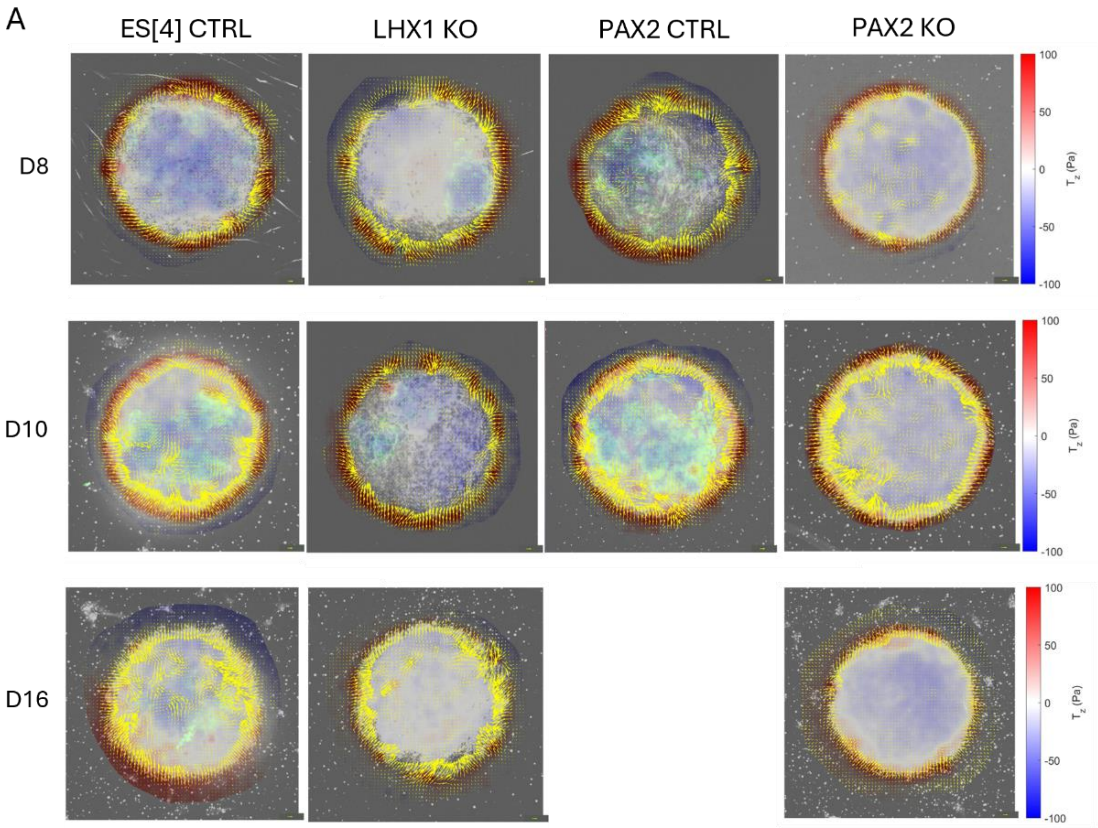
A
ES[4] CTRL
LHX1 KO
PAX2 CTRL
PAX2 KO
D8
D10
D16
100
50
0
-50
-100
T_z (Pa)

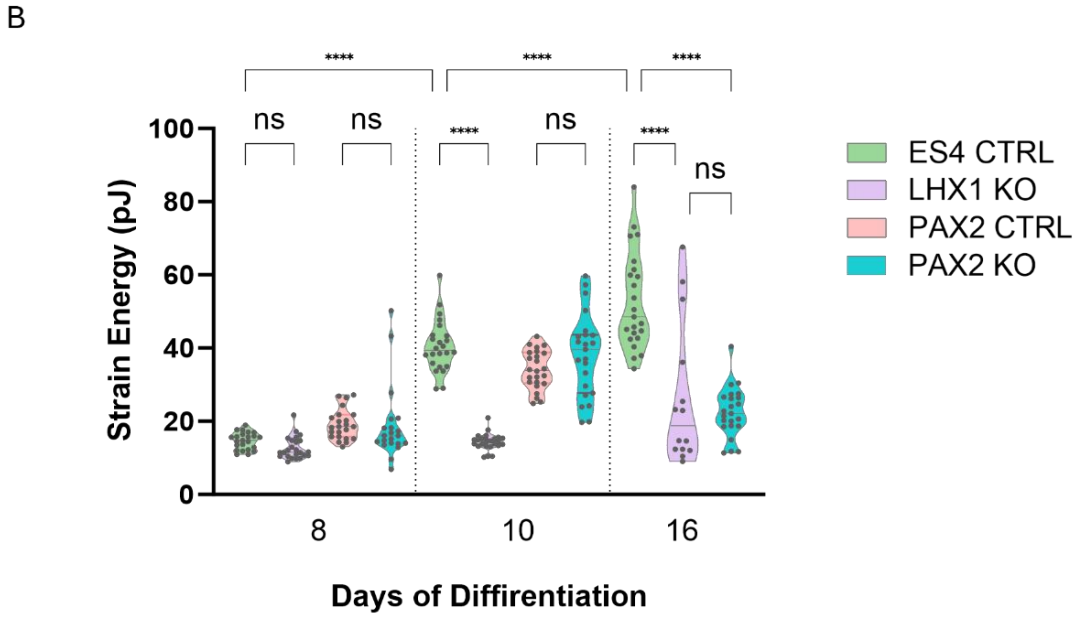
B
Strain Energy (pJ)
Days of Diffirentiation
ns
****
8
10
16
ES4 CTRL
LHX1 KO
PAX2 CTRL
PAX2 KO

Figure 21. Measurement of traction forces in ES[4] CTRL, LHX1 KO, PAX2 CTRL and PAX2 KO lines on 300 µm circle micropatterned 3kPa PDMS. A) Representative images of traction maps in z across D8, D10 and D16 of differentiation. Yellow vectors represent components tangential to the substrate, and the colour map represents vectors normal relative to the substrate. *PAX2* in green can be seen underneath the maps. B) Average strain energy measurements taken across 4 cells lines and 3 time points, from 3 biological experiments with 20-25 technical replicates per experiment (except for LHX1 KO and PAX2 KO D16 – N=2 experiments, and PAX2 CTRL D8 & D10 – N=1 experiment). Statistical significance was determined by a two-way ANOVA test: **** P < 0.0001, *** P < 0.001, ** P < 0.01, * P < 0.05, ns > 0.05.

At closer observation of traction measurements at D10 of differentiation, we noticed that there were rotational patterns present in the system, reminiscent of vortices commonly observed in turbulent fluids. Indeed, such mesoscale cell turbulences had been previously observed in other cell monolayer systems (S. Z. Lin et al., 2021).

To characterize vorticity, we computed the curl of traction fields as:

$$curl\ \vec{T} = \nabla \times \vec{T} = \frac{\partial T_y}{\partial x} - \frac{\partial T_x}{\partial y}$$

Taking inspiration from research in active matter and nematics (Guillamat et al., 2017), we made use of a mathematical criterion based on velocities and applied it to the traction vector fields. Briefly, by using the Okubo-Weiss parameter, $OW = \partial_x T_x{}^2 + \partial_y T_x * \partial_x T_y$, we could identify the areas of vortices and plot them on top of the rotations maps (Figure 22A).

Similar to the measurements of strain energies, mean traction curls displayed no differences among samples at D8 of differentiation (Figure 22B). At D10, however, significant differences were observed between the control and knock-out samples: LHX1 KO and PAX2 KO derived samples displayed weaker curls than their corresponding ES[4] CTRL and PAX2 CTRL samples. In the control background, mean curls grew from D8 until D10, after which there were no significant changes observed.

These results have suggested that RV emergence from hPSC-derived NPCs is a mechanically active process. Moreover, in the background of CAKUT-related mutations, mechanical forces arising in the system seem to be diminished, in direct relation to extent and capability of renal differentiation.

In 3D kidney organoids derived from the PAX2 KO background, RVs have been shown to be present at D12 of differentiation (RV emergence stage in 3D) and by D20 3D kidney organoids presented with few glomerular like structures and an absence of LTL positive proximal tubule segments (Aspiroz, 2021). Traction force measurements show that in terms of strain energies, PAX2 KO samples behave similar to control differentiation at time points of RV emergence (D10 in this system) and are reduced towards later stages of differentiation (Figure 21B).

In 3D kidney organoids of the LHX1 KO background, a complete abolition of nephrogenesis has been previously described (Gimenez, 2021). Indeed, the most drastic differences in total strain energy measurements in 2D, were also observed between ES[4] CTRL and LHX1 KO backgrounds. This further supports the idea that in the absence of nephrogenesis due to genetic aberrations, NPCs cannot exert any forces, meaning that RV emergence and nephrogenesis are mechanically active processes.

Moving forward, further experiments were conducted using only ES[4] CTRL and LHX1 KO backgrounds.

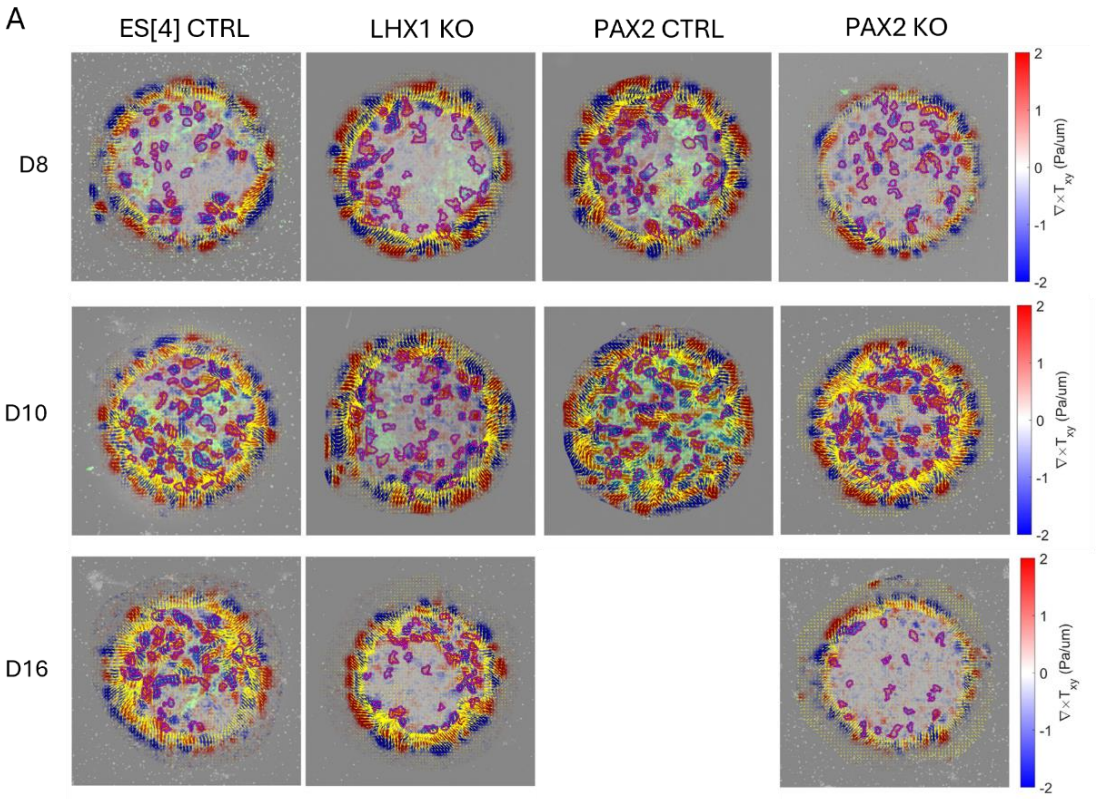
A
ES[4] CTRL
LHX1 KO
PAX2 CTRL
PAX2 KO
D8
D10
D16
2
1
0
-1
-2
∇×T_xy (Pa/um)

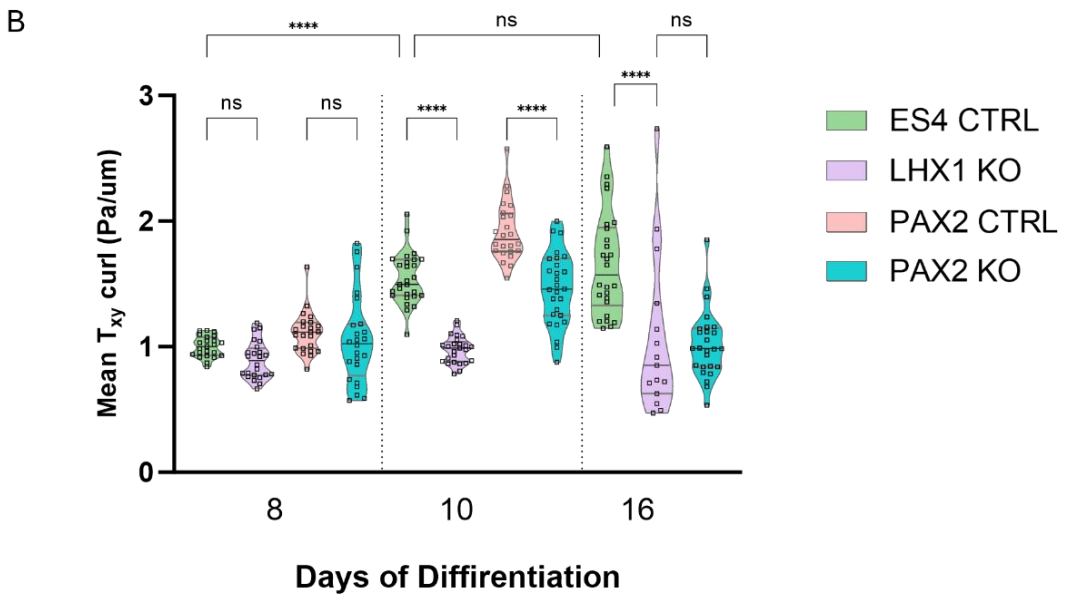
B
****
ns
ns
ns
ns
****
****
****
Mean T_xy curl (Pa/um)
3
2
1
0
8
10
16
Days of Diffirentiation
ES4 CTRL
LHX1 KO
PAX2 CTRL
PAX2 KO

Figure 22. Measurement of rotational movements in ES[4] CTRL, LHX1 KO, PAX2 CTRL and PAX2 KO lines on 300 µm circle micropatterned 3kPa PDMS. A) Representative images of rotation maps across D8, D10 and D16 of differentiation. Yellow vectors represent components tangential to the substrate, red represents clockwise rotational movements, blue represents counterclockwise rotational movements. *PAX2* in green can be seen underneath the maps. Pink highlighted regions represent vortices identified using the Okubo-Weiss parameter. B) Mean traction curl measurements taken across 4 cells lines and 3 time points, from 3 biological experiments with 20-25 technical replicates per experiment (except for LHX1 KO and PAX2 KO D16 – N=2 experiments, and PAX2 CTRL D8 & D10 – N=1 and N=2 experiments, respectively). Statistical significance was determined by a two-way ANOVA test: **** $P < 0.0001$, *** $P < 0.001$, ** $P < 0.01$, * $P < 0.05$, ns > 0.05

Exploring 2D kidney differentiation in ES[4] CTRL and LHX1 KO backgrounds on micropatterned 3kPa PDMS

Micropatterning by geometry allows a physical confinement of hPSCs cultured on substrates that support their differentiation and maintenance (Warmflash et al., 2014). Here, we further exploited this approach to externally modulate spatial polarization of cell-cell and cell-matrix adhesions, which has been previously shown to determine meso-endoderm differentiation patterns in hPSCs (Deglincerti et al., 2016). Indeed, this approach has also allowed for the mechanistic investigation of multiple hPSC-based developmental models (Karzbrun et al., 2021; Kaylan et al., 2018; Martyn et al., 2018; Xue et al., 2018).

By establishing a simple and robust method through the generation of 25-30 2D kidney differentiation micropatterns per sample, we aimed to establish an experimental model to investigate mesoderm renal progenitor organization and patterning during early steps of RV emergence and subsequent differentiation into nephron-like structures. To this aim, we explored immunofluorescence expression of key markers in RV emergence and differentiation, in the backgrounds of ES[4] CTRL and LHX1 KO hPSC lines between D8 and D16 of differentiation.

Overall, the 2D kidney differentiation set up on micropatterns of 3kPa PDMS supported kidney differentiation of the NPCs until D16 of differentiation, which will be discussed in detail further.

In the ES[4] background, from D8 until D10 of differentiation we observed the mesenchymal to epithelial transition of NPCs towards RVs (demarked by the expression of *PAX2, WT1* and *E-CADHERIN* in Figure 23A). At D10 of differentiation, we saw lumenized vesicle like structures, that by D14 of differentiation committed towards nephron like structures, as demarked by the expression of *WT1* in the proximal tubule like segments and podocyte-like cells, and *PAX2* and *E-CADHERIN* distal expression in emerging distal tubule like structures (Figure 23A). In general, from D8 until D16 of differentiation, we observed an increase in cell culture size (data not shown).

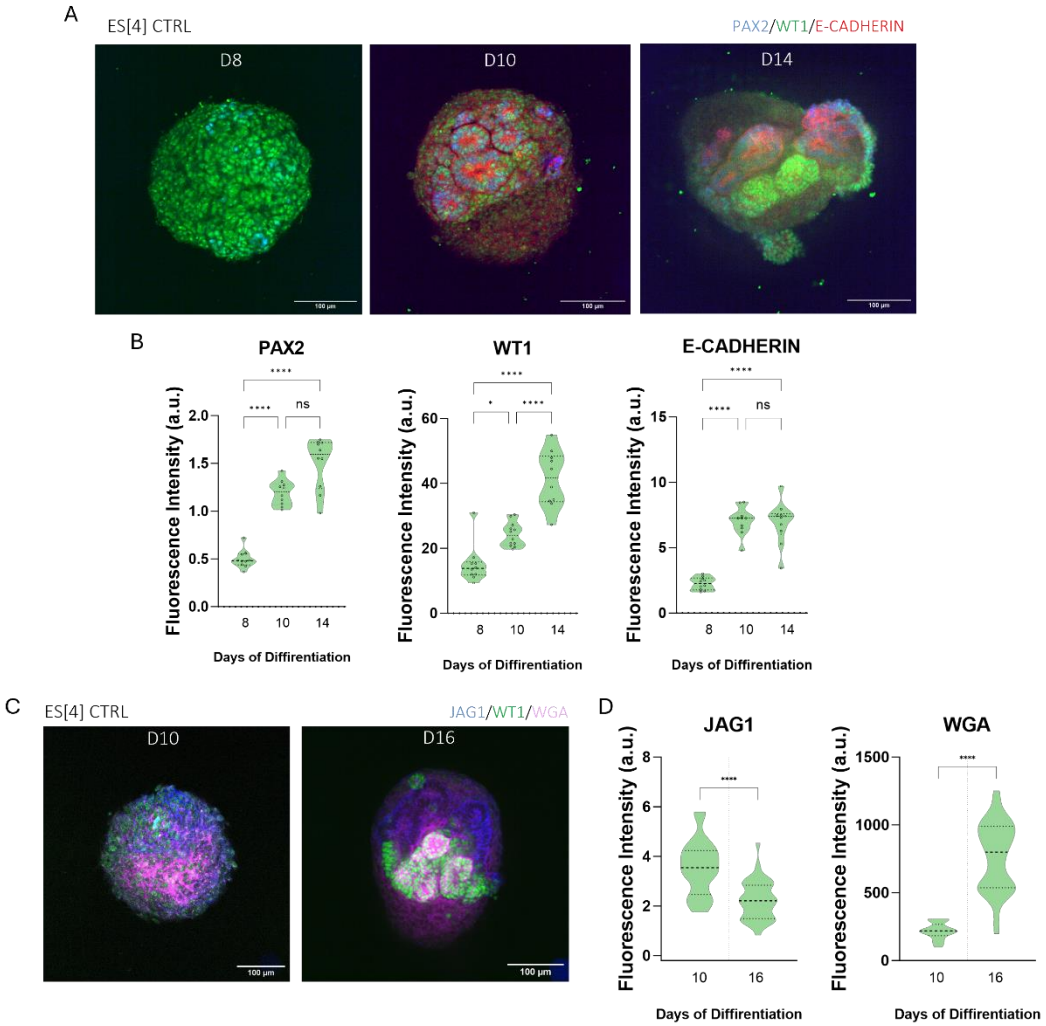

Figure 23. ES[4] CTRL 2D kidney differentiation on 300 µm circles micropatterned on 3kPa PDMS. A) Representative immunofluorescence images of at D8, D10 and D14 of differentiation. *PAX2* in blue, *WT1* in green and *E-CADHERIN* in red. Scale bar 100 µm. B) Average fluorescence intensity measurements of *PAX2*, *WT1* and *E-CADHERIN*, normalized by z slice and background intensity values. C) Representative immunofluorescence images of at D10 and D16 of differentiation. *JAG1* in blue, *WT1* in green and *WGA* in magenta. Scale bar 100 µm. D) Average fluorescence intensity measurements of *JAG1* and *WGA*, normalized by z slice and background intensity values. Images and data represent N=1 biological experiment with 15 micropatterns per experiment (B) and 10 micropatterns per experiment (D). Statistical significance was determined by an ordinary one-way ANOVA test: **** $P < 0.0001$, *** $P < 0.001$, ** $P < 0.01$, * $P < 0.05$, ns > 0.05.

When measuring the fluorescence intensity, we observed an increase in *WT1* expression over time: from RVs to proximal tubules and podocytes (Figure 23B). Similarly, we observed an increase of *PAX2* between D8 and D10 of differentiation: from RVs to becoming more distal. *E-CADHERIN* expression indicated mesenchymal to epithelial transition by D8 of differentiation. Studies have shown that *E-Cadherin* expression in mice, demarking the formation of mature epithelia, only occurs after the fusion of the RV to the ureteric tip, which occurs at late RV stages, after polarization. Then, as differentiation progresses, it obtains a more distal fate, being expressed solely in the distal segments of the nephron (Georgas et al., 2009). The increased expression of *E-CADHERIN* observed in the ES[4] CTRL background could indicate a transition towards mature epithelia over the course of differentiation (Figure 23B). Analysis of a medial marker of differentiation, such as *JAG1*, showed a switch between polarized RVs to segmented nephron like structures between D10 and D16 of differentiation (Figure 23C and D). Wheat germ agglutin (WGA), used as a tubule marker [as described previously in (Rizki-Safitri et al., 2022)], showed increased expressions towards late stages of differentiation, indicating an increase in tubule like structures (Figure 23C and D).

In the LHX1 KO background on the other hand, we observed an absence of RV formation at D10 and an absence of the formation of segmented nephron like structures, as demarked by *WT1, JAG1* and WGA (Figure 24A). We did not observe noticeable growth in the size of the cultures over differentiation time (data not shown). The average immunofluorescence intensity of the described markers was maintained constant throughout the entire differentiation (and lower in comparison to expressions seen in ES[4] CTRL background (see figure 23), with the exception of an increase observed in *WT1* and *WGA* expression by D16 (Figure 24B). Overall, this points to the cessation of RV emergence and differentiation in the LHX1 KO background, supporting the phenotypes previously observed in 3D kidney differentiation as well (Gimenez, 2021).

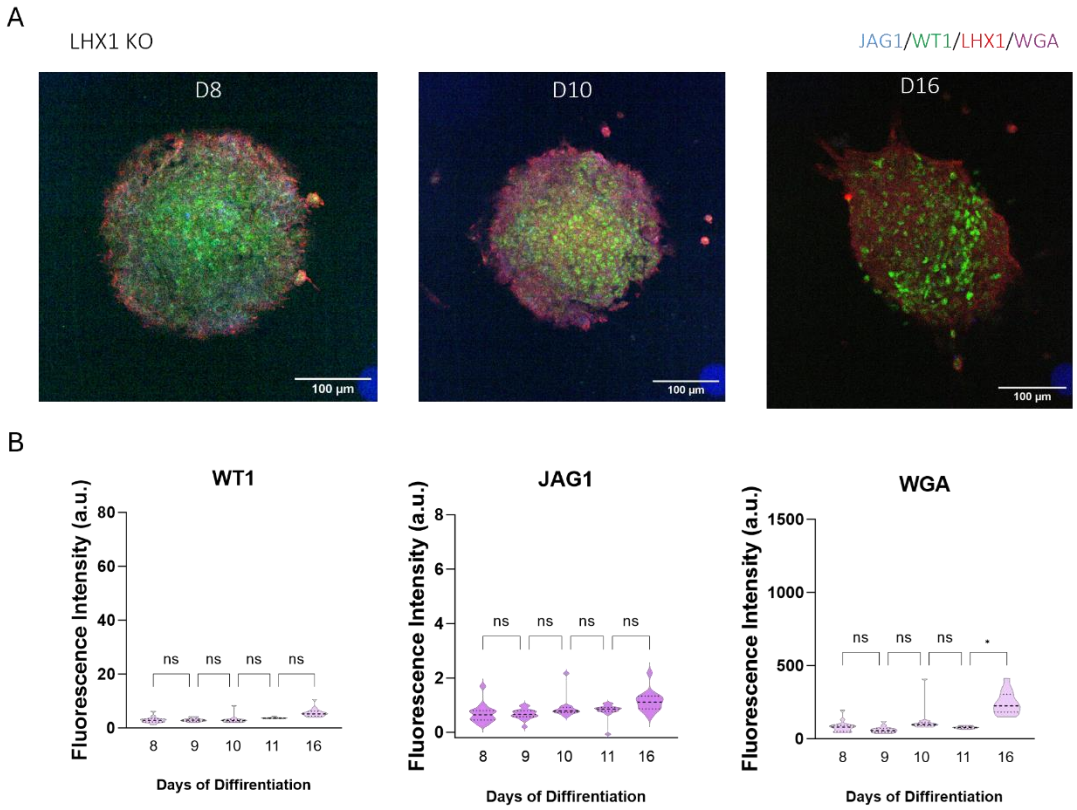

Figure 24. LHX1 KO 2D kidney differentiation on 300 µm circles micropatterned on 3kPa PDMS. A) Representative immunofluorescence images of at D8, D10 and D16 of differentiation. *JAG1* in blue, *WT1* in green, *LHX1* in red and *WGA* in magenta. Scale bar 100 µm. D) Average fluorescence intensity measurements of *WT1*, *JAG1* and *WGA*, normalized by z slice and background intensity values. Images and data represent N=1 biological experiment with 15 micropatterns per experiment. Statistical significance was determined by an ordinary one-way ANOVA test: **** P < 0.0001, *** P < 0.001, ** P < 0.01, * P < 0.05, ns > 0.05.

Exploring the effect of geometry on 2D kidney differentiation in ES[4] CTRL and LHX1 KO backgrounds

When cells are exposed to micropatterned ECM islands, they organize their focal adhesions (FAs) and actin filaments to spread until the edges of the islands. Studies have demonstrated, how depending on the size and curvature of the geometry, the cytoskeletal organization of the cells can vary (Parker et al., 2002; Thé et al., 2006; Versaevel et al., 2012). This in turn has been shown to regulate stem cell fate decisions (Connelly et al., 2010).

Others have demonstrated the generation of tensile stresses at the edges of geometries such as triangles, that in turn initiated BMP-mediated mesodermal specification of ESCs cultured on 2D ECM islands (Muncie et al., 2020).

In this regard, we explored the effect of different geometrical constraints on 2D kidney differentiation, for which we designed micropatterns of squares and isosceles triangles of equal surface area to the original 300 µm diameter circles.

We explored the expression of markers of RV emergence and differentiation, and monitored the organization and location of expression of these markers among the different patterns in ES[4] CTRL and LHX1 KO backgrounds.

2D kidney differentiation on square geometries

When NPCs of the ES[4] CTRL background were cultured on square micropatterned 3kPa PDMS substrates, we observed changes in expression and localization of markers such as *LHX1, JAG1, WT1* and WGA over time (Figure 25A). At D8 of differentiation we observed single cells expressing *LHX1,* at D11 - clustered expression of *LHX1* and *JAG1* and at D16 we observed the appearance of podocyte-like structures expressing *WT1* and tubular structures labelled with WGA (Figure 25A). By D16 of differentiation the cell cultures grew taller and outwards of the confined square geometry.

In the LHX1 KO background, while NPC organization into RVs could not be observed, we observed cell clusters expressing *WT1* at D8 (first in the centre) and D11 (around the edges of the pattern) of differentiation. At D16 we observed that the cultures remained small and bound to the square geometry (Figure 25B).

Upon quantification of the total immunofluorescence expression profiles, interestingly, we saw differences between the two cell lines only at certain time points (Figure 25C). *LHX1* expression was different between the two cell lines at D 10, 11 and 16 of differentiation, while *WT1* seemed to display no difference at the RV stages and higher expressions in the control background at D16, when nephron-like structures were present (Figure 25C). In the mouse, *WT1* expression has been identified in the proximal RVs and its absence has been associated with an overgrowth of NPCs and arrested tubular and glomerular differentiation (Drake et al., 2020; Georgas et al., 2009). At later stages of development, *WT1* has been associated with activating podocyte-specific genes and promoting epithelial tubule maturation (Berry et al., 2015; Kann et al., 2015). Indeed, in human iPSC-derived kidney organoids, time-controlled deletion of *WT1* has resulted in identification of its role in 1) exit from NPC state and mesenchymal to epithelial transition, and 2) podocyte and tubular differentiation (Waehle et al., 2021). Indeed, in ES[4] CTRL 2D kidney differentiation, *WT1* positive podocyte like cells could be observed at D16 of differentiation, validated by the increase observed in average immunofluorescence intensity (Figure 25C). While there seems to be no apparent difference in *WT1* average immunofluorescence intensities between the wildtype and KO samples until D16, the main differences lie in the localization of the markers. Between D8 and D11, a co-localization of RV specific markers, such as *JAG1* and *LHX1* together with *WT1* could be observed in the ES[4] CTRL background, indicating exit from NPC state and MET towards RV like structures (Figure 25A). In the LHX1 KO background on the other hand, such co-localization could not be observed, indicating a failure of NPCs to undergo MET (Figure 25B).

JAG1 expression was observed to be higher at D10 and D11 in the ES[4] CTRL squares, again, pointing to absence of RV emergence and consequent failure to undergo nephron segmentation in the LHX1 KO background. Interestingly, *WGA* expression was not different among the two cell lines, except for D11, raising the question of what structures (other than distal tubular segments of the nephron, which seem to be absent in the LHX1 KO background) *WGA* is demarking.

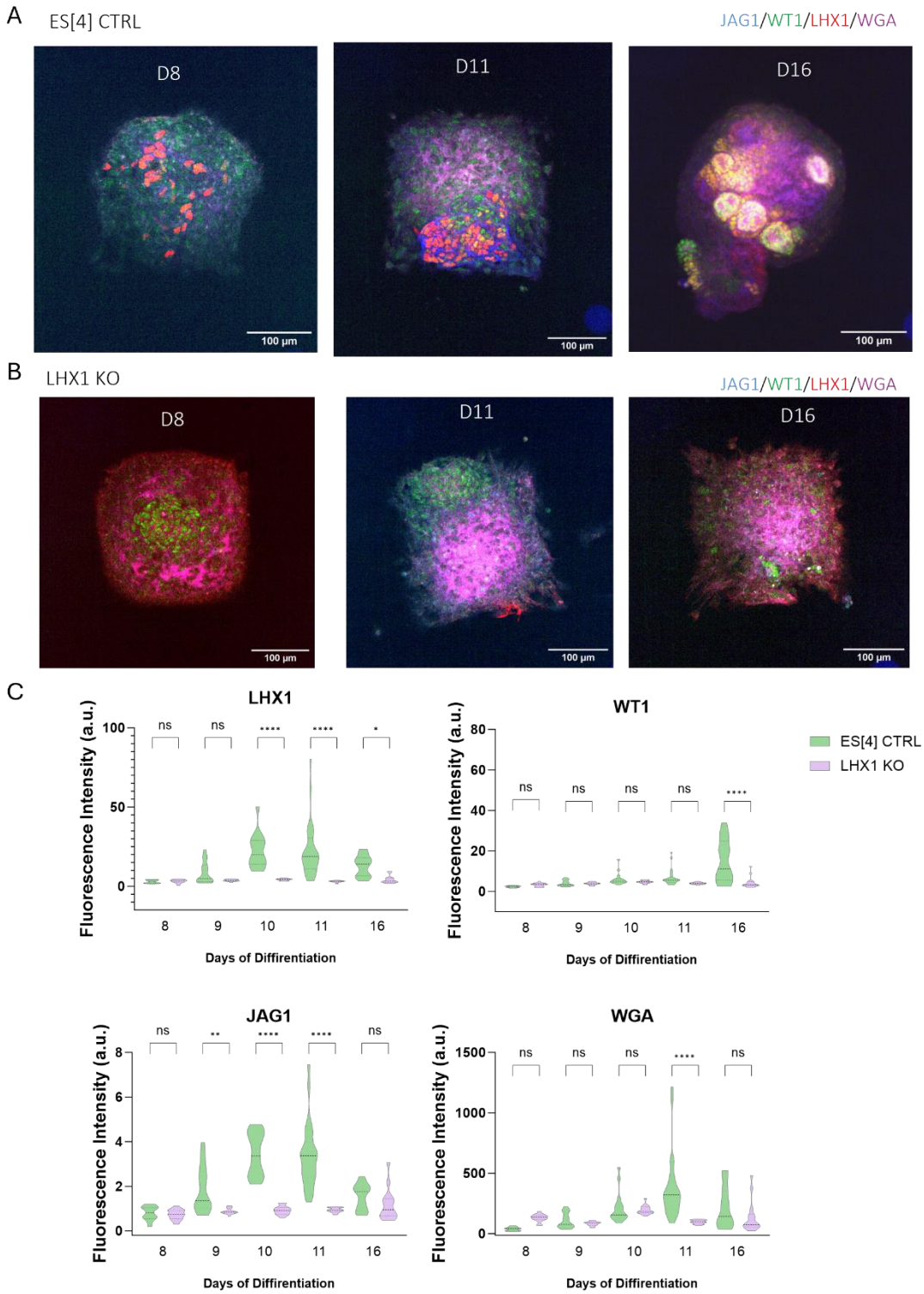
A
ES[4] CTRL
JAG1/WT1/LHX1/WGA
D8
D11
D16
100 µm
B
LHX1 KO
JAG1/WT1/LHX1/WGA
C
LHX1
WT1
JAG1
WGA
Fluorescence Intensity (a.u.)
Days of Differentiation
ES[4] CTRL
LHX1 KO
ns
*
**
***
****

Figure 25. ES[4] CTRL and LHX1 KO 2D kidney differentiation on squares micropatterned on 3kPa PDMS. Representative immunofluorescence images of at D8, D10 and D16 of differentiation of A) ES4 CTRL and B) LHX2 KO backgrounds. *JAG1* in blue, *WT1* in green and *LHX1* in red, *WGA* in magenta. Scale bar 100 µm. C) Average fluorescence intensity measurements of *JAG1*, *WT1* and *LHX1* and *WGA*, normalized by z slice and background intensity values. Images and data represent N=1 biological experiment with 15 micropatterns per experiment. Statistical significance was determined by an ordinary one-way ANOVA test: **** P < 0.0001, *** P < 0.001, ** P < 0.01, * P < 0.05, ns > 0.05.

2D kidney differentiation on triangle geometries

When ES[4] CTRL and LHX1 KO background NPCs were seeded onto triangular micropatterns, changes in expression and localization of *JAG1, LHX1* and *WT1* (like those observed in squares) were found over time (Figure 26A & B). Individual cells expressing *LHX1* were found in D8 ES[4] CTRL samples, and at D11 clusters expressing *LHX1, JAG1* and *WT1* were also identified. Similar to the observations made in square geometries, the co-localization of the three RV associated markers indicate correct NPC exit and MET occurring in the ES[4] CTRL background on triangle geometries. By D16 the 2D cultures grew in height and appeared to have a rounded morphology (Figure 26A).

On the contrary, the samples of LHX1 KO background did not appear to change in size over time. *WT1* and WGA expressions were sustained over time and had a tendency to localize along the edges (*WT1*) and in the centre (WGA) of the pattern (Figure 26B).

While no differences in the total immunofluorescence intensities of *LHX1, WT1* and WGA between the two cell lines was observed, the organization of cells expressing these markers was different among the two conditions (Figure 26C).

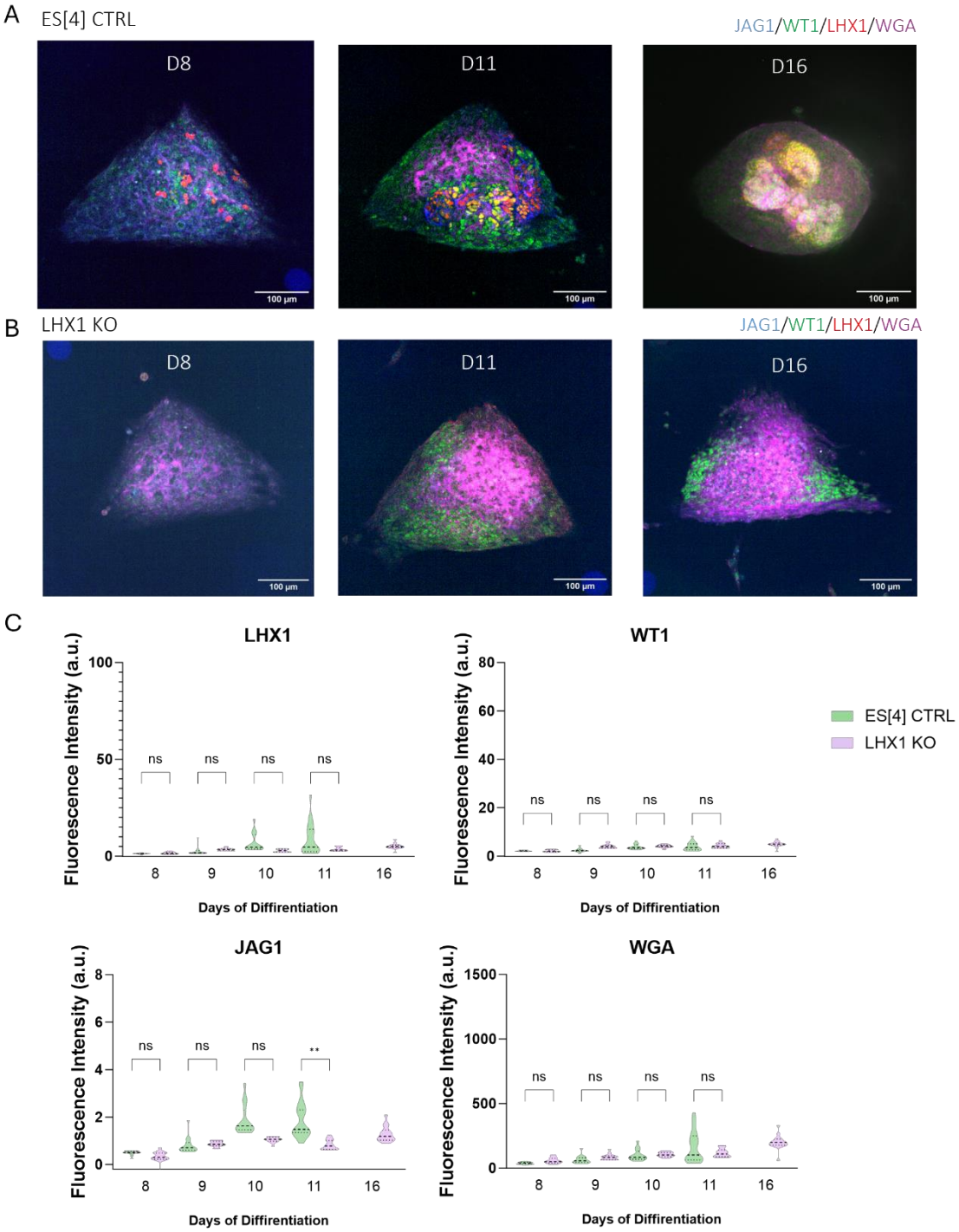
A
ES[4] CTRL
JAG1/WT1/LHX1/WGA
D8
D11
D16
100 µm
B
LHX1 KO
JAG1/WT1/LHX1/WGA
D8
D11
D16
100 µm
C
LHX1
WT1
JAG1
WGA
Fluorescence Intensity (a.u.)
Days of Differentiation
ns
**
ES[4] CTRL
LHX1 KO

Figure 26. ES[4] CTRL and LHX1 KO 2D kidney differentiation on triangles micropatterned on 3kPa PDMS. Representative immunofluorescence images of at D8, D10 and D16 of differentiation of A) ES4 CTRL and B) LHX2 KO backgrounds. *JAG1* in blue, *WT1* in green and *LHX1* in red, *WGA* in magenta. Scale bar 100 µm. C) Average fluorescence intensity measurements of *JAG1*, *WT1* and *LHX1* and *WGA*, normalized by z slice and background intensity values. Images and data represent N=1 biological experiment with 15 micropatterns per experiment. Statistical significance was determined by an ordinary one-way ANOVA test: **** P < 0.0001, *** P < 0.001, ** P < 0.01, * P < 0.05, ns > 0.05.

Effect of geometry on overall expression of RV emergence and differentiation markers

We then explored whether there were differences in expression intensity between cell cultures on different geometries.

In the ES[4] CTRL background, at D10 of differentiation (the timepoint of expected RV emergence), we saw a general trend of decreasing expression of *LHX1, WT1* and *JAG1* as the curvature of the geometry increase (i.e. circle > square > triangle) (Figure 27A and B) (see supplementary material for statistical analysis between geometries). This may indicate that higher curvature leads to reduced RV emergence. At D14/16 of differentiation, we observe a similar trend in the expression intensities of *WT1* (podocyte-like cells)*, WGA* (tubule like structures)*, PAX2* (distal tubule like structures)*, E-CADHERIN* (distal tubule like structures) between circle and square geometries (Figure 27A and B). This may indicate that higher curvature leads to reduced nephron like structure differentiation. Unfortunately, D16 samples of ES[4] CTRL differentiation on triangles were missing, however expression intensities of *PAX2, WT1* and *E-CADHERIN* in triangles at D14 were significantly higher than in squares, and non-different from circular patterns (Figure 27B).

In the LHX1 KO background, no differences in expression of *LHX1, WT1*, *JAG1* and WGA were observed between different geometries. However, an overall trend was observed between ES[4] CTRL and LHX1 KO samples, where the differences between immunofluorescence intensities of markers in CTRL and KO samples decreased with increasing geometry curvature, pointing to the possibility that ECM island geometry can regulate 2D kidney differentiation.

A

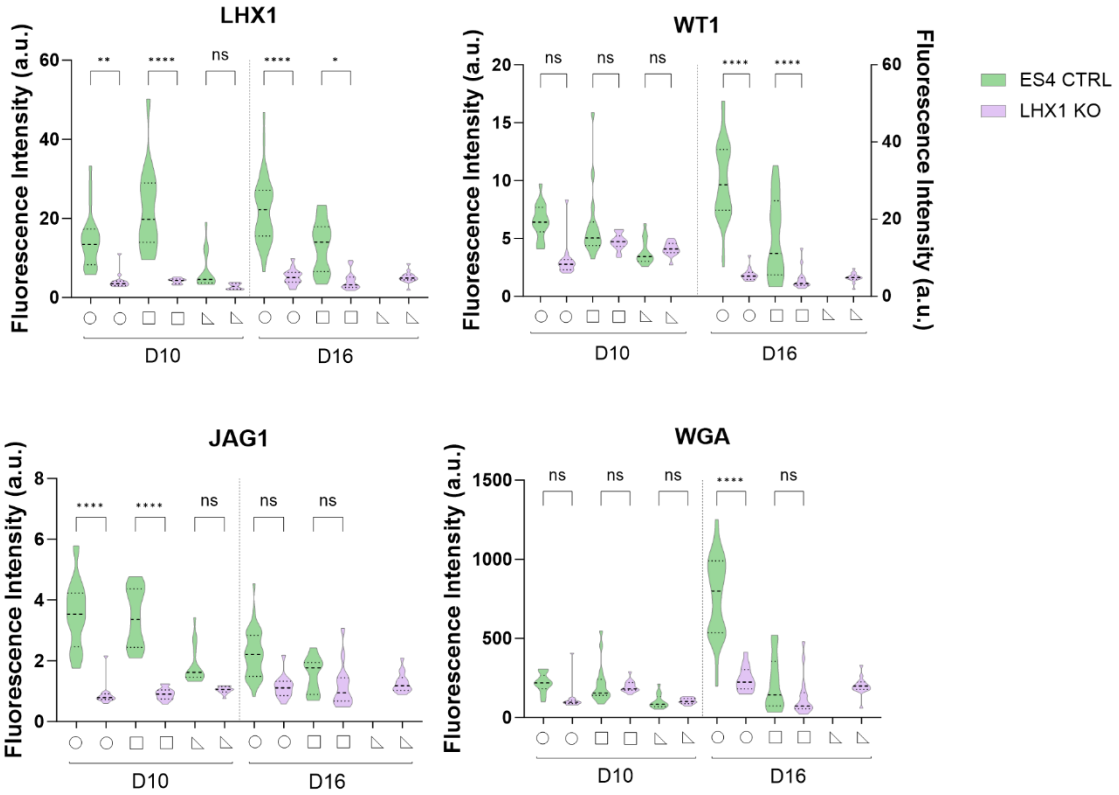
LHX1
WT1
JAG1
WGA
Fluorescence Intensity (a.u.)
D10
D16
ES4 CTRL
LHX1 KO

B

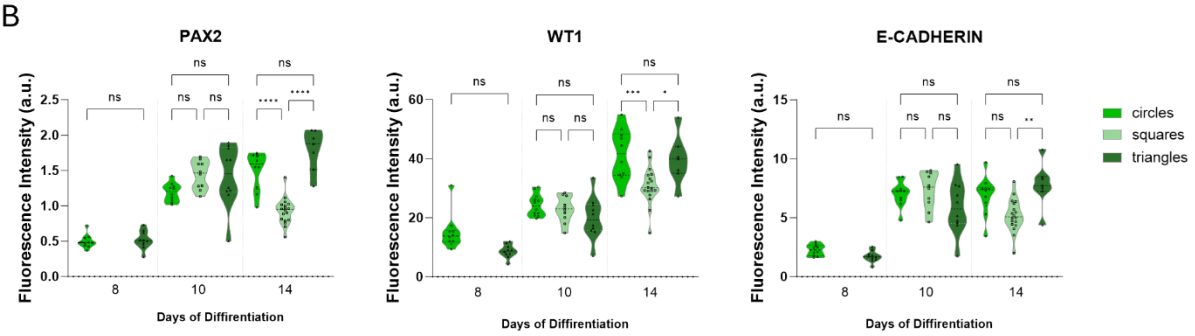
PAX2
WT1
E-CADHERIN
Fluorescence Intensity (a.u.)
Days of Diffirentiation
circles
squares
triangles

Figure 27. Comparison of average fluorescence intensities across different geometries in ES[4] CTRL and LHX1 KO differentiations. A) Average fluorescence intensity measurements of *JAG1*, *WT1* and *LHX1* and *WGA* at D10 and D16 of differentiation in ES[4] CTRL (in green) and LHX1 KO (in purple) samples in circle, square and triangle geometries. B) Average fluorescence intensity measurements of *PAX2*, *WT1* and *E-CADHERIN* at D8, D10 and D14 of differentiation in ES4 CTRL samples in circles (green), squares (light green) and triangles (dark green). Normalized by z slice and background intensity values. Data represent N=1 biological experiment with 15 micropatterns per experiment (A) and 10 micropatterns per experiment (B). Statistical significance was determined by an ordinary one-way ANOVA test: **** $P < 0.0001$, *** $P < 0.001$, ** $P < 0.01$, * $P < 0.05$, ns > 0.05.

Effect of geometry on the localization of expression markers of RV emergence and nephron differentiation

Micropatterns have been shown to influence various cell behaviours, including orientation, proliferation, migration and differentiation (Parker et al., 2002; Thé et al., 2006; Versaevel et al., 2012). Here, we further aimed to assess whether differentiating NPCs would adapt their morphology to match the shape of the micropatterns, and if those changes would influence spreading and adhesion, ultimately affecting renal differentiation (RV formation and subsequent nephron like structure formation). Indeed, previous studies have shown that micropatterns allow for dynamic changes in cell morphology and shape dependent expression of differentiation markers (Muncie et al., 2020; Smith et al., 2018). Our results indicate a possible geometry dependent localization of cells undergoing differentiation towards the RV fate.

In LHX1 KO background kidney differentiation on squares (Figure25B) and on triangles (Figure 26B), we observed a tendency of markers like *WT1* to be expressed in clusters along the edges of the pattern. To measure this, we divided the geometries into inner and outer regions, and re-calculated the average fluorescence intensities in the two regions (Figure 28 and 29).

In the ES[4] CTRL background in square geometries (Figure 28), we observed that the expression of *WT1* peaked in the inner region at D10 of differentiation (together with *LHX1* and *JAG1)*, which correlates with the appearance of RVs, and then again peaked at D16, associated with proximal tubule and podocyte development. This overall signifies that the square geometry sustains renal differentiation. In the LHX1 KO background we could not observe any obvious trend in expression of markers between inner and outer regions (Figure 28B).

Similar analysis was performed in the triangular geometries, however no clear differences were observed between the ES[4] CTRL and LHX1 KO samples, pointing to the fact that perhaps triangular geometries are not as efficient as circles and squares in sustaining RV emergence (Figure 29).

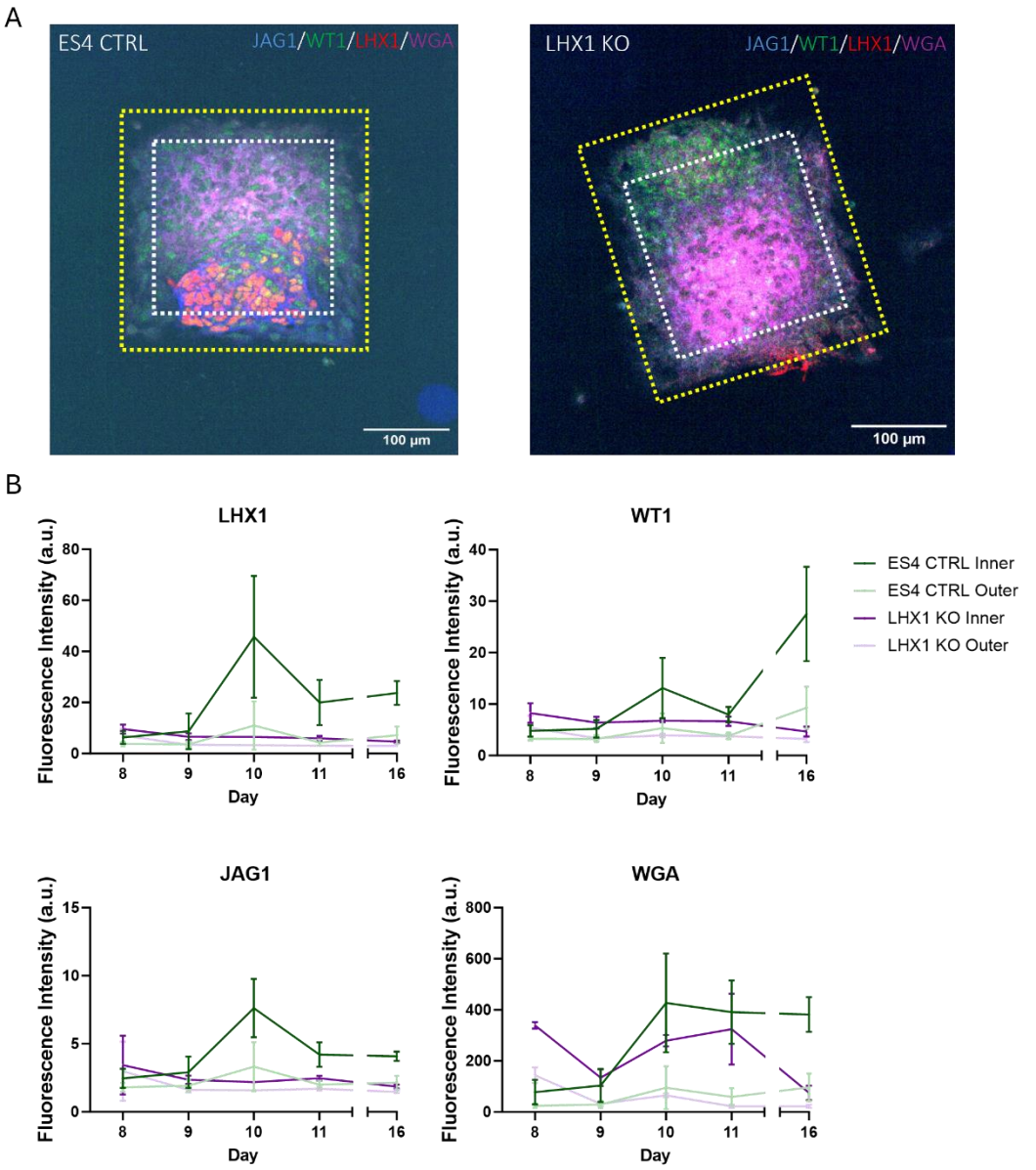

Figure 28. Inner and outer region fluorescence intensity measurements in square geometries. A) Representative IF image of ES[4] CTRL and LHX1 KO D11 differentiation on square 3kPa PDMS micropatterns, *JAG1* in blue, *WT1* in green, *LHX1* in red, *WGA* in magenta. Scale bar 100 µm. Yellow square represents outer region, white square represents inner region (calculated to be 20% smaller than the whole region). B) Inner vs outer fluorescence intensity measurements of *LHX1, JAG1, WT1* and *JAG1* expression in ES[4] CTRL (green) and LHX1 KO (purple) square samples. Darker lines indicate inner regions, lighter lines indicate outer regions. Normalized by z slice, background intensity and area. Data represent N=1 biological experiment with 10 micropatterns per experiment. Data points represented as mean ±SD

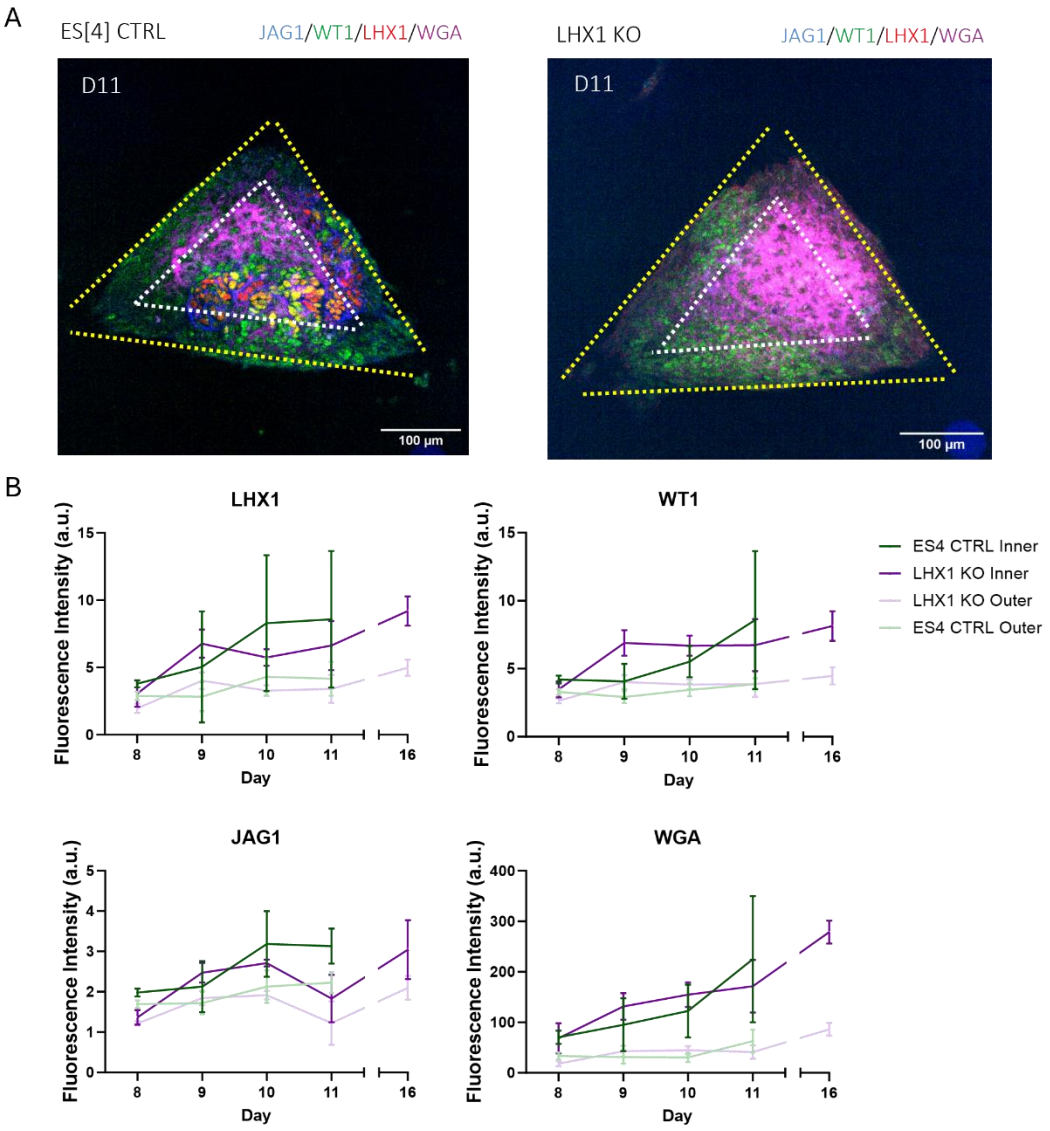

Figure 29. Inner and outer region fluorescence intensity measurements in triangle geometries. A) Representative IF image of ES[4] CTRL and LHX1 KO D11 differentiation on triangle 3kPa PDMS micropatterns, *JAG1* in blue, *WT1* in green, *LHX1* in red, *WGA* in magenta. Scale bar 100 µm. Yellow square represents outer region, white square represents inner region (calculated to be 20% smaller than the whole region). B) Inner vs outer fluorescence intensity measurements of *LHX1, JAG1, WT1* and *JAG1* expression in ES[4] CTRL (green) and LHX1 KO (purple) square samples. Darker lines indicate inner regions, lighter lines indicate outer regions. Normalized by z slice, background intensity and area. Data represent N=1 biological experiment with 10 micropatterns per experiment. Data points represented as mean ±SD.

When comparing *PAX2* expressions between circle, square and triangle samples at D10 of differentiation, we observed a similar trend of *PAX2* positive cells localizing along the edges of the geometries in LHX1 KO samples, while in the ES4 CTRL background they tended to be localized in the centre of the patterns (Figure 30A). Indeed, quantification of inner vs outer fluorescence intensities revealed increased inner intensities across all geometries in the ES[4] CTRL samples compared to LHX1 KO. Interestingly, LHX1 KO NPCs seeded onto square geometries seemed to have higher *PAX2* expression in the outer region compared to ES[4] CTRL NPCs on square micropatterns (Figure 30B). These findings suggest that the *PAX2* positive cell localization can be regulated by geometry.

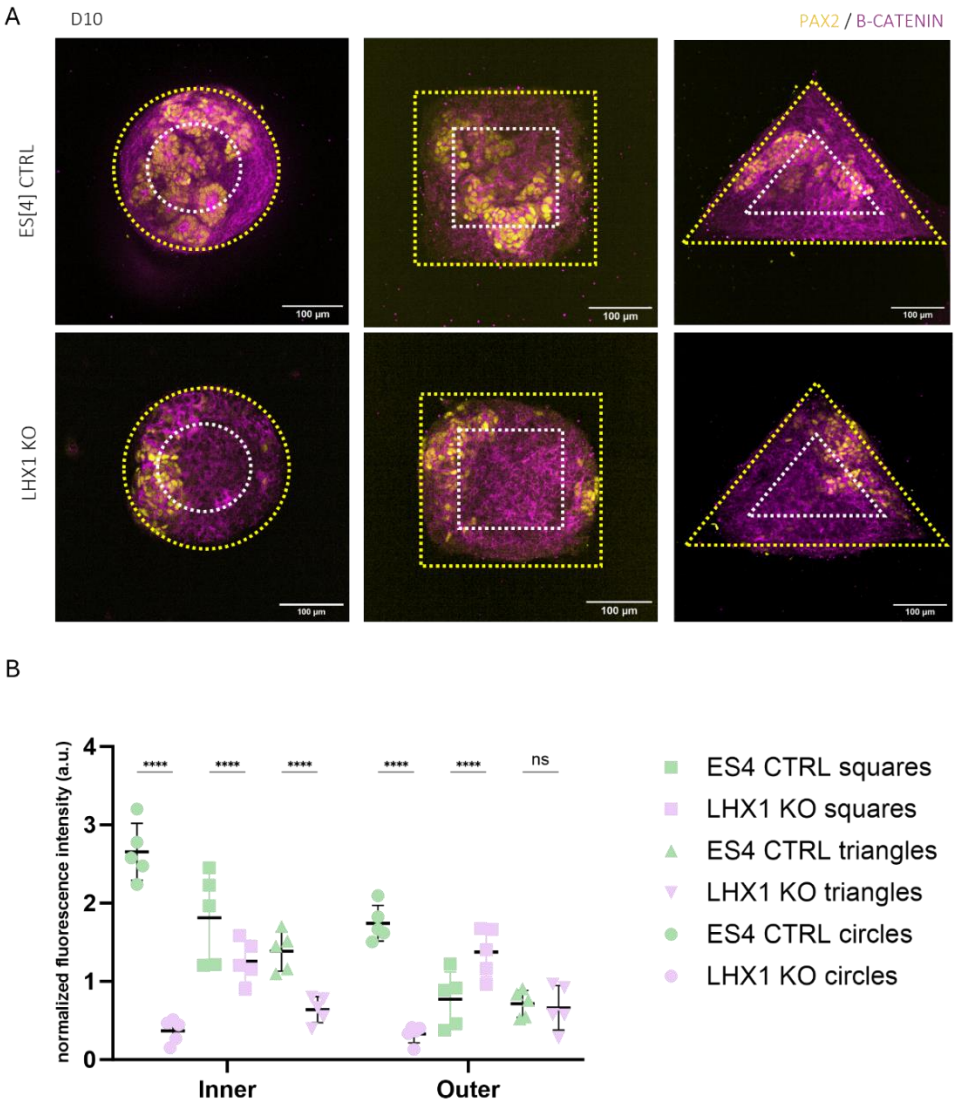

Figure 30. Inner and outer region fluorescence intensity measurements across different geometries. A) Representative IF image of ES[4] CTRL (upper panel) and LHX1 KO (lower panel) D10 differentiation on circle, square and triangle 3kPa PDMS micropatterns, *PAX2* in yellow and *B-CATENIN* in magenta. Scale bar 100 µm. Yellow lines represent outer region, white lines represent inner region (calculated to be 30% smaller than the whole region). B) Inner vs outer fluorescence intensity measurements of *PAX2* expression in ES[4] CTRL (green) and LHX1 KO (purple) circle, square and triangle samples. Normalized by z slice, background intensity and area. Data represent N=1 biological experiment with 5 micropatterns per experiment. Data points represented as mean ±SD. Statistical significance was determined by a one-way ANOVA test: **** $P < 0.0001$, *** $P < 0.001$, ** $P < 0.01$, * $P < 0.05$, ns > 0.05.

Measuring forces exerted by ES[4] CTRL and LHX1 KO NPCs on 3kPa PDMS of circle, square and triangle geometries

Several studies have previously measured forces exerted by different cell types, including ESCs, in colonies and on micropatterned ECM islands, and have identified higher traction forces along the boundaries of clusters (I. Jain et al., 2022; Nelson et al., 2005; Xue et al., 2018). Moreover, these regions of high tractions been linked, by monolayer stress microscopy, to areas of high cell adhesion tensions. Such tensions in turn have been shown experimentally to regulate signalling pathways such as Wnt/β-catenin and Notch, ultimately influencing ESC differentiation (I. Jain et al., 2022; Muncie et al., 2020).

Considering the important role that these pathways play in kidney development, it is possible that cellular tensions generated by exposure of NPSCs to geometries of varying curvatures could result in regions where signalling molecules/morphogens could accumulate and therefore influence cell organization and ultimately differentiation.

To further investigate these possibilities, we measured traction forces exerted by NPCs of ES[4] CTRL and LHX1 KO backgrounds seeded onto 3kPa PDMS substrates micropatterned with circle, square and triangle geometries.

Indeed, and as expected, in both cell lines, in all three geometries, we observe a higher traction force in the boundaries of the micropatterns, as has been previously described for other 2D micropatterned system (Figure 31A) (I. Jain et al., 2022; Nelson et al., 2005; Xue et al., 2018).

We focused the measurements on D10 of differentiations, the time point at which RVs are expected to be present in control differentiations.

We observed higher strain energies and traction curls being exerted in the ES[4] CTRL background compared to LHX1 KO across all three geometries (Figure 31B). Interestingly, we observed a trend of increasing strain energies in relation to increasing geometry curvature (i.e. circle > square > triangle) in both cell lines. Similarly, stronger traction curls were observed in the square and triangular geometries, compared to the circles in the ES[4] CTRL background and observed no (or minimal) differences in LHX1 KO (Figure 31B).

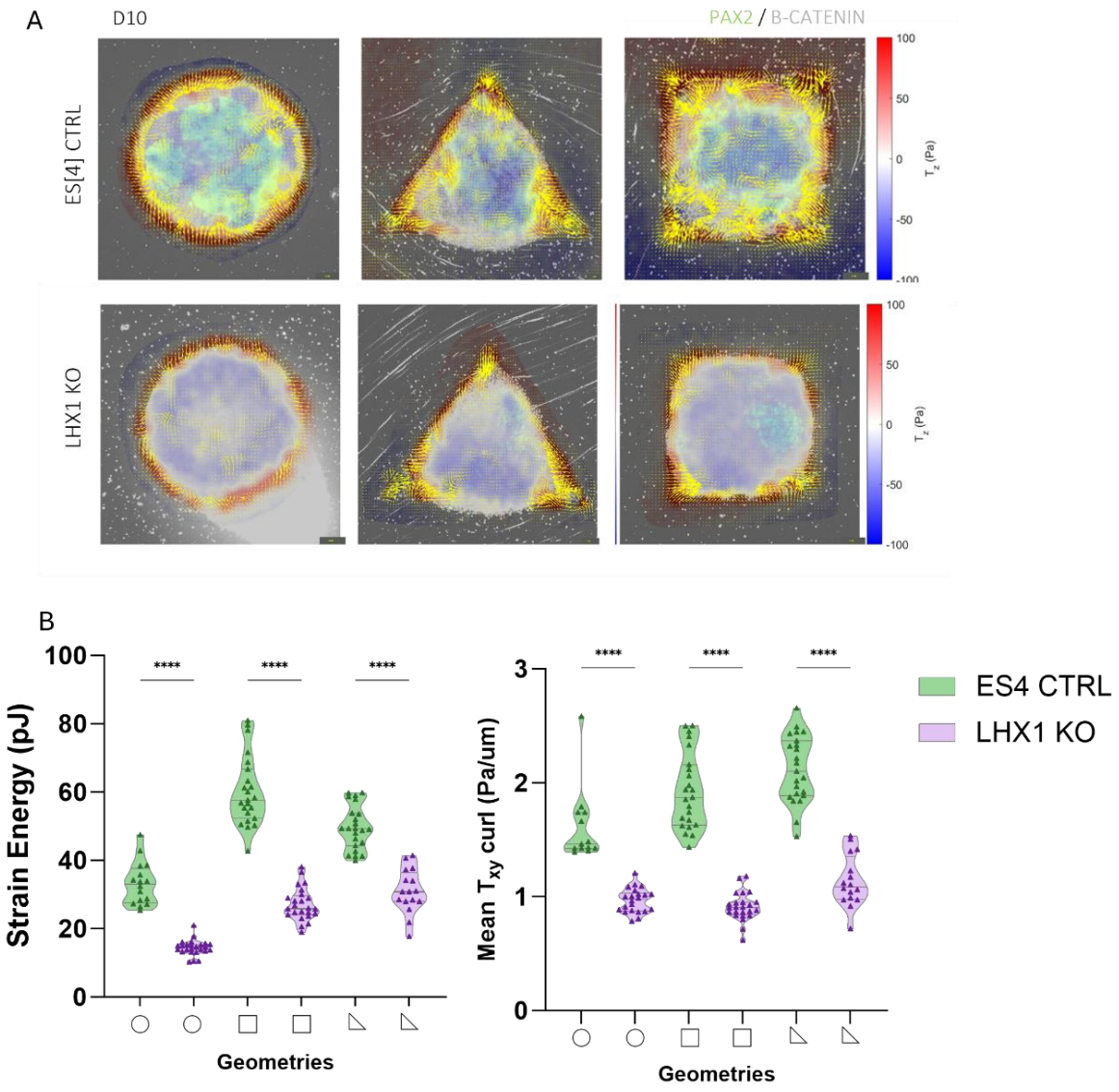

Figure 31. Measurement of traction forces in ES[4] CTRL and LHX1 KO lines on circle, square and triangle micropatterned 3kPa PDMS. A) Representative images of traction maps in z at D10 of differentiation. Yellow vectors represent components tangential to the substrate, and the colour map represents vectors normal relative to the substrate. *PAX2* in green can be seen underneath the maps. B) Average strain energy (left) and mean traction curl (right) measurements taken across 3 biological experiments (in circles) and 1 biological experiment (in squares and triangles) with 20-25 technical replicates per experiment. Statistical significance was determined by a one-way ANOVA test: **** P < 0.0001, *** P < 0.001, ** P < 0.01, * P < 0.05, ns > 0.05.

While most previous studies have associated differentiation with increased tension stresses, we in general have observed the opposite. While NPCs seeded onto triangular geometries seem to exert the highest overall traction forces, they also seem to be the geometry that results in a lesser degree of differentiation (using IF as a readout) in comparison to circular and square patterns. To further correlate extent of differentiation, effect of geometry and cellular forces, RNA analysis could provide a deeper insight into the different gene regulatory mechanisms involved.

Discussion

Generating a 2D system for interrogating mechanics in 2D kidney differentiation

Like in many biological systems, the development of the kidney relies on an intricate interplay of fate commitment of different stem cell populations and their shape and organization within the forming tissue. This is largely influenced by both the genetic pre-disposition of the cells to be guided to a particular fate, and by microenvironmental cues (including biophysical and biochemical signals), to guide cell migration and re-organization (Vining and Mooney, 2017). Indeed, like many other organs, the kidney is composed of a complex architectural network of ECM components such as collagens (the main structural scaffold), proteoglycans (responsible for the gel like structure and hydration) and glycoproteins (laminin and fibronectin, that are crucial for cell adhesion, migration, and signalling), that collectively form the basal membranes and interstitial spaces. In fact, these components are more than just a scaffold, they are crucial for providing mechanical support and for mediating a variety of signalling pathways, such as TGFβ/Smad signalling, Janus Kinase (JAK)/STAT signalling, Wnt/β-catenin signalling, ERK1/2 signalling, RhoA/ROCK signalling (Roskelley, Srebrow and Bissell, 1995; Bülow and Boor, 2019; Di et al., 2023; Novoseletskaya, Evdokimov and Efimenko, 2023).

Nephron patterning is a very dynamic process, where cells could be re-arranging as they commit to a particular fate. In the process of tubule formation, for example, cell-cell, and cell-ECM adhesions play an important role, as the cells are sensing their surroundings and using the input they receive to initiate lumen formation, polarization, and elongation of tubules. Recent studies have suggested that the stiffness of the surrounding ECM has an influence on renal tubule cell differentiation and tubule formation, opening the possibilities of using material stiffness to guide cell organization (Garreta et al., 2019; Love et al., 2019; Hamon et al., 2023).

Indeed, control of material stiffness, in the past, has been shown to improve *in vitro* 3D kidney organoid culture, where softer matrices enhanced maturation and reduced fibrosis (Garreta et al., 2019; Geuens et al., 2021; Ruiter et al., 2022; Nerger et al., 2024). Indeed, studies using hESCs cultured on soft PAA matrices

have demonstrated that the stiffness of the surrounding matrix can modulate Wnt/ β-catenin mediated mesodermal specification (Muncie et al., 2020; Przybyla et al., 2016). In fact, β-catenin has been previously shown to be mechanosensitive, where for the example, in the bone, it has been associated with activation via mechanical loading (Farge, 2003; Hens et al., 2005; Ou & Weaver, 2015). While the role of Wnt/β-catenin signalling in kidney morphogenesis has been described (Carroll et al., 2005; Park et al., 2007), it is not yet clear by which mechanisms softer matrices promote renal differentiation (as observed in hPSC-derived NPCs), which mechanosensitive proteins are at play, and how they correlate with the genetic program of kidney development.

Other studies in mice embryonic kidneys have discussed how the specific geometry of the branching ureteric tree guides the development of the organ by creating an up-concentration of morphogen gradients in certain regions (like under the branch tip), which in turn regulates the positioning of the future nephrons in the kidney (Mederacke et al., 2023). Similarly, the branching of the ureteric bud has been shown to be regulated by specific geometric packing phases, that control the interplay between the number of branches formed and the physical constraint of organ size during development (Viola et al., 2022; Prahl et al., 2023).

While such studies have provided very valuable insights into ureteric branching and morphogen gradient movements in kidney development (specifically in the mouse background), several gaps remain in understanding the morphogenesis of human metanephric mesenchyme (MM) - derived progenitor differentiation towards the mature nephron. Specifically, how renal vesicles (RV) form from the MM progenitor population, how they generate a lumen that undergoes elongation and polarization, and further patterning, from a mechanobiological perspective, is largely unexplored.

One of the main reasons for this is the lack of a system that would allow for direct interrogation of the human tissue at both biochemical and physical level, over long periods of time that covers the extent of nephron formation. While 3D kidney organoids have been a valuable alternative to human foetal tissue samples, their three dimensionality poses as an extra difficulty in addressing

questions regarding how the interplay of biochemical and genetic conditions together with cell mechanics impacts on morphogenesis.

Indeed, in this regard, certain research models for translating 3D organoid culture set ups into 2D systems (i.e. 2.5D culture) have been emerging (Tohyama et al., 2017; Abugomaa et al., 2020; Pérez-González et al., 2021).

In this thesis we aimed to map RV emergence and nephron differentiation in human kidney development. Towards this goal, we first developed a series of differentiation procedures (kidney organoids in 3D and 2D) based on the use genetically engineered hPSC lines in combination with micropatterning techniques, confocal and traction force microscopy analysis. This multifaceted approach allowed us to start mechanistically coupling how RV emergence and nephron differentiation is driven by changes in the expression of specific renal markers and cell force generation.

We started by evaluating RV emergence and differentiation into nephron like structures by making use of an established 3D kidney differentiation methodology (Garreta et al., 2019; Garreta, Moya-Rull, et al., 2022; Garreta, Prado, et al., 2022). By culturing kidney organoids (in free floating and Trans-well inserts) from distinct backgrounds (ES[4] hPSCs - male and CB40 hiPSCs - female) we could observe via immunofluorescence characterization, the key time points of RV emergence (as demarked by expression of *PAX2, JAG1, LHX1* and *WT1)* and their further evolution into segmented nephron like structures containing distal (*E-CADHERIN)*, medial (*JAG1)*, proximal (*LTL)* tubules and podocyte like cells (*WT1)*. The kidney organoids developed following the Garreta et al. protocol, have previously been shown to resemble embryonic kidneys of the 2nd trimester of human development. Moreover, the effect of the mechanical micro-environment (in the form of substrate rigidity) on kidney organoids differentiation was first explored in the same study. Here, the authors demonstrated how exposure of hPSCs to a soft (1kPa) PAA gel for a period of 4 days prior to organoid assembly by micro-centrifugation, resulted in kidney organoids developing RVs at an earlier timepoint and in higher numbers, compared to exposure to stiff PAA (60kPa). In addition, the kidney organoids developed from soft PAA gel exposure had developed more glomerular-like and tubule-like structures by D20 of differentiation, as well as presented with higher

mRNA expression of late-stage nephron markers such as *NPHS1*, *SCNN1B* (Garreta et al., 2019). Building up on these preliminary findings, we worked on identifying a culture set up that would allow long term 2D kidney differentiation from the hPSC-derived NPCs stage and be compatible with traction force measurements and confocal immunofluorescence analysis, as a quantitative measure of cellular forces exerted and NPC differentiation extent.

Polyacrylamide gels have previously been established as a valuable substrate for studying cell-cell and cell-ECM interactions in many systems studying morphogenesis (Muncie et al., 2020; Pérez-González et al., 2021; Jain et al., 2022). While this opened many opportunities for interrogating the mechanics of the ESC differentiation, liver, and intestinal epithelium (among other systems), in the context of this thesis, PAA gels could not support long term culture adhesion of hPSC-derived NPCs. Soft elastic PDMS, on the other hand, was able to support prolonged kidney differentiation culture in the context of this thesis, and has been shown to be compatible with traction force measurements [as described previously in epithelial monolayers (Bergert et al., 2016)]. Indeed, PDMS has been previously shown to support differentiation of cells into the myogenic, cardiac, and neural lineages as well (Kim et al., 2008; Świerczek-Lasek et al., 2019; Etezadi et al., 2022).

Importantly, PDMS, due to its mode of polymerization, is highly compatible with high-resolution photopatterning via PRIMO, unlike PAA (Strale et al., 2016). This was a significant advantage of the system we had been working with since it added the possibility of simultaneously imposing two physical constraints during kidney differentiation: rigidity and geometry. More importantly, the use of a maskless photopatterning technique allowed for robust reproduction of micropatterns and efficient passivation of undesired areas of the culture plate, that are common technical limitations that are present when using other patterning techniques such as microcontact printing (D'Arcangelo and McGuigan, 2015).

Micropatterning techniques have been traditionally used to manipulate cell adhesion patterns for studying cytoplasmic reorganization and cellular function via the shape, spread, cell polarity and migration of cells on substrates (Roca-Cusachs et al., 2008; Pitaval et al., 2010). In the context of stem cell

differentiation, several important works have demonstrated how environmental cues (such as physical constraints of geometries and rigidity) can influence cell fate decisions (McBeath et al., 2004; Connelly et al., 2010; Warmflash et al., 2014; Muncie et al., 2020; Britton et al., 2021; Karzbrun et al., 2021; Jain et al., 2022).

Particularly remarkable work in terms of tissue morphogenesis on 2D micropatterns has been the differentiation of the human neural tube by a rectangular geometric constraint (Karzbrun et al., 2021). This work highlighted the potential importance of neural ectoderm geometry in determining the morphology along the anterior-posterior axis of the developing neural tube.

Regarding kidney morphogenesis, the effect of physical constraints on differentiation, in the form of geometry, to our knowledge, has not yet been explored. In this thesis, we aimed to externally guide NPC differentiation using geometrical constraints to start mechanistically coupling how RV emergence and nephron differentiation is driven by changes in the expression of specific renal markers and cell force generation. In this regard, renal agenesis has been registered in patients carrying mutations in *ITGA8*, coding for α8-integrin, which is normally expressed on cells of the MM and mediate interactions with ECM proteins expressed by epithelial cells of the ureteric bud (Humbert et al., 2014; Marek et al., 2020). Considering that disturbances in cell-cell contact interactions have been identified as drivers of disease, we aimed to impose geometrical constraints on NPCs during differentiation, thereby modulating cell-cell and cell-ECM contact to interrogate for external conditions that have been hypothesized to account for CAKUT.

The high-resolution photopatterning via PRIMO on PDMS substrates has allowed us to annotate micropatterns, to ultimately be able to correlate traction force measurements during 2D kidney differentiation with cell identity markers via post-fixation immunofluorescence staining. This gives the opportunity to potentially explore any marker of interest, including markers for different stages of nephron patterning, cell death, or proliferation.

In this manner, the experimental set up we had developed for studying 2D hPSC-derived kidney development by imposing physical (geometric and rigidity)

constraints could be beneficial for monitoring RV emergence and differentiation into nephron-like structures and evaluating the effects of biochemical and physical cues on kidney differentiation in an *in vitro* setting.

Using the 2D system for interrogating mechanics in 2D kidney differentiation of ES[4] CTRL, PAX2 KO and LHX1 KO backgrounds

With the aim of monitoring RV emergence and nephron like differentiation in the CAKUT background *in vitro*, we employed the experimental set-up to assess the interplay between biochemical cues, genetics, and physical constraints of 2D kidney differentiation in wildtype and knock-out lines for *PAX2* and *LHX1*.

While CAKUT encompasses a wide variety of kidney and urinary tract developmental anomalies, they have a complex aetiology, potentially spanning disturbances in multiple important developmental genes. Only 10-15% of CAKUT cases are explained by single gene pathogenic variances, whereas most cases are a result of polygenic variances with environmental and epigenetic influences (Nicolaou et al., 2015). Mutations in over twenty genes have been identified as contributing factors in the development of CAKUT, potentially explaining the spectrum of clinical presentations observed in this condition. These mutations can manifest as either isolated kidney anomalies or can be integrated within a broader syndrome encompassing additional clinical features. Notably, several key regulatory genes, including *PAX2*, *HNF1B*, *BMP7*, *RET*, *GATA3*, *SALL1*, *SIX5*, and *EYA1*, have been implicated in CAKUT pathogenesis due to their critical roles in normal kidney development (Ichikawa et al., 2002; Nicolaou et al., 2015).

PAX2 in one of developmental genes with the most variances identified and associated with various renal phenotypes in the spectrum of CAKUT (Sanyanusin et al., 1995; Bower et al., 2012; Chang et al., 2022). Mutations in *LHX1* on the other hand, in humans have been associated mostly with congenital anomalies of the reproductive tract, leading to Mayer-Rokitansky-Kuster-Hauser (MRKH) syndrome (Ledig et al., 2012). However, studies in mouse and frog models have demonstrated the important role of *LHX1* (*Lim1* and X*lim-1* in mouse and frog) in

nephrogenesis, with KO mutations being associated with a complete absence of nephrons (and lethality) (Chan, Takahashi and Asashima, 2000; Kobayashi et al., 2005).

Moreover, genetic studies in mice have identified *Pax2, Gata3* and *Lim1* (*LHX1* in humans) as a core transcriptional network in kidney development that regulates several key players in pro/mesonephros morphogenesis (Boualia et al., 2013). These studies helped identify the genetically upstream localization of *Pax2* in relation to both *Gata3* and *Lim1*, showing that *Pax2* expression is independent of *Lhx1*, however, *Lhx1* expression in Wolffian ducts seems to require *Pax2* (Bouchard et al., 2002; Kobayashi et al., 2005; Boualia et al., 2013).

In hPSC-derived *PAX2* null kidney organoids, *PAX2* has been shown to be dispensable, resulting in successful NPC exit towards RV MET. Kaku et al., had reported undisturbed further tubulogenesis and glomerulogenesis, with the only remark in the columnar to squamous transition of glomerular parietal cells, indicating the potential importance of *PAX2* in the development of this cell type (Kaku et al., 2017). Findings in the Montserrat laboratory, on the other hand, demonstrated the formation of 3D kidney organoids with disrupted formation of proximal tubular structures and disrupted glomerulogenesis (Aspiroz, 2021). *LHX1,* on the other hand, was demonstrated to be vital for NPC exit and MET, with mutant kidney organoids resulting in abolished nephrogenesis all together (Gimenez, 2021).

In this thesis, we utilized our experimental set-up to study the mechanical responses of 2D kidney differentiation in normal (wildtype), disrupted (PAX2 KO) and complete absence (LHX1KO) of nephrogenesis backgrounds.

Indeed, our traction forces measurements revealed an interesting trend of decreasing traction forces, in relation to severity of genetic disruption of RV emergence and nephron like structure differentiation. We observed that during wildtype RV emergence and differentiation, the 2D cultures exert a certain amount of forces that seem to be drastically reduced when RVs are not able to form. Indeed, this points towards the fact that RV emergence and differentiation are mechanically dynamic processes.

It is important to note that in such 2D long term kidney differentiation, the cultures grew into a multi-cell layer structure, becoming taller as differentiation progresses. A limitation of the system was the difficulty to infer and dissect the exact structures exerting forces, since TFM measurements in 2D are restricted to the cells in contact with the surface of the gel. Given the fact that the TFM measurements were taken at single static timepoints, inferring the mechanical process by which RV form, lumenize and elongate over time, was not possible.

Despite these limitations, this methodology allowed us to monitor RV emergence and differentiation in 2D by immunofluorescence microscopy, and to gain an insight into the overall average traction forces of 2D kidney differentiation *in vitro,* which to our knowledge has not yet been explored in the field.

Further on, our traction force measurements revealed an interesting pattern of rotations present in the 2D kidney differentiation system. Indeed, such mesoscale such turbulences have been previously identified and described in 2D monolayers (Lin et al., 2021). We were curious to understand the magnitude of the rotational forces observed in the 2D kidney differentiation and whether they were correlated with the formation of renal vesicles.

To characterize the magnitude of rotations, we calculated average traction curls in the different cell lines across three time points. We found that when RVs were present in the system (D10) there was a tendency of increased average traction curls (compared to when RVs were absent, i.e. at D8 of differentiation). Interestingly, the PAX2 KO background displayed a lower magnitude of rotations at D10, compared to its corresponding wildtype background (PAX2 CTRL). At this stage of differentiation, the presence of RVs in the PAX2 KO background has been previously demonstrated in 3D (Kaku et al., 2017; Aspiroz, 2021). While the presence of RVs in the 2D kidney differentiation system are yet to be verified, this raises the question of whether in fact something else may be contributing to the formation of traction curls.

In order to identify the location of the curls, we employed the Okubo-Weiss mathematical parameter in our system (Guillamat, Ignés-Mullol and Sagués, 2017). The parameter is defined by a mathematical formula (see in results

chapter 2), that gives a binary condition, when the area in which OW is negative, there is a vortex, when it is positive, no vortex is present.

We wondered whether these vortices could be correlated with forming renal vesicles, however some limitations of our current system did not allow us to provide a concrete answer to this question yet.

First, the measurement of these curls was limited to the surface of the PDMS substrate and to the cells that were in direct contact with it, whereas the expression of *PAX2* (as a marker for RVs) was often seen at higher levels of the multi-cell layer structures. Inferring the effect of *PAX2* positive cells through several layers of intermediate cells onto the surface of the gel would not provide accurate information. Here, further IF analysis would be required, to identify other cell populations in 2D kidney differentiation. Alternatively, another approach would be the incorporation of reporter cell lines for monitoring cell fate, either by targeting specific loci or via an unbiased manner, such as the confetti system, allowing multi-color lineage tracing (Cre-reporter) through time (Snippert et al., 2010; Weissman & Pan, 2014).

Furthermore, the exact moment of RV emergence in the 2D kidney differentiation has not yet been registered since the measurement taken thus far had been of single specific time points. Here, a long-term traction force measurements taken over the course of days between D8 and D10 of differentiation could allow for a better overview of RV emergence. In this regard, it would be possible to use the ES[4]-WT1-GFP cell line, as *WT1* also demarks RV emergence and further is expressed in glomeruli-like structures. The expression pattern of *WT1* increases from RV emergence until the formation of podocytes in the 3D kidney organoid system, allowing for live monitoring of kidney differentiation.

In the 2D kidney differentiation system, this cell line could provide a clearer overview of RV emergence and help identify where traction curls stem from.

While we could not yet correlate renal vesicle formation with the vortices observed in our system, a future exploration could involve the cells that are in direct contact with the PDMS surface, that could be responsible for the generation of such curls. It is not excluded that some mechanical effects could be stemming from stromal cells that surround the renal structures. Indeed,

stromal cells in renal development were first defined as the supportive construction surround the nephrons and ureteric bud, giving rise to the ECM and growth factors necessary for kidney development (Cullen-McEwen, Caruana and Bertram, 2005). In 3D kidney organoids, populations of *MEIS-1* positive stromal cells have been previously identified (Garreta, Prado, et al., 2022). In the 2D kidney differentiation system, the use of a *MEIS-1* reporter hPSC line (developed in the Montserrat laboratory) could further help in the investigation of the origin of traction vorticities observed.

The 2D micropatterning set up has further allowed us to monitor the effect of geometry as a physical constraint on 2D kidney differentiation. While the effect of geometry as a physical constraint on kidney morphogenesis has not yet been explored, other studies have started demonstrating the power of geometrical confinement on driving embryonic organization and differentiation (Warmflash et al., 2014; Britton et al., 2021). It has been shown how embryonic stem cells seeded on geometries, such as triangles generate tensile stresses at corners of the geometry, that in turn, initiated BMP-mediated mesodermal specification (Muncie et al., 2020). Such tensile stresses have been further correlated with signalling in the Wnt/β-catenin and Notch signalling. pathways, both of which are key in embryonic kidney development (Carroll et al., 2005; Park, Valerius and McMahon, 2007; Lindström et al., 2015; Muncie et al., 2020; Jain et al., 2022).

While the results of our investigations were preliminary, we observed certain geometry related differences in 2D kidney differentiation. When culturing 2D kidney differentiation in the wildtype ES[4] CTRL background, all three geometries were able to support the formation of renal vesicles and further nephron like structures. We noticed however that immunofluorescence expression of markers during RV emergence such as *WT1, LHX1* and *JAG1* were higher in circle and square geometries in comparison to triangles. This hinted at the potential effect of geometry curvature on extent of 2D kidney differentiation.

When compared with LHX1 KO backgrounds, we noticed a tendency, where the difference in total fluorescence intensity of markers of differentiation between the two cell lines would reduce, in relation to geometry curvature.

Overall, in the LHX1 KO background, we noticed a tendency of *WT1* or *PAX2* positive cells to cluster along the edges of the geometries. When analysing this phenomenon by dividing the patterns into inner vs outer regions, we observed, on square geometries, some preference of *PAX2* positive cells to localize on the outer region in LHX1 KO cultures compared with ES[4] CTRL cultures on the same geometry. This points to the potential effect of curvature sensing by the cells on their localization within the pattern. Indeed, in the scenario of genetic disruption of nephron patterning, differentiating cells could be depending on instructive cues from the surrounding environment, prompting them to organize around areas of increased curvature/tension.

It should be noted that the analysis was performed considering approximately 50 µm in height of cells of the (100 µm) multi-cell layer from the surface of the PDMS substrate, in attempt to only capture the effect of the geometry on marker localization. Moreover, the definition of the outer region was decided by taking between 20-30% distance from the edge of the pattern. Considering that these are preliminary data, it is possible that the variability of the samples is too high, requiring a larger n for gaining a better overview of the phenomenon. There is still room for improvement of this methodology, perhaps by also considering the total volume of the system instead of a projection of the first 50 µm.

To evaluate if the localization of cells during kidney differentiation on 2D micropatterns could be linked to tensile stresses of the monolayer [as has been previously described in ESC differentiation to mesodermal fate (Muncie et al., 2020)] we measured overall strain energies of the cell cultures via traction force microscopy.

In the square and triangular geometries, we observed a higher tendency of average strain energies and traction curls, than in circles, in both the wildtype and knockout cell lines. While these findings are still very preliminary, we observe a correlation between average strain energies in the geometries and extent of 2D kidney differentiation in the wildtype background, as defined by IF markers such as *LHX1, WT1* and *JAG1* at D10 of differentiation.

It seems that NPCs confined by triangular geometries seem to exert overall higher strain energies, while sustaining less differentiation as compared to

circular and square micropatterns. While the exact mechanisms by which this may occur are not yet clear, we can speculate the effect of the sharper angles on generating greater tensile stresses, that ultimately could influence morphogen signalling during differentiation.

More and more studies are supporting the importance of mechanical sensing in the embryonic kidney microenvironment (Weinbaum et al., 2010; Hamon et al., 2023; Nerger et al., 2024), yet not much is known about the effects of physical constraints such as rigidity and geometry on the transcriptomic landscape of nephrogenesis. Previous RNA-seq analysis of hPSCs cultured on soft vs still PAA matrices showed an increase in embryo and mesoderm related markers in the soft milieu at the hPSCs-stage, and a downregulation of ECM and basement membrane at the posterior primitive streak stage (Garreta et al., 2019). Future work would include performing an RNA analysis over the time course of nephrogenesis on different geometries and rigidities to investigate correlations between genes of nephron patterning and cell adhesion, spreading, polarization etc. in the background of wildtype, PAX2 KO and LHX1 KO human lines. Previous single – cell RNA analysis (and re-analysis) of mouse embryonic kidneys at D18.5 of development has shown an enrichment of genes in cell adhesion, cadherin expression, cortical cytoskeletal organization and actomyosin structure organization in cells of pre-tubular aggregates (PTAs) and renal vesicles (RVs) (Combes et al., 2019; Liu et al., 2024).

It is also important to note that here we have not explored the role of YAP as a mechano-sensitive transcription factor, that is also involved in differentiation of stem cells via the HIPPO pathway (Dupont et al., 2011; Piccolo, Dupont and Cordenonsi, 2014; Elosegui-Artola et al., 2017; Totaro et al., 2017). Uncoupling the role of YAP in morphogenesis of 2D kidney differentiation under the different physical constraints could provide valuable information on the mechanosensing and transduction during steps of nephrogenesis. Similarly, the mechanisms of other mechanosensing proteins in kidney function, such as Piezo1, crucial for sensing shear stress and wall tension for proper filtration, is largely unexplored, while its importance in the urinary tract is undeniable (Dalghi et al., 2019; Li et al., 2022).

In summary, our 2D kidney differentiation system on PDMS substrates, with the limitations discussed above, has provided us with some insights into the interplay between biochemical signalling, genetics and cell mechanics of *in vitro* human RV emergence and nephron differentiation. Our experimental pipeline and quantitative analysis set the bases for further experiments to mechanistically couple how RV emergence and nephron differentiation is driven by changes in the expression of specific renal markers and cell force generation.

Conclusions

1. We have developed a high-throughput system for 2D kidney differentiation (namely RV emergence and nephron-like formation) on soft PDMS substrates which allows the exposure of hPSCs-derived kidney progenitor cells to physical constraints in the form of substrate rigidity and geometry, and which is compatible with traction force measurements.

2. We have validated the system developed in this thesis in supporting RV emergence and nephron-like formation in 2D in the background of male ES[4]-, ES[4] PAX2 KO-, ES[4] LHX1 KO and female CB40 kidney progenitor cells.

3. Wild type ES[4] (ES4[4] CTRL)-kidney progenitor cells exert increasing traction forces on 3kPa PDMS substrates over time.

4. ES4[4] CTRL kidney progenitor cells exert higher traction forces compared to both PAX2 KO and LHX1 KO-derived kidney progenitor cells at the RV (D10) and nephron-like (D16) stages of differentiation.

5. ES4[4] CTRL kidney progenitor cells exhibit higher vorticity of traction fields compared to PAX2 KO and LHX1 KO counterparts at D10 and D16 of differentiation.

6. Geometric confinements in the form of circles results in higher expression of RV emergence and nephron differentiation markers in the background of ES[4] CTRL NPCs, compared to squares and triangulars.

7. ES4[4] CTRL kidney progenitor cells exhibit higher traction forces and vorticity on square and triangle patterns compared to circles.

8. Our experimental pipeline and quantitative analysis set the bases for further experiments to mechanistically couple how RV emergence and nephron differentiation is driven by changes in the expression of specific renal markers and cell force generation.

Contributions

Contributions to the thesis

The cell lines ES[4] WT1 GFP, LHX1 KO, PAX2 CTRL and PAX2 KO were generated by Carolina Tarantino and characterized by Lucia Selfa and Andres Marco. All kidney differentiation experiments (both in 3D and 2D) presented in Chapter 1 were performed by Zarina Nauryzgaliyeva. Gaia Amato performed the qPCR analysis of Figure 14C. The MATLAB codes for measuring traction forces were developed by Manuel Gomez and adapted by Miquel Bosch. Codes for measuring traction curls were developed by Miquel Bosch. All traction force experiments of Chapter 2 were performed and analysed by Zarina Nauryzgaliyeva. Image J macros for quantifying immunofluorescence intensities (both total and inner vs outer) were developed by Andres Marco. Analysis of images for chapter 2 was performed by Zarina Nauryzgaliyeva with the help of Agnes Resto and Gaia Amato.

All along the project we received guidance, supervision, and support from Elena Garreta, Nuria Montserrat and Xavier Trepat. The project was conceptualized by Nuria Montserrat.

References

Abugomaa, A., Elbadawy, M., Yamanaka, M., Goto, Y., Hayashi, K., Mori, T., Uchide, T., Azakami, D., Fukushima, R., Yoshida, T., Shibutani, M., Yamashita, R., Kobayashi, M., Yamawaki, H., Shinohara, Y., Kaneda, M., Usui, T., & Sasaki, K. (2020). Establishment of 2.5D organoid culture model using 3D bladder cancer organoid culture. *Scientific Reports*, *10*(1), 3–5. https://doi.org/10.1038/s41598-020-66229-w

Alcaraz, J., Xu, R., Mori, H., Nelson, C. M., Mroue, R., Spencer, V. A., Brownfield, D., Radisky, D. C., Bustamante, C., & Bissell, M. J. (2008). Laminin and biomimetic extracellular elasticity enhance functional differentiation in mammary epithelia. *EMBO Journal*, *27*(21), 2829–2838. https://doi.org/10.1038/emboj.2008.206

Andreu, I., Falcones, B., Hurst, S., Chahare, N., Quiroga, X., Roux, A. Le, Kechagia, Z., Beedle, A. E. M., & Elosegui-artola, A. (2021). The force loading rate drives cell mechanosensing through both reinforcement and cytoskeletal softening. *Nature Communications*, 1–12. https://doi.org/10.1038/s41467-021-24383-3

Andreu, I., Granero-moya, I., Chahare, N. R., Clein, K., Molina-jordán, M., Beedle, A. E. M., Elosegui-artola, A., Abenza, J. F., Rossetti, L., Trepat, X., Raveh, B., & Roca-cusachs, P. (2022). Mechanical force application to the nucleus regulates nucleocytoplasmic transport. *Nature Cell Biology*, *24*(June), 896–905. https://doi.org/10.1038/s41556-022-00927-7

Aragona, M., Panciera, T., Manfrin, A., Giulitti, S., Michielin, F., Elvassore, N., Dupont, S., & Piccolo, S. (2013). A mechanical checkpoint controls multicellular growth through YAP/TAZ regulation by actin-processing factors. *Cell*, *154*(5), 1047–1059. https://doi.org/10.1016/j.cell.2013.07.042

Arellano-Viera, E., Zabaleta, L., Castaño, J., Azkona, G., Carvajal-Vergara, X., & Giorgetti, A. (2019). Generation of two transgene-free human iPSC lines from CD133 + cord blood cells. *Stem Cell Research*, *36*(February), 101410. https://doi.org/10.1016/j.scr.2019.101410

Armstrong, J. F., Pritchard-Jones, K., Bickmore, W. A., Hastie, N. D., & Bard, J. B. L. (1993). The expression of the Wilms' tumour gene, WT1, in the developing mammalian embryo. *Mechanisms of Development*, *40*(1–2), 85–97. https://doi.org/10.1016/0925-4773(93)90090-K

Armstrong, P. B. (1989). Cell sorting out: The self-assembly of tissues in vitro. *Critical Reviews in Biochemistry and Molecular Biology*, *24*(2), 119–149. https://doi.org/10.3109/10409238909086396

Aspiroz, I. L. S. (2021). *Engineering human pluripotent stem cells to understand kidney development and disease*. Universitat Pompeu Fabra.

Badique, F., Stamov, D. R., Davidson, P. M., Veuillet, M., Reiter, G., Freund, J. N., Franz, C. M., & Anselme, K. (2013). Directing nuclear deformation on micropillared surfaces by substrate geometry and cytoskeleton organization. *Biomaterials*, *34*(12), 2991–3001. https://doi.org/10.1016/j.biomaterials.2013.01.018

Ban, E., Franklin, J. M., Nam, S., Smith, L. R., Wang, H., Wells, R. G., Chaudhuri, O., Liphardt, J. T., & Shenoy, V. B. (2018). Mechanisms of Plastic Deformation in Collagen Networks Induced by Cellular Forces. *Biophysical Journal*, *114*(2), 450–461. https://doi.org/10.1016/j.bpj.2017.11.3739

Barak, H., Huh, S.-H., Chen, S., Jeanpierre, C., Martinovic, J., Parisot, M., Bole-Feysot, C., Nitschké, P., Salomon, R., Antignac, C., Ornitz, D. M., & Kopan, R. (2012). Fgf9 and FGF20 maintain the stemness of nephron progenitors in mice and man. *Developmental Cell*, *22*(6), 1191–1207. https://doi.org/10.1016/j.devcel.2012.04.018.Fgf9

Barker, N., Huch, M., Kujala, P., van de Wetering, M., Snippert, H. J., van Es, J. H., Sato, T., Stange, D. E., Begthel, H., van den Born, M., Danenberg, E., van den Brink, S., Korving, J., Abo, A., Peters, P. J., Wright, N., Poulsom, R., & Clevers, H. (2010). Lgr5+ve Stem Cells Drive Self-Renewal in the Stomach and Build Long-Lived Gastric Units In Vitro. *Cell Stem Cell*, *6*(1), 25–36. https://doi.org/10.1016/j.stem.2009.11.013

Batchelder, C. A., Martinez, M. L., & Tarantal, A. F. (2015). Natural scaffolds for renal differentiation of human embryonic stem cells for kidney tissue

engineering. *PLoS ONE*, *10*(12), 1–18. https://doi.org/10.1371/journal.pone.0143849

Bauer, J., Emon, M. A. B., Staudacher, J. J., Thomas, A. L., Zessner-Spitzenberg, J., Mancinelli, G., Krett, N., Saif, M. T., & Jung, B. (2020). Increased stiffness of the tumor microenvironment in colon cancer stimulates cancer associated fibroblast-mediated prometastatic activin A signaling. *Scientific Reports*, *10*(1), 1–11. https://doi.org/10.1038/s41598-019-55687-6

Beloussov, L. V., Saveliev, S. V., Naumidi, I. I., & Novoselov, V. V. (1994). Mechanical Stresses in Embryonic Tissues: Patterns, Morphogenetic Role, and Involvement in Regulatory Feedback. *International Review of Cytology*, *150*(C), 1–34. https://doi.org/10.1016/S0074-7696(08)61535-1

Bergert, M., Lendenmann, T., Zündel, M., Ehret, A. E., Panozzo, D., Richner, P., Kim, D. K., Kress, S. J. P., Norris, D. J., Sorkine-Hornung, O., Mazza, E., Poulikakos, D., & Ferrari, A. (2016). Confocal reference free traction force microscopy. *Nature Communications*, *7*. https://doi.org/10.1038/ncomms12814

Berry, R. L., Ozdemir, D. D., Aronow, B., Lindström, N. O., Dudnakova, T., Thornburn, A., Perry, P., Baldock, R., Armit, C., Joshi, A., Jeanpierre, C., Shan, J., Vainio, S., Baily, J., Brownstein, D., Davies, J., Hastie, N. D., & Hohenstein, P. (2015). Deducing the stage of origin of Wilms' tumours from a developmental series of Wt1-mutant mice. *DMM Disease Models and Mechanisms*, *8*(8), 903–917. https://doi.org/10.1242/dmm.018523

Bertram, J. F., Douglas-Denton, R. N., Diouf, B., Hughson, M. D., & Hoy, W. E. (2011). Human nephron number: Implications for health and disease. *Pediatric Nephrology*, *26*(9), 1529–1533. https://doi.org/10.1007/s00467-011-1843-8

Bier, E., & De Robertis, E. M. (2015). BMP gradients: A paradigm for morphogen-mediated developmental patterning. *Science*, *348*(6242). https://doi.org/10.1126/science.aaa5838

Binari, R. C., Staveley, B. E., Johnson, W. A., Godavarti, R., Sasisekharan, R., & Manoukian, A. S. (1997). Genetic evidence that heparin-like glycosaminoglycans are involved in wingless signaling. *Development*, *124*(13), 2623–2632. https://doi.org/10.1242/dev.124.13.2623

Blackburn, A. T. M., & Miller, R. K. (2019). Modeling congenital kidney diseases in Xenopus laevis. *DMM Disease Models and Mechanisms*, *12*(4). https://doi.org/10.1242/dmm.038604

Blum, M., & Ott, T. (2019). Xenopus: An undervalued model organism to study and model human genetic disease. *Cells Tissues Organs*, *205*(5–6), 303–312. https://doi.org/10.1159/000490898

Bohn, S., Thomas, H., Turan, G., Ellard, S., Bingham, C., Hattersley, A. T., & Ryffel, G. U. (2003). Distinct molecular and morphogenetic properties of mutations in the human HNF1β gene that lead to defective kidney development. *Journal of the American Society of Nephrology*, *14*(8), 2033–2041. https://doi.org/10.1097/01.ASN.0000078808.70309.C4

Boualia, S. K., Gaitan, Y., Tremblay, M., Sharma, R., Cardin, J., Kania, A., & Bouchard, M. (2013). A core transcriptional network composed of Pax2/8, Gata3 and Lim1 regulates key players of pro/mesonephros morphogenesis. *Developmental Biology*, *382*(2), 555–566. https://doi.org/10.1016/j.ydbio.2013.07.028

Bouchard, M., Souabni, A., Mandler, M., Neubüser, A., & Busslinger, M. (2002). Nephric lineage specification by Pax2 and Pax8. *Genes and Development*, *16*(22), 2958–2970. https://doi.org/10.1101/gad.240102

Bower, M., Salomon, R., Allanson, J., Antignac, C., Benedicenti, F., Benetti, E., Binenbaum, G., Jensen, U. B., Cochat, P., Decramer, S., Dixon, J., Drouin, R., Falk, M. J., Feret, H., Gise, R., Hunter, A., Johnson, K., Kumar, R., Lavocat, M. P., … Heidet, L. (2012). Update of PAX2 mutations in renal coloboma syndrome and establishment of a locus-specific database. *Human Mutation*, *33*(3), 457–466. https://doi.org/10.1002/humu.22020

Britton, G., Chhabra, S., Massay, J., & Warmflash, A. (2021). Fate-Patterning of 2D Gastruloids and Ectodermal Colonies Using Micropatterned Human

Pluripotent Stem Cells. In M. R. Ebrahimikhani & J. Hislop (Eds.), *Programmed Morphogenesis. Methods and Protocols* (pp. 119–130). Springer. http://www.springer.com/series/7651

Broguiere, N., Isenmann, L., Hirt, C., Ringel, T., Placzek, S., Cavalli, E., Ringnalda, F., Villiger, L., Züllig, R., Lehmann, R., Rogler, G., Heim, M. H., Schüler, J., Zenobi-Wong, M., & Schwank, G. (2018). Growth of Epithelial Organoids in a Defined Hydrogel. *Advanced Materials*, *30*(43). https://doi.org/10.1002/adma.201801621

Brophy, P. D., Ostrom, L., Lang, K. M., & Dressler, G. R. (2001). Regulation of ureteric bud outgrowth by Pax2-dependent activation of the glial derived neurotrophic factor gene. *Development*, *128*(23), 4747–4756. https://doi.org/10.1242/dev.128.23.4747

Brown, A. C., Muthukrishnan, S. D., & Oxburgh, L. (2015). A synthetic Niche for Nephron Progenitor Cells. *Developmental Cell*, *34*(2), 229–241. https://doi.org/10.1016/j.devcel.2015.06.021.A

Brown, X. Q., Ookawa, K., & Wong, J. Y. (2005). Evaluation of polydimethylsiloxane scaffolds with physiologically-relevant elastic moduli: Interplay of substrate mechanics and surface chemistry effects on vascular smooth muscle cell response. *Biomaterials*, *26*(16), 3123–3129. https://doi.org/10.1016/j.biomaterials.2004.08.009

Buisson, I., Le Bouffant, R., Futel, M., Riou, J. F., & Umbhauer, M. (2015). Pax8 and Pax2 are specifically required at different steps of Xenopus pronephros development. *Developmental Biology*, *397*(2), 175–190. https://doi.org/10.1016/j.ydbio.2014.10.022

Bülow, R. D., & Boor, P. (2019). Extracellular Matrix in Kidney Fibrosis: More Than Just a Scaffold. *Journal of Histochemistry and Cytochemistry*, *67*(9), 643–661. https://doi.org/10.1369/0022155419849388

Butler, J. P., Toli-Nørrelykke, I. M., Fabry, B., & Fredberg, J. J. (2002). Traction fields, moments, and strain energy that cells exert on their surroundings. *American Journal of Physiology - Cell Physiology*, *282*(3 51-3), 595–605. https://doi.org/10.1152/ajpcell.00270.2001

Call, K. M., Glaser, T., Ito, C. Y., Buckler, A. J., Pelletier, J., Haber, D. A., Rose, E. A., Kral, A., Yeger, H., Lewis, W. H., Jones, C., & Housman, D. E. (1990). Isolation and characterization of a zinc finger polypeptide gene at the human chromosome 11 Wilms' tumor locus. *Cell*, *60*(3), 509–520. https://doi.org/10.1016/0092-8674(90)90601-A

Campàs, O. (2016). A toolbox to explore the mechanics of living embryonic tissues. *Seminars in Cell and Developmental Biology*, *55*, 119–130. https://doi.org/10.1016/j.semcdb.2016.03.011

Capeling, M. M., Czerwinski, M., Huang, S., Tsai, Y. H., Wu, A., Nagy, M. S., Juliar, B., Sundaram, N., Song, Y., Han, W. M., Takayama, S., Alsberg, E., Garcia, A. J., Helmrath, M., Putnam, A. J., & Spence, J. R. (2019). Nonadhesive Alginate Hydrogels Support Growth of Pluripotent Stem Cell-Derived Intestinal Organoids. *Stem Cell Reports*, *12*(2), 381–394. https://doi.org/10.1016/j.stemcr.2018.12.001

Carroll, T. J., Park, J. S., Hayashi, S., Majumdar, A., & McMahon, A. P. (2005). Wnt9b plays a central role in the regulation of mesenchymal to epithelial transitions underlying organogenesis of the mammalian urogenital system. *Developmental Cell*, *9*(2), 283–292. https://doi.org/10.1016/j.devcel.2005.05.016

Carroll, T. J., & Vize, P. D. (1999). Synergism between Pax-8 and lim-1 in embryonic kidney development. *Developmental Biology*, *214*(1), 46–59. https://doi.org/10.1006/dbio.1999.9414

Cassel De Camps, C., Aslani, S., Stylianesis, N., Nami, H., Mohamed, N. V., Durcan, T. M., & Moraes, C. (2022). Hydrogel Mechanics Influence the Growth and Development of Embedded Brain Organoids. *ACS Applied Bio Materials*, *5*(1), 214–224. https://doi.org/10.1021/acsabm.1c01047

Cattelan, G., Guerrero Gerbolés, A., Foresti, R., Pramstaller, P. P., Rossini, A., Miragoli, M., & Caffarra Malvezzi, C. (2020). Alginate Formulations: Current Developments in the Race for Hydrogel-Based Cardiac Regeneration. *Frontiers in Bioengineering and Biotechnology*, *8*(May). https://doi.org/10.3389/fbioe.2020.00414

Chaigne, A., Campillo, C., Gov, N. S., Voituriez, R., Azoury, J., Umaña-diaz, C., Almonacid, M., Queguiner, I., Nassoy, P., & Sykes, C. (2013). A soft cortex is essential for asymmetric spindle positioning in mouse oocytes. *Nature Cell Biology*, *15*(8), 958–966. https://doi.org/10.1038/ncb2799

Chambers, S. M., Fasano, C. A., Papapetrou, E. P., Tomishima, M., Sadelain, M., & Studer, L. (2009). Highly efficient neural conversion of human ES and iPS cells by dual inhibition of SMAD signaling. *Nature Biotechnology*, *27*(3), 275–280. https://doi.org/10.1038/nbt.1529

Chan, T. chuan, Takahashi, S., & Asashima, M. (2000). A role for Xlim-1 in pronephros development in Xenopus laevis. *Developmental Biology*, *228*(2), 256–269. https://doi.org/10.1006/dbio.2000.9951

Chang, Y. M., Chen, C. C., Lee, N. C., Sung, J. M., Chou, Y. Y., & Chiou, Y. Y. (2022). PAX2 Mutation-Related Renal Hypodysplasia: Review of the Literature and Three Case Reports. *Frontiers in Pediatrics*, *9*(January), 1–8. https://doi.org/10.3389/fped.2021.765929

Chatterjee, R., Ramos, E., Hoffman, M., Vanwinkle, J., Martin, D. R., Davis, T. K., Hoshi, M., Hmiel, S. P., Beck, A., Hruska, K., Coplen, D., Liapis, H., Mitra, R., Druley, T., Austin, P., & Jain, S. (2012). Traditional and targeted exome sequencing reveals common, rare and novel functional deleterious variants in RET-signaling complex in a cohort of living US patients with urinary tract malformations. *Human Genetics*, *131*(11), 1725–1738. https://doi.org/10.1007/s00439-012-1181-3

Chaudhuri, O., Cooper-White, J., Janmey, P. A., Mooney, D. J., & Shenoy, V. B. (2020). Effects of extracellular matrix viscoelasticity on cellular behaviour. *Nature*, *584*(7822), 535–546. https://doi.org/10.1038/s41586-020-2612-2

Chaudhuri, O., Gu, L., Klumpers, D., Darnell, M., Bencherif, S. A., Weaver, J. C., Huebsch, N., Lee, H. P., Lippens, E., Duda, G. N., & Mooney, D. J. (2016). Hydrogels with tunable stress relaxation regulate stem cell fate and activity. *Nature Materials*, *15*(3), 326–334. https://doi.org/10.1038/nmat4489

Chen, X., Zhao, X., & Wang, G. (2020). Review on marine carbohydrate-based gold nanoparticles represented by alginate and chitosan for biomedical application. *Carbohydrate Polymers*, *244*(May), 116311. https://doi.org/10.1016/j.carbpol.2020.116311

Cheng, S., Clarke, E. C., & Bilston, L. E. (2008). Rheological properties of the tissues of the central nervous system: A review. *Medical Engineering and Physics*, *30*(10), 1318–1337. https://doi.org/10.1016/j.medengphy.2008.06.003

Cheroki, C., Krepischi-Santos, A. C. V., Szuhai, K., Brenner, V., Kim, C. A. E., Otto, P. A., & Rosenberg, C. (2008). Genomic imbalances associated with müllerian aplasia. *Journal of Medical Genetics*, *45*(4), 228–232. https://doi.org/10.1136/jmg.2007.051839

Choudhury, M. I., Li, Y., Mistriotis, P., Vasconcelos, A. C. N., Dixon, E. E., Yang, J., Benson, M., Maity, D., Walker, R., Martin, L., Koroma, F., Qian, F., Konstantopoulos, K., Woodward, O. M., & Sun, S. X. (2022). Kidney epithelial cells are active mechano-biological fluid pumps. *Nature Communications*, *13*(1). https://doi.org/10.1038/s41467-022-29988-w

Chrisnandy, A., Blondel, D., Rezakhani, S., Broguiere, N., & Lutolf, M. P. (2022). Synthetic dynamic hydrogels promote degradation-independent in vitro organogenesis. *Nature Materials*, *21*(4), 479–487. https://doi.org/10.1038/s41563-021-01136-7

Chuah, Y. J., Koh, Y. T., Lim, K., Menon, N. V., Wu, Y., & Kang, Y. (2015). Simple surface engineering of polydimethylsiloxane with polydopamine for stabilized mesenchymal stem cell adhesion and multipotency. *Scientific Reports*, *5*(November), 1–12. https://doi.org/10.1038/srep18162

Clark, A. G., Maitra, A., Jacques, C., Bergert, M., Pérez-González, C., Simon, A., Lederer, L., Diz-Muñoz, A., Trepat, X., Voituriez, R., & Vignjevic, D. M. (2022). Self-generated gradients steer collective migration on viscoelastic collagen networks. In *Nature Materials* (Vol. 21, Issue 10). Springer US. https://doi.org/10.1038/s41563-022-01259-5

Colombo, K., Grill, S. W., Kimple, R. J., Willard, F. S., Siderovski, D. P., & Gönczy, P. (2003). Translation of polarity cues into asymmetric spindle positioning in Caenorhabditis elegans embryos. *Science*, *300*(5627), 1957–1961. https://doi.org/10.1126/science.1084146

Combes, A. N., Phipson, B., Lawlor, K. T., Dorison, A., Patrick, R., Zappia, L., Harvey, R. P., Oshlack, A., & Little, M. H. (2019). Correction: Single cell analysis of the developing mouse kidney provides deeper insight into marker gene expression and ligand-receptor crosstalk (Development, (2019) 146, 12, 10.1242/dev.178673). *Development (Cambridge)*, *146*(13). https://doi.org/10.1242/dev.182162

Connelly, J. T., Gautrot, J. E., Trappmann, B., Tan, D. W. M., Donati, G., Huck, W. T. S., & Watt, F. M. (2010). Actin and serum response factor transduce physical cues from the microenvironment to regulate epidermal stem cell fate decisions. *Nature Cell Biology*, *12*(7), 711–718. https://doi.org/10.1038/ncb2074

Cruciat, C. M., & Niehrs, C. (2013). Secreted and transmembrane Wnt inhibitors and activators. *Cold Spring Harbor Perspectives in Biology*, *5*(3). https://doi.org/10.1101/cshperspect.a015081

Cruz, N. M., Song, X., Czerniecki, S. M., Gulieva, R. E., Churchill, A. J., Kim, Y. K., Winston, K., Tran, L. M., Diaz, M. A., Fu, H., Finn, L. S., Pei, Y., Himmelfarb, J., & Freedman, B. S. (2017). Organoid cystogenesis reveals a critical role of microenvironment in human polycystic kidney disease. *Nature Materials*, *16*(11), 1112–1119. https://doi.org/10.1038/NMAT4994

Cullen-McEwen, L. A., Caruana, G., & Bertram, J. F. (2005). The where, what and why of the developing renal stroma. *Nephron - Experimental Nephrology*, *99*(1), 1–8. https://doi.org/10.1159/000081792

Cullen-McEwen, L. A., Kett, M. M., Dowling, J., Anderson, W. P., & Bertram, J. F. (2003). Nephron number, renal function, and arterial pressure in aged GDNF heterozygous mice. *Hypertension*, *41*(2), 335–340. https://doi.org/10.1161/01.HYP.0000050961.70182.56

Cullen-McEwen, L., Sutherland, M. R., & Black, M. J. (2015). The Human Kidney: Parallels in Structure, Spatial Development, and Timing of Nephrogenesis. In *Kidney Development, Disease, Repair and Regeneration* (Vol. 1). Elsevier Inc. https://doi.org/10.1016/B978-0-12-800102-8.00003-5

Czerniecki, S. M., Cruz, N. M., Harder, J. L., Menon, R., Annis, J., Otto, E. A., Gulieva, R. E., Islas, L. V., Kim, Y. K., Tran, L. M., Martins, T. J., Pippin, J. W., Fu, H., Kretzler, M., Shankland, S. J., Himmelfarb, J., Moon, R. T., Paragas, N., & Freedman, B. S. (2018). High-Throughput Screening Enhances Kidney Organoid Differentiation from Human Pluripotent Stem Cells and Enables Automated Multidimensional Phenotyping. *Cell Stem Cell*, *22*(6), 929-940.e4. https://doi.org/10.1016/j.stem.2018.04.022

Daley, W. P., Kohn, J. M., & Larsen, M. (2011). A focal adhesion protein-based mechanochemical checkpoint regulates cleft progression during branching morphogenesis. *Developmental Dynamics*, *240*(9), 2069–2083. https://doi.org/10.1002/dvdy.22714

Dalghi, M. G., Clayton, D. R., Ruiz, W. G., Al-Bataineh, M. M., Satlin, L. M., Kleyman, T. R., Ricke, W. A., Carattino, M. D., & Apodaca, G. (2019). Expression and distribution of PIEZO1 in the mouse urinary tract. *American Journal of Physiology - Renal Physiology*, *317*(2), F303–F321. https://doi.org/10.1152/ajprenal.00214.2019

D'Arcangelo, E., & McGuigan, A. P. (2015). Micropatterning strategies to engineer controlled cell and tissue architecture in vitro. *BioTechniques*, *58*(1), 13–23. https://doi.org/10.2144/000114245

Davies, J. A., Ladomery, M., Hohenstein, P., Michael, L., Shafe, A., Spraggon, L., & Hestie, N. (2004). Development of an siRNA-based method for repressing specific genes in renal organ culture and its use to show that the Wt1 tumour suppressor is required for nephron differentiation. *Human Molecular Genetics*, *13*(2), 235–246. https://doi.org/10.1093/hmg/ddh015

Davis, J. O., Carpenter, C. C., Ayers, C. R., Holman, J. E., & Bahn, R. C. (1961). Evidence for secretion of an aldosterone-stimulating hormone by the

kidney. *The Journal of Clinical Investigation*, *40*, 684–696. https://doi.org/10.1172/JCI104301

De Belly, H., Paluch, E. K., & Chalut, K. J. (2022). Interplay between mechanics and signalling in regulating cell fate. *Nature Reviews Molecular Cell Biology*, *23*(7), 465–480. https://doi.org/10.1038/s41580-022-00472-z

De Robertis, E. M., Larraín, J., Oelgeschläger, M., & Wessely, O. (2000). The establishment of Spemann's organizer and patterning of the vertebrate embryo. *Nature Reviews Genetics*, *1*(3), 171–181. https://doi.org/10.1038/35042039

Deacon, P., Concodora, C. W., Chung, E., & Park, J. S. (2019). B-Catenin Regulates the Formation of Multiple Nephron Segments in the Mouse Kidney. *Scientific Reports*, *9*(1), 1–13. https://doi.org/10.1038/s41598-019-52255-w

Deglincerti, A., Etoc, F., Guerra, M. C., Martyn, I., Metzger, J., Ruzo, A., Simunovic, M., Yoney, A., Brivanlou, A. H., Siggia, E., & Warmflash, A. (2016). Self-organization of human embryonic stem cells on micropatterns. *Nature Protocols*, *11*(11), 2223–2232. https://doi.org/10.1038/nprot.2016.131

DeLay, B. D., Corkins, M. E., Hanania, H. L., Salanga, M., Deng, J. M., Sudou, N., Taira, M., Horb, M. E., & Miller, R. K. (2018). Tissue-Specific Gene Inactivation in Xenopus laevis: Knockout of lhx1 in the Kidney with CRISPR/Cas9. *Genetics*, *208*(February), 673–686. https://doi.org/10.1534/genetics.117.300468/-/DC1.1

Dembo, M., & Wang, Y.-L. (1999). Stresses at the Cell-to-Substrate Interface during Locomotion of Fibroblasts. *Biophysical Journal*, *76*(April), 2307–2316. https://www.ncbi.nlm.nih.gov/pmc/articles/PMC1300203/pdf/10096925.pdf%0Apapers://93f2eea4-15a4-4ebf-aabd-9521e30fc280/Paper/p1429

Dhillon, P., Park, J., Hurtado del Pozo, C., Li, L., Doke, T., Huang, S., Zhao, J., Kang, H. M., Shrestra, R., Balzer, M. S., Chatterjee, S., Prado, P., Han, S. Y., Liu, H., Sheng, X., Dierickx, P., Batmanov, K., Romero, J. P., Prósper, F., …

Susztak, K. (2021). The Nuclear Receptor ESRRA Protects from Kidney Disease by Coupling Metabolism and Differentiation. *Cell Metabolism*, *33*(2), 379-394.e8. https://doi.org/10.1016/j.cmet.2020.11.011

Discher, D. E., Janmey, P., & Wang, Y. L. (2005). Tissue cells feel and respond to the stiffness of their substrate. *Science*, *310*(5751), 1139–1143. https://doi.org/10.1126/science.1116995

Dong, C., & Lv, Y. (2016). Application of collagen scaffold in tissue engineering: Recent advances and new perspectives. *Polymers*, *8*(2), 1–20. https://doi.org/10.3390/polym8020042

Drake, K. A., Chaney, C. P., Das, A., Roy, P., Kwartler, C. S., Rakheja, D., & Carroll, T. J. (2020). Stromal β-catenin activation impacts nephron progenitor differentiation in the developing kidney and may contribute to Wilms tumor. *Development (Cambridge)*, *147*(21), 1–14. https://doi.org/10.1242/DEV.189597

Drash, A., Sherman, F., Hartman, W. H., & Blizzard, R. M. (1970). A syndrome ofpseudobermapbroditism , Wilms ' tumor , bypertemion , and degenerative renal disease. *Journal of Pediatrics*, *76*(4), 585–593.

Dressler, G. R. (2006). The cellular basis of kidney development. *Annual Review of Cell and Developmental Biology*, *22*, 509–529. https://doi.org/10.1146/annurev.cellbio.22.010305.104340

Dressler, G. R. (2009). Advances in early kidney specification, development and patterning. *Development*, *136*(23), 3863–3874. https://doi.org/10.1242/dev.034876

Dressler, G. R., Deutsch, U., Chowdhury, K., Nornes, H. O., & Gruss, P. (1990). Pax2, a new murine paired-box-containing gene and its expression in the developing excretory system. *Development*, *109*(4), 787–795. https://doi.org/10.1242/dev.109.4.787

Drury, J. L., & Mooney, D. J. (2003). Hydrogels for tissue engineering: Scaffold design variables and applications. *Biomaterials*, *24*(24), 4337–4351. https://doi.org/10.1016/S0142-9612(03)00340-5

Duffy, D. C., McDonald, J. C., Schueller, O. J. A., & Whitesides, G. M. (1998). Rapid prototyping of microfluidic systems in poly(dimethylsiloxane). *Analytical Chemistry*, *70*(23), 4974–4984. https://doi.org/10.1021/ac980656z

Dupont, S., Morsut, L., Aragona, M., Enzo, E., Giulitti, S., Cordenonsi, M., Zanconato, F., Le Digabel, J., Forcato, M., Bicciato, S., Elvassore, N., & Piccolo, S. (2011). Role of YAP/TAZ in mechanotransduction. *Nature*, *474*(7350), 179–184. https://doi.org/10.1038/nature10137

Edelstein, Arthur, D., Tsuchida, M. A., Amodaj, N., Henry, P., Vale, R. D., & Stuurman, N. (2015). Advanced methods of microscope control using μManager software. *Journal of Biological Methods*, *1*(2). https://doi.org/10.14440/jbm.2014.36.Advanced

Eiraku, M., Watanabe, K., Matsuo-Takasaki, M., Kawada, M., Yonemura, S., Matsumura, M., Wataya, T., Nishiyama, A., Muguruma, K., & Sasai, Y. (2008). Self-Organized Formation of Polarized Cortical Tissues from ESCs and Its Active Manipulation by Extrinsic Signals. *Cell Stem Cell*, *3*(5), 519–532. https://doi.org/10.1016/j.stem.2008.09.002

Eisenhoffer, G. T., Loftus, P. D., Yoshigi, M., Otsuna, H., Chien, C. Bin, Morcos, P. A., & Rosenblatt, J. (2012). Crowding induces live cell extrusion to maintain homeostatic cell numbers in epithelia. *Nature*, *484*(7395), 546–549. https://doi.org/10.1038/nature10999

Elosegui-Artola, A. (2021). The extracellular matrix viscoelasticity as a regulator of cell and tissue dynamics. *Current Opinion in Cell Biology*, *72*, 10–18. https://doi.org/10.1016/j.ceb.2021.04.002

Elosegui-Artola, A., Andreu, I., Beedle, A. E. M., Lezamiz, A., Uroz, M., Kosmalska, A. J., Oria, R., Kechagia, J. Z., Rico-Lastres, P., Le Roux, A. L., Shanahan, C. M., Trepat, X., Navajas, D., Garcia-Manyes, S., & Roca-Cusachs, P. (2017a). Force Triggers YAP Nuclear Entry by Regulating Transport across Nuclear Pores. *Cell*, *171*(6), 1397-1410.e14. https://doi.org/10.1016/j.cell.2017.10.008

Elosegui-Artola, A., Andreu, I., Beedle, A. E. M., Lezamiz, A., Uroz, M., Kosmalska, A. J., Oria, R., Kechagia, J. Z., Rico-Lastres, P., Le Roux, A. L., Shanahan, C. M., Trepat, X., Navajas, D., Garcia-Manyes, S., & Roca-Cusachs, P. (2017b). Force Triggers YAP Nuclear Entry by Regulating Transport across Nuclear Pores. *Cell*, *171*(6), 1397-1410.e14. https://doi.org/10.1016/j.cell.2017.10.008

Elosegui-Artola, A., Gupta, A., Najibi, A. J., Seo, B. R., Garry, R., Darnell, M., Gu, W., Zhou, Q., Weitz, D. A., Mahadevan, L., & Mooney, D. J. (2022). Matrix viscoelasticity controls spatio-temporal tissue organization. *Nature Materials*, *22*, 117–127. https://doi.org/10.1038/s41563-022-01400-4

Elosegui-Artola, A., Oria, R., Chen, Y., Kosmalska, A., Pérez-González, C., Castro, N., Zhu, C., Trepat, X., & Roca-Cusachs, P. (2016). Mechanical regulation of a molecular clutch defines force transmission and transduction in response to matrix rigidity. *Nature Cell Biology*, *18*(5), 540–548. https://doi.org/10.1038/ncb3336

Engler, A. J., Sen, S., Sweeney, H. L., & Discher, D. E. (2006). Matrix Elasticity Directs Stem Cell Lineage Specification. *Cell*, *126*(25), 677–689. https://doi.org/10.1016/j.cell.2006.06.044

Essafi, A., Webb, A., Berry, R. L., Slight, J., Burn, S. F., Spraggon, L., Velecela, V., Martinez-Estrada, O. M., Wiltshire, J. H., Roberts, S. G. E., Brownstein, D., Davies, J. A., Hastie, N. D., & Hohenstein, P. (2011). A Wt1-Controlled chromatin switching mechanism underpins tissue-specific wnt4 activation and repression. *Developmental Cell*, *21*(3), 559–574. https://doi.org/10.1016/j.devcel.2011.07.014

Etezadi, F., Tuyet Le, M. N., Shahsavarani, H., Alipour, A., Moazzezy, N., Samani, S., Amanzadeh, A., Pahlavan, S., Bonakdar, S., Shokrgozar, M. A., & Hasegawa, K. (2022). Optimization of a PDMS-Based Cell Culture Substrate for High-Density Human-Induced Pluripotent Stem Cell Adhesion and Long-Term Differentiation into Cardiomyocytes under a Xeno-Free Condition. *ACS Biomaterials Science and Engineering*, *8*(5), 2040–2052. https://doi.org/10.1021/acsbiomaterials.2c00162

Faa, G., Gerosa, C., Fanni, D., Monga, G., Zaffanello, M., Van Eyken, P., & Fanos, V. (2012). Morphogenesis and molecular mechanisms involved in human kidney development. *Journal of Cellular Physiology*, *227*(3), 1257–1268. https://doi.org/10.1002/jcp.22985

Farge, E. (2003). Mechanical Induction of Twist in the Drosophila Foregut/Stomodeal Primordium. *Current Biology*, *13*, 1365–1377. https://doi.org/10.1016/S

Favor, J., Sandulache, R., Neuhäuser-Klaus, A., Pretsch, W., Chatterjee, B., Senft, E., Wurst, W., Blanquet, V., Grimes, P., Spörle, R., & Schughart, K. (1996). The mouse Pax21Neu mutation is identical to a human PAX2 mutation in a family with renal-coloboma syndrome and results in developmental defects of the brain, ear, eye, and kidney. *Proceedings of the National Academy of Sciences of the United States of America*, *93*(24), 13870–13875. https://doi.org/10.1073/pnas.93.24.13870

Feroze, R., Shawky, J. H., von Dassow, M., & Davidson, L. A. (2015). Mechanics of blastopore closure during amphibian gastrulation. *Developmental Biology*, *398*(1), 57–67. https://doi.org/10.1016/j.ydbio.2014.11.011

Forbes, J. M. (2016). Mitochondria-Power Players in Kidney Function? *Trends in Endocrinology and Metabolism*, *27*(7), 441–442. https://doi.org/10.1016/j.tem.2016.05.002

Frasier, S. D., Crudo, F. S., & Farrell, F. J. (1964). Buccal smears in the newborn female. *The Journal of Pediatrics*, *65*(2), 222–225. https://doi.org/10.1016/S0022-3476(64)80523-0

Freedman, B. S., Brooks, C. R., Lam, A. Q., Fu, H., Morizane, R., Agrawal, V., Saad, A. F., Li, M. K., Hughes, M. R., Werff, R. Vander, Peters, D. T., Lu, J., Baccei, A., Siedlecki, A. M., Valerius, M. T., Musunuru, K., McNagny, K. M., Steinman, T. I., Zhou, J., … Bonventre, J. V. (2015). Modelling kidney disease with CRISPR-mutant kidney organoids derived from human pluripotent epiblast spheroids. *Nature Communications*, *6*(May). https://doi.org/10.1038/ncomms9715

Freund, J. B., Goetz, J. G., Hill, K. L., & Vermot, J. (2012). Erratum to Fluid flows and forces in development: Functions, features and biophysical principles (Development, 139, (1229-1245)). *Development (Cambridge)*, *139*(16), 3063. https://doi.org/10.1242/dev.085902

Fu, S., Thacker, A., Sperger, D. M., Boni, R. L., Velankar, S., Munson, E. J., & Block, L. H. (2010). Rheological evaluation of inter-grade and inter-batch variability of sodium alginate. *AAPS PharmSciTech*, *11*(4), 1662–1674. https://doi.org/10.1208/s12249-010-9547-0

Garreta, E., Moya-Rull, D., Stanifer, M. L., Monteil, V., Prado, P., Marco, A., Tarantino, C., Gallo, M., Jonsson, G., Hagelkruys, A., Mirazimi, A., Boulant, S., Penninger, J. M., & Montserrat, N. (2022). Protocol for SARS-CoV-2 infection of kidney organoids derived from human pluripotent stem cells. *STAR Protocols*, *3*(4). https://doi.org/10.1016/j.xpro.2022.101872

Garreta, E., Oria, R., Tarantino, C., Pla-Roca, M., Prado, P., Fernández-Avilés, F., Campistol, J. M., Samitier, J., & Montserrat, N. (2017). Tissue engineering by decellularization and 3D bioprinting. *Materials Today*, *20*(4), 166–178. https://doi.org/10.1016/j.mattod.2016.12.005

Garreta, E., Prado, P., Stanifer, M. L., Monteil, V., Marco, A., Ullate-Agote, A., Moya-Rull, D., Vilas-Zornoza, A., Tarantino, C., Romero, J. P., Jonsson, G., Oria, R., Leopoldi, A., Hagelkruys, A., Gallo, M., González, F., Domingo-Pedrol, P., Gavaldà, A., del Pozo, C. H., … Montserrat, N. (2022). A diabetic milieu increases ACE2 expression and cellular susceptibility to SARS-CoV-2 infections in human kidney organoids and patient cells. *Cell Metabolism*, *34*(6), 857-873.e9. https://doi.org/10.1016/j.cmet.2022.04.009

Garreta, E., Prado, P., Tarantino, C., Oria, R., Fanlo, L., Martí, E., Zalvidea, D., Trepat, X., Roca-Cusachs, P., Gavaldà-Navarro, A., Cozzuto, L., Campistol, J. M., Izpisúa Belmonte, J. C., Hurtado del Pozo, C., & Montserrat, N. (2019). Fine tuning the extracellular environment accelerates the derivation of kidney organoids from human pluripotent stem cells. *Nature Materials*, *18*(4), 397–405. https://doi.org/10.1038/s41563-019-0287-6

Geerligs, M., Peters, G. W. M., Ackermans, P. A. J., Oomens, C. W. J., & Baaijens, F. P. T. (2008). Linear viscoelastic behavior of subcutaneous adipose tissue. *Biorheology*, *45*(6), 677–688. https://doi.org/10.3233/BIR-2008-0517

Georgas, K., Rumballe, B., Valerius, M. T., Chiu, H. S., Thiagarajan, R. D., Lesieur, E., Aronow, B. J., Brunskill, E. W., Combes, A. N., Tang, D., Taylor, D., Grimmond, S. M., Potter, S. S., McMahon, A. P., & Little, M. H. (2009). Analysis of early nephron patterning reveals a role for distal RV proliferation in fusion to the ureteric tip via a cap mesenchyme-derived connecting segment. *Developmental Biology*, *332*(2), 273–286. https://doi.org/10.1016/j.ydbio.2009.05.578

Geuens, T., Ruiter, F. A. A., Schumacher, A., Morgan, F. L. C., Rademakers, T., Wiersma, L. E., van den Berg, C. W., Rabelink, T. J., Baker, M. B., & LaPointe, V. L. S. (2021). Thiol-ene cross-linked alginate hydrogel encapsulation modulates the extracellular matrix of kidney organoids by reducing abnormal type 1a1 collagen deposition. *Biomaterials*, *275*(June), 120976. https://doi.org/10.1016/j.biomaterials.2021.120976

Gimenez, A. M. (2021). *Generation and Validation of a CRISPR Platform for Rapid and Inducible Genome Editing in Human Pluripotent Stem Cells and Kidney Organoids Andrés Marco Giménez*. Universitat Pompeu Fabra.

Girardo, S., Träber, N., Wagner, K., Cojoc, G., Herold, C., Goswami, R., Schlüßler, R., Abuhattum, S., Taubenberger, A., Reichel, F., Mokbel, D., Herbig, M., Schürmann, M., Müller, P., Heida, T., Jacobi, A., Ulbricht, E., Thiele, J., Werner, C., & Guck, J. (2018). Standardized microgel beads as elastic cell mechanical probes. *Journal of Materials Chemistry B*, *6*(39), 6245–6261. https://doi.org/10.1039/c8tb01421c

Gjorevski, N., Nikolaev, M., Brown, T. E., Mitrofanova, O., Brandenberg, N., DelRio, F. W., Yavitt, F. M., Liberali, P., Anseth, K. S., & Lutolf, M. P. (2022). Tissue geometry drives deterministic organoid patterning. *Science*, *375*(6576). https://doi.org/10.1126/science.aaw9021

Gjorevski, N., Sachs, N., Manfrin, A., Giger, S., Bragina, M. E., Ordóñez-Morán, P., Clevers, H., & Lutolf, M. P. (2016). Designer matrices for intestinal stem cell and organoid culture. *Nature*, *539*(7630), 560–564. https://doi.org/10.1038/nature20168

Glowacki, J., & Mizuno, S. (2008). Collagen scaffolds for tissue engineering. *Biopolymers*, *89*(5), 338–344. https://doi.org/10.1002/bip.20871

Godeau, A. L., Leoni, M., Comelles, J., Guyomar, T., Lieb, M., Delanoë-Ayari, H., Ott, A., Harlepp, S., Sens, P., & Riveline, D. (2022). 3D single cell migration driven by temporal correlation between oscillating force dipoles. *ELife*, *11*, 1–24. https://doi.org/10.7554/ELIFE.71032

Goodwin, K., & Nelson, C. M. (2021). Mechanics of Development. *Developmental Cell*, *56*(2), 240–250. https://doi.org/10.1016/j.devcel.2020.11.025

Grashoff, C., Hoffman, B. D., Brenner, M. D., Zhou, R., Parsons, M., Yang, M. T., McLean, M. A., Sligar, S. G., Chen, C. S., Ha, T., & Schwartz, M. A. (2010). Measuring mechanical tension across vinculin reveals regulation of focal adhesion dynamics. *Nature*, *466*(7303), 263–266. https://doi.org/10.1038/nature09198

Grobstein, C. (1956). Trans-filter induction of tubules in mouse metanephrogenic mesenchyme. *Experimental Cell Research*, *10*(2), 424–440. https://doi.org/10.1016/0014-4827(56)90016-7

Guilak, F., Cohen, D. M., Estes, B. T., Gimble, J. M., Liedtke, W., & Chen, C. S. (2009). Control of Stem Cell Fate by Physical Interactions with the Extracellular Matrix. *Cell Stem Cell*, *5*(1), 17–26. https://doi.org/10.1016/j.stem.2009.06.016

Guillamat, P., Ignés-Mullol, J., & Sagués, F. (2017). Taming active turbulence with patterned soft interfaces. *Nature Communications*, *8*(1), 1–8. https://doi.org/10.1038/s41467-017-00617-1

Gupta, A. K., Ivancic, D. Z., Naved, B. A., Wertheim, J. A., & Oxburgh, L. (2021). An efficient method to generate kidney organoids at the air-liquid interface.

Journal of Biological Methods, *8*(2), e150. https://doi.org/10.14440/jbm.2021.357

Gurdon, J. B., Elsdale, T. R., & Fischberg, M. (1958). Sexually Mature Individuals of Xenopus laevis from the Transplantation of Single Somatic Nuclei. *Nature*, *182*(4627), 64–65.

Guyette, J. P., Gilpin, S. E., Charest, J. M., Tapias, L. F., Ren, X., & Ott, H. C. (2014). Perfusion decellularization of whole organs. *Nature Protocols*, *9*(6), 1451–1468. https://doi.org/10.1038/nprot.2014.097

Halt, K., & Vainio, S. (2014). Coordination of kidney organogenesis by Wnt signaling. *Pediatric Nephrology*, *29*(4), 737–744. https://doi.org/10.1007/s00467-013-2733-z

Hamon, M., Chen, Y., Srivastava, P., Chang, H. M., Gupta, V., Jin, L., Yanagawa, N., & Hauser, P. V. (2023). Matrix Stiffness Influences Tubular Formation in Renal Tissue Engineering. *Applied Sciences (Switzerland)*, *13*(7). https://doi.org/10.3390/app13074510

Han, S. J., Oak, Y., Groisman, A., & Danuser, G. (2015). Traction microscopy to identify force modulation in subresolution adhesions. *Nature Methods*, *12*(7), 653–656. https://doi.org/10.1038/nmeth.3430

Han, W., Chen, S., Yuan, W., Fan, Q., Tian, J., Wang, X., Chen, L., Zhang, X., Wei, W., Liu, R., Qu, J., Jiao, Y., Austin, R. H., & Liu, L. (2016). Oriented collagen fibers direct tumor cell intravasation. *Proceedings of the National Academy of Sciences of the United States of America*, *113*(40), 11208–11213. https://doi.org/10.1073/pnas.1610347113

Harrington, W. F. (1979). On the origin of the contractile force in skeletal muscle. *Proceedings of the National Academy of Sciences of the United States of America*, *76*(10), 5066–5070. https://doi.org/10.1073/pnas.76.10.5066

Harris, A. R., Peter, L., Bellis, J., Baum, B., Kabla, A. J., & Charras, G. T. (2012). Characterizing the mechanics of cultured cell monolayers. *Proceedings of*

the National Academy of Sciences of the United States of America, *109*(41), 16449–16454. https://doi.org/10.1073/pnas.1213301109

Heisenberg, C. P., & Bellaïche, Y. (2013). Forces in tissue morphogenesis and patterning. *Cell*, *153*(5), 948. https://doi.org/10.1016/j.cell.2013.05.008

Heliot, C., Desgrange, A., Buisson, I., Prunskaite-Hyyryläinen, R., Shan, J., Vainio, S., Umbhauer, M., & Cereghini, S. (2013). HNF1B controls proximal-intermediate nephron segment identity in vertebrates by regulating Notch signalling components and Irx1/2. *Development (Cambridge)*, *140*(4), 873–885. https://doi.org/10.1242/dev.086538

Hellsten, U., Harland, R. M., Gilchrist, M. J., Hendrix, D., Jurka, J., Kapitonov, V., Ovcharenko, I., Putnam, N. H., Shu, S., Taher, L., Blitz, I. L., Blumberg, B., Dichmann, D. S., Dubchak, L., Amaya, E., Detter, J. C., Fletcher, R., Gerhard, D. S., Goodstein, D., … Rokhsar, D. S. (2010). The genome of the western clawed frog xenopus tropicalis. *Science*, *328*(5978), 633–636. https://doi.org/10.1126/science.1183670

Hens, J. R., Wilson, K. M., Dann, P., Chen, X., Horowitz, M. C., & Wysolmerski, J. J. (2005). TOPGAL mice show that the canonical Wnt signaling pathway is active during bone development and growth and is activated by mechanical loading in vitro. *Journal of Bone and Mineral Research*, *20*(7), 1103–1113. https://doi.org/10.1359/JBMR.050210

Homan, K. A., Gupta, N., Kroll, K. T., Kolesky, D. B., Skylar-Scott, M., Miyoshi, T., Mau, D., Valerius, M. T., Ferrante, T., Bonventre, J. V., Lewis, J. A., & Morizane, R. (2019). Flow-enhanced vascularization and maturation of kidney organoids in vitro. *Nature Methods*, *16*(3), 255–262. https://doi.org/10.1038/s41592-019-0325-y

Hong, X., Yuan, Y., Sun, X., Zhou, M., Guo, G., Zhang, Q., Hescheler, J., & Xi, J. (2018). Skeletal Extracellular Matrix Supports Cardiac Differentiation of Embryonic Stem Cells: A Potential Scaffold for Engineered Cardiac Tissue. *Cellular Physiology and Biochemistry*, *45*(1), 319–331. https://doi.org/10.1159/000486813

Howden, S. E., Vanslambrouck, J. M., Wilson, S. B., Tan, K. S., & Little, M. H. (2019). Reporter-based fate mapping in human kidney organoids confirms nephron lineage relationships and reveals synchronous nephron formation. *EMBO Reports*, *20*(4), 1–13. https://doi.org/10.15252/embr.201847483

Howe, K., Clark, M. D., Torroja, C. F., Torrance, J., Berthelot, C., Muffato, M., Collins, J. E., Humphray, S., McLaren, K., Matthews, L., McLaren, S., Sealy, I., Caccamo, M., Churcher, C., Scott, C., Barrett, J. C., Koch, R., Rauch, G.-J., White, S., … Stemple, D. L. (2013). The zebrafish reference genome sequence and its relationship to the human genome. *Nature*, *496*(April 2013), 498–503.

Huch, M., Bonfanti, P., Boj, S. F., Sato, T., Loomans, C. J. M., Van De Wetering, M., Sojoodi, M., Li, V. S. W., Schuijers, J., Gracanin, A., Ringnalda, F., Begthel, H., Hamer, K., Mulder, J., Van Es, J. H., De Koning, E., Vries, R. G. J., Heimberg, H., & Clevers, H. (2013). Unlimited in vitro expansion of adult bi-potent pancreas progenitors through the Lgr5/R-spondin axis. *EMBO Journal*, *32*(20), 2708–2721. https://doi.org/10.1038/emboj.2013.204

Huebsch, N., Arany, P. R., Mao, A. S., Shvartsman, D., Ali, O. A., Bencherif, S. A., Rivera-Feliciano, J., & Mooney, D. J. (2010). Harnessing traction-mediated manipulation of the cell/matrix interface to control stem-cell fate. *Nature Materials*, *9*(6), 518–526. https://doi.org/10.1038/nmat2732

Humbert, C., Silbermann, F., Morar, B., Parisot, M., Zarhrate, M., Masson, C., Tores, F., Blanchet, P., Perez, M. J., Petrov, Y., Khau Van Kien, P., Roume, J., Leroy, B., Gribouval, O., Kalaydjieva, L., Heidet, L., Salomon, R., Antignac, C., Benmerah, A., … Jeanpierre, C. (2014). Integrin alpha 8 recessive mutations are responsible for bilateral renal agenesis in humans. *American Journal of Human Genetics*, *94*(2), 288–294. https://doi.org/10.1016/j.ajhg.2013.12.017

Ichikawa, I., Kuwayama, F., Pope, J. C., Stephens, F. D., & Miyazaki, Y. (2002). Paradigm shift from classic anatomic theories to contemporary cell biological views of CAKUT. *Kidney International*, *61*(3), 889–898. https://doi.org/10.1046/j.1523-1755.2002.00188.x

Irianto, J., Xia, Y., Pfeifer, C. R., Greenberg, R. A., & Discher, D. E. (2016). As a nucleus enters a small pore , chromatin stretches and maintains integrity even with DNA breaks. *Biophys. J.*, *112*, 446–449. https://doi.org/10.1016/j.bpj.2016.09.047

Jain, I., Berg, I. C., Acharya, A., Blaauw, M., Gosstola, N., Perez-Pinera, P., & Underhill, G. H. (2022). Delineating cooperative effects of Notch and biomechanical signals on patterned liver differentiation. *Communications Biology*, *5*(1), 1–16. https://doi.org/10.1038/s42003-022-03840-9

Jain, S. (2009). The many faces of RET dysfunction in kidney. *Organogenesis*, *5*(4). https://doi.org/10.4161/org.5.4.10048

Jee, J. H., Lee, D. H., Ko, J., Hahn, S., Jeong, S. Y., Kim, H. K., Park, E., Choi, S. Y., Jeong, S., Lee, J. W., Cho, H. J., Kwon, M. S., & Yoo, J. (2019). Development of Collagen-Based 3D Matrix for Gastrointestinal Tract-Derived Organoid Culture. *Stem Cells International*, *2019*. https://doi.org/10.1155/2019/8472712

Juskowiak, B. (2011). Nucleic acid-based fluorescent probes and their analytical potential. *Analytical and Bioanalytical Chemistry*, *399*(9), 3157–3176. https://doi.org/10.1007/s00216-010-4304-5

Kaku, Y., Taguchi, A., Tanigawa, S., Haque, F., Sakuma, T., Yamamoto, T., & Nishinakamura, R. (2017). PAX2 is dispensable for in vitro nephron formation from human induced pluripotent stem cells. *Scientific Reports*, *7*(1), 1–12. https://doi.org/10.1038/s41598-017-04813-3

Kann, M., Ettou, S., Jung, Y. L., Lenz, M. O., Taglienti, M. E., Park, P. J., Schermer, B., Benzing, T., & Kreidberg, J. A. (2015). Genome-wide analysis of Wilms' tumor 1-controlled gene expression in podocytes reveals key regulatory mechanisms. *Journal of the American Society of Nephrology*, *26*(9), 2097–2104. https://doi.org/10.1681/ASN.2014090940

Karp, S., Pollak, M. R., & Subramanian, B. (2022). Disease Modeling with Kidney Organoids. *Micromachines*, *13*(9). https://doi.org/10.3390/mi13091384

Karzbrun, E., Khankhel, A. H., Megale, H. C., Glasauer, S. M. K., Wyle, Y., Britton, G., Warmflash, A., Kosik, K. S., Siggia, E. D., Shraiman, B. I., & Streichan, S. J. (2021). Human neural tube morphogenesis in vitro by geometric constraints. *Nature*, *599*(7884), 268–272. https://doi.org/10.1038/s41586-021-04026-9

Karzbrun, E., Kshirsagar, A., Cohen, S. R., Hanna, J. H., & Reiner, O. (2018). Human brain organoids on a chip reveal the physics of folding. *Nature Physics*, *14*(5), 515–522. https://doi.org/10.1038/s41567-018-0046-7

Kaylan, K. B., Berg, I. C., Biehl, M. J., Brougham-Cook, A., Jain, I., Jamil, S. M., Sargeant, L. H., Cornell, N. J., Raetzman, L. T., & Underhill, G. H. (2018). Spatial patterning of liver progenitor cell differentiation mediated by cellular contractility and Notch signaling. *ELife*, *7*, 1–23. https://doi.org/10.7554/eLife.38536

Kechagia, J. Z., Ivaska, J., & Roca-Cusachs, P. (2019). Integrins as biomechanical sensors of the microenvironment. *Nature Reviews Molecular Cell Biology*, *20*(8), 457–473. https://doi.org/10.1038/s41580-019-0134-2

Khan, K., Ahram, D. F., Liu, Y. P., Westland, R., Sampogna, R. V., Katsanis, N., Davis, E. E., & Sanna-Cherchi, S. (2022). Multidisciplinary approaches for elucidating genetics and molecular pathogenesis of urinary tract malformations. *Kidney International*, *101*(3), 473–484. https://doi.org/10.1016/j.kint.2021.09.034

Khoshdel Rad, N., Aghdami, N., & Moghadasali, R. (2020). Cellular and Molecular Mechanisms of Kidney Development: From the Embryo to the Kidney Organoid. *Frontiers in Cell and Developmental Biology*, *8*(March), 1–16. https://doi.org/10.3389/fcell.2020.00183

Kibbey, M. C., Grant, D. S., & Kleinman, H. K. (1992). Role of the SIKVAV site of laminin in promotion of angiogenesis and tumor growth: An in vivo matrigel model. *Journal of the National Cancer Institute*, *84*(21), 1633–1638. https://doi.org/10.1093/jnci/84.21.1633

Kiehart, D. P., Galbraith, C. G., Edwards, K. A., Rickoll, W. L., & Montague, R. A. (2000). Multiple Forces Contribute to Cell Sheet Morphogenesis for Dorsal Closure in Drosophila. *Journal of Cell Biology*, *149*(2), 1–20. papers2://publication/uuid/01B6DCD5-E195-434F-B1FC-2BFB4BEF489D

Kim, S. J., Lee, J. K., Kim, J. W., Jung, J. W., Seo, K., Park, S. B., Roh, K. H., Lee, S. R., Hong, Y. H., Kim, S. J., Lee, Y. S., Kim, S. J., & Kang, K. S. (2008). Surface modification of polydimethylsiloxane (PDMS) induced proliferation and neural-like cells differentiation of umbilical cord blood-derived mesenchymal stem cells. *Journal of Materials Science: Materials in Medicine*, *19*(8), 2953–2962. https://doi.org/10.1007/s10856-008-3413-6

Kobayashi, A., Kwan, K. M., Carroll, T. J., McMahon, A. P., Mendelsohn, C. L., & Behringer, R. R. (2005). Distinct and sequential tissue-specific activitites of the LIM-class homeobox gene Lim1 for tubular morphogenesis during kidney development. *Development*, *132*(12), 2809–2823. https://doi.org/10.1242/dev.01858

Kolahi, K. S., Donjacour, A., Liu, X., Lin, W., Simbulan, R. K., Bloise, E., Maltepe, E., & Rinaudo, P. (2012). Effect of substrate stiffness on early mouse embryo development. *PLoS ONE*, *7*(7). https://doi.org/10.1371/journal.pone.0041717

Kopanska, K. S., Alcheikh, Y., Staneva, R., Vignjevic, D., & Betz, T. (2016). Tensile forces originating from cancer spheroids facilitate tumor invasion. *PLoS ONE*, *11*(6), 1–23. https://doi.org/10.1371/journal.pone.0156442

Kramer-Zucker, A. G., Olale, F., Haycraft, C. J., Yoder, B. K., Schier, A. F., & Drummond, I. A. (2005). Cilia-driven fluid flow in the zebrafish pronephros, brain and Kupffer's vesicle is required for normal organogenesis. *Development*, *132*(8), 1907–1921. https://doi.org/10.1242/dev.01772

Kreidberg, J. A., Sariola, H., Loring, J. M., Maeda, M., Pelletier, J., Housman, D., & Jaenisch, R. (1993). WT-1 is required for early kidney development. *Cell*, *74*(4), 679–691. https://doi.org/10.1016/0092-8674(93)90515-R

Krieg, M., Arboleda-Estudillo, Y., Puech, P. H., Käfer, J., Graner, F., Müller, D. J., & Heisenberg, C. P. (2008). Tensile forces govern germ-layer organization in

zebrafish. *Nature Cell Biology*, *10*(4), 429–436. https://doi.org/10.1038/ncb1705

Kubota, Y., Kleinman, H. K., Martin, G. R., & Lawley, T. J. (1988). Role of laminin and basement membrane in the morphological differentiation of human endothelial cells into capillary-like structures. *The Journal of Cell Biology*, *107*(4), 1589–1598. https://doi.org/10.1083/jcb.107.4.1589

Kuure, S., & Sariola, H. (2018). Mouse models of Congenital Kidney Anomalies. In A. Liu (Ed.), *Animal Models of Human Birth Defects* (Vol. 1236, pp. 109–136). Springer.

Kuure, S., Vuolteenaho, R., & Vainio, S. (2000). Kidney morphogenesis: Cellular and molecular regulation. *Mechanisms of Development*, *92*(1), 31–45. https://doi.org/10.1016/S0925-4773(99)00323-8

Laflamme, M. A., Chen, K. Y., Naumova, A. V., Muskheli, V., Fugate, J. A., Dupras, S. K., Reinecke, H., Xu, C., Hassanipour, M., Police, S., O'Sullivan, C., Collins, L., Chen, Y., Minami, E., Gill, E. A., Ueno, S., Yuan, C., Gold, J., & Murry, C. E. (2007). Cardiomyocytes derived from human embryonic stem cells in pro-survival factors enhance function of infarcted rat hearts. *Nature Biotechnology*, *25*(9), 1015–1024. https://doi.org/10.1038/nbt1327

Lancaster, M. A., & Knoblich, J. A. (2014). Organogenesisin a dish: Modeling development and disease using organoid technologies. *Science*, *345*(6194). https://doi.org/10.1126/science.1247125

Latorre, E., Kale, S., Casares, L., Gómez-González, M., Uroz, M., Valon, L., Nair, R. V., Garreta, E., Montserrat, N., del Campo, A., Ladoux, B., Arroyo, M., & Trepat, X. (2018). Active superelasticity in three-dimensional epithelia of controlled shape. *Nature*, *563*(7730), 203–208. https://doi.org/10.1038/s41586-018-0671-4

Ledig, S., Brucker, S., Barresi, G., Schomburg, J., Rall, K., & Wieacker, P. (2012). Frame shift mutation of LHX1 is associated with Mayer-Rokitansky- Küster-Hauser (MRKH) syndrome. *Human Reproduction*, *27*(9), 2872–2875. https://doi.org/10.1093/humrep/des206

Lee, E. J., Seo, E., Kim, J. W., Nam, S. A., Lee, J. Y., Jun, J., Oh, S., Park, M., Jho, E. H., Yoo, K. H., Park, J. H., & Kim, Y. K. (2020). TAZ/Wnt-β-catenin/c-MYC axis regulates cystogenesis in polycystic kidney disease. *Proceedings of the National Academy of Sciences of the United States of America*, *117*(46), 29001–29012. https://doi.org/10.1073/pnas.2009334117

Li, X., Han, L., Nookaew, I., Mannen, E., Silva, M. J., Almeida, M., & Xiong, J. (2019). Stimulation of piezo1 by mechanical signals promotes bone anabolism. *ELife*, *8*, 1–22. https://doi.org/10.7554/eLife.49631

Li, X., Hu, J., Zhao, X., Li, J., & Chen, Y. (2022). Piezo channels in the urinary system. *Experimental and Molecular Medicine*, *54*(6), 697–710. https://doi.org/10.1038/s12276-022-00777-1

Lian, I., Kim, J., Okazawa, H., Zhao, J., Zhao, B., Yu, J., Chinnaiyan, A., Israel, M. A., Goldstein, L. S. B., Abujarour, R., Ding, S., & Guan, K. L. (2010). The role of YAP transcription coactivator in regulating stem cell self-renewal and differentiation. *Genes and Development*, *24*(11), 1106–1118. https://doi.org/10.1101/gad.1903310

Lin, C. C., & Anseth, K. S. (2009). PEG hydrogels for the controlled release of biomolecules in regenerative medicine. *Pharmaceutical Research*, *26*(3), 631–643. https://doi.org/10.1007/s11095-008-9801-2

Lin, S. Z., Zhang, W. Y., Bi, D., Li, B., & Feng, X. Q. (2021). Energetics of mesoscale cell turbulence in two-dimensional monolayers. *Communications Physics*, *4*(1), 1–9. https://doi.org/10.1038/s42005-021-00530-6

Lindström, N. O., Guo, J., Kim, A. D., Tran, T., Guo, Q., De Sena Brandine, G., Ransick, A., Parvez, R. K., Thornton, M. E., Basking, L., Grubbs, B., McMahon, J. A., Smith, A. D., & McMahon, A. P. (2018). Conserved and divergent features of mesenchymal progenitor cell types within the cortical nephrogenic niche of the human and mouse kidney. *Journal of the American Society of Nephrology*, *29*(3), 806–824. https://doi.org/10.1681/ASN.2017080890

Lindstrom, N. O., Hohenstein, P., & Davies, J. A. (2013). Nephrons require Rho-kinase for proximal-distal polarity development. *Scientific Reports*, *3*, 1–8. https://doi.org/10.1038/srep02692

Lindström, N. O., Lawrence, M. L., Burn, S. F., Johansson, J. A., Bakker, E. R. M., Ridgway, R. A., Chang, C. H., Karolak, M. J., Oxburgh, L., Headon, D. J., Sansom, O. J., Smits, R., Davies, J. A., & Hohenstein, P. (2015). Integrated β-catenin, BMP, PTEN, and Notch signalling patterns the nephron. *ELife*, *3*. https://doi.org/10.7554/eLife.04000

Lindström, N. O., Tran, T., Guo, J., Rutledge, E., Parvez, R. K., Thornton, M. E., Grubbs, B., McMahon, J. A., & McMahon, A. P. (2018). Conserved and divergent molecular and anatomic features of human and mouse nephron patterning. *Journal of the American Society of Nephrology*, *29*(3), 825–840. https://doi.org/10.1681/ASN.2017091036

Ling, L., Mulligan, J. A., Ouyang, Y., Shimpi, A. A., Williams, R. M., Beeghly, G. F., Hopkins, B. D., Spector, J. A., Adie, S. G., & Fischbach, C. (2020). Obesity-Associated Adipose Stromal Cells Promote Breast Cancer Invasion through Direct Cell Contact and ECM Remodeling. *Advanced Functional Materials*, *1910650*, 1–13. https://doi.org/10.1002/adfm.201910650

Little, M. H., & McMahon, A. P. (2012). Mammalian kidney development: Principles, progress, and projections. *Cold Spring Harbor Perspectives in Biology*, *4*(5), 3. https://doi.org/10.1101/cshperspect.a008300

Liu, H., Wang, Y., Wang, H., Zhao, M., Tao, T., Zhang, X., & Qin, J. (2020). A Droplet Microfluidic System to Fabricate Hybrid Capsules Enabling Stem Cell Organoid Engineering. *Advanced Science*, *7*(11). https://doi.org/10.1002/advs.201903739

Liu, J., Prahl, L. S., Huang, A., & Hughes, A. J. (2024). Measurement of adhesion and traction of cells at high yield (MATCHY) reveals an energetic ratchet driving nephron condensation. *BioRxiv*, 22–26.

Liu, M., Cardilla, A., Ngeow, J., Gong, X., & Xia, Y. (2022). Studying Kidney Diseases Using Organoid Models. *Frontiers in Cell and Developmental Biology*, *10*(March), 1–12. https://doi.org/10.3389/fcell.2022.845401

Love, H. D., Ao, M., Jorgensen, S., Swearingen, L., Ferrell, N., Evans, R., Gewin, L., Harris, R. C., Zent, R., Roy, S., & Fissell, W. H. (2019). Substrate Elasticity Governs Differentiation of Renal Tubule Cells in Prolonged Culture. *Tissue Engineering - Part A*, *25*(13–14), 1013–1022. https://doi.org/10.1089/ten.tea.2018.0182

Lutolf, M. P., Lauer-Fields, J. L., Schmoekel, H. G., Metters, A. T., Weber, F. E., Fields, G. B., & Hubbell, J. A. (2003). Synthetic matrix metalloproteinase-sensitive hydrogels for the conduction of tissue regeneration: Engineering cell-invasion characteristics. *Proceedings of the National Academy of Sciences of the United States of America*, *100*(9), 5413–5418. https://doi.org/10.1073/pnas.0737381100

Ma, Z., Wang, J., Loskill, P., Huebsch, N., Koo, S., Svedlund, F. L., Marks, N. C., Hua, E. W., Grigoropoulos, C. P., Conklin, B. R., & Healy, K. E. (2015). Self-organizing human cardiac microchambers mediated by geometric confinement. *Nature Communications*, *6*(May). https://doi.org/10.1038/ncomms8413

Maître, J. L., Niwayama, R., Turlier, H., Nedelec, F., & Hiiragi, T. (2015). Pulsatile cell-autonomous contractility drives compaction in the mouse embryo. *Nature Cell Biology*, *17*(7), 849–855. https://doi.org/10.1038/ncb3185

Mammoto, A., Mammoto, T., & Ingber, D. E. (2012). Mechanosensitive mechanisms in transcriptional regulation. *Journal of Cell Science*, *125*(13), 3061–3073. https://doi.org/10.1242/jcs.093005

Marek, I., Hilgers, K. F., Rascher, W., Woelfle, J., & Hartner, A. (2020). A role for the alpha-8 integrin chain (itga8) in glomerular homeostasis of the kidney. *Molecular and Cellular Pediatrics*, *7*(1), 5–8. https://doi.org/10.1186/s40348-020-00105-5

Martyn, I., Kanno, T. Y., Ruzo, A., Siggia, E. D., & Brivanlou, A. H. (2018). Self-organization of a human organizer by combined Wnt and Nodal signaling. *Nature*, *558*(7708), 132–135. https://doi.org/10.1038/s41586-018-0150-y

Mata, A., Fleischman, A. J., & Roy, S. (2005). Characterization of Polydimethylsiloxane (PDMS) Properties for Biomedical

Micro/Nanosystems. *Biomedical Microdevices*, *7*(4), 281–293. https://doi.org/10.1007/s10544-005-6070-2

Matejčić, M., & Trepat, X. (2023). Mechanobiological approaches to synthetic morphogenesis: learning by building. *Trends in Cell Biology*, *33*(2), 95–111. https://doi.org/10.1016/j.tcb.2022.06.013

McBeath, R., Pirone, D. M., Nelson, C. M., Bhadriraju, K., & Chen, C. S. (2004). Cell Shape, Cytoskeletal Tension, and RhoA Regulate Stem Cell Lineage Commitment. *Developmental Cell*, *6*(1), 483–495.

Mederacke, M., Conrad, L., Doumpas, N., Vetter, R., & Iber, D. (2023). Geometric effects position renal vesicles during kidney development. *Cell Reports*, *42*(12), 113526. https://doi.org/10.1016/j.celrep.2023.113526

Mellott, M. B., Searcy, K., & Pishko, M. V. (2001). Release of protein from highly cross-linked hydrogels of polyethelyne glycol diacrylate fabricated by UV polymerization. *Biomaterials*, *22*, 929–941.

Mongera, A., Pochitaloff, M., Gustafson, H. J., Stooke-Vaughan, G. A., Rowghanian, P., Kim, S., & Campàs, O. (2023). Mechanics of the cellular microenvironment as probed by cells in vivo during zebrafish presomitic mesoderm differentiation. *Nature Materials*, *22*(1), 135–143. https://doi.org/10.1038/s41563-022-01433-9

Monteil, V., Kwon, H., Prado, P., Hagelkrüys, A., Wimmer, R. A., Stahl, M., Leopoldi, A., Garreta, E., Hurtado del Pozo, C., Prosper, F., Romero, J. P., Wirnsberger, G., Zhang, H., Slutsky, A. S., Conder, R., Montserrat, N., Mirazimi, A., & Penninger, J. M. (2020). Inhibition of SARS-CoV-2 Infections in Engineered Human Tissues Using Clinical-Grade Soluble Human ACE2. *Cell*, *181*(4), 905-913.e7. https://doi.org/10.1016/j.cell.2020.04.004

Moon, J. J., Saik, J. E., Poché, R. A., Leslie-Barbick, J. E., Lee, S. H., Smith, A. A., Dickinson, M. E., & West, J. L. (2010). Biomimetic hydrogels with pro-angiogenic properties. *Biomaterials*, *31*(14), 3840–3847. https://doi.org/10.1016/j.biomaterials.2010.01.104

Moore, S. W., Keller, R. E., & Koehl, M. A. R. (1995). The dorsal involuting marginal zone stiffens anisotropically during its convergent extension in the gastrula of Xenopus laevis. *Development*, *121*(10), 3131–3140. https://doi.org/10.1242/dev.121.10.3131

Morizane, R., Lam, A. Q., Freedman, B. S., Kishi, S., Valerius, M. T., & Bonventre, J. V. (2015). Nephron organoids derived from human pluripotent stem cells model kidney development and injury. *Nature Biotechnology*, *33*(11), 1193–1200. https://doi.org/10.1038/nbt.3392

Moscona, A., & Moscona, H. (1952). The dissociation and aggregation of cells from organ rudiments of the early chick embryo. *Journal of Anatomy*, *86*(3), 287–301. http://www.ncbi.nlm.nih.gov/pubmed/12980879%0Ahttp://www.pubmedcentral.nih.gov/articlerender.fcgi?artid=PMC1273752

Mosqueira, D., Pagliari, S., Uto, K., Ebara, M., Romanazzo, S., Escobedo-Lucea, C., Nakanishi, J., Taniguchi, A., Franzese, O., Di Nardo, P., Goumans, M. J., Traversa, E., Pinto-Do-Ó, P., Aoyagi, T., & Forte, G. (2014). Hippo pathway effectors control cardiac progenitor cell fate by acting as dynamic sensors of substrate mechanics and nanostructure. *ACS Nano*, *8*(3), 2033–2047. https://doi.org/10.1021/nn4058984

Mulligan, J. A., Feng, X., & Adie, S. G. (2019). Quantitative reconstruction of time-varying 3D cell forces with traction force optical coherence microscopy. *Scientific Reports*, *9*(1), 1–14. https://doi.org/10.1038/s41598-019-40608-4

Muncie, J. M., Ayad, N. M. E., Lakins, J. N., Xue, X., Fu, J., & Weaver, V. M. (2020). Mechanical Tension Promotes Formation of Gastrulation-like Nodes and Patterns Mesoderm Specification in Human Embryonic Stem Cells. *Developmental Cell*, *55*(6), 679-694.e11. https://doi.org/10.1016/j.devcel.2020.10.015

Murugapoopathy, V., & Gupta, I. R. (2020). A primer on congenital anomalies of the kidneys and urinary tracts (CAKUT). *Clinical Journal of the American*

Society of Nephrology, *15*(5), 723–731. https://doi.org/10.2215/CJN.12581019

Musah, S., Wrighton, P. J., Zaltsman, Y., Zhong, X., Zorn, S., Parlato, M. B., Hsiao, C., Palecek, S. P., Chang, Q., Murphy, W. L., & Kiessling, L. L. (2014). Substratum-induced differentiation of human pluripotent stem cells reveals the coactivator YAP is a potent regulator of neuronal specification. *Proceedings of the National Academy of Sciences of the United States of America*, *111*(38), 13805–13810. https://doi.org/10.1073/pnas.1415330111

Nagamani, S. C. S., Erez, A., Shen, J., Li, C., Roeder, E., Cox, S., Karaviti, L., Pearson, M., Kang, S. H. L., Sahoo, T., Lalani, S. R., Stankiewicz, P., Sutton, V. R., & Cheung, S. W. (2010). Clinical spectrum associated with recurrent genomic rearrangements in chromosome 17q12. *European Journal of Human Genetics*, *18*(3), 278–284. https://doi.org/10.1038/ejhg.2009.174

Nauli, S. M., Alenghat, F. J., Luo, Y., Williams, E., Vassilev, P., Li, X., Elia, A. E. H., Lu, W., Brown, E. M., Quinn, S. J., Ingber, D. E., & Zhou, J. (2003). Polycystins 1 and 2 mediate mechanosensation in the primary cilium of kidney cells. *Nature Genetics*, *33*(2), 129–137. https://doi.org/10.1038/ng1076

Nauryzgaliyeva, Z., Goux Corredera, I., Garreta, E., & Montserrat, N. (2023). Harnessing mechanobiology for kidney organoid research . In *Frontiers in Cell and Developmental Biology* (Vol. 11). https://www.frontiersin.org/articles/10.3389/fcell.2023.1273923

Naylor, R. W., Przepiorski, A., Ren, Q., Yu, J., & Davidson, A. J. (2013). HNF1β is essential for nephron segmentation during nephrogenesis. *Journal of the American Society of Nephrology*, *24*(1), 77–87. https://doi.org/10.1681/ASN.2012070756

Nelson, C. M. (2016). On buckling morphogenesis. *Journal of Biomechanical Engineering*, *138*(2), 1–6. https://doi.org/10.1115/1.4032128

Nelson, C. M., Jean, R. P., Tan, J. L., Liu, W. F., Sniadecki, N. J., Spector, A. A., & Chen, C. S. (2005). Emergent patterns of growth controlled by multicellular

form and mechanics. *Proceedings of the National Academy of Sciences of the United States of America*, *102*(33), 11594–11599. https://doi.org/10.1073/pnas.0502575102

Nerger, B., Sinha, S., Lee, N., Cheriyan, M., Bertsch, P., Johnson, C., Mahadevan, L., Bonventre, J., & Mooney, D. (2024). 3D Hyrgogel encapsulation Regulates Nephrogenesis in Kidney Organoids. *Advanced Materials*, *36*.

Ng, S. S., Xiong, A., Nguyen, K., Masek, M., No, D. Y., Elazar, M., Shteyer, E., Winters, M. A., Voedisch, A., Shaw, K., Rashid, S. T., Frank, C. W., Cho, N. J., & Glenn, J. S. (2017). Long-term culture of human liver tissue with advanced hepatic functions. *JCI Insight*, *2*(11), 1–11. https://doi.org/10.1172/jci.insight.90853

Nicolaou, N., Renkema, K. Y., Bongers, E. M. H. F., Giles, R. H., & Knoers, N. V. A. M. (2015). Genetic, environmental, and epigenetic factors involved in CAKUT. *Nature Reviews Nephrology*, *11*(12), 720–731. https://doi.org/10.1038/nrneph.2015.140

O'Brien, L. L., Guo, Q., Lee, Y. J., Tran, T., Benazet, J. D., Whitney, P. H., Valouev, A., & McMahon, A. P. (2016). Differential regulation of mouse and human nephron progenitors by the six family of transcriptional regulators. *Development (Cambridge)*, *143*(4), 595–608. https://doi.org/10.1242/dev.127175

O'Brien, L. L., & McMahon, A. P. (2014). Induction and patterning of the metanephric nephron. *Seminars in Cell and Developmental Biology*, *36*, 31–38. https://doi.org/10.1016/j.semcdb.2014.08.014

Orkin, R. W., Gehron, P., Mcgoodwin, E. B., George, R., Valentine, T., & Swarm, R. (1977). A Murine Tumor Producing A Matrix of Basement Membrane. *The Journal of Experimental Medicine*, *145*, 204–220.

Orlando, G., Booth, C., Wang, Z., Totonelli, G., Ross, C. L., Moran, E., Salvatori, M., Maghsoudlou, P., Turmaine, M., Delario, G., Al-Shraideh, Y., Farooq, U., Farney, A. C., Rogers, J., Iskandar, S. S., Burns, A., Marini, F. C., De Coppi, P., Stratta, R. J., & Soker, S. (2013). Discarded human kidneys as a source

of ECM scaffold for kidney regeneration technologies. *Biomaterials*, *34*(24), 5915–5925. https://doi.org/10.1016/j.biomaterials.2013.04.033

Ou, G., & Weaver, V. M. (2015). Tumor-induced solid stress activates β-catenin signaling to drive malignant behavior in normal, tumor-adjacent cells. *BioEssays*, *37*(12), 1293–1297. https://doi.org/10.1002/bies.201500090

Pagliarini, D. J., Calvo, S. E., Chang, B., Sheth, S. A., Vafai, S. B., Ong, S. E., Walford, G. A., Sugiana, C., Boneh, A., Chen, W. K., Hill, D. E., Vidal, M., Evans, J. G., Thorburn, D. R., Carr, S. A., & Mootha, V. K. (2008). A Mitochondrial Protein Compendium Elucidates Complex I Disease Biology. *Cell*, *134*(1), 112–123. https://doi.org/10.1016/j.cell.2008.06.016

Pahuja, A., Goux Corredera, I., Moya-Rull, D., Garreta, E., & Montserrat, N. (2024). Engineering physiological environments to advance kidney organoid models from human pluripotent stem cells. *Current Opinion in Cell Biology*, *86*, 102306. https://doi.org/10.1016/j.ceb.2023.102306

Palakkan, A. A., Tarnick, J., Waterfall, M., Sallam, M., Glykofrydis, F., Elhendawi, M., & Davies, J. A. (2022). Production of kidney organoids arranged around single ureteric bud trees, and containing endogenous blood vessels, solely from embryonic stem cells. *Scientific Reports*, *12*(1), 1–16. https://doi.org/10.1038/s41598-022-16768-1

Park, J. S., Valerius, M. T., & McMahon, A. P. (2007). Wnt/β-catenin signaling regulates nephron induction during mouse kidney development. *Development*, *134*(13), 2533–2539. https://doi.org/10.1242/dev.006155

Parker, K. K., Brock, A. L., Brangwynne, C., Mannix, R. J., Wang, N., Ostuni, E., Geisse, N. A., Adams, J. C., Whitesides, G. M., & Ingber, D. E. (2002). Directional control of lamellipodia extension by constraining cell shape and orienting cell tractional forces. *The FASEB Journal*, *16*(10), 1195–1204. https://doi.org/10.1096/fj.02-0038com

Pathak, M. M., Nourse, J. L., Tran, T., Hwe, J., Arulmoli, J., Le, D. T. T., Bernardis, E., Flanagan, L. A., & Tombola, F. (2014). Stretch-activated ion channel Piezo1 directs lineage choice in human neural stem cells. *Proceedings of*

the National Academy of Sciences of the United States of America, *111*(45), 16148–16153. https://doi.org/10.1073/pnas.1409802111

Pelham, R. J., & Wang, Y. L. (1997). Cell locomotion and focal adhesions are regulated by substrate flexibility. *Proceedings of the National Academy of Sciences of the United States of America*, *94*(25), 13661–13665. https://doi.org/10.1073/pnas.94.25.13661

Pelletier, J., Bruening, W., Kashtan, C. E., Mauer, S. M., Manivel, J. C., Striegel, J. E., Houghton, D. C., Junien, C., Habib, R., Fouser, L., Fine, R. N., Silverman, B. L., Haber, D. A., & Housman, D. (1991). Germline mutations in the Wilms' tumor suppressor gene are associated with abnormal urogenital development in denys-drash syndrome. *Cell*, *67*(2), 437–447. https://doi.org/10.1016/0092-8674(91)90194-4

Pérez-González, C., Ceada, G., Greco, F., Matejčić, M., Gómez-González, M., Castro, N., Menendez, A., Kale, S., Krndija, D., Clark, A. G., Gannavarapu, V. R., Álvarez-Varela, A., Roca-Cusachs, P., Batlle, E., Vignjevic, D. M., Arroyo, M., & Trepat, X. (2021). Mechanical compartmentalization of the intestinal organoid enables crypt folding and collective cell migration. *Nature Cell Biology*, *23*(7), 745–757. https://doi.org/10.1038/s41556-021-00699-6

Phelps, E. A., Enemchukwu, N. O., Fiore, V. F., Sy, J. C., Murthy, N., Sulchek, T. A., Barker, T. H., & García, A. J. (2012). Maleimide cross-linked bioactive PEG hydrogel exhibits improved reaction kinetics and cross-linking for cell encapsulation and in situ delivery. *Advanced Materials*, *24*(1), 64–70. https://doi.org/10.1002/adma.201103574

Philpott, A., & Yew, P. R. (2008). The xenopus cell cycle: An overview. *Molecular Biotechnology*, *39*(1), 9–19. https://doi.org/10.1007/s12033-008-9033-z

Piccolo, S., Dupont, S., & Cordenonsi, M. (2014). The biology of YAP/TAZ: Hippo signaling and beyond. *Physiological Reviews*, *94*(4), 1287–1312. https://doi.org/10.1152/physrev.00005.2014

Pitaval, A., Tseng, Q., Bornens, M., & Théry, M. (2010). Cell shape and contractility regulate ciliogenesis in cell cycle-arrested cells. *Journal of Cell Biology*, *191*(2), 303–312. https://doi.org/10.1083/jcb.201004003

Polacheck, W. J., & Chen, C. S. (2016). Measuring cell-generated forces: A guide to the available tools. *Nature Methods*, *13*(5), 415–423. https://doi.org/10.1038/nmeth.3834

Polacheck, W. J., Li, R., Uzel, S. G. M., & Kamm, R. D. (2013). Microfluidics platforms for mechanobiology. *Lab Chip*, *13*(12), 2252–2267. https://doi.org/10.1016/j.biotechadv.2011.08.021.Secreted

Prahl, L. S., Porter, C. M., Liu, J., Viola, J. M., & Hughes, A. J. (2023). Independent control over cell patterning and adhesion on hydrogel substrates for tissue interface mechanobiology. *IScience*, *26*(5), 106657. https://doi.org/10.1016/j.isci.2023.106657

Prahl, L. S., Viola, J. M., Liu, J., & Hughes, A. J. (2023). The developing murine kidney actively negotiates geometric packing conflicts to avoid defects. *Developmental Cell*, *58*(2), 110-120.e5. https://doi.org/10.1016/j.devcel.2022.12.008

Przepiorski, A., Sander, V., Tran, T., Hollywood, J. A., Sorrenson, B., Shih, J. H., Wolvetang, E. J., McMahon, A. P., Holm, T. M., & Davidson, A. J. (2018a). A Simple Bioreactor-Based Method to Generate Kidney Organoids from Pluripotent Stem Cells. *Stem Cell Reports*, *11*(2), 470–484. https://doi.org/10.1016/j.stemcr.2018.06.018

Przepiorski, A., Sander, V., Tran, T., Hollywood, J. A., Sorrenson, B., Shih, J. H., Wolvetang, E. J., McMahon, A. P., Holm, T. M., & Davidson, A. J. (2018b). A Simple Bioreactor-Based Method to Generate Kidney Organoids from Pluripotent Stem Cells. *Stem Cell Reports*, *11*(2), 470–484. https://doi.org/10.1016/j.stemcr.2018.06.018

Przybyla, L., Lakins, J. N., & Weaver, V. M. (2016). Tissue Mechanics Orchestrate Wnt-Dependent Human Embryonic Stem Cell Differentiation. *Cell Stem Cell*, *19*(4), 462–475. https://doi.org/10.1016/j.stem.2016.06.018

Rajagopalan, J., & Saif, M. Taher. A. (2011). MEMS Sensors and Microsystems of Cell Mechanobiology. *J Micromech Microeng.*, *21*(5), 054002. https://doi.org/10.1088/0960-1317/21/5/054002.MEMS

Rak-Raszewska, A., Hauser, P. V., & Vainio, S. (2015). Organ in vitro culture: What have we learned about early kidney development? *Stem Cells International*, *2015*. https://doi.org/10.1155/2015/959807

Ranade, S. S., Qiu, Z., Woo, S. H., Hur, S. S., Murthy, S. E., Cahalan, S. M., Xu, J., Mathur, J., Bandell, M., Coste, B., Li, Y. S. J., Chien, S., & Patapoutian, A. (2014). Piezo1, a mechanically activated ion channel, is required for vascular development in mice. *Proceedings of the National Academy of Sciences of the United States of America*, *111*(28), 10347–10352. https://doi.org/10.1073/pnas.1409233111

Ranade, S. S., Syeda, R., & Patapoutian, A. (2015). Mechanically Activated Ion Channels. *Neuron*, *87*(6), 1162–1179. https://doi.org/10.1016/j.neuron.2015.08.032

Ranga, A., Girgin, M., Meinhardt, A., Eberle, D., Caiazzo, M., Tanaka, E. M., & Lutolf, M. P. (2016). Neural tube morphogenesis in synthetic 3D microenvironments. *Proceedings of the National Academy of Sciences of the United States of America*, *113*(44), E6831–E6839. https://doi.org/10.1073/pnas.1603529113

Ransick, A., Lindström, N. O., Liu, J., Zhu, Q., Guo, J. J., Alvarado, G. F., Kim, A. D., Black, H. G., Kim, J., & McMahon, A. P. (2019). Single-Cell Profiling Reveals Sex, Lineage, and Regional Diversity in the Mouse Kidney. *Developmental Cell*, *51*(3), 399-413.e7. https://doi.org/10.1016/j.devcel.2019.10.005

Rauzi, M., Verant, P., Lecuit, T., & Lenne, P. F. (2008). Nature and anisotropy of cortical forces orienting Drosophila tissue morphogenesis. *Nature Cell Biology*, *10*(12), 1401–1410. https://doi.org/10.1038/ncb1798

Reidy, K. J., & Rosenblum, N. D. (2009). Cell and Molecular Biology of Kidney Development. *Seminars in Nephrology*, *29*(4), 321–337. https://doi.org/10.1016/j.semnephrol.2009.03.009

Rizki-Safitri, A., Gupta, N., Hiratsuka, K., Kobayashi, K., Zhang, C., Ida, K., Satlin, L. M., & Morizane, R. (2022). Live functional assays reveal longitudinal maturation of transepithelial transport in kidney organoids. *Frontiers in Cell and Developmental Biology*, *10*(August), 1–11. https://doi.org/10.3389/fcell.2022.978888

Roca-Cusachs, P., Alcaraz, J., Sunyer, R., Samitier, J., Farré, R., & Navajas, D. (2008). Micropatterning of single endothelial cell shape reveals a tight coupling between nuclear volume in G1 and proliferation. *Biophysical Journal*, *94*(12), 4984–4995. https://doi.org/10.1529/biophysj.107.116863

Roca-Cusachs, P., Conte, V., & Trepat, X. (2017). Quantifying forces in cell biology. *Nature Cell Biology*, *19*(7), 742–751. https://doi.org/10.1038/ncb3564

Romagnani, P., Lasagni, L., & Remuzzi, G. (2013). Renal progenitors: An evolutionary conserved strategy for kidney regeneration. *Nature Reviews Nephrology*, *9*(3), 137–146. https://doi.org/10.1038/nrneph.2012.290

Ross, A. J., May-Simera, H., Eichers, E. R., Kai, M., Hill, J., Jagger, D. J., Leitch, C. C., Chapple, J. P., Munro, P. M., Fisher, S., Tan, P. L., Phillips, H. M., Leroux, M. R., Henderson, D. J., Murdoch, J. N., Copp, A. J., Eliot, M. M., Lupski, J. R., Kemp, D. T., … Beales, P. L. (2005). Disruption of Bardet-Biedl syndrome ciliary proteins perturbs planar cell polarity in vertebrates. *Nature Genetics*, *37*(10), 1135–1140. https://doi.org/10.1038/ng1644

Rozario, T., & DeSimone, D. W. (2010). The Extracellular Matrix in Development and Morphogenesis: A Dynamic View. *Developmental Biology*, *341*(1), 126–140. https://doi.org/10.1007/978-1-4842-3402-0_18

Ruiter, F. A. A., Morgan, F. L. C., Roumans, N., Schumacher, A., Slaats, G. G., Moroni, L., LaPointe, V. L. S., & Baker, M. B. (2022). Soft, Dynamic Hydrogel Confinement Improves Kidney Organoid Lumen Morphology and Reduces Epithelial–Mesenchymal Transition in Culture. *Advanced Science*, *9*(20). https://doi.org/10.1002/advs.202200543

Safshekan, F., Tafazzoli-Shadpour, M., Abdouss, M., & Shadmehr, M. B. (2017). Viscoelastic Properties of Human Tracheal Tissues. *Journal of*

Biomechanical Engineering, *139*(1), 1–9. https://doi.org/10.1115/1.4034651

Sahay, M., Kalra, S., & Bandgar, T. (2012). Renal endocrinology: The new frontier. *Indian Journal of Endocrinology and Metabolism*, *16*(2), 154. https://doi.org/10.4103/2230-8210.93729

Samarage, C. R., White, M. D., Álvarez, Y. D., Fierro-González, J. C., Henon, Y., Jesudason, E. C., Bissiere, S., Fouras, A., & Plachta, N. (2015). Cortical Tension Allocates the First Inner Cells of the Mammalian Embryo. *Developmental Cell*, *34*(4), 435–447. https://doi.org/10.1016/j.devcel.2015.07.004

Sanyanusin, P., Mcnoe, L. A., Sullivan, M. J., Weaver, R. G., & Eccles, M. R. (1995). Mutation of PAX2 in two siblings with renal-coloboma syndrome. *Human Molecular Genetics*, *4*(11), 2183–2184. https://doi.org/10.1093/hmg/4.11.2183

Sauert, K., Kahnert, S., Roose, M., Gull, M., Brändli, A. W., Ryffel, G. U., & Waldner, C. (2012). Heat-shock mediated overexpression of HNF1β mutations has differential effects on gene expression in the xenopus pronephric kidney. *PLoS ONE*, *7*(3). https://doi.org/10.1371/journal.pone.0033522

Saxen, L. (1987). *Organogenesis of the Kidney* (Developmen). Cambridge University Press.

Saxen, L., & Sariola, H. (1987). Early organogenesis of the kidney. *Pediatr Nephrol*, *1*, 385–392.

Schedl, A. (2007). Renal abnormalities and their developmental origin. *Nature Reviews Genetics*, *8*(October), 791–802.

Schillers, H., Rianna, C., Schäpe, J., Luque, T., Doschke, H., Wälte, M., Uriarte, J. J., Campillo, N., Michanetzis, G. P. A., Bobrowska, J., Dumitru, A., Herruzo, E. T., Bovio, S., Parot, P., Galluzzi, M., Podestà, A., Puricelli, L., Scheuring, S., Missirlis, Y., … Radmacher, M. (2017). Standardized Nanomechanical Atomic Force Microscopy Procedure (SNAP) for

Measuring Soft and Biological Samples. *Scientific Reports*, *7*(1), 1–9. https://doi.org/10.1038/s41598-017-05383-0

Schmidt-Ott, K. M., & Barasch, J. (2008). WNT/β-catenin signaling in nephron progenitors and their epithelial progeny. *Kidney International*, *74*(8), 1004–1008. https://doi.org/10.1038/ki.2008.322

Selfa, I. L., Gallo, M., Montserrat, N., & Garreta, E. (2021). Directed Differentiation of Human Pluripotent Stem Cells for the Generation of High-Order Kidney Organoids. *Methods in Molecular Biology*, 171–192.

Sen, D., Voulgaropoulos, A., & Keung, A. J. (2021). Effects of early geometric confinement on the transcriptomic profile of human cerebral organoids. *BMC Biotechnology*, 1–16. https://doi.org/10.1186/s12896-021-00718-2

Seo, B. R., Bhardwaj, P., Choi, S., Gonzalez, J., Eguiluz, R. C. A., Wang, K., Mohanan, S., Morris, P. G., Du, B., Zhou, X. K., Vahdat, L. T., Verma, A., Elemento, O., Hudis, C. A., Williams, R. M., Gourdon, D., Dannenberg, A. J., & Fischbach, C. (2015). Obesity-dependent changes in interstitial ECM mechanics promote breast tumorigenesis. *Science Translational Medicine*, *7*(301), 1–12.

Sha, W., Moore, J., Chen, K., Lassaletta, A. D., Yi, C. S., Tyson, J. J., & Sible, J. C. (2003). Hysteresis drives cell-cycle transitions in Xenopus laevis egg extracts. *Proceedings of the National Academy of Sciences of the United States of America*, *100*(3), 975–980. https://doi.org/10.1073/pnas.0235349100

Shawlot, W., & Behringer, R. R. (1995). Requirement for liml in head-organizer function. In *Nature* (Vol. 374, Issue 6521, pp. 425–430). https://doi.org/10.1038/374425a0

Shi, M., McCracken, K. W., Patel, A. B., Zhang, W., Ester, L., Valerius, M. T., & Bonventre, J. V. (2023). Human ureteric bud organoids recapitulate branching morphogenesis and differentiate into functional collecting duct cell types. *Nature Biotechnology*, *41*(2), 252–261. https://doi.org/10.1038/s41587-022-01429-5

Smith, Q., Rochman, N., Carmo, A. M., Vig, D., Chan, X. Y., Sun, S., & Gerecht, S. (2018). Cytoskeletal tension regulates mesodermal spatial organization and subsequent vascular fate. *Proceedings of the National Academy of Sciences of the United States of America*, *115*(32), 8167–8172. https://doi.org/10.1073/pnas.1808021115

Snippert, H. J., van der Flier, L. G., Sato, T., van Es, J. H., van den Born, M., Kroon-Veenboer, C., Barker, N., Klein, A. M., van Rheenen, J., Simons, B. D., & Clevers, H. (2010). Intestinal crypt homeostasis results from neutral competition between symmetrically dividing Lgr5 stem cells. *Cell*, *143*(1), 134–144. https://doi.org/10.1016/j.cell.2010.09.016

Song, J. W., & Munn, L. L. (2011). Fluid forces control endothelial sprouting. *Proceedings of the National Academy of Sciences of the United States of America*, *108*(37), 15342–15347. https://doi.org/10.1073/pnas.1105316108

Stange, D. E., Koo, B. K., Huch, M., Sibbel, G., Basak, O., Lyubimova, A., Kujala, P., Bartfeld, S., Koster, J., Geahlen, J. H., Peters, P. J., Van Es, J. H., Van De Wetering, M., Mills, J. C., & Clevers, H. (2013). XDifferentiated Troy+ chief cells act as reserve stem cells to generate all lineages of the stomach epithelium. *Cell*, *155*(2), 357. https://doi.org/10.1016/j.cell.2013.09.008

Steinwachs, J., Metzner, C., Skodzek, K., Lang, N., Thievessen, I., Mark, C., Münster, S., Aifantis, K. E., & Fabry, B. (2016). Three-dimensional force microscopy of cells in biopolymer networks. *Nature Methods*, *13*(2), 171–176. https://doi.org/10.1038/nmeth.3685

Stone, A. V, Vanderman, K. S., Willey, J. S., David, L., Register, T. C., Shively, C. A., Jr, J. R. S., Loeser, F., & Ferguson, C. M. (2016). Single-Gene Causes of Congenital Anomalies of the Kidney and Urinary Tract (CAKUT) in Humans. *Pediatr Nephrol*, *23*(10), 1780–1789. https://doi.org/10.1007/s00467-013-2684-4.Single-Gene

Strale, P. O., Azioune, A., Bugnicourt, G., Lecomte, Y., Chahid, M., & Studer, V. (2016a). Multiprotein Printing by Light-Induced Molecular Adsorption.

Advanced Materials, *28*(10), 2024–2029. https://doi.org/10.1002/adma.201504154

Strale, P. O., Azioune, A., Bugnicourt, G., Lecomte, Y., Chahid, M., & Studer, V. (2016b). Multiprotein Printing by Light-Induced Molecular Adsorption. *Advanced Materials*, *28*(10), 2024–2029. https://doi.org/10.1002/adma.201504154

Świerczek-Lasek, B., Keremidarska-Markova, M., Hristova-Panusheva, K., Vladkova, T., Ciemerych, M. A., Archacka, K., & Krasteva, N. (2019). Polydimethylsiloxane materials with supraphysiological elasticity enable differentiation of myogenic cells. *Journal of Biomedical Materials Research - Part A*, *107*(12), 2619–2628. https://doi.org/10.1002/jbm.a.36768

Taguchi, A., Kaku, Y., Ohmori, T., Sharmin, S., Ogawa, M., Sasaki, H., & Nishinakamura, R. (2014). Redefining the in vivo origin of metanephric nephron progenitors enables generation of complex kidney structures from pluripotent stem cells. *Cell Stem Cell*, *14*(1), 53–67. https://doi.org/10.1016/j.stem.2013.11.010

Taguchi, A., & Nishinakamura, R. (2017). Higher-Order Kidney Organogenesis from Pluripotent Stem Cells. *Cell Stem Cell*, *21*(6), 730-746.e6. https://doi.org/10.1016/j.stem.2017.10.011

Taira, M., Jamrich, M., Good, P. J., & Dawid, I. B. (1992). The LIM domain-containing homeo box gene Xlim-1 is expressed specifically in the organizer region of Xenopus gastrula embryos. *Genes and Development*, *6*(3), 356–366. https://doi.org/10.1101/gad.6.3.356

Taira, M., Otani, H., Saint-Jeannet, J. P., & Dawid, I. B. (1994). Role of the LIM class homeodomain protein Xlim-1 in neural and muscle induction by the Spemann organizer in Xenopus. In *Nature* (Vol. 372, Issue 6507, pp. 677–679). https://doi.org/10.1038/372677a0

Takahashi, K., Tanabe, K., Ohnuki, M., Narita, M., Ichisaka, T., Tomoda, K., & Yamanaka, S. (2007). Induction of Pluripotent Stem Cells from Adult Human Fibroblasts by Defined Factors. *Cell*, *131*(5), 861–872. https://doi.org/10.1016/j.cell.2007.11.019

Takahashi, K., & Yamanaka, S. (2006). Induction of Pluripotent Stem Cells from Mouse Embryonic and Adult Fibroblast Cultures by Defined Factors. *Cell*, *126*(4), 663–676. https://doi.org/10.1016/j.cell.2006.07.024

Takasato, M., Er, P. X., Becroft, M., Vanslambrouck, J. M., Stanley, E. G., Elefanty, A. G., & Little, M. H. (2014). Directing human embryonic stem cell differentiation towards a renal lineage generates a self-organizing kidney. *Nature Cell Biology*, *16*(1), 118–126. https://doi.org/10.1038/ncb2894

Takasato, M., Er, P. X., Chiu, H. S., & Little, M. H. (2016). Generation of kidney organoids from human pluripotent stem cells. *Nature Protocols*, *11*(9), 1681–1692. https://doi.org/10.1038/nprot.2016.098

Takasato, M., Er, P. X., Chiu, H. S., Maier, B., Baillie, G. J., Ferguson, C., Parton, R. G., Wolvetang, E. J., Roost, M. S., De Sousa Lopes, S. M. C., & Little, M. H. (2015). Kidney organoids from human iPS cells contain multiple lineages and model human nephrogenesis. *Nature*, *526*(7574), 564–568. https://doi.org/10.1038/nature15695

Tan, J. L., Tien, J., Pirone, D. M., Gray, D. S., Bhadriraju, K., & Chen, C. S. (2002). Cells lying on a bed of microneedles : An approach to isolate mechanical force. *PNAS*, *100*(4), 1484–1489. https://doi.org/10.1073/pnas.0235407100

Tanaka, Y., Okada, Y., & Hirokawa, N. (2005). FGF-induced vesicular release of Sonic hedgehog and retinoic acid in leftward nodal flow is critical for left-right determination. *Nature*, *435*(7039), 172–177. https://doi.org/10.1038/nature03494

Tanigawa, S., Naganuma, H., Kaku, Y., Era, T., Sakuma, T., Yamamoto, T., Taguchi, A., & Nishinakamura, R. (2019). Activin Is Superior to BMP7 for Efficient Maintenance of Human iPSC-Derived Nephron Progenitors. *Stem Cell Reports*, *13*(2), 322–337. https://doi.org/10.1016/j.stemcr.2019.07.003

Tanigawa, S., Tanaka, E., Miike, K., Ohmori, T., Inoue, D., Cai, C. L., Taguchi, A., Kobayashi, A., & Nishinakamura, R. (2022). Generation of the organotypic kidney structure by integrating pluripotent stem cell-derived renal stroma.

Nature Communications, *13*(1), 1–15. https://doi.org/10.1038/s41467-022-28226-7

Taubenberger, A. V., Hutmacher, D. W., & Muller, D. J. (2014). Single-cell force spectroscopy, an emerging tool to quantify cell adhesion to biomaterials. *Tissue Engineering - Part B: Reviews*, *20*(1), 40–55. https://doi.org/10.1089/ten.teb.2013.0125

Thé, M., Racine, V., Piel, M., Pépin, A., Dimitrov, A., Chen, Y., Sibarita, J. B., & Bornens, M. (2006). Anisotropy of cell adhesive microenvironment governs cell internal organization and orientation of polarity. *Proceedings of the National Academy of Sciences of the United States of America*, *103*(52), 19771–19776. https://doi.org/10.1073/pnas.0609267103

Thomson, J. A., Itskovitz-eldor, J., Shapiro, S. S., Waknitz, M. A., Swiergiel, J. J., Marshall, V. S., & Jones, J. M. (1998). Embryonic Stem Cell Lines Derived from Human Blastocysts. *Science*, *282*(November), 1145–1147.

Tohyama, S., Fujita, J., Fujita, C., Yamaguchi, M., Kanaami, S., Ohno, R., Sakamoto, K., Kodama, M., Kurokawa, J., Kanazawa, H., Seki, T., Kishino, Y., Okada, M., Nakajima, K., Tanosaki, S., Someya, S., Hirano, A., Kawaguchi, S., Kobayashi, E., & Fukuda, K. (2017). Efficient Large-Scale 2D Culture System for Human Induced Pluripotent Stem Cells and Differentiated Cardiomyocytes. *Stem Cell Reports*, *9*(5), 1406–1414. https://doi.org/10.1016/j.stemcr.2017.08.025

Torres, M., Gómez-Pardo, E., Dressler, G. R., & Gruss, P. (1995). Pax-2 controls multiple steps of urogenital development. *Development*, *121*(12), 4057–4065. https://doi.org/10.1242/dev.121.12.4057

Totaro, A., Castellan, M., Battilana, G., Zanconato, F., Azzolin, L., Giulitti, S., Cordenonsi, M., & Piccolo, S. (2017). YAP/TAZ link cell mechanics to Notch signalling to control epidermal stem cell fate. *Nature Communications*, *8*(May), 1–13. https://doi.org/10.1038/ncomms15206

Träber, N., Uhlmann, K., Girardo, S., Kesavan, G., Wagner, K., Friedrichs, J., Goswami, R., Bai, K., Brand, M., Werner, C., Balzani, D., & Guck, J. (2019). Polyacrylamide Bead Sensors for in vivo Quantification of Cell-Scale

Stress in Zebrafish Development. *Scientific Reports*, *9*(1), 1–14. https://doi.org/10.1038/s41598-019-53425-6

Tran, T., Song, C. J., Nguyen, T., Cheng, S. Y., McMahon, J. A., Yang, R., Guo, Q., Der, B., Lindström, N. O., Lin, D. C. H., & McMahon, A. P. (2022). A scalable organoid model of human autosomal dominant polycystic kidney disease for disease mechanism and drug discovery. *Cell Stem Cell*, *29*(7), 1083-1101.e7. https://doi.org/10.1016/j.stem.2022.06.005

Trepat, X., Wasserman, M. R., Angelini, T. E., Millet, E., Weitz, D. A., Butler, J. P., & Fredberg, J. J. (2009). Physical forces during collective cell migration. *Nature Physics*, *5*(6), 426–430. https://doi.org/10.1038/nphys1269

Trowell, O. A. (1954). A Modified Technique for Organ Culture In Vitro. *Experimental Cell Research*, *6*, 246–248.

Uchimura, K., Wu, H., Yoshimura, Y., & Humphreys, B. D. (2020). Human Pluripotent Stem Cell-Derived Kidney Organoids with Improved Collecting Duct Maturation and Injury Modeling. *Cell Reports*, *33*(11), 108514. https://doi.org/10.1016/j.celrep.2020.108514

Vanslambrouck, J. M., Wilson, S. B., Tan, K. S., Groenewegen, E., Rudraraju, R., Neil, J., Lawlor, K. T., Mah, S., Scurr, M., Howden, S. E., Subbarao, K., & Little, M. H. (2022). Enhanced metanephric specification to functional proximal tubule enables toxicity screening and infectious disease modelling in kidney organoids. *Nature Communications*, *13*(1). https://doi.org/10.1038/s41467-022-33623-z

Vanslambrouck, J. M., Wilson, S. B., Tan, K. S., Soo, J. Y. C., Scurr, M., Spijker, H. S., Starks, L. T., Neilson, A., Cui, X., Jain, S., Little, M. H., & Howden, S. E. (2019). A toolbox to characterize human induced pluripotent stem cell-derived kidney cell types and organoids. *Journal of the American Society of Nephrology*, *30*(10), 1811–1823. https://doi.org/10.1681/ASN.2019030303

Versaevel, M., Grevesse, T., & Gabriele, S. (2012). Spatial coordination between cell and nuclear shape within micropatterned endothelial cells. *Nature Communications*, *3*. https://doi.org/10.1038/ncomms1668

Vining, K. H., & Mooney, D. J. (2017). Mechanical forces direct stem cell behaviour in development and regeneration. *Nature Reviews Molecular Cell Biology*, *18*(12), 728–742. https://doi.org/10.1038/nrm.2017.108

Viola, J. M., Liu, J., Prahl, L. S., Huang, A., Chan, T. J., Hayward-Lara, G., Porter, C. M., & Hughes, A. J. (2022). Tubule jamming in the developing kidney creates cyclical mechanical stresses instructive to nephron formation. *BioRxiv*, 2022.06.03.494718. https://www.biorxiv.org/content/10.1101/2022.06.03.494718v1.abstract

von Dassow, M., Strother, J. A., & Davidson, L. A. (2010). Surprisingly simple mechanical behavior of a complex embryonic tissue. *PLoS ONE*, *5*(12). https://doi.org/10.1371/journal.pone.0015359

Waehle, V., Ungricht, R., Hoppe, P. S., & Betschinger, J. (2021). The tumor suppressor WT1 drives progenitor cell progression and epithelialization to prevent Wilms tumorigenesis in human kidney organoids. *Stem Cell Reports*, *16*(9), 2107–2117. https://doi.org/10.1016/j.stemcr.2021.07.023

Wagh, K., Ishikawa, M., Garcia, D. A., Stavreva, D. A., Upadhyaya, A., & Hager, G. L. (2021). Cell Biology Mechanical Regulation of Transcription : Recent Advances. *Trends in Cell Biology*, *31*(6), 457–472. https://doi.org/10.1016/j.tcb.2021.02.008

Wang, H., & Heilshorn, S. C. (2015). Adaptable Hydrogel Networks with Reversible Linkages for Tissue Engineering. *Advanced Materials*, *27*(25), 3717–3736. https://doi.org/10.1002/adma.201501558

Wang, P. C. (2005). Reconstruction of renal glomerular tissue using collagen vitrigel scaffold. *Journal of Bioscience and Bioengineering*, *99*(6), 529–540. https://doi.org/10.1263/jbb.99.529

Wang, W., Jin, S., & Ye, K. (2017). Development of Islet Organoids from H9 Human Embryonic Stem Cells in Biomimetic 3D Scaffolds. *Stem Cells and Development*, *26*(6), 394–404. https://doi.org/10.1089/scd.2016.0115

Wang, Y., Lee, J. H., Shirahama, H., Seo, J., Glenn, J. S., & Cho, N. J. (2016). Extracellular Matrix Functionalization and Huh-7.5 Cell Coculture Promote

the Hepatic Differentiation of Human Adipose-Derived Mesenchymal Stem Cells in a 3D ICC Hydrogel Scaffold. *ACS Biomaterials Science and Engineering*, *2*(12), 2255–2265. https://doi.org/10.1021/acsbiomaterials.6b00487

Warmflash, A., Sorre, B., Etoc, F., Siggia, E. D., & Brivanlou, A. H. (2014). A method to recapitulate early embryonic spatial patterning in human embryonic stem cells. *Nature Methods*, *11*(8), 847–854. https://doi.org/10.1038/nMeth.3016

Weinbaum, S., Duan, Y., Satlin, L. M., Wang, T., & Weinstein, A. M. (2010). Mechanotransduction in the renal tubule. *American Journal of Physiology - Renal Physiology*, *299*(6), 1220–1236. https://doi.org/10.1152/ajprenal.00453.2010

Weissman, T. A., & Pan, Y. A. (2014). Brainbow: New resources and emerging biological applications for multicolor genetic labeling and analysis. *Genetics*, *199*(2), 293–306. https://doi.org/10.1534/genetics.114.172510

Wen, J. H., Vincent, L. G., Fuhrmann, A., Choi, Y. S., Hribar, K. C., Taylor-Weiner, H., Chen, S., & Engler, A. J. (2014). Interplay of matrix stiffness and protein tethering in stem cell differentiation. *Nature Materials*, *13*(10), 979–987. https://doi.org/10.1038/nmat4051

Westland, R., Renkema, K. Y., & Knoers, N. V. A. M. (2021). Clinical integration of genome diagnostics for congenital anomalies of the kidney and urinary tract. *Clinical Journal of the American Society of Nephrology*, *16*(1), 128–137. https://doi.org/10.2215/CJN.14661119

Wilkinson, D. C., Mellody, M., Meneses, L. K., Hope, A. C., Dunn, B., & Gomperts, B. N. (2018). Development of a Three-Dimensional Bioengineering Technology to Generate Lung Tissue for Personalized Disease Modeling. *Current Protocols in Stem Cell Biology*, *46*(1). https://doi.org/10.1002/cpsc.56

Wilson, L., Gale, E., & Maden, M. (2003). The role of retinoic acid in the morphogenesis of the neural tube. *Journal of Anatomy*, *203*(4), 357–368. https://doi.org/10.1046/j.1469-7580.2003.00230.x

Wingert, R. A., & Davidson, A. J. (2008). The zebrafish pronephros: A model to study nephron segmentation. *Kidney International*, *73*(10), 1120–1127. https://doi.org/10.1038/ki.2008.37

Wolpert, L. (1981). Positional information and pattern formation. *Philosophical Transactions of the Royal Society of London. Series B, Biological Sciences*, *295*(1078), 441–450. https://doi.org/10.1098/rstb.1981.0152

Wong, L., Kumar, A., Gabela-Zuniga, B., Chua, J., Singh, G., Happe, C. L., Engler, A. J., Fan, Y., & McCloskey, K. E. (2019). Substrate stiffness directs diverging vascular fates. *Acta Biomaterialia*, *96*, 321–329. https://doi.org/10.1016/j.actbio.2019.07.030

Wullkopf, L., West, A. K. V., Leijnse, N., Cox, T. R., Madsen, C. D., Oddershede, L. B., & Erler, J. T. (2018). Cancer cells' ability to mechanically adjust to extracellular matrix stiffness correlates with their invasive potential. *Molecular Biology of the Cell*, *29*(20), 2378–2385. https://doi.org/10.1091/mbc.E18-05-0319

Xia, Y., Sancho-Martinez, I., Nivet, E., Rodriguez Esteban, C., Campistol, J. M., & Izpisua Belmonte, J. C. (2014). The generation of kidney organoids by differentiation of human pluripotent cells to ureteric bud progenitor-like cells. *Nature Protocols*, *9*(11), 2693–2704. https://doi.org/10.1038/nprot.2014.182

Xue, X., Sun, Y., Resto-Irizarry, A. M., Yuan, Y., Aw Yong, K. M., Zheng, Y., Weng, S., Shao, Y., Chai, Y., Studer, L., & Fu, J. (2018). Mechanics-guided embryonic patterning of neuroectoderm tissue from human pluripotent stem cells. *Nature Materials*, *17*(7), 633–641. https://doi.org/10.1038/s41563-018-0082-9

Yamaguchi, N., Zhang, Z., Schneider, T., Wang, B., Panozzo, D., & Knaut, H. (2022). Rear traction forces drive adherent tissue migration in vivo. *Nature Cell Biology*, *24*(2), 194–204. https://doi.org/10.1038/s41556-022-00844-9

Yang, L., Soonpaa, M. H., Adler, E. D., Roepke, T. K., Kattman, S. J., Kennedy, M., Henckaerts, E., Bonham, K., Abbott, G. W., Linden, R. M., Field, L. J., & Keller, G. M. (2008). Human cardiovascular progenitor cells develop from a

KDR+ embryonic-stem-cell-derived population. *Nature*, *453*(7194), 524–528. https://doi.org/10.1038/nature06894

Yang, Y., Beqaj, S., Kemp, P., Ariel, I., & Schuger, L. (2000). Stretch-induced alternative splicing of serum response factor promotes bronchial myogenesis and is defective in lung hypoplasia. *Journal of Clinical Investigation*, *106*(11), 1321–1330. https://doi.org/10.1172/JCI8893

Zeng, Z., Huang, B., Parvez, R. K., Li, Y., Chen, J., Vonk, A. C., Thornton, M. E., Patel, T., Rutledge, E. A., Kim, A. D., Yu, J., Grubbs, B. H., McMahon, J. A., Pastor-Soler, N. M., Hallows, K. R., McMahon, A. P., & Li, Z. (2021). Generation of patterned kidney organoids that recapitulate the adult kidney collecting duct system from expandable ureteric bud progenitors. *Nature Communications*, *12*(1), 1–15. https://doi.org/10.1038/s41467-021-23911-5

Zhang, H., & Liu, K. K. (2008). Optical tweezers for single cells. *Journal of the Royal Society Interface*, *5*(24), 671–690. https://doi.org/10.1098/rsif.2008.0052

Zhu, P., Qiu, Q., Harris, P. C., Xu, X., & Lin, X. (2021). mtor Haploinsufficiency Ameliorates Renal Cysts and Cilia Abnormality in Adult Zebrafish tmem67 Mutants. *Journal of the American Society of Nephrology : JASN*, *32*(4), 822–836. https://doi.org/10.1681/ASN.2020070991

Zimmermann, W. H., Fink, C., Kralisch, D., Remmers, U., Weil, J., & Eschenhagen, T. (2000). Three-dimensional engineered heart tissue from neonatal rat cardiac myocytes. *Biotechnology and Bioengineering*, *68*(1), 106–114. https://doi.org/10.1002/(SICI)1097-0290(20000405)68:1<106::AID-BIT13>3.0.CO;2-3